UNIVERSITY OF CALIFORNIA

Los Angeles

Adipose Tissue and Translation Machinery in Metabolic Regulation

A dissertation submitted in partial satisfaction of the requirements for the degree Doctor of Philosophy in Molecular, Cellular, and Integrative Physiology

by

Mirian Krystel De Siqueira

2024

ABSTRACT OF THE DISSERTATION

Adipose Tissue and Translation Machinery

in Metabolic Regulation

by

Mirian Krystel De Siqueira

Doctor of Philosophy in Molecular, Cellular, and Integrative Physiology

University of California, Los Angeles, 2024

Professor Claudio Javier Villanueva, Chair

Adipose tissue plays a pivotal role in energy homeostasis and metabolic regulation. However, in obesity, the remarkable adaptability of adipose tissue becomes impaired. The underlying mechanisms behind this limited adaptability remain poorly understood. Here, we initially discuss on chapter one an overview about adipose tissue plasticity in health and disease. Then, we investigate a novel layer of regulation involving translation in the adipose tissue, examining its response to obesity and acute PPARγ agonist treatment with rosiglitazone. First, using single-cell RNA sequencing, we establish a transcriptional profile atlas of stromal cellular remodeling from obese to lean-like states in inguinal and epididymal adipose tissue following rosiglitazone treatment. Notably, both stromal fractions exhibit a downregulation of inflammation-related transcripts and an upregulation of lipid-related metabolism and ribosomal transcripts. Adipocyte progenitor and preadipocyte populations display enhanced *ex-vivo* differentiation potential and upregulation in ribosome and peptide chain elongation pathways. This ribosomal

remodeling is directly driven by PPARγ binding to gene promoters of ribosomal factors. Furthermore, we have characterized the translatome in the epididymal stromal fraction, highlighting a buffering response and fat-exclusive preferential translation after rosiglitazone treatment. Enhanced translation efficiency in rosiglitazone-elicited polysomes promotes the translation of transcripts containing G-rich sequences in their 5' untranslated regions. Our findings shed light and provide a resource on how rosiglitazone remodels the adipose stromal vascular fraction, both dependent and independent of PPARγ. Importantly, we uncover translatome remodeling as a major new mechanism for maintaining translation homeostasis and preserving adipose tissue health in obesity.

Second, we focused on the mature adipocytes, and how rosiglitazone modulates their translation machinery. Transcriptional analysis of brown and white adipose tissue after thiazolidinedione treatment has shown translation as a highly upregulated process. Therefore, we hypothesized that thiazolidinediones may have an uncharacterized mechanism of action by enhancing translation efficiency in adipocytes. A mechanism that may be mediated by specific induced proteins such as PIXL. Our laboratory has identified a largely uncharacterized PPARγ - responsive, X-linked gene, PIXL that is primarily expressed in the cytoplasm. Notably, PIXL and PPARγ expression is reduced in ob/ob mice and with high-fat feeding, results that are consistent with impaired expansion of adipose tissue. Our *in vivo* studies demonstrated that PIXL loss-of-function in mature adipocytes leads to a dysfunctional tissue characterized by adipocyte hypertrophy, impaired glucose metabolism, inflammation, hypertriglyceridemia, enhanced cold sensitivity, and decreased energy expenditure. Mechanistically, immunoprecipitation studies have uncovered PIXL interactome, highlighting the close association with eukaryotic initiation factors, ribonucleoprotein complexes, and 40S ribosomal proteins. Indeed, co-immunoprecipitation studies have demonstrated that PIXL associated with the eIF4E complex. Additionally, polysome profiling have shown PIXL at protein levels associated with initiation factors and subunits of

ribosomes. Taken together, we propose that PPARγ induces the expression of PIXL, which in turn may be an important factor regulating translational control and directing the translation of defined mRNA networks. Finally, we propose a novel layer of molecular regulation of thiazolidinediones by targeting translation efficiency and adipocyte proteostasis - a process that may be impaired during obesity and restored after treatment with rosiglitazone.

The dissertation of Mirian Krystel De Siqueira is approved.

Peter John Tontonoz

Thomas Aguiar Vallim

Thomas M. Vondriska

Xia Yang

Claudio Javier Villanueva, Committee Chair

University of California, Los Angeles

2024

To my late grandmother Maria Przeybilovicz whose love remains the heartwarming tale that I carry with me on every page of my life.

TABLE OF CONTENTS

LIST OF FIGURES

ACKNOWLEDGMENTS

In recognition of the invaluable contributions and unwavering support, I extend my sincerest gratitude to those who have made this journey possible!

First and foremost, I would like to thank my supervisor, Dr. Claudio J. Villanueva whose guidance, expertise, and unwavering support were indispensable in completing this doctoral dissertation. His mentorship has been invaluable, and I am profoundly grateful for his dedication to my academic and professional development.

To the members of my dissertation committee: Dr. Peter J. Tontonoz, Dr. Thomas A. Vallim, Dr. Thomas M. Vondriska, and Dr. Xia Yang for their time, expertise, and valuable feedback during our meetings. Their guidance and constructive criticism have been instrumental in shaping the direction and quality of this research.

To my family, Goncalo M. De Siqueira, Miguelina C. De Siqueira, Katia R. De Siqueira, Joao P. M. Neto and Maria Julia S. Maia, for their unconditional love, encouragement, and understanding throughout this doctoral degree. Their support has been my rock, enabling me to pursue my academic aspirations with confidence and determination.

To my fiancé Cesar Antonio Martinez whose love, support, and understanding have been my guiding light throughout this doctoral journey. Your encouragement and belief in me have been the driving force behind my success. I am profoundly grateful for your presence in my life and for standing by my side every step of the way (also thank you for supplying snacks and lots of coffee!).

To my best MCIP friends Dr. Julianne Yang and Irene Santiago, whose support and belief in me have been a constant source of strength during my PhD. Our countless pep talks, and shared laughter have infused joy into even the most challenging moments. I am immensely thankful to your friendship.

To my two dear friends, Luane F. T. Silveira and Gabriela Cateb, whose friendship has spanned the test of time, and merits a debt of gratitude beyond the capacity of words to convey fully. Thank you for all the long-distance calls and advice!

To the Villanueva Lab members: Dr. Lucydalila Cedillo, Dr. Sicheng Zhang, Stacy Tletlepantzi, Jakeline Larios, Ezekiel Delgado, Jasmine Tzeng, Kelly Kiremidjian, Jeslyn Zhang, and Vishnu Nair, for their invaluable contributions to our research endeavors and their friendship over these past five years.

To the Metabolism Theme Gang, especially to Luciano T. Moraes, Andrew Caliri, and Akash Saha, for the countless laughs, shared dramas, snack-fueled discussions, and exchanged reagents during our meetings and daily interactions. Your friendship is deeply appreciated.

To the Thermogenesis Posse, Dr. Marcus Tol and Dr. Yuta Shimanaka, I extend my heartfelt gratitude for welcoming me into this scientific niche and generously sharing your knowledge, help, and support (also thank you for all the happy-hour invitations!).

To all my uncited friends, whose path have crossed mine during this PhD, you are deeply appreciated. In special to my first friend in LA (and also roommate) Dr. Frederick Vu – thank you for accepting me as your roommate for the past 5 years and for your friendship.

To all my co-authors, thank you for their collaboration, expertise, and dedication in bringing this work to fruition. Your contributions have been invaluable, and I am grateful for the opportunity to work alongside such talented individuals.

To the Molecular, Cellular, and Integrative Program (MCIP), and in special to our Graduate Student Services Advisor, Yesenia Rayos, your tireless efforts ensured that I could navigate the doctoral academic journey with confidence and ease.

To the funding resources, Ursula Mandel Fellowship, Graduate Council Diversity Fellowship, Eureka Fellowship, American Heart Association Pre-doctoral fellowship, your financial assistance has been instrumental in bringing this project to fruition, and I am thankful for your commitment to advancing knowledge and innovation in our field.

BIOGRAPHICAL SKETCH

EDUCATION/TRAINING

INSTITUTION AND LOCATION	DEGREE *(if applicable)*	Completion Date MM/YYYY	FIELD OF STUDY
University Tuiuti of Parana, Parana, Brazil	B.S.	07/2016	Biomedical Sciences
Rowan University, New Jersey, U.S.A.	Visitor Fellow	12/2014	Biology
State University of Campinas, Sao Paulo, Brazil	M.S.	08/2019	Genetics and Molecular Biology
National Institutes of Health, Maryland, U.S.A.	Visitor Fellow	05/2019	Mucosal Immunology

FULL-TIME POSITIONS

2018 - 2019	Master Student Visitor Fellow with Yasmine Belkaid, Ph.D., Laboratory of Immune System Biology, National Institutes of Health, Bethesda, MD, USA
2016 - 2019	Master Student with Denise Morais da Fonseca, Ph.D., Laboratory of Mucosal Immunology, University of Sao Paulo, Sao Paulo, SP, Brazil
2019 -present	Ph.D. Candidate with Claudio J. Villanueva, Ph.D., UCLA David Geffen School of Medicine, University of California, Los Angeles, California, USA

TEACHING

2019	Teaching Assistant Physiological Sciences 121: Disease Mechanism and Therapies. Professor: Rachelle Crosbie, Ph.D. Upper division class - University of California, Los Angeles
2022	Teaching Assistant Physiological Sciences 148: Physiological Regulation of Metabolism and Nutrient Sensing. Professor: Claudio Villanueva, Ph.D. Upper division class - University of California, Los Angeles

SCHOLASTIC HONORS

2006	Medal of Brazil Application and Study, Elementary School Trajano Ehlke Pires
2014	Brazilian Scientific Mobility Program (Science Without Borders)
2016	Honorable Mention at the XXIV Annual Meeting of Scientific Initiation, Fiocruz, Carlos Chagas Institute
2016	Best Student of 2016' Class, GPA Ranked, University Tuiuti of Parana, Brazil
2017	Honorable Mention - SBI Scientific Abstract Award, XLII Congress of the Brazilian Society of Immunology 2017, X Extra Section of Clinical Immunology
2022	UCLA Life Sciences Mautner Graduate Award for Excellence in Academics and Research
2023	University of California Lindau Fellow: 72nd Lindau Nobel Laureate Meeting (Physiology and Medicine)
2024	Best Oral Presentation 10th SoCal Graduate Student Symposium
2024	Best Oral Presentation MCIP 2024 Retreat

SELECTED MEETINGS AND PRESENTATIONS

2018	XLIII Congress of the Brazilian Society of Immunology 2018 - XI Extra Section of Clinical Immunology, Ouro Preto, Brazil. Poster presentation: Metabolic Imprint following Acute Intestinal Infection
2019	Microbiome retreat, National Institute of Health. Bethesda, USA
2020	DEUEL Conference on Lipids. San Diego, California. Poster presentation: Novel mechanism controlling adipose tissue heterogeneity
2022	MCIP 2022 Retreat. Los Angeles, California. Poster presentation: Role of Bhlhb9 in adipose tissue biology and metabolism
2022	Sigman Symposium. Los Angeles, California. Poster presentation: Role of PIXL in adipose tissue proteostasis
2023	Keystone Conference Adipose Tissue: Energizing Good Fat. Poster and Oral presentation: PPARg-induced regulation of PIXL interacts with ribosomal machinery and improves glucose metabolism
2023	ASBMB Deuel Conference on Lipids. Poster presentation: PPARg-induced regulation of PIXL interacts with ribosomal machinery to maintain adipose tissue homeostasis
2023	72nd Lindau Nobel Laureate Meeting (Physiology and Medicine): 600-most promising young scientists and Nobel Laureates
2023	10th SoCal Graduate Student Symposium. Oral Presentation: Heating Up Fat: Unveiling the Ribosomal Secrets of Brown Adipose Tissue Homeostasis.
2024	20th Annual Stem Cell Symposium UCLA Broad Stem Cell Research Center. Poster Presentation: Rosiglitazone-dependent remodeling of adipose stromal vascular fraction reveals translational selectivity in adipose progenitors.
2024	MCIP 2024 Retreat. Oral Presentation: Adipose tissue plasticity and translation machinery in metabolic regulation.

PUBLICATIONS

1. **De Siqueira, M. K.** & Pires, L. Review: Epigenetic process involved in multiple sclerosis pathophysiology with emphasis in miRNAs function. *Semin. Ciências Biológicas e da Saúde* 37, 125 (2017)
2. Mosimann, A. L. P., **De Siqueira, M. K.,** Ceole, L. F. & Nunes Duarte Dos Santos, C. A new Aura virus isolate in Brazil shows segment duplication in the variable region of the nsP3 gene. *Parasites and Vectors* 11, (2018)
3. Alberca-Custodio, R.W.; Faustino, L.D.; Gomes, E.; Nunes, F.P.B.; **De Siqueira, M.K.;** Labrada, A.; Almeida, R.R.; Camara, N.O.S.; Fonseca, D.M.; Russo, M. Allergen-specific immunotherapy with liposome containing CpG-ODN in Murine Model of Asthma Relies on MyD88 Signaling in Dendritic Cells. *Frontiers in Immunology*, 11 (2020)
4. **De Siqueira, M. K.,** & Villanueva, C. J. (2021). When fat talks, the gut listens: IRONing out metabolism. *Cell Metabolism*, *33*(8), 1505-1506
5. Sakers*, A., **De Siqueira*, M. K.**, Seale, P., & Villanueva, C. J. (2022). Adipose-tissue plasticity in health and disease. *Cell*, *185*(3), 419-446 *equal contribution
6. **De Siqueira, M. K.**, Oliveira, V.A., Stacy, A., Santos, J.M., Ferreira, M.D., Guimarães, J.P.T., Han, S., Zaretsky, A.G., Silva, L.M., Terra, F.F., Turato, W.T., Jancar, S., Russo, M., Camara, N.O.S., Belkaid, Y. & Fonseca, D.M Infection-elicited microbiota promotes host adaptation to nutrient restriction. *Proceedings of the National Academy of Sciences* 120.4 (2023): e2214484120
7. Han, S.J., Stacy, A., Corral, D., Link, V.M., **De Siqueira, M.K.**, Chi, L., Teijeiro, A., Yong, D.S., Perez-Chaparro, P.J., Bouladoux, N. and Lim, A.I. Enamorado, M., Belkaid, Y. and Collins, N. Microbiota configuration determines nutritional immune optimization. *Proceedings of the National Academy of Sciences* 120, no. 49 (2023): e2304905120

INTRODUCTION

CHAPTER 1: OVERVIEW OF ADIPOSE TISSUE BIOLOGY

This article was published in Adipose-tissue plasticity in health and disease, Cell, Volume 185, Issue 3, 2022, Pages 419-446 (Sakers, De Siqueira et al. 2022). Granted permission to reprint by Cell.

Adipose tissue is defined by the presence of specialized lipid handling cells called adipocytes, which function as the body's primary energy reservoir. Throughout much of our evolution, access to food was sporadic and stores of adipose tissue were advantageous for surviving extended periods of food insecurity. However, in current times, chronic over nutrition is driving an epidemic of obesity and cardiometabolic disease (e.g., type 2 diabetes, coronary artery disease and stroke) in large parts of the world. Furthermore, obesity increases the risk of developing numerous cancers and predisposes to adverse outcomes in other diseases (Donohoe, Lysaght et al. 2017). The increased mortality among obese patients in the COVID-19 pandemic is a notable example. This expanding health crisis is reversing recent gains in life expectancy and imposes an enormous strain on healthcare systems (Mehta, Abrams et al. 2020).

The association between excess adiposity and disease has been recognized since antiquity, with notable thinkers like Hippocrates writing over 2,000 years ago "sudden death is more common in those who are naturally fat than in the lean" (Haslam and Rigby 2010). Indeed, obesity, especially central (abdominal) obesity, is associated with several metabolic pathologies, including hyperglycemia, low HDL cholesterol, hypertriglyceridemia, and hypertension, which together are often called "the metabolic syndrome" (Lanktree and Hegele 2017). Recent discoveries have revealed a complex and nuanced relationship between adipose tissue and health. Epidemiologic studies indicate that excess fat mass strongly correlate with a higher incidence of metabolic disease (Di Angelantonio, Bhupathiraju et al. 2016, Padwal, Leslie et al. 2016). However, there is substantial inter-individual variation, with some obese people remaining metabolically healthy and some thin people exhibiting metabolic disease. Furthermore, patients

with lipodystrophy have low amounts of adipose tissue yet suffer many of the same ailments as those with severe obesity.

The distribution of adipose tissue into multiple heterogeneous depots and their myriad functions add to the challenges in deciphering the roles of adipose tissue in disease. Beyond its critical role in energy storage, adipose tissue produces hormones that regulate many physiological processes, serves as a hub for inflammatory responses, provides mechanical cushioning and insulation, and participates in heat production for the regulation of body temperature (Rosen and Spiegelman 2014, Zwick, Guerrero-Juarez et al. 2018). All these processes may change in adaptive or maladaptive ways during weight loss or gain.

How then should we consider the relationship between adipose tissue and metabolic health? Adipose tissue plays a central role in maintaining whole body insulin sensitivity and energy levels. Adipose tissue regulates insulin action via the secretion of insulin-sensitizing factors like Adiponectin and by sequestering lipids, which would otherwise accumulate in other tissues and have deleterious effects. Indeed, adipose tissue insufficiency (as in lipodystrophy) or dysfunction (as in obesity) leads to the excessive deposition of lipids in other organs like liver and muscle, which is a hallmark of and major contributor to insulin resistance (Petersen and Shulman 2018). Insulin resistance and high insulin secretion define the pre-diabetic state, which often progresses to type 2 diabetes and contributes to the pathogenesis of other disease processes.

This chapter discusses the function and regulation of adipose tissue, emphasizing its ability to undergo profound metabolic, structural, and phenotypic remodeling in response to physiologic cues **(Figure 1).** We further consider how the maintenance of adipose tissue plasticity helps to preserve metabolic health.

Placental mammals have three main types of adipocytes – white, beige, and brown, organized into discrete depots throughout the body (**Figure 2**). White adipocytes are specialized

for lipid storage and release, while beige and brown adipocytes are specialized thermogenic cells able to expend nutritional energy in the form of heat.

White Adipose Tissue (WAT)

WAT is the most abundant form of adipose tissue, found in almost every area of the body (Zwick, Guerrero-Juarez et al. 2018) (**Figure 2**). The major WAT depots are classified according to their anatomic location as either subcutaneous or visceral. In humans, visceral fat is located in the peritoneal cavity, corresponding to the omental and mesenteric depots (Chusyd, Wang et al. 2016). Subcutaneous fat is located beneath the skin and typically represents 80% or more of total fat mass in humans, concentrated in the abdominal and gluteofemoral depots (Karastergiou and Fried 2017). Mice and rats have somewhat analogous visceral (mesenteric, perirenal, and gonadal) and subcutaneous (inguinal and axillary) depots (**Figure 2**). A notable difference is that murine gonadal fat drains into the systemic circulation while human visceral fat drains into the portal circulation (Rytka, Wueest et al. 2011). In addition to the major fat depots discussed above, smaller deposits of adipocytes serve important mechanical and signaling roles in diverse locations, such as the muscle, breast, bone marrow, orbits, face, joints, feet, and dermis (Zwick, Guerrero-Juarez et al. 2018).

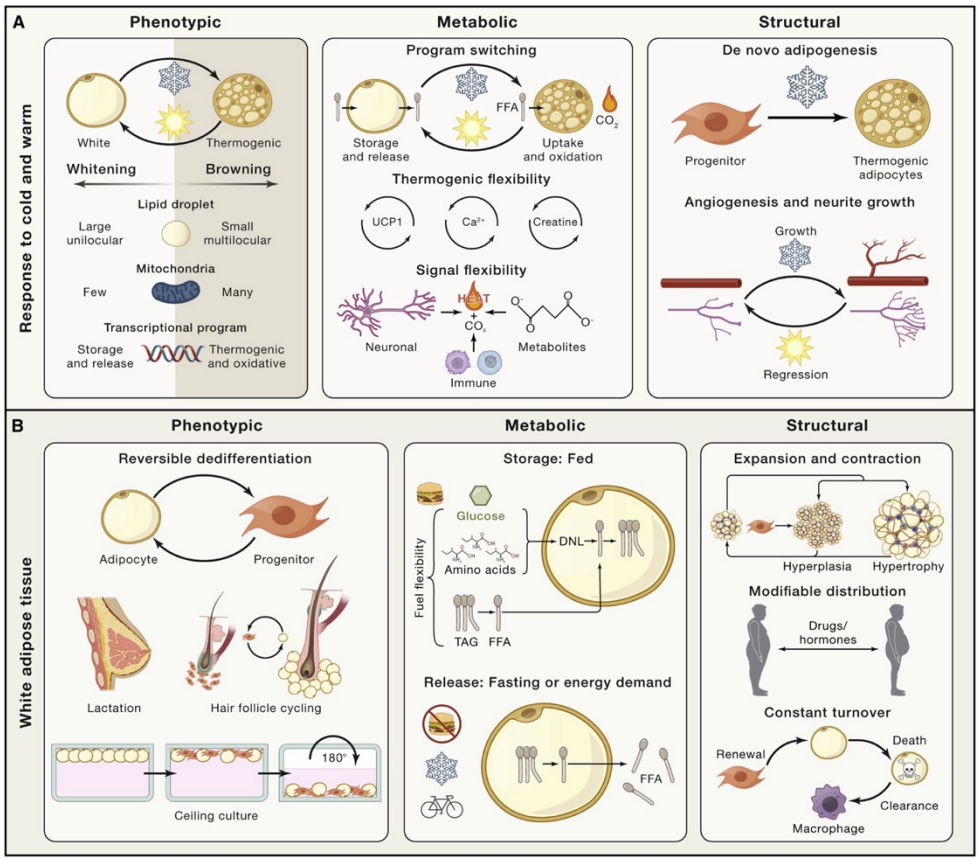

Figure 1 Adipose tissue plasticity.

Adipose tissue engages in multiple adaptive processes to maintain homeostasis which can be classified into distinct categories of plasticity. (A) Adipose tissue changes dynamically in response to cold and warm environments. Phenotypic: in response to cold, individual adipocytes remodel their internal architecture to facilitate thermogenesis in a process called beiging or browning. Beiging involves alterations to the structure of lipid droplets, robust mitochondrial biogenesis, and upregulation of a transcriptional program that supports high levels of local fuel oxidation. These changes are reversible and regress with the removal of cold stimulus through the reverse process called whitening. Metabolic: cold exposure promotes a metabolic switch from energy storage to fuel utilization and uncoupled respiration. Thermogenesis is classically achieved by a futile cycle involving Uncoupling Protein 1 (UCP1), although recent work has demonstrated that adipocytes employ several mechanisms of futile cycling that promote thermogenesis, including calcium and creatine cycling. Adipocytes respond to several cues for thermogenesis, including neuronal, immune, and metabolite derived signals, allowing tight and context specific control of heat production. Structural: during the response to cold, the structure of adipose tissue remodels to facilitate thermogenesis. Cold induces the production of new adipocytes from adipogenic progenitor cells via *de novo* differentiation. Additionally, cold induces angiogenesis and sympathetic nerve-fiber branching, which regress upon removal of thermogenic stress. (B) White adipose tissue plasticity. Phenotypic: in specific contexts, white adipocytes are capable of reversible dedifferentiation *in vivo* and *in vitro*, most notably during lactation (dedifferentiation) and involution (redifferentiation), hair-follicle cycling, and in “ceiling culture,” a specific technique for primary cell culture of isolated adipocytes. Metabolic: white adipocytes switch between two opposing metabolic programs: nutrient storage and nutrient release. Nutrient storage involves the uptake of glucose, amino acids, and fatty acids (TAG: triacylglycerol. FFA: free fatty acid). By the process of *de novo* lipogenesis (DNL) excess nutrients are converted into fatty acids allowing for efficient storage in lipid droplets. During periods of fasting or high energy demand (e.g., exercise, cold exposure), adipocytes release nutrients into the systemic circulation by breaking down stored TAGs and releasing FFAs through lipolysis. Structural: adipose tissue has a remarkable ability to expand and contract in response to over- and under nutrition, respectively. Expansion is mediated by a combination of one of two mechanisms: hypertrophy (increases in individual adipocyte size) and hyperplasia (increases fat-cell number mediated by *de novo* differentiation of adipocyte progenitor cells). The distribution of adipose tissue is variable and can be modified toward a more metabolically favorable peripheral distribution (or a more metabolically maladaptive central distribution by numerous factors including sex hormones, growth hormones, cortisol, and pharmaceuticals. The structure of adipose tissue is in constant flux due to persistent low-level turnover and replacement of adipocytes at a rate of ~10% per year in humans.

White adipocytes generally possess a single large lipid droplet occupying most of the cell

and relatively few mitochondria. A major function of these cells is to store and release energy in response to changes in systemic energy levels. These processes occur on multiple time scales, with lipolysis (fatty acid release) versus lipogenesis (fatty acid uptake/synthesis) acting in the acute setting, the balance of which drives tissue expansion and contraction over longer periods.

WAT is an essential endocrine organ, secreting numerous hormones and other factors, collectively termed adipokines. Adipokines play major roles in regulating whole body metabolism, including promoting insulin sensitivity (e.g. Adiponectin), insulin resistance (e.g. Resistin, RBP4, Lipocalin), and inflammation (e.g. TNF, IL6, IL-1b, IL-8, IL-18, sFRP5) (Funcke and Scherer 2019). Leptin is particularly well studied as it plays a major role in controlling energy homeostasis. High levels of Leptin signal high levels of energy storage in adipose tissue. Leptin acts in the hypothalamus and other brain regions to promote satiety and augment energy expenditure (Pan and Myers 2018). Rare loss-of-function mutations in Leptin or the Leptin receptor cause severe forms of monogenic obesity. In common forms of obesity, the brain becomes resistant to higher levels of Leptin. An intriguing recent study shows that reducing leptin levels in obese mice alleviates Leptin resistance, decreases obesity, and improves metabolic parameters (Zhao, Zhu et al. 2019).

Brown and beige adipose tissue

Brown and beige adipocytes, while representing a small proportion of total adipose tissue, can exert a sizable metabolic impact due to their capacity to engage in thermogenesis. When fully active, BAT can increase whole body energy expenditure by over 100% in mice and by 40-80% in humans (Ouellet, Labbe et al. 2012, Angueira, Shapira et al. 2020). Both cell types are characterized by multilocular lipid droplets, high mitochondrial density, and expression of Uncoupling Protein 1 (UCP1) (**Figure 2**). Upon activation, UCP1 separates nutrient catabolism

from ATP synthesis by dissipating the proton gradient in the inner mitochondrial membrane, releasing potential energy in the form of heat (Cannon and Nedergaard 2004).

Brown adipocytes develop in dedicated deposits of brown adipose tissue (BAT) that are specified prior to birth whereas beige adipocytes develop in WAT depots, predominantly in response to cold exposure. The major murine BAT depot is located in the interscapular region, with additional depots found in cervical, axillary, perivascular, and perirenal regions (Zhang, Hao et al. 2018) (**Figure 2**). Human infants also possess an interscapular BAT depot, which later regresses and is absent in adults (Lidell, Betz et al. 2013). Adult humans possess substantial, though variable, amounts of BAT and beige fat tissue in the paravertebral junctions, cervical/axillary region, along the trachea and blood vessels, and in perirenal/adrenal locations (Ouellet, Routhier-Labadie et al. 2011). Several groups have isolated populations of thermogenic adipocytes from adult humans: some report more transcriptional similarity to mouse beige adipocytes, while others report more similarity to mouse brown adipocytes (Jespersen, Larsen et al. 2013, Lidell, Betz et al. 2013). The results from these studies are probably influenced by the biopsy site and history of cold exposure, so it is likely that humans have both brown and beige adipocytes.

Thermogenic fat is critical for adaptation to environmental cold in mice and humans, but current interest in these tissues focuses on their ability to act as a metabolic sink for excess nutrients. Many studies have shown that mice with increased thermogenic fat activity are protected against weight gain and metabolic dysfunction (Harms and Seale 2013). Moreover, transplantation of brown or beige fat into obese mice enhances insulin sensitivity and decreases fat mass (Liu, Wang et al. 2015, Min, Kady et al. 2016). Similarly, in humans, augmenting brown fat activity is associated with beneficial metabolic effects (Chondronikola, Volpi et al. 2016). In addition to suppressing weight gain by elevating energy expenditure, thermogenic adipocytes improve systemic metabolism and insulin-action via clearing triglyceride-rich lipoproteins,

acylcarnitines, glucose and other potentially toxic metabolites such as branched chain amino acids (BCAAs) that have been closely linked to metabolic dysfunction (Bartelt, Bruns et al. 2011, Yoneshiro, Wang et al. 2019).

1.1 Metabolic plasticity of white adipocytes

WAT metabolism rapidly shifts to meet the energetic needs of the organism, which vary greatly during times of fasting, feeding, cold, and exercise. WAT switches between two opposing metabolic programs, one driving nutrient uptake and the other nutrient release, to ensure that other organs always have an adequate, but not excessive, level of energy (**Figure 3**). The metabolic plasticity of white adipocytes is controlled by hormonal and neuronal signals acting through a cadre of effector proteins and transcriptional regulators.

Nutrient Uptake and Lipogenesis

During periods of positive-energy balance and after feeding, WAT takes up nutrients from the bloodstream and stores them as lipids. This process is mediated by both fatty acid uptake and through the conversion of other nutrients (e.g., glucose) into lipids via *de novo* lipogenesis. The major signal for nutrient uptake into adipocytes is the hormone insulin, secreted by pancreatic β-cells in response to increased circulating levels of glucose and fatty acids (Petersen and Shulman 2018). Insulin drives lipid storage in adipocytes by: (1) stimulating glucose uptake, (2) promoting *de novo* lipogenesis (DNL), and (3) suppressing lipolysis (Carpentier 2021). Insulin signaling is also critical for the differentiation and maintenance of adipocytes; genetic deletion of the insulin receptor or downstream effectors in adipocytes causes varying degrees of lipodystrophy along with insulin resistance (Shearin, Monks et al. 2016, Vazirani, Verma et al. 2016, Sakaguchi, Fujisaka et al. 2017).

Adipocytes contain specialized machinery to take up FFAs from circulating chylomicrons and very low-density lipoprotein (VLDL) **(Figure 3)**. A major constituent of this machinery is lipoprotein lipase (LPL), an enzyme responsible for the hydrolysis of triacylglycerols (TAG) into FFAs and monoacylglycerols. LPL, produced from adipocytes is transported to the apical membrane of capillaries in adipose tissue via the action of the GPi anchored protein GpiHBP1 (Davies, Beigneux et al. 2010). After LPL releases FFAs, specialized FA binding and transport proteins (FATPs), such as FATP1 and CD36, facilitate the uptake of fatty acids into adipocytes. Insulin stimulates the translocation of FATP1 to the plasma membrane to promote FA uptake. Once taken up by adipocytes, FAs are activated by acyl-CoA synthetase to generate acyl-CoAs, which are the substrate for successive acylation reactions with glycerol through the Kennedy pathway. The last step in triglyceride synthesis joins an acyl-CoA and diacylglycerol (DAG) through diacylglycerol acyltransferase enzymes (DGAT1 and DGAT2) (Carpentier 2021).

Adipocytes also synthesize acyl chains through DNL. Adipose tissue and liver are the two major sites for DNL, with adipose tissue accounting for more whole-body lipogenesis in humans and the liver accounting for more in rodents (Song, Xiaoli et al. 2018). DNL is essential for maintaining energy balance, since it converts excess energy from carbohydrates and protein into fatty acids and ultimately triglycerides, for storage in lipid droplets. DNL initially involves the breakdown of nutrients through the TCA cycle, followed by export of citrate to the cytoplasm which is converted through a series of steps into Acetyl-CoA, Malonyl-CoA, and finally into FAs. DNL is regulated at multiple levels, including: (1) the buildup of malonyl coA, which signals to suppress FA oxidation, and (2) transcriptional activation of key enzymes in the DNL pathway. In particular, carbohydrate response element binding protein (ChREBP), LXRa, and sterol response element binding protein 1c (SREBP1c) stimulate the expression of key DNL, enzymes fatty acid synthase (FAS) and acetyl-CoA carboxylase (ACC) (Herman, Peroni et al. 2012). ChREBP is a major transcriptional regulator of DNL in adipocytes, and its expression is controlled by mammalian

rapamycin complex 2 (mTORC2), linking the regulation of *de novo* lipogenesis to growth factor responses (**Figure 3**) (Tang, Wallace et al. 2016).

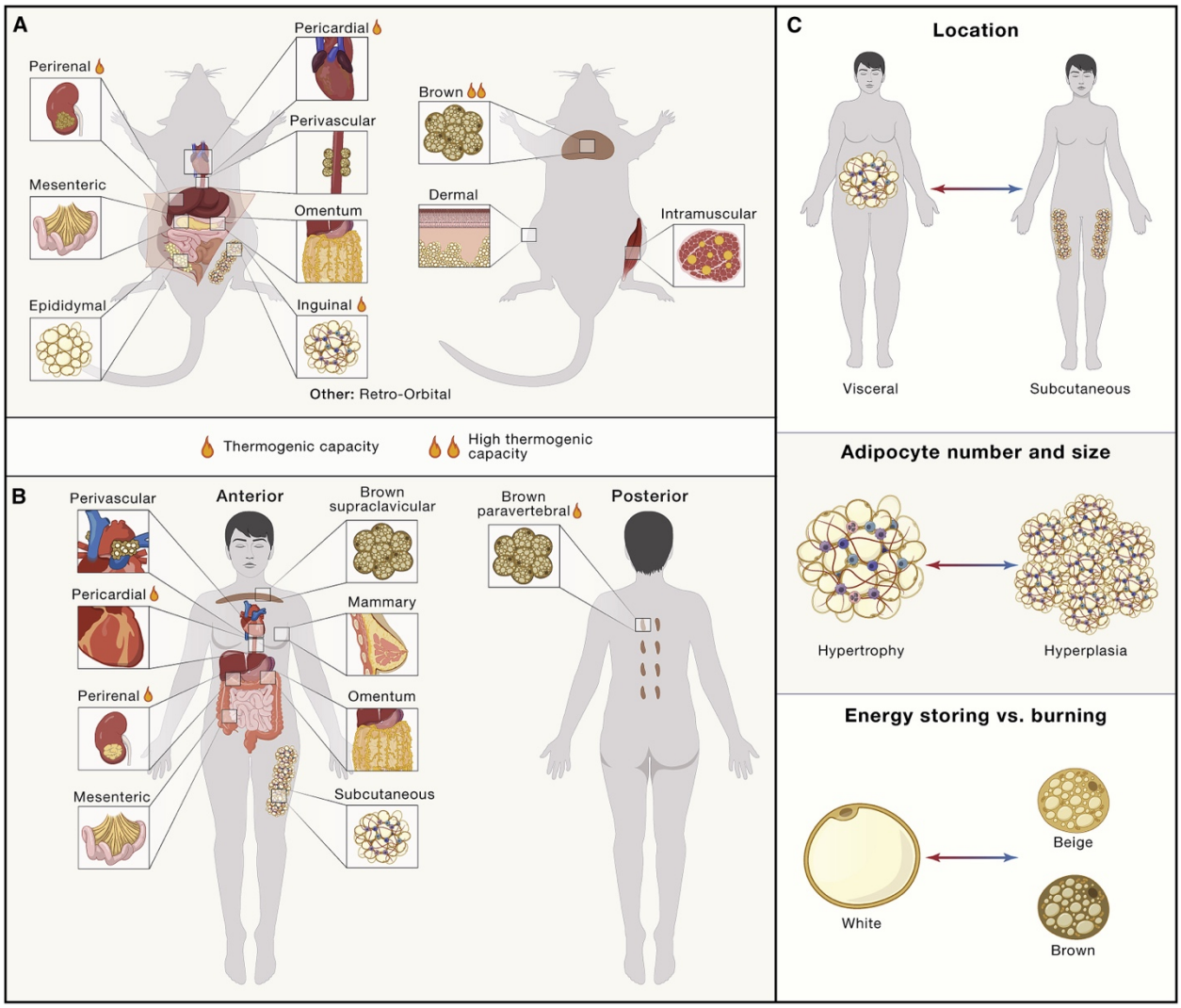

Figure 2 Location of Major Adipose Tissue Depots in Mice and Humans.

Both mice (A) and humans (B) have thermogenic brown adipose tissue (interscapular, cervical, paravertebral). Epididymal adipose tissue (eWAT) is comparable to visceral human adipose tissue (omental, mesenteric adipose tissue (MAT)), while murine inguinal adipose tissue (iWAT) is comparable to human subcutaneous adipose tissue. Fat depots differ in their propensity for thermogenesis. (C) The three axes of adipose tissue variance relevant to metabolic health: location (visceral vs subcutaneous); expansion mechanism (hypertrophy vs hyperplasia), and metabolic phenotype (energy storing vs burning).

Adipocyte DNL maintains insulin sensitivity by converting excess nutrients into lipids for sequestration in adipocytes. Additionally, DNL in adipocytes results in the production of several lipid species with anti-inflammatory and insulin sensitizing effects (Yore, Syed et al. 2014, Yilmaz, Claiborn et al. 2016). These lipids largely correspond to branched fatty acid esters of hydroxy fatty

acids (FAHFA), of which there are many variants, based on the position of the branched ester (Zhou, Santoro et al. 2019). Among these, palmitic acid esters of hydroxy stearic acid (PAHSA) have been singled out for their insulin sensitizing properties. PAHSAs signal through GPR120 to enhance insulin stimulated glucose uptake into adipocytes and also have direct and indirect insulin sensitizing effects in the liver (Yang, Vijayakumar et al. 2018, Zhou, Santoro et al. 2019). Finally, branched chain amino acids (BCAAs) are also used as substrate for DNL, thereby limiting their buildup in (A) Fasted state. Adipocytes release free fatty acids (FFAs) and glycerol via lipolysis in response to external stimulation (i.e., norepinephrine, glucagon). Binding of norepinephrine to the adrenergic receptor (AR) on adipocytes drives the elevation of cAMP and PKA activation. PKA stimulates the hydrolysis of triglycerides (TAG), diacylglycerol (DAG), and subsequently monoacylglycerol (MAG) through activation of the endogenous lipases ATGL and HSL. FFAs and glycerol are secreted into the systemic circulation to supply fuel to other tissues. (B) Fed State. Adipocytes have access to multiple sources of circulating nutrients, including: 1) Long Chain Fatty Acids (LCFA) from Very Low-Density Lipoprotein (VLDL) (LPL-mediated hydrolysis of triacylglycerols from VLDL in capillaries to generate FFAs); 2) glucose; 3) branched-chain amino acids (BCAA). De novo lipogenesis (DNL) uses Acetyl-CoA (AcCoA) as the primary building block for fatty acid synthesis. Synthesized fatty acids are esterified into triglycerides (TAG) and stored in lipid droplets. Expression of enzymes involved in DNL (i.e., fatty acid synthase (FAS); acetyl-CoA carboxylase (ACC)) are positively regulated by hormones (i.e., insulin) and by transcription factors such as Carbohydrate response element binding protein (ChREBP), Liver X receptor alpha (LXRa) and Sterol response element binding protein 1c (SREBP1c). TAGs stored in the lipid droplet are released by lipolysis during periods of energy demanded circulation, which has been linked to insulin resistance (Yoon 2016).

Energy Mobilization through Adipose Tissue Lipolysis

Lipolysis is the process of hydrolyzing triacylglycerols into glycerol and free fatty acids (FFAs) **(Figure 3)**. Sympathetic nerve-derived catecholamines stimulate lipolysis, and this process is repressed by insulin (Fruhbeck, Mendez-Gimenez et al. 2014). In particular, epinephrine and norepinephrine release are induced by fasting or exercise and signal through the adrenergic receptor-PKA pathway in adipocytes to increase lipolysis. Lipolysis depends on the inhibitory phosphorylation of the lipid droplet membrane protein PLIN1 (Sztalryd and Brasaemle 2017). In a basal or anabolic state, PLIN1 is bound to comparative gene identification 58 (CGI-58) (Chouchani and Kajimura 2019). Upon stimulation of lipolysis, PLIN1 is phosphorylated, triggering the release of CG1-58 and subsequent activation of adipose triglyceride lipase (ATGL). ATGL moves to the lipid droplet surface to hydrolyze triglycerides. PKA also phosphorylates HSL, which binds to PLIN1 to favor the hydrolysis of diacylglycerol, and subsequently monoacylglycerol. The final products, glycerol and FFAs are exported into the bloodstream (**Figure 3**). While lipolysis is viewed as the main pathway for lipid release, a recent study demonstrates that lipids are also exported from adipocytes in exosomes, providing an important local signal for macrophage differentiation (Flaherty, Grijalva et al. 2019). Lipolysis is further regulated by several endocrine factors. Leptin promotes lipolysis via stimulation of neuro-adipose junctions (Zeng, Pirzgalska et al. 2015). Growth hormone (GH), adrenocorticotropic hormone, cortisol, thyroid hormones, PTH, and glucagon also provide regulatory roles in lipolysis (Fruhbeck, Mendez-Gimenez et al. 2014). By contrast, insulin signaling functions as the major anti-lipolytic factor by blocking production of intracellular cAMP, leading to suppression of PKA-activity and lipolysis.

1.2 Thermogenic adaptation in adipose tissue

A striking example of adipose tissue plasticity is observed during environmental cold exposure. Initially, animals shiver and activate pre-existing BAT to help defend their body temperature. Longer exposure recruits additional thermogenic capacity, mediated by increases in BAT mass and elevated expression of thermogenic genes (Cannon and Nedergaard 2004). In

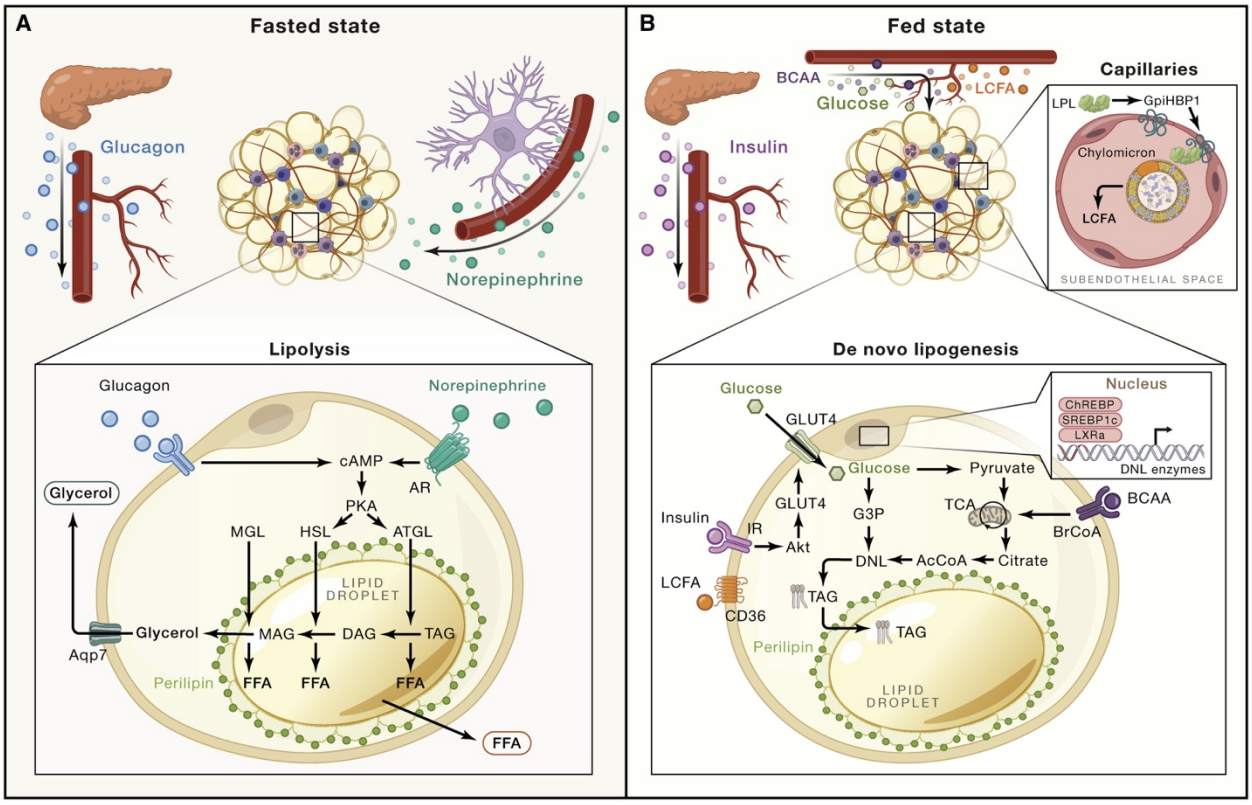

Figure 3 Metabolic Plasticity of White Adipose Tissue.

(A) Fasted state. Adipocytes release free fatty acids (FFAs) and glycerol via lipolysis in response to external stimulation (i.e., norepinephrine, glucagon). Binding of norepinephrine to the adrenergic receptor (AR) on adipocytes drives the elevation of cAMP and PKA activation. PKA stimulates the hydrolysis of triglycerides (TAG), diacylglycerol (DAG), and subsequently monoacylglycerol (MAG) through activation of the endogenous lipases ATGL and HSL. FFAs and glycerol are secreted into the systemic circulation to supply fuel to other tissues. (B) Fed State. Adipocytes have access to multiple sources of circulating nutrients, including: 1) Long Chain Fatty Acids (LCFA) from Very Low-Density Lipoprotein (VLDL) (LPL-mediated hydrolysis of triacylglycerols from VLDL in capillaries to generate FFAs); 2) glucose; 3) branched-chain amino acids (BCAA). De novo lipogenesis (DNL) uses Acetyl-CoA (AcCoA) as the primary building block for fatty acid synthesis. Synthesized fatty acids are esterified into triglycerides (TAG) and stored in lipid droplets. Expression of enzymes involved in DNL (i.e., fatty acid synthase (FAS); acetyl-CoA carboxylase (ACC)) are positively regulated by hormones (i.e., insulin) and by transcription factors such as Carbohydrate response element binding protein (ChREBP), Liver X receptor alpha (LXRa) and Sterol response element binding protein 1c (SREBP1c). TAGs stored in the lipid droplet are released by lipolysis during periods of energy demand.

WAT, especially in rodents, cold exposure induces the development of mitochondria-rich, thermogenic beige adipocytes. The rapid induction of beige adipocytes is accompanied by

remarkable changes in tissue structure, including increased nerve fiber arborization and angiogenesis. Importantly, these cold-induced changes in BAT and WAT are reversible and regress in the absence of cold, highlighting the flexibility of the tissue.

Beige adipocytes can be generated via three mechanisms: (1) the differentiation of progenitor cells into new beige adipocytes (i.e. *de novo* beige adipogenesis), (2) the activation (or re-activation) of the thermogenic program in mature adipocytes and (3) the proliferation of mature beige adipocytes (Wang, Tao et al. 2013, Shao, Wang et al. 2019, Park, Shin et al. 2021). Activation of the beige program in adipocytes involves upregulation of thermogenic genes such as *Ucp1*, mitochondrial biogenesis and lipid droplet remodeling from a unilocular to multilocular morphology (Kim, Park et al. 2019)

BAT undergoes an analogous thermogenic recruitment process during cold exposure. Histological studies show that expression of UCP1 in brown adipocytes is not homogeneous, suggesting a level of cellular heterogeneity in BAT (Cinti, Cancello et al. 2002). A recent study identified two distinct populations of thermogenic cells in mouse BAT, classical brown adipocytes and 'low-thermogenic' brown adipocytes exhibiting fewer mitochondria, lower levels of UCP1, and larger lipid droplets (Song, Dai et al. 2020). Interestingly, cold exposure activated the 'low-thermogenic' cells to become highly thermogenic. Another recent study identified a new subset of 'thermogenesis-inhibitory' adipocytes in mouse and human BAT that restrain the thermogenic capacity of brown adipocytes via local production of acetate (Sun, Dong et al. 2020). These inhibitory adipocytes are enriched in BAT under thermoneutral (non-stimulated) conditions, suggesting that BAT function is regulated by the coordinated activity of distinct adipocyte subpopulations.

Adrenergic signaling is the major physiologic signal controlling both the formation and thermogenic activity of brown and beige adipocytes. Adipose tissue, especially BAT, is densely innervated by sympathetic neurons (Morrison 2016). Upon cold exposure, sympathetic neurons

release the neurotransmitter norepinephrine (NE), which activates the β-adrenergic receptor-cAMP-PKA pathway in adipocytes. This signaling cascade induces lipolysis, thermogenesis and stimulates brown fat-selective gene transcription in brown and beige adipocytes. UCP1 function and thus thermogenic respiration is acutely activated by long-chain FAs and inhibited by purine nucleotides (Fedorenko, Lishko et al. 2012, Bertholet and Kirichok 2017).

A key hub of the thermogenic transcriptional response is the coactivator protein PPARγ coactivator-1a (PGC1-α), which is upregulated by cold exposure (Puigserver, Wu et al. 1998). PGC1-α is phosphorylated and activated by p38 mitogen-activated protein kinase (MAPK) in response to β-adrenergic signaling (Cao, Daniel et al. 2004). PGC1-α co-activates several transcription factors, including PPAR and ESRR family members, Thyroid Receptor and IRF4 to increase the transcription of *Ucp1* and other mitochondrial genes involved in thermogenesis (Shapira and Seale 2019).

Adrenergic stimulation of adipocytes also activates the nutrient-sensing mTOR pathway, a central integrator of cell and tissue metabolism that functions in two distinct complexes, mTORC1 and mTORC2 (Ye, Liu et al. 2019). PKA phosphorylates Raptor and activates the mTORC1 complex in β-adrenergic agonist-stimulated adipocytes (Liu, Bordicchia et al. 2016). Mice with genetic loss or inhibition of Raptor display reduced WAT beiging and impaired brown fat activity (Labbe, Mouchiroud et al. 2016, Liu, Bordicchia et al. 2016, Tran, Mukherjee et al. 2016). The mTORC2 complex, containing the Rictor subunit, is also required for glucose uptake and glycolysis in brown fat tissue during cold exposure (Albert, Svensson et al. 2016). Interestingly, inhibition of mTORC2 in brown adipocytes reduces glucose uptake and lipid storage while also leading to enhanced lipid catabolism, associated with protection against cold and obesity (Jung, Hung et al. 2019). By contrast, loss of mTORC2 in all adipocytes leads to systemic insulin resistance, which can indirectly decrease BAT function (Tang, Wallace et al. 2016).

A new study shows that cold and β-adrenergic signaling also activate expression of the ligand-independent G-protein coupled receptor, GPR3 in brown adipocytes (Sveidahl Johansen, Ma et al. 2021). GPR3 amplifies the β-adrenergic response to enable high levels of thermogenesis. Forced expression of GPR3 in adipose tissues dramatically augments energy expenditure and can reduce obesity in mice. Finally, numerous other extracellular signals, hormones, and metabolites (e.g. FGF21, natriuretic peptides, acetylcholine, and Irisin) promote WAT beiging and add an additional layer of regulation to the control of thermogenesis (Cohen and Kajimura 2021).

Immune cells and beiging

Immune cells, including M2 macrophages, mast cells, eosinophils and ILC2s regulate adipose tissue remodeling and thermogenesis during cold exposure. Type 2 cytokines, especially IL-4, promote beige fat biogenesis and ameliorate obesity, although the involved mechanisms remain uncertain (Qiu, Nguyen et al. 2014, Fischer, Ruiz et al. 2017, Henriques, Bedard et al. 2020). Innate lymphoid ILC2 cells, activated by IL-33, promote beiging through two proposed pathways: (1) the production of methionine-enkephalin peptides, that act on adipocytes to stimulate UCP1 expression (Brestoff, Kim et al. 2015); and (2) the induction of IL-4 and IL-13, which act on adipocyte progenitor cells to promote beige adipocyte differentiation (Lee, Odegaard et al. 2015). Recent work has identified stromal cells as a critical source of IL-33 in adipose tissue, illustrating the crosstalk between mesenchymal cells and immune cells in regulating adipose tissue phenotypes (Mahlakoiv, Flamar et al. 2019, Spallanzani, Zemmour et al. 2019, Shan, Shao et al. 2021). The anti-inflammatory cytokine IL-10 suppresses thermogenic genes in adipocytes. Deletion of the IL-10 receptor in adipocytes augments thermogenesis and reduces obesity (Rajbhandari, Arneson et al. 2019). Additionally, recent studies demonstrate an important role for γδ T cells in regulating innervation, especially in BAT. Specifically, IL-17 secreted from γδ T cells

acts on brown adipocytes, leading to TGFβ production and increased sympathetic innervation. Deletion of the γδ T cells or IL-17R on brown adipocytes reduces energy expenditure in mice and exacerbates obesity (Hu, Jin et al. 2020).

Adipose tissue whitening

The thermogenic phenotype of fat cells, especially beige fat cells, is unstable, requiring persistent stimulation. Elegant cell tracking studies revealed that UCP1+ beige fat cells become unilocular white-appearing adipocytes following re-warming (Rosenwald, Perdikari et al. 2013, Roh, Tsai et al. 2018). During this "whitening process", fat cells lose UCP1 expression and mitochondrial density, and remodel their lipid droplets from a multilocular to a unilocular architecture over the course of ~4 weeks (Roh, Tsai et al. 2018). This process involves direct conversion of beige adipocytes rather than proceeding through a progenitor cell state and depends on mitochondrial clearance (Altshuler-Keylin, Shinoda et al. 2016). Decreased adrenergic signaling in beige fat cells induces the recruitment of the E3 ubiquitin ligase complex, Parkin, to mitochondria, triggering mitophagy. Impairing this process by deletion of autophagy components, *Atg5*, *Atg12*, or *Parkin* prevents the "beige-to-white" phenotype transition (Lu, Altshuler-Keylin et al. 2018). Mitophagy in adipocytes is also driven by the kinases STK3 and STK4. STK3 and STK4 are highly expressed in 'white-appearing' (unstimulated) adipocytes and downregulated during cold exposure. Genetic loss or inhibition of STK3/4 activity increases mitochondrial content and uncoupled respiratory activity in beige and brown adipocytes via reducing mitophagy (Cho, Son et al. 2021). Remarkably, inhibiting mitochondrial clearance in the above mouse models ameliorates obesity and improves systemic metabolism, though this may be expected to cause aberrant mitochondrial function over the long term. A similar whitening process occurs in BAT with exposure to warmer temperatures and during aging. The gene expression profile of 'previously beige adipocytes' is nearly indistinguishable from 'white' adipocytes (never beige) after rewarming (Roh, Tsai et al. 2018). However, 'previously beige'

cells rapidly reactivate the thermogenic program upon a second exposure to cold (Rosenwald, Perdikari et al. 2013). Compared to white adipocytes, 'previously beige' adipocytes display increased levels of H3K4me1, a chromatin mark associated with active or primed enhancers, at certain thermogenic genes, indicating an epigenetic memory of cold exposure (Roh, Tsai et al. 2018). Because of the plasticity of mature adipocytes, the balance between new beige adipocyte differentiation and re-activation of 'previously beige' adipocytes during beiging depends on the environmental exposure history of the animal. For example, in mice that have recently undergone cold exposure, reactivation of dormant beige cells predominates, whereas in cold naïve animals, *de novo* beige adipocyte differentiation from progenitor cells is favored (Shao, Wang et al. 2019). Interestingly, UCP1+ cells, specifically in the central region of iWAT (near the lymph nodes) exhibit proliferative capacity and generate new beige adipocytes in response to β-adrenergic stimulation (Park, Shin et al. 2021).

Metabolic Programming for Thermogenesis

The thermogenic capacity of brown and beige adipocytes relies on burning FAs via oxidative metabolism (Gonzalez-Hurtado, Lee et al. 2018). Classically, adipose tissue thermogenesis is driven by sympathetic nerve-mediated adrenergic signaling, which stimulates lipolysis (**Figure 4**). Free fatty acids (FFAs) serve as both a fuel for thermogenesis and as an allosteric activator of UCP1 function. Surprisingly, lipolysis in UCP1+ adipocytes is dispensable for thermogenesis. However, disrupting lipolysis in all adipocytes compromises thermogenesis in the absence of food, demonstrating that white fat cells can supply the FFAs necessary to support adipose tissue thermogenesis (Schreiber, Diwoky et al. 2017, Shin, Ma et al. 2017). Furthermore, even lipid droplets in BAT are dispensable for thermogenesis. Deletion of core lipogenesis components DGAT1 and DGAT2 in UCP1+ adipocytes produce lipid droplet-less adipocytes, that remain competent for thermogenesis (Chitraju, Fischer et al. 2020).

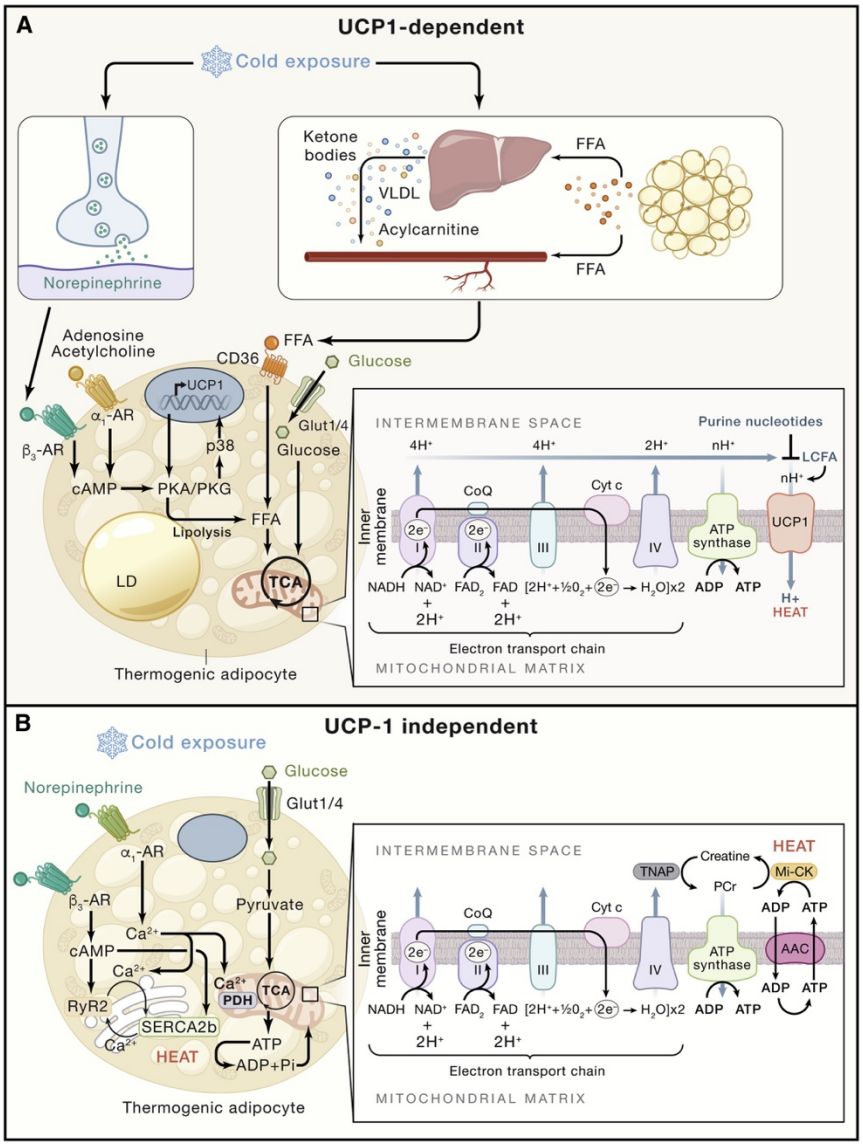

Figure 4 Metabolic Plasticity of Thermogenesis

(A) UCP-1 dependent: Cold exposure or adrenergic stimulation increases cAMP levels, driving activation of PKA/PKG signaling and lipolysis. P38MAPK (p38) in turn promotes activation of transcriptional regulators that drive mitochondrial biogenesis and expression of thermogenic genes (*Ucp1, Cidea, Dio2*). When activated, UCP1 drives proton leak in the mitochondria, leading to uncoupling of mitochondrial respiration from ATP synthesis and driving greater consumption of fuels (e.g., glucose and free fatty acids (FFA)). FFA secreted by WAT also drives hepatic production of acylcarnitines and ketones to help fuel thermogenesis. (B) UCP1-independent: beige thermogenic cells use Ca^{2+} futile cycling through the SERCA2b-RyR2 pathway in the endoplasmic reticulum (ER) to produce heat during cold exposure. Creatine cycling in the mitochondria is an additional mechanism to produce heat independent of UCP1. UCP-1 independent pathways require glycolysis and mitochondrial ATP-synthesis to provide fuel for futile cycling.

Brown fat in mice and humans also oxidize branched-chain amino acids (BCAAs) during cold exposure (Yoneshiro, Wang et al. 2019). This pathway likely contributes to the metabolic benefits of BAT given the well-established link between elevated circulating BCAAs and insulin resistance. Interestingly, recent studies show that brown fat cells take up and concentrate large amounts of the TCA intermediate succinate, which promotes thermogenic respiration (Mills,

Pierce et al. 2018). Mechanistically, the oxidation of succinate generates reactive oxygen species that promote UCP1-activity (Chouchani, Kazak et al. 2016).

Adipocytes can also carry out thermogenesis through an expanding array of UCP1-independent mechanisms. The existence of such mechanisms were initially invoked when it was observed that UCP1-null mice can adapt to the cold if ambient temperature is gradually decreased (Ukropec, Anunciado et al. 2006). These alternative mechanisms have been extensively reviewed elsewhere and include Ca^{2+} futile cycling, creatine-dependent substrate cycling, and triacylglycerol futile cycling (Kazak, Chouchani et al. 2015, Ikeda, Kang et al. 2017, Chouchani and Kajimura 2019). Of note, the futile creatine cycle is required for high fat diet-induced energy expenditure in adipocytes. Ablation of this pathway in mice sensitizes them to obesity and metabolic complications (Kazak, Chouchani et al. 2017) (**Figure 4**).

Structural Remodeling to Optimize Thermogenesis

Sympathetic innervation is critical for brown and beige fat thermogenesis. BAT is more densely innervated than WAT depots; however, a recent study shows that >90% of adipocytes in inguinal WAT are closely opposed to sympathetic fibers, which likely relates to the high beiging potential of this depot (Murano, Barbatelli et al. 2009, Jiang, Ding et al. 2017). Sympathetic arborization increases (by over 3-fold) during cold exposure and is likely essential for sustaining high levels of thermogenic activation (Cao, Wang et al. 2018). Indeed, ablation of nerve fiber arborizations blunts the development of beige adipocytes in response to cold exposure (Jiang, Ding et al. 2017, Cao, Jing et al. 2019). The expansion of neurites is reversible and neurite density normalizes to baseline within approximately 4 weeks after removal of cold stimulus (Cao, Wang et al. 2018). The growth and branching of sympathetic neurites during cold exposure is regulated by adipocytes. For example, adipocyte-specific deletion of the brown fat transcription factor PRDM16 impairs nerve fiber growth and branching in WAT following cold exposure (Chi, Wu et

al. 2018). Adipose cells have been shown to produce a variety of neurotrophic factors, including Nerve Growth Factor (NGF), Neuregulin-4 (NRG4), TGFβ and S100b (Rosell, Kaforou et al. 2014, Zeng, Ye et al. 2019, Hu, Jin et al. 2020).

Vascular density also increases in adipose tissue during cold exposure to support the increase in metabolic activity (Xue, Petrovic et al. 2009). Vascular density doubles within just 5 days and is reversible upon warming (Cao, Wang et al. 2018). As with angiogenesis in other organs, vascular endothelial growth factor (VEGF) is a critical regulator of this process in adipose tissue. Knockout of VEGF in adipose cells leads to whitening of both brown and beige fat (Shimizu, Aprahamian et al. 2014, During, Liu et al. 2015). Interestingly, overexpression of VEGF stimulates browning of WAT and BAT, suggesting that VEGF and/or angiogenesis plays an instructive role in beiging, in addition to supporting the increase in tissue metabolism (Sun, Kusminski et al. 2014, During, Liu et al. 2015).

1.3 Phenotypic plasticity of adipose tissue

Intriguing work over the past few years shows that adipocytes are not necessarily terminally differentiated. Under certain conditions adipocytes reversibly de-differentiate and re-differentiate, cycling between a progenitor cell and adipocyte state.

The capacity for adipocytes to dedifferentiate *ex vivo* was noted in the 1980's with the development of the ceiling culture method to isolate adipogenic primary cell lines. In this method, mature adipocytes are induced to adhere to the top surface of a flask, where they de-differentiate into a fibroblastic pre-adipocyte state (Cote, Ostinelli et al. 2019). However, whether de-differentiation of adipocytes occurs *in vivo* had been unclear until recently. Bi et al. demonstrated that activation of Notch signaling induces the de-differentiation of adipocytes, leading to the development of liposarcomas (Bi, Yue et al. 2016). In lactation, the posterior mammary fat pads (inguinal fat) in mice remodel, with proliferation of mammary alveolar structures and a relative

loss of adipocytes in the areas of high ductal density. During this process, mature adipocytes de-differentiate into proliferative fibroblasts that retain their adipocyte differentiation capacity *in vitro* and *in vivo* (Wang, Song et al. 2018). Similarly, adipocytes within the dermis undergo reversible dedifferentiation during hair follicle cycling and wound healing (Zhang, Shao et al. 2019, Shook, Wasko et al. 2020). In the dermis, mature adipocytes de-differentiate and give rise to myofibroblasts, specialized contractile fibroblasts which secrete extracellular matrix for wound repair. Adipocytes undergoing de-differentiation stimulate lipolysis and release of FFA, which also plays a critical role in regulating the wound inflammatory response (Shook, Wasko et al. 2020). It remains unknown if adipocyte de-differentiation occurs in the major WAT and BAT depots under other physiological conditions, such as during fasting, weight loss, or wound healing outside of the skin.

1.4 Adipose tissue expandability

Adipose tissue has an unparalleled ability to expand, and contract compared to other organs. In humans, the proportion of body fat varies widely, ranging from normal levels of 10-20% in men and 15-30% in women, to below 5% in bodybuilders and anorexic patients, and above 70% in severe obesity. These differences in fat mass are driven by long term calorie surplus or deficit, and the structural changes are enabled by the coordinated action of several cell types, including adipocytes, adipocyte progenitor cells, and immune cells.

The Structure of Adipose Tissue

Human subcutaneous WAT is organized by fibrous septa that define progressively smaller tissue compartments at each scale. The highest-level division is formed by a collagen and elastin rich sheet called the fascia superficialis, often referred to as Scarpa's fascia in the abdominal wall and a "membranous layer" in other body regions (Markman and Barton 1987). The fascia

superficialis runs parallel to the plane of the skin and separates subcutaneous fat into a superficial (sSAT) and a deep compartment (dSAT). At the next level, thinner fibrous septa, sometimes referred to as retinacula cutis superficialis (in sSAT) and profundus (in dSAT), define centimeter scale compartments, and anchor the fascia superficialis to the dermis above and to the deep fascia below. Together, the fascia superficialis, retinacula cutis, and compartments of sSAT and dSAT, are referred to as the superficial fascial system, and are identifiable in nearly all areas of the body (Lockwood 1991). Finally, within the compartments of the superficial fascial system, 500 μm-1000 μm lobules of adipocyte rich stroma are encapsulated by fibrous septa, representing the smallest structural unit of subcutaneous adipose tissue (Esteve, Boulet et al. 2019).

The distinctions between sSAT and dSAT are not purely anatomic. During obesity, both the abdominal sSAT and dSAT expand, with males exhibiting a tendency to expand the abdominal dSAT preferentially (Kim, Chung et al. 2016). Compared to abdominal sSAT, the dSAT is more prone to inflammation, contains more saturated lipids, and adipocyte progenitor cells from this layer are more resistant to differentiation (Cancello, Zulian et al. 2013). Accordingly, expansion of the dSAT, especially in men, is associated with adverse metabolic outcomes (Kelley, Thaete et al. 2000).

Mice have two main subcutaneous WAT depots, the posterior inguinal WAT (iWAT) and anterior axillary WAT (axWAT). The inguinal WAT is heavily studied, due to its larger size, high propensity for beiging, and ease of dissection. Both the iWAT and axWAT lie directly beneath the panniculus carnosus, a layer of striated muscle which separates the subcutaneous structures from the overlying dermis, that some have speculated is an evolutionarily analogous structure to the fascia superficialis (Fodor 1993). Both depots are encased on all sides by a thin fibrous membrane containing mostly DPP4+ fibroblasts that can also serve as adipocyte progenitors (Merrick, Sakers et al. 2019, Stefkovich, Traynor et al. 2021). At the next scale, the tissue can be subdivided into lobular areas (the central areas within the tissue) and non-lobular areas

(surrounding, at the periphery) (Barreau, Labit et al. 2016, Peurichard, Delebecque et al. 2017). The lobular areas are delineated by fibrous septations, analogous to those found in humans that create discrete compartments of adipocytes on the order of 300 μm (Chi, Wu et al. 2018, Dichamp, Barreau et al. 2019). Several studies have noted clear anatomic regionality within the iWAT, with the more ventral regions and central lobular areas being more prone to cold-induced beiging, as compared to the peripheral and posterior regions (Barreau, Labit et al. 2016, Chi, Wu et al. 2018).

The structure of visceral adipose tissue has been less well studied. A defining feature of visceral fat is that, like other intraperitoneal organs, it is surrounded by a layer of mesothelium (Chau, Bandiera et al. 2014). Thus, both visceral and subcutaneous fat are encased by a lining of specialized cells (mesothelial cells for visceral fat, DPP4+ fibroblasts for subcutaneous fat), although in contrast to subcutaneous fat, this lining does not appear to contribute to adipocyte generation in visceral adipose tissue (Westcott, Emont et al. 2021). Furthermore, a recent report demonstrates the presence of lobules in human visceral adipose tissue, analogous to those present at the smallest scale in subcutaneous fat (Esteve, Boulet et al. 2019). By contrast, mouse visceral fat depots do not have a readily apparent lobular structure.

Adipose Tissue Expansion

Adipose tissue expansion is intricately linked to metabolic health. While high fat mass generally correlates with poor metabolic health, a high capacity for expansion protects against metabolic disease. The apparent contradiction in this relationship can be understood by considering the fate of excess nutrients. Once ingested and absorbed, excess nutrients must be either burned or stored. WAT is uniquely capable of safely storing large quantities of excess nutrients as lipids. In contrast, accumulation of excess lipids in other tissues drives insulin resistance (Petersen and Shulman 2018). Therefore, the proper partitioning of excess nutrients into WAT for storage or into BAT for heat generation promote metabolic health. Notably, the site

of adipose tissue expansion (into visceral or subcutaneous depots) and the mechanism of expansion, via increases in adipocyte number (hyperplasia) or size (hypertrophy), have profound impacts on metabolic health.

Adipose Tissue Distribution: Metabolic Consequences

Fat tissue distribution is highly variable, driven by differences between sexes, genetics, development, aging, and in response to hormones or drugs. The most common distinction between types of adipose tissue distribution is whether fat is stored viscerally or subcutaneously, and countless studies have examined the relative effects of visceral versus subcutaneous adiposity on overall health. Almost universally, since the first descriptions of “android” (central) vs “gynoid” (subcutaneous/peripheral) obesity by the French physician Jean Vague in the 1950’s, studies have shown that increased visceral/central adiposity correlates with worse insulin resistance and an increased risk of cardiometabolic disease, even in normal weight subjects (Chait and den Hartigh 2020). By contrast, the preferential expansion of subcutaneous adipose tissue, especially in the superficial region, is associated with a more favorable metabolic profile (Kelley, Thaete et al. 2000). It should be noted that, despite its metabolic importance, visceral fat represents only a small portion (~6-20%) of total fat mass, with this proportion generally higher in males (Karastergiou and Fried 2017).

Differences in body fat distribution may also explain the existence of “metabolically healthy obese” and “metabolically unhealthy normal-weight” individuals (Smith, Mittendorfer et al. 2019). Estimates from the United States suggest that 23.5% of normal weight adults are metabolically unhealthy while 31.7% of obese are metabolically healthy (Wildman, Muntner et al. 2008). Metabolically healthy obese people have unexpectedly low levels of visceral adiposity for their body weight while the situation is exactly reversed in those who are metabolically unhealthy but normal weight.

What makes visceral fat unhealthy and why do we have it? Visceral adipocytes are more metabolically and lipolytically active, exhibiting higher levels of both basal and catecholamine-induced lipolysis. Mechanistically, these differences may be due to increased expression of the stimulatory β-AR, lower expression of the inhibitory α-AR and reduced insulin-mediated lipolysis suppression in visceral adipocytes (Item and Konrad 2012). Consistent with these observations, fasting and weight loss in mice induce the preferential mobilization of visceral fat stores, with visceral depots losing mass earlier and losing a greater proportion of their mass overall (Ding, Zheng et al. 2016, Tang, Tang et al. 2017). Similarly, studies of weight loss in humans consistently show that a greater proportion (but not total amount) of the visceral fat is lost compared to subcutaneous fat (Merlotti, Ceriani et al. 2017). It is reasonable to speculate that a rapidly mobilized source of energy for internal organs may be advantageous under certain conditions.

The high lipolytic activity of visceral fat also underlies the basis for the “portal hypothesis”, which posits that visceral depots, since they drain into the portal circulation, expose the liver to high levels of FFAs, which impair hepatic insulin action. However, this version of the portal hypothesis has fallen out of favor because studies in humans show that, while the proportion of portal vein and circulating FFAs from visceral fat increase in obesity (from 5 to 20% and from 6% to 14% respectively), the visceral fat-derived FFAs still only represent a small proportion of the total circulating pool (Nielsen, Guo et al. 2004).

Alternative versions of the portal hypothesis highlighting a central role for inflammation are more compelling. Visceral adipose tissue is more prone to immune cell infiltration and inflammatory cytokine production than subcutaneous adipose tissue, especially in obesity (Item and Konrad 2012). Several factors that are preferentially produced by visceral fat and secreted into the portal circulation have been linked to the development of insulin resistance, including IL-6, IL-1b, and Retinol Binding Protein-4. For example, IL-6 levels are 50% higher and leptin levels are 20% lower in the portal compared to systemic circulation of severely obese subjects (Fontana,

Eagon et al. 2007). Transplantation studies further support the idea that increased intraperitoneal adipose tissue, whether from a visceral or subcutaneous source, is not harmful *per se* and may even be protective. Instead, the portal delivery of inflammatory cytokines appears to drive the detrimental effects of visceral fat. (Item and Konrad 2012). In transplant experiments, portal-draining visceral fat transplants impair insulin sensitivity whereas systemic-draining visceral fat transplants improve insulin sensitivity. Furthermore, portal-draining transplants from IL-6-deficient mice did not reduce host insulin sensitivity (Rytka, Wueest et al. 2011).

The inflammatory properties of visceral adipose tissue may have been selected for during evolution, by providing a defense against intra-peritoneal pathogens and helping to heal abdominal injuries (West-Eberhard 2019). Consistent with this notion, the omentum has important immunological functions and contains lymphoid cells organized into structures called milky spots, which are key mediators of peritoneal immunity (Meza-Perez and Randall 2017). Moreover, the omentum and mesenteric fat commonly adhere to sites of injury, including ruptured bowels, ovaries, or surgical trauma (West-Eberhard 2019). These fat depots can even wall off foreign bodies within the abdomen. A dramatic example of these properties is the phenomenon of creeping fat in Crohn's disease, in which mesenteric adipose tissue adheres to sites of gut barrier dysfunction, walling of the diseased areas and preventing dissemination of bacteria (Ha, Martin et al. 2020). Overall, the metabolic and immunological properties of visceral fat, which serve important protective roles, also trigger metabolic dysfunction in the setting of obesity.

Distributional Plasticity

Body fat distribution is not fixed and can be modified by hormones. Redistribution of adipose tissue is accomplished by varying the rates of nutrient uptake and lipolysis until a new steady state distribution is achieved. A famous example occurs during Cushing's syndrome, which results from excess secretion or administration of glucocorticoids. In addition to promoting weight

gain via effects on the CNS, glucocorticoids induce a redistribution of lipids to visceral adipose tissue, while causing wasting of adipose tissue from the extremities (Lee, Pramyothin et al. 2014).

Androgens and estrogens also produce characteristic effects on adipose tissue leading to the “android” and “gynoid” adipose tissue distributions in men and women, respectively (Karastergiou and Fried 2017). The plasticity of this distribution is most apparent in studies of gender transition, in which estrogen or androgen treatment produce characteristic shifts toward a gynoid distribution in transwomen and an android distribution in transmen, respectively (Klaver, de Blok et al. 2018). Prior to puberty there are discernable but small differences in the fat distribution of male and female children which become much more pronounced as sex hormone levels rise (Shen, Punyanitya et al. 2009). Likewise, during the transition to menopause, as estrogen levels fall, women begin to accumulate adipose tissue in a more android pattern, with an increase in the amount of centrally stored adipose tissue; these effects are reversed by estrogen replacement therapy (Reubinoff, Wurtman et al. 1995, Lovejoy, Champagne et al. 2008). Reciprocally, androgens tend to promote preferential visceral fat accumulation in women, as observed in polycystic ovarian syndrome (Dumesic, Akopians et al. 2016).

Finally, several drugs produce stereotyped effects on adipose tissue distribution. For example, certain HIV medications promote peripheral subcutaneous fat wasting (lipoatrophy) and central fat accumulation (Koethe, Lagathu et al. 2020). Conversely, TZDs, which promote insulin sensitivity, induce the preferential expansion of subcutaneous adipose tissue (Miyazaki, Mahankali et al. 2002).

Adipocyte hypertrophy and hyperplasia

Adipose tissue expands through adipocyte hypertrophy (increases in fat cell size) and/or hyperplasia (increases in fat cell number). Hypertrophic growth is linked with higher levels of adipose tissue inflammation, fibrosis, and hypoxia, along with poor metabolic health (Vishvanath

and Gupta 2019). In contrast, hyperplastic growth does not provoke these pathologic changes and is generally more metabolically favorable.

Association studies in humans provide evidence for the divergent consequences of hypertrophic versus hyperplastic expansion. First, obese subjects, have both more adipocytes and larger, more hypertrophic, adipocytes than normal weight controls (Salans, Cushman et al. 1973). Adipocyte size increases up to the point of moderate obesity, after which subsequent increases in fat mass are characterized by increases in adipocyte number (Hirsch and Batchelor 1976). Notably, there is substantial inter-individual variation; at any given fat mass, people can exhibit a more hypertrophic or more hyperplastic adipose tissue phenotype. Second, these studies showed that hypertrophic adipose tissue is associated with poor metabolic health, including increased fasting insulin, decreased insulin sensitivity, and elevated blood glucose levels (Bjorntorp 1971). Importantly, a body of recent work continues to support these conclusions (McLaughlin, Craig et al. 2016). Third, longitudinal and cross sectional studies suggest that the total number of adipocytes increases throughout childhood before stabilizing in adulthood (Spalding, Arner et al. 2008). Normal weight children experience two developmental periods (from age 0-2 and from age 13-18 years) characterized by rapid increases in adipocyte number; in contrast, obese children produce significantly more adipocytes than lean children and show ever increasing adipocyte numbers from age 0-18 (Knittle, Timmers et al. 1979). By the time they reach adulthood, those who were obese as children have about twice as many fat cells as their normal weight counterparts. The apparent stabilization of adipocyte numbers in adulthood has led to considerable confusion, with many erroneously believing that people have a “fixed” number of adipocytes.

While many obese children become obese adults, most obese adults were not obese as children. When do obese adults make their extra adipocytes? Adults produce new adipocytes during the normal process of adipose tissue turnover (Spalding, Arner et al. 2008). Therefore, it

seems likely that independent of the age of onset, adipocyte numbers increase during the development of obesity. To prove this, a longitudinal study quantifying adipocyte numbers in the transition from leanness to obesity during adulthood would be needed. The converse experiment, tracking adipocyte numbers during weight loss, has been performed. Weight loss induced by dietary changes or bariatric surgery leads to a reduction in subcutaneous adipocyte size but a maintenance of adipocyte number (Bjorntorp, Carlgren et al. 1975, Andersson, Eriksson Hogling et al. 2014). These results suggest that adipocyte number might function as a one-way ratchet, expanding in obesity, but not declining after weight loss. This may have evolved to allow the quick expansion of adipose tissue to accommodate calories during cycles of feast and famine.

Hypertrophic adipose tissue is dysfunctional

Hypertrophic expansion of adipose tissue is a risk factor, independent of body mass index, for the development of the metabolic syndrome (Weyer, Foley et al. 2000). Interestingly, the WAT of non-obese patients with insulin resistance or diabetes is characterized by large hypertrophic adipocytes further indicating a link between adipocyte hypertrophy (rather than total fat mass) and metabolic dysfunction (Acosta, Douagi et al. 2016). Molecular and functional analyses of large versus small adipocytes from the same individual provide some insights for why this is the case. In particular, large adipocytes undergo higher rates of lipolysis, and produce higher levels of inflammatory cytokines (Laurencikiene, Skurk et al. 2011, Xiao, Yang et al. 2016). Additionally, small adipocytes may secrete higher levels of the insulin sensitizing hormone adiponectin (Meyer, Ciaraldi et al. 2013). Consistent with this, WAT from insulin resistant patients features larger adipocytes, more fibrosis, hypoxia, and inflammation (Hepler and Gupta 2017). At a tissue level, this dysfunctional fat produces lower levels of insulin sensitizing adipokines such as adiponectin (Henninger, Eliasson et al. 2014, Kloting and Bluher 2014).

Pharmacologic and Genetic Manipulation of Tissue Expandability

Genetic and pharmacological studies suggest that it is not hypertrophic adipocytes *per se* that drive systemic metabolic dysfunction, but rather a failure of adipose tissue "expandability". In this model, hypertrophic adipocytes are a symptom more than a cause of dysfunctional adipose tissue. Once adipose tissue becomes "full" and can no longer take up excess nutrients, ectopic lipid begins to accumulate in peripheral organs leading to metabolic decline.

The first line of evidence for this concept comes from two genetic models of healthy obesity, one characterized by extreme adipose tissue hyperplasia and the other by extreme hypertrophy. Leptin deficient (*ob/ob*) mice, a model of severe obesity, exhibit glucose intolerance, hyperphagia, and adipose tissue replete with large hypertrophic adipocytes and inflammatory macrophages. Strikingly, the metabolic dysfunction of *ob/ob* mice is ameliorated by concomitant overexpression of the insulin sensitizing hormone adiponectin (AdiponectinTG) or by knockout of collagen 6 (*Col6* KO) (Kim, van de Wall et al. 2007, Khan, Muise et al. 2009). Both models are characterized by massively increased adipose tissue mass which normalizes insulin sensitivity, presumably by preventing ectopic lipid deposition in other tissues. The adipose tissue of *ob*/*ob* AdiponectinTG mice exhibits extreme hyperplasia and contains many small adipocytes. Interestingly, the adipose of *ob*/*ob Col6* KO mice contains enormous, highly hypertrophic adipocytes.

If hypertrophic adipocytes are truly harmful, why do *ob*/*ob Col6* KO mice have less severe metabolic disease than control ob/ob mice? Collagen 6 is selectively produced by adipocytes compared to other cell types (Divoux, Tordjman et al. 2010). It surrounds fat cells and is responsible for the pericellular fibrosis that restrains adipocytes from expanding past a certain size. Mice lacking collagen 6 therefore have a more permissive extracellular matrix, allowing for unrestricted expansion. Importantly, other genetic models which increase adipose ECM flexibility (ex. MMP14 overexpression) produce similar results to *Col6* KO (Li, Zhao et al. 2020). Thus, it

appears that hypertrophic adipocytes are not deleterious because they are large, but rather because they are prevented by the ECM from getting even larger.

Further evidence comes from experiments with thiazolidinediones (TZDs) which demonstrate that augmenting the expansion capacity of adipose tissue is beneficial in metabolic disease. TZDs are pharmacological ligands for PPARγ, the master regulator of adipogenesis (Tontonoz 1994). Activation of PPARγ leads to enhanced adipocyte differentiation (hyperplasia) and, in some depots, to enhanced expansion capacity (hypertrophy) (Tang, Zeve et al. 2011). Although PPARγ is expressed in other cell types, notably macrophages, endothelium, muscle, and liver, the utility of TZDs as anti-diabetic drugs is believed to come, in large part, from their ability to promote healthy adipose tissue expansion (Yki-Jarvinen 2004).

Elegant mouse genetic studies further show that enhancing *de novo* adipocyte differentiation by overexpression of PPARγ in a subset of progenitor cells in visceral adipose tissue improves insulin sensitivity in mice fed a high fat diet (HFD), without affecting body weight. Reciprocally, deletion of PPARγ in these cells provokes adipose tissue fibrosis and inflammation, along with worsened insulin resistance (Shao, Vishvanath et al. 2018). Similarly, loss of function mutations in humans and adipocyte specific deletion in mice of phosphate and tensin homologue (PTEN), a negative regulator of adipogenesis, increase nutrient partitioning into adipose tissue and enhance insulin sensitivity despite obesity (Pal, Barber et al. 2012, Morley, Xia et al. 2015). Other studies have described consistent results, with genetic models characterized by enhanced lipid sequestration into adipocytes and insulin sensitive obesity (Kusminski, Holland et al. 2012). Genome wide association studies in humans have also begun to link genetic variants associated with reduced subcutaneous adipocyte storage capacity to increased risk for insulin resistance (Majithia, Flannick et al. 2014, Chu, Deng et al. 2017, Gulati, Day et al. 2017).

Adipose Tissue Turnover

Adipose tissue is in a constant state of low-level turnover, with mature adipocytes dying and being replaced by new adipocytes. Several studies have attempted to estimate the rate of this turnover in mice and humans. The most widely cited study employed ^{14}C measurements of adipocytes, taking advantage of the spike in atmospheric ^{14}C that occurred due to nuclear tests in the 1960's (Spalding, Arner et al. 2008). This group found that about 10% of adipocytes turn over per year in both lean and obese subjects. They note that obese people have similar rates of turnover when normalizing to the number of adipocytes, but higher absolute levels of turnover due to their increased number of adipocytes. Follow up work using ^{14}C measurements to track long term lipid flux in adipose tissue further indicated that there is no long-term lipid pool in fat; i.e. all lipid in the tissue (and thus presumably every adipocyte) is subject to turnover (Arner, Bernard et al. 2019). Other studies tracking the proliferation of cells and turnover of substrates in slow turnover tissues using $^{2}H_2O$ long term labeling suggested more rapid turnover, of 0.16-0.29% of adipocytes and 4.5% of stromal-vascular cells per day (Neese, Misell et al. 2002).

In mice, the rates of adipocyte turnover are higher than in humans. Several studies employing distinct methods largely agree that ~5% of cells in the stromal vascular fraction are replicating at any time and that 1-5% of adipocytes are replaced each day (Neese, Misell et al. 2002, Rigamonti, Brennand et al. 2011). As in humans, obese mice exhibit higher rates of proliferation and adipocyte turnover (Rigamonti, Brennand et al. 2011). Notably, ^{15}N thymidine labeling studies in mice indicate that the renewal and differentiation of adipocyte progenitors are uncoupled (Kim, Lun et al. 2014). The biological basis of this phenomenon is likely accounted for by specialization of adipocyte progenitor cells into discrete cell types, some of which are more proliferative and others which are more primed for differentiation (see below) (Merrick, Sakers et al. 2019). Therefore, assessments of turnover which rely on assessing proliferation may understate the true rate of *de novo* adipogenesis, as committed preadipocytes may differentiate without first dividing.

The turnover of adipose tissue requires the coordinated action of multiple cell types. Dying adipocytes must be cleared away in an orderly manner to avoid the harmful effects of releasing lipids into the tissue. This clearing process is dependent upon adipose tissue macrophages, which engulf dying adipocytes and are detected within the tissue as crown-like structures. Interestingly, there is evidence that macrophages recruit adipocyte progenitor cells to sites of dying adipocytes via a CD44-Osteopontin axis, thereby linking the process of adipocyte death to adipogenesis (Lee, Petkova et al. 2013).

1.5 Adipose progenitor cells

The activity of APCs is a key mechanism by which adipose tissue achieves its plasticity. The major adaptive processes in adipose tissue, including expansion, beiging, and maintenance of adipocyte number, all involve *de novo* adipogenesis and therefore rely on the proper functioning of APCs. Could imbalances between the rate of adipocyte loss vs. replacement lead to metabolically maladaptive adipose tissue remodeling during aging? Likewise, since APCs must differentiate regularly, could we modulate their cell fate decisions, to encourage the formation of thermogenic adipose tissue instead of white adipose? Finally, do APCs make maladaptive cell fate decisions, for example by differentiating into pro-fibrogenic cell types, and can these decisions be intervened upon?

It has been known for decades that the stromal-vascular fraction (SVF) of adipose tissue contains cells capable of differentiating into adipocytes. The SVF is a heterogeneous mixture containing all the non-adipocyte cells which pellet after tissue digestion, and therefore the identity of the adipogenic cells was unclear. A groundbreaking study in 2008 utilized candidate cell surface markers to prospectively isolate and characterize APCs in WAT (Rodeheffer, Birsoy et al. 2008). In this study, APCs were defined based on their lack of expression of hematopoietic and endothelial cell markers (CD45 and CD31, hereafter celled Lin-) and their selective expression of

CD29, CD34, LY6A/Sca1, and CD24. This refined cell population produced adipocytes *in vitro* and *in vivo* following cell transplantation (Rodeheffer, Birsoy et al. 2008).

Another landmark study from Graff and colleagues identified a population of *Pparγ*-expressing APCs residing alongside blood vessels in WAT. In addition to *Pparγ*, these cells express the mural (vessel wall cell) marker *Pdgfrβ* (Tang, Zeve et al. 2008). Genetic lineage tracing studies in mice show that *Pdgfrβ*-expressing cells develop into *Pparγ* + mural cells and white adipocytes. Further lineage tracing experiments show that *Pdgfrβ*-expressing cells generate new adipocytes in the epididymal WAT upon high fat diet feeding, contributing to 10-30% of the total adipocytes in this depot after several weeks (Vishvanath, MacPherson et al. 2016, Gao, Daquinag et al. 2018). Together, these findings led to the conclusion that (at least a subset of) APCs occupy a peri-vascular niche and are identifiable as a population of PDGFRβ+ cells, often termed mural cells, which are distinct from smooth muscle cells. Many papers in the field have taken this view. However, a parallel body of work suggests that use of the marker PDGFRβ to identify APCs results in the inclusion of numerous, non-perivascular cell types. Indeed, PDGFRβ is also expressed by adventitial fibroblasts that co-express PDGFRα and potentially represent a major source of APCs (Hong, Bae et al. 2015, Vishvanath, MacPherson et al. 2016, Cattaneo, Mukherjee et al. 2020).

PDGFRα was first identified as a marker of adipogenic cells in regenerating muscle (Joe, Yi et al. 2010, Uezumi, Fukada et al. 2010). Lineage tracing studies indicate that PDGFRα is a common marker of APCs in WAT and BAT depots (Lee and Granneman 2012, Lee, Petkova et al. 2012, Berry and Rodeheffer 2013). These PDGFRα+ cells are characterized as adventitial fibroblasts with multiple elongated processes touching components of the ECM and vasculature. Numerous confirmatory studies have been done, by separate groups employing different *Pdgfrα-Cre* lineage reporters, which consistently demonstrate tracing of *Pdgfrα*+ cells to adipocytes in

both visceral and subcutaneous fat (Berry, Jeffery et al. 2014, Cattaneo, Mukherjee et al. 2020, Sun, Sakashita et al. 2020, Han, Zhang et al. 2021).

An elegant recent study utilized intersectional lineage tracing with Cre/Lox and Dre/Rox reporters, showing that *Pdgfrα*+/*Pdgfrβ*+ and *Pdgfrα*+/*Pdgfrβ*- progenitors, but not *Pdgfrα*-/*Pdgfrβ*+ cells, generated adipocytes during basal turnover and cold-induced adipogenesis in subcutaneous WAT and during wound healing-induced adipogenesis in dermal WAT (Han, Zhang et al. 2021). Consistent with this, another recent lineage tracing study revealed that *Pdgfra*+ cells but not *Tbx18*+ pericytes contribute to adipocyte formation (Cattaneo, Mukherjee et al. 2020). Taken together, these results suggest that *Pdgfrα*+ (±*Pdgfrβ)* adventitial fibroblasts rather than mural cells are the primary source of new adipocytes in WAT (**Figure 5**).

An APC hierarchy?

Recent single cell transcriptomic-based studies have enabled an unbiased analysis and further refinement of APC populations, suggestion specialization of APCs for different functions (Ferrero, Rainer et al. 2020). One source of APC specialization relates to their degree of adipocyte lineage commitment. This concept was originally introduced by Rodeheffer *et al*., who demonstrated that Lin-/CD29+/CD34+ cells could be subdivided into more and less committed cell populations based on CD24 expression. Compared CD24+ cells, CD24- cells are less proliferative and show higher expression of adipocyte identity genes such as *Pparγ, Lpl*, *AdipoQ*, and *Fabp4* (Berry and Rodeheffer 2013). Moreover, transplantation studies indicate that CD24+ cells produce CD24- cells during adipogenesis (Jeffery, Church et al. 2015, Jeffery, Wing et al. 2016).

Recent single cell transcriptomic studies have further refined this concept, identifying distinct cell types on the basis of unique gene expression signatures. Studies in mouse adipose tissue consistently identify a continuum of adipogenic cells which subdivides into two broad

categories, namely progenitor cells (also called adipocyte stem cells (ASC) or interstitial progenitors) and preadipocytes (Burl, Ramseyer et al. 2018, Hepler, Shan et al. 2018, Schwalie, Dong et al. 2018, Cho, Lee et al. 2019, Merrick, Sakers et al. 2019, Ferrero, Rainer et al. 2020, Han, Zhang et al. 2021, Nguyen, Lin et al. 2021, Sarvari, Van Hauwaert et al. 2021, Shao, Hepler et al. 2021). Likewise, studies of human subcutaneous adipose tissue have identified a similar continuum of APCs (Raajendiran, Ooi et al. 2019, Vijay, Gauthier et al. 2020, Hildreth, Ma et al. 2021).

Progenitor cells are the most "stem-like" cells found in the tissue and are characterized by expression of *Pdgfr*α, as well as *Dpp4, Pi16, Cd55, Ly6a*, and numerous *Wnt* pathway genes. Interestingly, fibroblasts with this gene expression signature are present in nearly every tissue of the body (Buechler, Pradhan et al. 2021). Preadipocytes are characterized by the expression of adipocyte-related genes, including *Pparγ*, *Fabp4*, *Lpl*, and *Cd36,* suggesting commitment to the adipocyte lineage. Interestingly, preadipocytes express similar levels of *Pdgfr*α but higher levels of *Pdgfr*β than progenitors, suggesting that earlier studies using these markers were in fact isolating distinct APC subtypes (Han, Zhang et al. 2021, Sarvari, Van Hauwaert et al. 2021).

Computational lineage prediction suggest that the APCs are arranged into a lineage hierarchy, with progenitors producing committed preadipocytes, before finally generating adipocytes (Burl, Ramseyer et al. 2018, Merrick, Sakers et al. 2019). This work implies that APCs likely exist in a continuum, from least to most committed to the adipocyte lineage, rather than occupying discrete states. Consistent with this, transplantation and lineage tracing studies show that DPP4+ progenitors, mainly localized in the layer of fibrous tissue which envelopes adipose tissue depots and subdivides it into lobes, produce preadipocytes and adipocytes *in vivo* (**Figure 5**) (Merrick, Sakers et al. 2019, Stefkovich, Traynor et al. 2021).

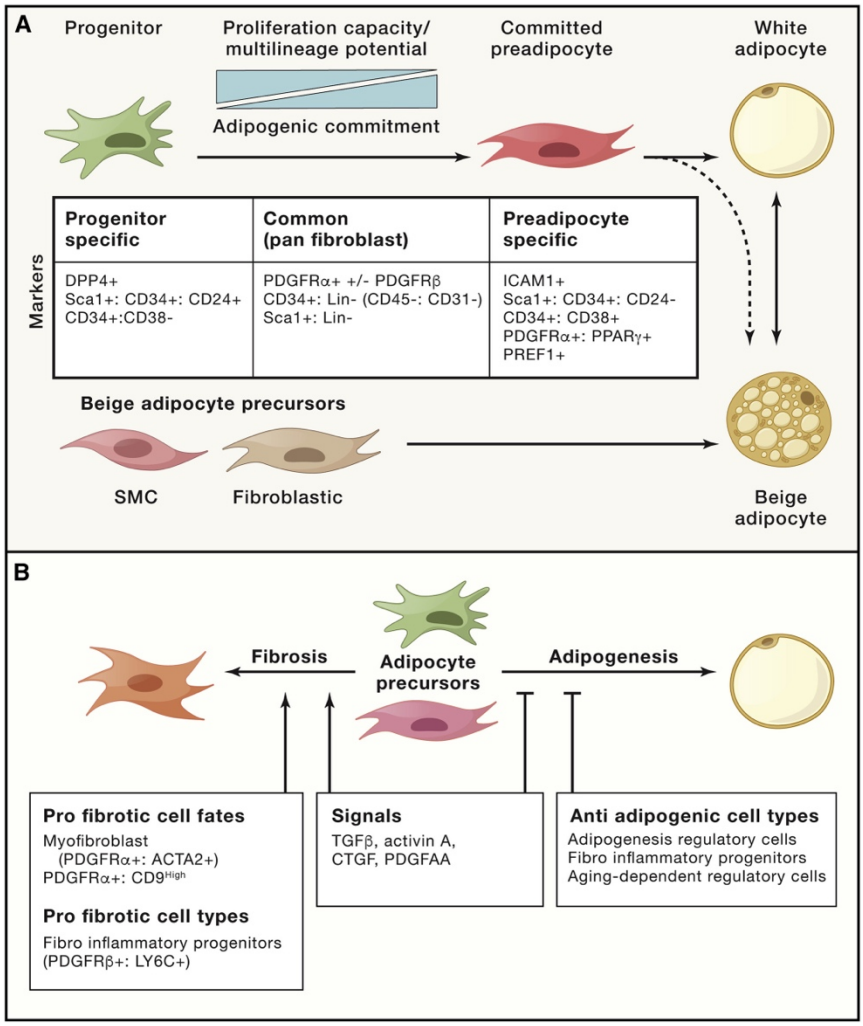

Figure 5 Adipocyte Progenitors and their Contribution to Adipose Tissue Homeostasis.

(A) Adipocyte progenitors are specialized according to their degree of commitment to the adipocyte lineage. A consensus has emerged that the major contributors to the adipocyte lineage are adventitial fibroblasts sharing a common set of fibroblastic markers including *Pdgfra and Cd34.* These fibroblasts can produce both white and beige adipocytes (which can interconvert in response to environmental temperature). (B) Adipocyte progenitor cells make critical cell fate decisions including whether to differentiate or adopt a more pro-fibrogenic state. Several lines of evidence suggest that, at a tissue level, there is competition between fibrosis and adipogenesis, with key mediators acting on adipocyte progenitors to alter their cell fate decisions.

Adipogenesis-inhibitory cells

Several recent studies have identified fibroblast populations that are capable of inhibiting adipogenesis, including: fibro-Inflammatory-Progenitors (FIPs) in visceral fat, $CD142^{High}$ AREGs (adipogenesis-regulatory cells) in visceral and subcutaneous fat and aging-dependent regulatory cells (ARCs) in aged subcutaneous WAT (Hepler, Shan et al. 2018, Schwalie, Dong et al. 2018,

Nguyen, Lin et al. 2021). Their anti-adipogenic effects are presumed to come from secretion of inflammatory mediators (ARCs and FIPs) or other secreted factors (AREGs). Of note, the anti-adipogenic properties of AREGs have been called into question, since other groups report robust adipogenesis from this population (Merrick, Sakers et al. 2019, Nguyen, Lin et al. 2021). Overall, the concept that stromal cells modulate the adipogenic commitment and differentiation of APCs is compelling and suggests an added layer of regulation to adipogenesis.

Depot and Development Specific Progenitors

Several groups have investigated the embryonic origin and development of adipocytes, and this work has been reviewed in recent articles (Sanchez-Gurmaches, Hung et al. 2016, Sebo and Rodeheffer 2019). To summarize, selective marker genes have been identified for adipocyte lineage cells that give rise to the broad categories of adipose tissue depots. For example, Paired related homeobox 1 (*Prx1*) is a selective marker of the subcutaneous adipocyte lineage (Sanchez-Gurmaches, Hsiao et al. 2015). Wilms Tumor 1 (WT1), a transcription factor with key roles in heart and kidney development, is a selective marker gene for visceral (versus subcutaneous) APCs (Chau, Bandiera et al. 2014). Notably, since mesothelial cells express WT1, lineage tracing from WT1+ cells into visceral adipocytes initially suggested that mesothelial cells contribute to adipogenesis. However, recent work demonstrates that bona fide mesothelial cells are not adipogenic; instead, a population of fibroblastic PDGFRα+/WT1+ accounts for this result (Westcott, Emont et al. 2021). Lineage tracing studies show that fat depots in the dorsal anterior aspect of the mouse, including interscapular BAT and WAT, develop from somitic mesodermal cells expressing *Myf5*, *Engrailed1* and *Pax7* which also give rise to dermal fibroblasts and skeletal muscle cells (Sebo and Rodeheffer 2019).

Elegant studies using a *Pparγ* lineage tracing system showed that distinct populations of APCs are responsible for adipose tissue development and maintenance (Jiang, Berry et al. 2014).

Pparγ + cells are detectable in the region which develops into inguinal WAT as early as E10.5. Interestingly, deletion of *Pparγ* in these embryonic *Pparγ*+ cells at E10.5 does not affect adipose tissue formation but causes progressive lipodystrophy during ageing. These results indicate that the adult progenitor cells responsible for adipocyte renewal are specified early in development and do not mediate the initial development of adipose tissue (organogenesis). The specification of adipocyte progenitors in embryogenesis suggests that *in utero* exposures may modulate the future differentiation potential or fate of these cells.

White vs. Beige adipogenesis

Beige and white fat-specific progenitor cell populations can be isolated and cloned from subcutaneous WAT, suggesting that beige and white fat cells represent distinct cell types/lineages (Wu, Bostrom et al. 2012). In this regard, PDGFRβ+ cells expressing *Cd81* have been reported to possess enhanced beige adipogenic potential, though this marker gene appears to be quite broadly expressed in many/most fibroblasts (Oguri, Shinoda et al. 2020). Additionally, smooth muscle-related cells expressing certain SMC marker genes (i.e. *Myh11*, *Acta2*, *Trpv1*) contribute to beige adipocyte development (Long, Svensson et al. 2014, Berry, Jiang et al. 2016, Shamsi, Piper et al. 2021). Remarkably, in the absence of β-adrenergic receptor signaling, a completely different progenitor cell population expressing skeletal muscle genes, including *Myod*, are recruited to generate a distinct type of beige fat exhibiting high levels of glycolysis (Chen, Ikeda et al. 2019). These results show that there are multiple paths for beige adipocyte development, though the inter-relationships between these different cell types and their differentiation trajectories are uncertain.

APC Regulation and Adipogenesis

APCs differentiate into adipocytes via the process of adipogenesis. The molecular regulation of this process has been extensively studied using *in vitro* cell model systems. Adipogenesis is governed by two main waves of transcription factor activation (Lefterova, Haakonsson et al. 2014). At the onset of differentiation, C/EBPβ and C/EBPδ bind to "semi-closed" chromatin at adipogenic target genes. At later time points, these regions become transcription factor 'hotspots' that are bound and regulated by multiple transcription factors, including Glucocorticoid receptor (GR), retinoid X receptor (RXR), and STAT5a. Amongst the second wave of factors, the master adipogenic factor PPARγ plays a dominant role in activating the expression of adipocyte-selective genes to confer the mature fat cell phenotype (Steger, Grant et al. 2010, Siersbaek, Nielsen et al. 2012).

An additional layer of transcriptional regulation in adipocytes is provided by numerous factors that determine the energy-storing white vs. energy-burning brown phenotype. The transcriptional co-activator PGC-1α along with IRF4, ERR factors, c/EBPb, CREB and ZFP516 are key regulators of the β-adrenergic-stimulated thermogenic gene program in adipocytes (Shapira and Seale 2019). Several other transcriptional factors play pivotal roles in specifying thermogenic adipocyte identity, including EBF2, NFIA, Zc3h10 and PRDM16 (Shapira and Seale 2019). Conversely, ZFP423 enforces white fat cell identity, acting through suppression of EBF2 activity. Adipocyte-specific deletion of ZFP423 or activation of EBF2 in mice enhances beige fat formation and improves metabolic health (Shao, Ishibashi et al. 2016, Stine, Shapira et al. 2016, Shao, Zhang et al. 2021). TLE3 also represses the thermogenic program of adipocytes both by impeding the function of pro-thermogenic factors PRDM16 and EBF2 and by increasing the expression of white-selective genes. Activation of TLE3 in BAT impairs lipid oxidation and thermogenesis, while deletion of TLE3 in WAT promotes thermogenesis and energy expenditure (Villanueva, Vergnes et al. 2013, Pearson, Loft et al. 2019).

A full understanding of adipocyte lineage commitment (i.e., progenitor-to-preadipocyte transition) in adult tissues has been hampered by the lack of molecular markers that define these cell types. However, as discussed above, recent studies have identified distinct cell types/states which appear to be positioned at different stages along the adipogenic trajectory. The adipogenic commitment process likely involves the integration of several pro- and anti- adipogenic growth factor signals. Anti-adipogenic signals include: canonical and noncanonical WNT pathways (especially WNT5, WNT6, WNT10a, and WNT10b), TGFβ, platelet derived growth factor (PDGF), and hedgehog signaling (Ghaben and Scherer 2019). Pro-adipogenic signals include: Insulin, Bone Morphogenic Protein (BMP) signaling (especially BMP2 and BMP4), and extracellular matrix composition (Ghaben and Scherer 2019). For example, BMP2 and BMP4 induce activation of SMAD4 and its heterodimeric partners, which subsequently stimulates the transcription of PPARγ, driving adipogenic commitment (Huang, Song et al. 2009). Of note, ZFP423, a regulator of adipogenic commitment and PPARγ expression, sensitizes cells to the pro-adipogenic effects of BMP signaling (Gupta, Arany et al. 2010).

While many pathways and factors have been shown to regulate adipocyte differentiation in cell culture models, the physiologic mechanisms that control adipocyte differentiation *in vivo* remain poorly defined. There is substantial literature implicating a role for fatty acids in promoting adipocyte differentiation, suggesting that lipolysis or lipid accumulation in fat tissue provides a signal for adipogenesis. In this regard, certain fatty acids can serve as activating ligands for PPAR proteins, providing an attractive mechanistic link between diet, lipid levels and adipocyte differentiation. However, a high affinity natural ligand for PPARγ has yet to be identified. A notable recent study showed that omega-3 fatty acids stimulate preadipocytes to undergo differentiation via the FFAR4 G-protein coupled receptor, located specifically in cilia (Hilgendorf, Johnson et al. 2019).

A number of pathways have been proposed to inhibit adipocyte differentiation, though in many cases *in vivo* evidence is lacking. The presence of committed preadipocyte cells expressing detectable levels of PPARγ suggest that the adipocyte differentiation program is actively inhibited in these cells under basal conditions. A widespread problem in the field relates to the misinterpretation of mouse models exhibiting changes in adipose tissue mass. Such effects are often attributed to primary changes in APC activity and adipogenesis. However, adipose tissue size is highly sensitive and responsive to changes in systemic energy levels. Many papers presenting an obesity-resistant mouse model with a metabolically healthy phenotype will attribute the phenotype to a defect in adipogenesis. However, impaired adipogenesis is expected to cause lipodystrophy, resulting in ectopic lipid accumulation in muscle and liver along with insulin resistance.

1.6 Limitations to plasticity

The functional decline of adipose tissue during obesity and aging is associated with a loss of plasticity. A prevailing model posits that maladaptive adipose tissue remodeling, characterized by fibrosis and inflammation, is triggered by a failure of angiogenesis which leads to tissue hypoxia as well as the accumulation of senescent cells (Crewe, An et al. 2017, Hepler and Gupta 2017). In this model, adipose tissue expansion outstrips vascular supply, causing local hypoxia, which inhibits adipogenesis and induces hypertrophic adipocytes to secrete inflammatory cytokines, die via necrosis and spill lipid in an uncontrolled manner. Consequently, adipose tissue becomes insulin resistant, inflamed, and fibrotic, further compromising its function. All of these processes are continuous and mutually reinforcing, making it difficult to disentangle cause and effect (**Figure 6**).

Reduced APC function in aging?

The capacity for hyperplastic adipose tissue expansion declines during aging (Caso, McNurlan et al. 2013, Kim, Lun et al. 2014). Aging-induced defects in APCs include decreased expression of sirtuins, reduced expression of pro-adipogenic transcription factors, and impaired proliferative capacity (Caso, McNurlan et al. 2013, Khanh, Zulkifli et al. 2018). Moreover, the adipose tissue of aged mice and humans accumulate senescent APCs (Baker, Childs et al. 2016, Tabula Muris 2020). Clearance of senescent cells from the adipose tissue of old mice improves adipogenesis and systemic metabolism (Xu, Palmer et al. 2015). Similarly, suppression of the SASP in human preadipocytes enhances adipogenic differentiation (Gustafson, Nerstedt et al. 2019). Interestingly, aging in mice also leads to the accumulation of a distinct population of anti-adipogenic cells, specifically in subcutaneous fat, called “aging-dependent regulatory cells” (ARCs). ARCs, which express inflammatory markers, inhibit both the proliferation and adipogenic capacity of APCs (Nguyen, Lin et al. 2021).

Adipose tissue fibrosis

In healthy adipose tissue, adipocytes are embedded in a loose mesh of ECM, composed of multiple collagens (especially I, III, and VI), fibrillins, and proteoglycans, that provides structural support and modulates the activity of growth factors and signaling molecules (Marcelin, Silveira et al. 2019). In contrast, fibrosis is a hallmark of dysfunctional fat, characterized by the excessive accumulation of extracellular matrix (ECM) and tissue stiffening. As with fibrosis in other organs, adipose tissue fibrosis is both a symptom of and contributor to the functional decline of the tissue.

Obesity in mice and humans is generally associated with increased adipose tissue fibrosis, especially in visceral depots, with higher levels of fibrosis correlating with more metabolic complications (Sun, Tordjman et al. 2013). Fibrosis appears to cause tissue dysfunction through several mechanisms. First, adipocytes themselves are mechanosensitive and thus dysregulated ECM can alter mechanical cues and impair adipocyte function. Indeed, mechanical compression

of adipocytes impairs lipolysis, decreases the expression of adipokines like leptin and adiponectin, and increases the expression of ECM genes and proinflammatory cytokines (Pellegrinelli, Heuvingh et al. 2014). Second, the ECM serves as a reservoir of growth factors and fibrotic ECM can alter tissue function by disrupting the signaling milieu (Marcelin, Silveira et al. 2019). Third, fibrotic ECM increases the rigidity of the tissue, physically impeding adipose tissue expansion by adipocyte hypertrophy (Khan, Muise et al. 2009). Fourth, dysregulated ECM impairs the function of APCs, which must remodel the local ECM to undergo adipocyte differentiation (Chun, Hotary et al. 2006). Finally, APCs are mechanosensitive and exhibit decreased adipogenic capacity on stiffer substrates (Young, Choi et al. 2013).

The signaling pathways, gene regulatory networks, and cellular mediators responsible for adipose tissue fibrosis have been extensively reviewed elsewhere (Crewe, An et al. 2017). Transforming growth factor beta (TGFβ) especially, as well as many other factors, including Activin A, Connective Tissue Growth Factor (CTGF), Platelet Derived Growth Factor (PDGFα), and inflammatory cytokines have been implicated in the development of adipose tissue fibrosis (Zaragosi, Wdziekonski et al. 2010, Iwayama, Steele et al. 2015, Yoshino, Patterson et al. 2019). Additionally, during obesity, hypoxia-induced signaling through HIF1α exerts potent pro-fibrotic rather than angiogenic effects in adipose tissue, further driving adipose tissue dysfunction (Halberg, Khan et al. 2009, Sun, Halberg et al. 2013).

The role of APCs in adipose tissue fibrosis has received significant attention. While other cell types in adipose tissue, such as macrophages and adipocytes, produce collagens and secrete pro-fibrotic factors, fibroblasts express the highest levels of collagens and fibrosis genes (Marcelin, Ferreira et al. 2017). Several studies suggest that APCs may have the capacity to adopt either an adipogenic or pro-fibrogenic fate, depending on the signaling context. In this regard, fibrosis would be pathogenic not only because of direct effects on the ECM but also because of aberrant cell fate choices by APCs, compromising their capacity for adipogenesis

(**Figure 6**). Genetic mouse models provide additional evidence that the pro-fibrotic and adipogenic activities of APCs are opposed. As an example, expression of constitutively active PDGFRα in APCs results in lipodystrophy and profoundly fibrotic tissue, while deletion of PDGFRα has opposite effects (Marcelin, Ferreira et al. 2017, Sun, Berry et al. 2017, Sun, Sakashita et al. 2020). Additionally, HIF1α inhibits APC differentiation through inhibitory phosphorylation of PPARγ and targeting this pathway augments adipogenesis and ameliorates metabolic dysfunction (Shao, Hepler et al. 2021).

Several studies have defined subsets of APCs in WAT that exhibit high fibrotic and low adipogenic potential. For example, $CD9^{High}$/PDGFRα+ cells, which increase during obesity in visceral fat, exhibit a pro-fibrotic phenotype and are less adipogenic (Marcelin, Ferreira et al. 2017). Hepler *et al*. identified a related population of PDGFRβ+/LY6a+/CD9+ cells in visceral WAT, which they termed fibro inflammatory progenitors (FIPs) (Hepler, Shan et al. 2018). FIPs are transcriptionally similar to (DPP4+) progenitor cells in subcutaneous WAT, suggesting that the division between pro-fibrotic and pro-adipogenic adipocyte progenitor cell subtypes is conserved across depots (Burl, Ramseyer et al. 2018, Merrick, Sakers et al. 2019, Ferrero, Rainer et al. 2020).

Finally, a fibrosis vs. adipogenesis (or lipid storage) fibroblast fate axis exists in other tissues. A well-studied example occurs in the skin, in which conversion of myofibroblasts into adipocytes and vice-versa occurs during wound healing (Marangoni, Korman et al. 2015, Plikus, Guerrero-Juarez et al. 2017, Shook, Wasko et al. 2020). In skeletal muscle, PDGFRα+ fibroblastic cells also give rise to both adipocytes and pro-fibrogenic cells (Uezumi, Ito et al. 2011). Furthermore, in models of idiopathic pulmonary fibrosis (IPF), treatment with PPARγ agonists alleviates fibrosis by promoting differentiation of lung fibroblasts into lipid storing and less fibrogenic lipofibroblasts (El Agha, Moiseenko et al. 2017).

Adipose tissue inflammation

Immune cells play many critical roles in regulating adipose tissue phenotypes in response to physiological and pathological stimuli (Lu, Zhao et al. 2019). Evidence that obesity results in chronic inflammation emerged in the 1990s, through the study of Hotamisligil *et al.,* showing increased concentrations of the inflammatory cytokine TNFα in the adipose tissue of obese rats (Hotamisligil, Shargill et al. 1993). Neutralization of TNFα signaling improves insulin sensitivity, establishing a link between immune responses and metabolism. Following these early studies, an extensive amount of research has demonstrated that chronic inflammation is a hallmark of adipose tissue dysfunction and systemic metabolic dysregulation.

Obesity in mice and humans dramatically increases the number of adipose tissue macrophages, linked to the activation of several inflammatory pathways (Weisberg, McCann et al. 2003, Patsouris, Li et al. 2008, Amano, Cohen et al. 2014). Seminal work showed that obesity induces a phenotypic switch in adipose tissue macrophages from an anti-inflammatory “type 2” profile to a pro-inflammatory “type 1” state (Lumeng, Bodzin et al. 2007, Nguyen, Favelyukis et al. 2007, Lumeng, DelProposto et al. 2008). These “type 1” macrophages represent a major source of pro-inflammatory cytokines and can be found surrounding dead or dying adipocytes in adipose tissue, forming characteristic crown-like structures. Ablation of pro-inflammatory macrophages in obese mice decreases adipose tissue inflammation and enhances insulin sensitivity (Patsouris, Li et al. 2008). Similarly, reducing macrophage recruitment into adipose tissue ameliorates metabolic complications in high fat fed mice (Kanda, Tateya et al. 2006, Weisberg, Hunter et al. 2006).

T cells also increase during obesity and play prominent roles in adipose tissue inflammation (Wu, Ghosh et al. 2007, Nishimura, Manabe et al. 2009). CD8+ effector T cells infiltrate adipose tissue at early stages of obesity development, stimulating macrophage recruitment and inflammation (Rausch, Weisberg et al. 2008, Nishimura, Manabe et al. 2009). Of

note, high fat feeding in mice led to an accumulation of a particular subset of T cells exhibiting a senescent phenotype and expressing high levels of the pro-inflammatory factor Osteopontin (*Spp1*) in visceral adipose tissue (Shirakawa, Yan et al. 2016). Conversely, regulatory T (Treg) cells play a critical role in suppressing adipose tissue inflammation in the visceral depot (Feuerer, Herrero et al. 2009, Ilan, Maron et al. 2010). Adipose tissue Treg cells are abundant in the lean state and decrease in obesity. Ablation of these cells in fat tissue increases inflammation and insulin resistance, whereas adoptive transfer of Treg cells blunts inflammatory response and improves metabolic parameters.

Another important immune cell type in adipose tissue is innate lymphoid type 2 cells (ILC2). ILC2 cells express IL-5 and IL-13, which regulate the maintenance of alternatively activated macrophages and eosinophils to limit inflammation and promote the development of thermogenic adipocytes (Hams, Locksley et al. 2013, Molofsky, Nussbaum et al. 2013). Like Treg cells, adipose tissue ILC2 decrease in the setting of obesity. ILC2 cells also decrease in abundance and lose their identity in the visceral adipose tissue of mice during aging (Goldberg, Shchukina et al. 2021).

The mechanisms responsible for triggering and sustaining adipose tissue inflammation have been intensively studied over the past decade. Obesity-induced alterations in the gut microbiome, along with increased gut permeability promote the translocation of endotoxins like LPS, driving inflammation in many tissues including adipose tissue. Within adipose tissue, fatty acids released from fat cells (or insufficiently sequestered by fat cells) have been proposed to elicit inflammatory responses, though these effects have not been observed consistently across studies (Tilg, Zmora et al. 2020). Additionally, the chronic uptake and increased storage of fatty acids as lipid droplets in macrophages may cause lipotoxicity, leading to pro-inflammatory changes within macrophages. In support of this idea, lipid-storing macrophages, resembling foam cells, accumulate in obese adipose tissue (Lumeng, Deyoung et al. 2007). More recently, single

cell transcriptomic studies defined a population of lipid-laden macrophages in adipose tissue of obese animals marked by the expression of CD9. These CD9+ macrophages are sufficient to induce pathologic programing of adipose tissue when transferred into lean mice (Hill, Lim et al. 2018). Interestingly, the capacity for macrophages to take up and store lipid exerts beneficial, metabolically protective effects, suggesting that lipid-storage *per se* is adaptive and that other signals are necessary to provoke inflammatory changes (Aouadi, Vangala et al. 2014). Further studies show that the lipid receptor TREM2 is a key functional regulator and marker of lipid-storing macrophages in rodent and human fat tissue (Jaitin, Adlung et al. 2019). Notably, a recent study shows that adipocytes, in addition to releasing fatty acids via lipolysis, transfer lipids to macrophages *via* exosomes (Flaherty, Grijalva et al. 2019). This exosomal lipid transfer pathway is increased in obesity and promotes macrophage differentiation.

Adipocytes modulate inflammation through the production of adipokines. In particular, Leptin, which increases during obesity, exerts pro-inflammatory effects through direct actions on many types of immune cells (Francisco, Pino et al. 2018). By contrast, adiponectin promotes an anti-inflammatory profile in macrophages (Ohashi, Parker et al. 2010). An emerging concept in the field demonstrates important functions for various types of fibroblasts in modulating adipose tissue immune responses. For example, the Gupta lab has defined a subset of fibroblasts, called fibro-inflammatory progenitors that stimulate macrophage accrual in adipose tissue during obesity development (Shan, Shao et al. 2020). Additionally, certain subpopulations of mesenchymal cells in adipose tissue are a major source of IL-33, which regulates the activity of Treg and ILC2 cells (Spallanzani, Zemmour et al. 2019). Unfortunately, despite a huge body of literature implicating inflammation as a driver of obesity-related metabolic disease, anti-inflammatory therapies have, thus far, not been successful. Given the pleiotropic effects of immune cells in adipose tissue, it will likely be necessary to identify approaches that selectively block the maladaptive effects of

inflammation, without compromising the critical functions of immune cells that support adipose tissue health and plasticity.

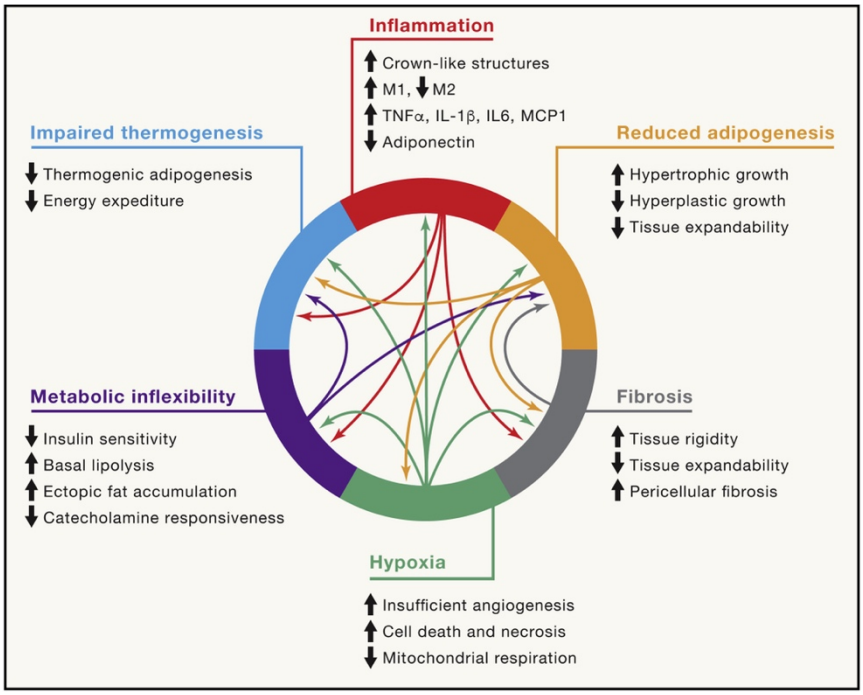

Figure 6 The Hallmarks of Adipose Tissue Dysfunction
Several interconnected and mutually reinforcing processes contribute to adipose tissue dysfunction during the pathogenesis of metabolic disease. Excessive expansion of adipose tissue and insufficient angiogenesis drives hypoxia, which triggers an inflammatory response and promotes fibrosis. The inflammatory milieu drives the secretion of cytokines that maintain adipose inflammation, promote fibrosis, and impair metabolic flexibility by interfering with both nutrient uptake and nutrient release. Diminished progenitor cell differentiation capacity, due to progenitor autonomous defects, inflammation, or fibrotic ECM, limits expansion via hyperplasia, favoring adipocyte hypertrophy. Thermogenesis, which is highly dependent on the metabolic flexibility of adipose tissue is blunted, diminishing energy expenditure. These processes are continuous and synergistic, leading to a vicious cycle that culminates in adipose tissue dysfunction.

Limitations to Metabolic Plasticity

Healthy WAT exhibits extensive metabolic flexibility, responding to anabolic and catabolic signals (via lipogenesis and lipolysis respectively) to preserve whole organism energy homeostasis. However, in the setting of chronic positive energy balance, WAT develops metabolic inflexibility, characterized by a decreased amplitude of response to signals regulating both the storage and mobilization of nutrients.

In the fed-state, adipose tissue metabolic inflexibility manifests as insulin resistance, resulting in decreased post-prandial glucose and lipid sequestration, unrestrained lipolysis, and

elevated circulating FFA levels (Gastaldelli, Gaggini et al. 2017, Petersen and Shulman 2018). The molecular pathogenesis of adipose tissue insulin resistance is complex and incompletely understood, but inflammation, hypoxia, fibrosis, and impaired expandability appear to be key contributors; comprehensive reviews offering integrated perspectives on whole body and adipose tissue specific insulin resistance have been recently published elsewhere (Czech 2020).

In the fasted-state, adipose tissue metabolic inflexibility manifests as diminished catecholamine-stimulated lipolysis in subcutaneous WAT, despite elevations in basal lipolysis in all fat depots (Arner 2005). This lipolysis impairment is due to alterations in the catecholamine-stimulated signaling cascade, including reduced β_2-adrenergic receptor expression, increased anti-lipolytic α_2-receptor activity, and decreased HSL stimulation by cAMP; these phenomena have been extensively reviewed elsewhere (Morigny, Houssier et al. 2016). These changes are likely exacerbated by obesity-induced decreases in sympathetic nerve fiber density (Jiang, Ding et al. 2017, Cao, Wang et al. 2018).

Chronic inflammation is believed to be a major contributor to the impairment in the metabolic plasticity of fat (Zatterale, Longo et al. 2019). As an example, secretion of the proinflammatory cytokines TNFα and MCP1 by adipocytes and infiltrating macrophages activates JNK signaling, which phosphorylates the insulin receptor and reduces its activity (Hirosumi, Tuncman et al. 2002). Similarly, chronic inflammation diminishes catecholamine responsiveness. For example, TNFα-induced expression of the kinases IKKe and TBK1 activates the phosphodiesterase PDE3B, which directly reduces the levels of cAMP. This reduction in cAMP signaling reduces HSL phosphorylation and UCP1 expression thereby diminishing both lipolysis and thermogenesis (Mowers, Uhm et al. 2013, Li, Wang et al. 2019).

Hypoxia is another key driver of adipose tissue dysfunction and metabolic inflexibility during aging and obesity. Hypoxia is believed to develop due to (1) the presence of hypertrophic adipocytes (reaching 200+ μm in diameter), which exceed the diffusion limit of O_2 (typically 100-

200 μm in tissues) and (2) defects in post-prandial blood flow and vascular density (Trayhurn 2013). In obesity, rather than stimulating angiogenesis, HIF1α, the master regulator of the hypoxia response, promotes the expression of pro-inflammatory and pro-fibrotic genes (Halberg, Khan et al. 2009, Lee, Kim et al. 2014). Interestingly, expression levels of an anti-angiogenic form of VEGF ($VEGFA_{165}b$) are elevated in obesity and likely contribute to impaired angiogenesis in adipose tissue (Ngo, Farb et al. 2014). Obese humans exhibit diminished adipose tissue blood flow and a notable failure to augment blood flow in response to feeding, prolonged fasting, and exercise (Frayn and Karpe 2014). Consistent with this finding, obese mice show precipitous declines in adipose tissue capillary density (Cao, Wang et al. 2018). Together these results suggest that targeting adipose tissue angiogenesis to promote healthy vascular growth and avoid hypoxia may be a promoting future therapeutic avenue.

Thermogenesis

Obesity and aging are associated with reductions in the abundance and activity of thermogenic adipose tissue in both mice and humans (Wang, Ishibashi et al. 2019, Becher, Palanisamy et al. 2021). Interestingly, distinct mechanisms may underlie age- and obesity-linked declines in thermogenic fat activity. For example, Song et al. observed that the conversion of low-thermogenic cells to high-thermogenic cells in BAT is impaired in aging but not in diet-induced obesity (Song, Dai et al. 2020). Likewise, Nguyen et al. showed that aging but not obesity causes the emergence of pro-inflammatory precursor (ARC) cells in subcutaneous adipose tissue, which impede adipocyte differentiation (Nguyen, Lin et al. 2021). Targeting BAT to increase longevity has been the aim of several studies and is reviewed elsewhere (Darcy and Tseng 2019).

1.7 Translational regulation of adipose tissue

As discussed earlier on this chapter, the adipose tissue has an incredible ability to adapt and remodel its structure and function in response to the host needs. Even though transcription regulation has been largely studied as an import process regulating adipose tissue plasticity, translational control is the final level of regulation to make a functional gene product: a protein.

Interestingly, there is little known about the interplay of metabolism, adipose tissue, and translational control. In the early 80's, the ability of insulin to regulate fat cells ribosomes activity and protein synthesis rates was reported. Insulin induced a shift in the polysome profile by increasing the size of the polysomes pool and decreasing monosomes abundancy (Vydelingum, Drake et al. 1983). A few papers since then have demonstrated how hormones and growth factors directly impact the translation machinery. For example, activation mTOR/PI3K and MAPK pathways, drives the downstream activation of kinases S6K and RSK that phosphorylate eukaryotic initiation factor 4B (eIF4B) (Shahbazian, Roux et al. 2006). eIF4B phosphorylation at Ser422 increases the ability of this initiation factor to interact with initiation factor complex 3, therefore increasing rates of translation initiation. However, how these pathways and translation rate respond to pathologies such as obesity is still under investigation.

Evidence of a finely tuned regulation has been demonstrated by the studies with global heterozygous mice for negative regulators of the cap-binding protein eIF4E (4E-BP1 and 4E-BP2), eukaryotic initiation factor 4E (eIF4E) and eukaryotic initiation factor 6 (eIF6). Le Bacquer and collaborators (Le Bacquer, Petroulakis et al. 2007) demonstrated that ablation of negative regulators 4E-BP1 and 4E-BP2 promoted an increased sensitivity to diet induced obesity and insulin resistance. A mechanism driven by increased adipogenesis, and reduced energy expenditure/lipolysis(Tsukiyama-Kohara, Poulin et al. 2001). Consistent with these findings, a more recent study, demonstrated that hemizygous mice for eIF4E are resistant to diet-induced obesity (Conn, Yang et al. 2021). Specifically, eIF4E in liver selects for mRNAs involved in lipid

storage and lipid metabolic processing - a process that is disrupted in the eIF4E+/- mice resulting in increased fatty acid oxidation and consequently enhancement in energy expenditure. These two seminal papers together demonstrate that in the absence of translational break (4E-BP1 and 4E-BP2), eIF4E is free to drive initiation of translation, and as a consequence drives more adipogenesis, and increase in fat mass. However, if you reduce eIF4E dose (eIF4E+/- mice), that drives a lean phenotype, with increase in beta-oxidation and decrease in lipid storage. Finally, eIF6 heterozygous mice have shown a decrease in body mass, and triglyceride content in liver and increased insulin sensitivity (Brina, Miluzio et al. 2015). Mechanistically, eIF6 promotes the translation of a specific set of mRNAs (e.g. Fasn), involved in *de novo* lipogenesis increasing lipid storage as a consequence. Therefore, modulating the expression and activation of essential initiation factors seems crucial to regulate metabolism and energy homeostasis.

In conclusion, given the interconnected roles of translation and metabolism, shaping physiological outcomes and metabolic diseases (e.g. obesity, diabetes, fatty liver), a continued and comprehensive exploration of their intricate interrelationships is indispensable for advancing our mechanistic understanding about obesity in health and disease.

1.8 Conclusions

There is an urgent need to develop new therapies to combat the expanding dual epidemics of obesity and cardiometabolic disease. Adipose tissue lies at the center of these health problems, representing a major contributor to disease pathogenesis and a promising target for therapies. As highlighted in this chapter, adipose tissue possesses extraordinary plasticity, including its: (1) rapid titration of metabolic programs to maintain systemic energy levels in the face of fluctuating changes in nutrient supply and demand; (2) unparalleled capacity to expand and contract to accommodate long term trends in energy balance; (3) remarkable structural and metabolic

transformation during cold exposure to engage in heat production; (4) capacity for de-differentiation to regulate lactation and wound healing.

Obesity often leads to a decline in adipose tissue plasticity, which is associated with fibrosis, inflammation, progenitor cell senescence, and catecholamine resistance. Ultimately, these pathological changes impair the critical nutrient-buffering function of adipose tissue, leading to insulin resistance and metabolic disease. The central role of adipose tissue dysfunction in disease and the incredible plasticity of fat tissue supports the promise of modulating fat tissue phenotypes for therapeutic purposes. The viability of this approach has already been demonstrated with the success of thiazolidinediones, which promote healthy adipose tissue expansion and enhance insulin sensitivity. Unfortunately, unfavorable side effects of some thiazolidinediones have caused this class of drugs to fall out of favor.

New insights into the identity and regulation of APCs, adipocytes, immune cells, and other diverse cell types in adipose tissue promise to reveal novel drug targets to promote metabolically beneficial tissue remodeling. For example, it may be possible to promote favorable APC-fate decisions, encouraging adipogenesis at the expense of adipocyte hypertrophy, fibrosis, and inflammation. Additionally, increasing the abundance and activity of thermogenic adipose tissue is a promising strategy to enhance energy expenditure to combat both metabolic disease and obesity. Many questions and opportunities for future discovery remain, which will yield new insights into adipose tissue biology and hopefully lead to improved therapies for human disease.

RESULTS

CHAPTER 2: PPARγ-DEPENDENT REMODELING OF TRANSLATIONAL MACHINERY IN ADIPOSE PROGENITORS IS IMPAIRED IN OBESITY

2.1 Introduction: Overview of rosiglitazone-induced response in adipose tissue

Obesity is a complex and multifactorial condition that results from an imbalance between energy intake and energy expenditure. This leads to an excessive accumulation of body fat, which in some cases can negatively impact an individual's physical, psychological, and social well-being, as well as increases the risk of developing several chronic diseases, such as cardiovascular disease, type 2 diabetes, and certain cancers, among others. This complex interplay of adipose tissue adaptation and expansion during obesity can ultimately lead to maladaptive changes in its structure and function (CDC 2023, WHO 2023).

While the maladaptation of the adipose tissue during obesity has been studied extensively (Sakers, De Siqueira et al. 2022), it is not clear how distinct cell types within adipose tissue are impacted. Furthermore, the role of adipose progenitor cells (APCs) and their response to different stimuli is still not fully understood. Recent single-cell and single-nuclei RNA sequencing studies started uncovering the tremendous heterogeneity and plasticity of these cells in mice and humans (Hepler, Shan et al. 2018, Merrick, Sakers et al. 2019, Min, Desai et al. 2019, Rajbhandari, Arneson et al. 2019, Spallanzani, Zemmour et al. 2019, Henriques, Bedard et al. 2020, Oguri, Shinoda et al. 2020, Ramirez, Dankel et al. 2020, Song, Dai et al. 2020, Vijay, Gauthier et al. 2020, Angueira, Sakers et al. 2021, Hildreth, Ma et al. 2021, Sárvári, Van Hauwaert et al. 2021, Maniyadath, Zhang et al. 2023). External factors such as β-adrenergic stimulation drive dynamic remodeling of APCs, both in brown adipose tissue and inguinal white adipose tissue (Oguri, Shinoda et al. 2020, Song, Dai et al. 2020), while obesity is characterized by a decline in the number of APCs and a shift towards a fibroinflammatory and less lipogenic profile (Merrick,

Sakers et al. 2019, Sárvári, Van Hauwaert et al. 2021). Whether the stromal vascular fraction and specifically the APCs contribute to whole-body metabolic homeostasis and how they can be potentially targeted is still not fully characterized.

Evidence of such a crucial function was first reported using an inducible adipocyte-specific PPARγ knockout system, where after mice were treated with thiazolidinediones (TZDs - PPARγ agonists) several pathways were modulated in the white adipose tissue in the absence of PPARγ. This remodeling suggests that there are either indirect effects of TZDs or PPARγ-independent targets in the adipose tissue (Wang, Zhang et al. 2018). TZDs have been studied for a long time and specifically, rosiglitazone has been shown to improve insulin sensitivity in adipocytes directly through the activation of PPARγ receptors which promotes lipogenesis and secretion of adiponectin, reduces inflammation in adipose tissue, and decreases hepatic and peripheral triglycerides levels (Chao, Marcus-Samuels et al. 2000, Tontonoz and Spiegelman 2008, Kang, Park et al. 2010, Cariou, Charbonnel et al. 2012, Soccio, Li et al. 2017, Lebovitz 2019). At the molecular level, the occupancy of PPARγ in the promoter regions of multiple adipose genes is indeed significantly decreased in adipocytes following a high-fat diet. Consequently, these cells exhibit an increased expression of myofibroblast genes triggered by the TGFβ1 effector protein SMAD. Notably, rosiglitazone does revert the molecular and cellular phenotype in fat cells from obese animals highlighting a crucial role of PPARγ in remodeling the transcriptional architecture (Roh, Kumari et al. 2020). Even though the transcriptional landscape reconfiguration by rosiglitazone in the adipose tissue is well described, the translational regulation of these messenger RNA networks is not fully understood.

Indirect evidence has shown that after rosiglitazone treatment, there is an increase in the mammalian target of rapamycin complex 1 (mTORC1) activity and that deficiency of mTORC1 blocks the rosiglitazone effect on transcriptional remodeling in the adipose tissue (Blanchard, Festuccia et al. 2012, Andrade, Gilio et al. 2021). One of the downstream effector functions of

mTORC1 activation is the phosphorylation and consequently, dissociation of eukaryotic translation initiation factor 4E-binding protein 1 (eIF-4EBP1) from the major cap-dependent eukaryotic translation initiation factor 4E (eIF4E) (Pause, Belsham et al. 1994, von Manteuffel, Gingras et al. 1996, Burnett, Barrow et al. 1998, Gingras, Gygi et al. 1999, Roux and Topisirovic 2012). As a consequence, eIF4E can then be recruited to the translation initiation complex eIF4F. In addition, mTORC1 is known to phosphorylate S6K, which in turn phosphorylates several components of the translation machinery (e.g., S6, eIF4B) (Valvezan and Manning 2019). However, it's not clear how rosiglitazone directly impacts the translation machinery in the adipose tissue to promote adipocyte differentiation.

Here we investigated the impact of an acute PPARγ agonist treatment in obese mice at single cell level in both inguinal and epididymal adipose stromal vascular fraction. We demonstrated that rosiglitazone profoundly remodels the molecular landscape in both depots and restores the obese transcriptional profile to what we observed in lean mice. In addition to developing a single-cell transcriptome atlas of leptin deficient mice (*ob/ob*), and their response to rosiglitazone in each cell type, we identified a novel role of PPARγ agonists in regulating translation. We have shown that rosiglitazone increased the expression of ribosomal genes in the APCs and that this remodeling is induced by PPARγ directly binding to enhancers in close proximity to these genes. Moreover, heavily translating ribosomes (polysomes) were not only occupied by fat-specific PPARγ targets but also by a distinct selection of transcripts containing specific G-rich motifs in their 5' untranslated region (5'UTR) after rosiglitazone treatment. In conclusion, we propose that this remodeling drives a translation selectivity in the polysomes of the stromal vascular fraction characterizing a specialized adipose tissue translation response to rosiglitazone to drive adipogenesis and maintain adipose homeostasis.

2.2 Results

2.2.1 Acute Rosiglitazone Treatment Confers Improvement in Glucose Tolerance and Remodeling in the Adipose Tissue

To evaluate the impact of an acute PPARγ agonist treatment on host physiology, we treated wild-type (WT) C57BL/6 lean mice and obese *Lep^{ob}/Lep^{ob}* (*ob/ob*) mice with either Rosiglitazone (Rosi) or vehicle (Veh) by oral gavage for three days (**Fig7A**). Lean mice treated either with vehicle (WT-Veh) or Rosi (WT-Rosi) did not present changes in total body weight, nor improvement in glucose clearance (**Fig7B-C)**. ob/ob mice treated with vehicle (ob/ob-Veh) or rosiglitazone (ob/ob-Rosi) also did not show changes in body weight (**Fig7B**), however, ob/ob-Rosi mice presented a remarkable improvement in glucose tolerance, comparable to lean mice (**Fig7C**). Thus, Rosi leads to the normalization of glucose excursion curves within 3 days of acute treatment in the absence of changes in body weight.

To assess whether acute treatment with Rosi leads to morphological changes in adipose tissue, we analyzed histological sections from liver and adipose tissue. WT-Rosi mice presented no hepatic histological changes but a minor increase in total mass (**FigS1A-B**). In contrast, the liver of ob/ob-Rosi mice exhibited a decrease in lipid accumulation (**FigS1A**) characterized by a reduction in lipid droplet numbers and size (**FigS1C**). Next, we examined whether Rosi impacted the weight and histology of the main fat depots: brown adipose tissue (BAT), epididymal white adipose tissue (eWAT), and inguinal adipose tissue (iWAT). We found that BAT mass increased with Rosi treatment in both lean and obese mice (**Fig7D**)**,** while the weight of eWAT and iWAT were similar when compared between vehicle and Rosi (**Fig7E-F**). Notably, ob/ob mice treated with Rosi had decreased crown-like structures in the eWAT with no major alterations in the iWAT and BAT in both obese and lean conditions (**Fig7G**).

In order to evaluate the distribution of glucose with Rosi treatment, we adapted the conventional glucose tolerance test by mixing a bolus of glucose with 18F fluorodeoxyglucose

([^{18}F]-FDG). After one hour of conscious glucose uptake, mice were subjected to PET/CT scans (**FigS1D**). ob/ob-Rosi mice presented an increase in glucose uptake in the brain, heart, liver, muscle, and adipose tissue (axillary) and a trend in the BAT compared to ob/ob-Veh mice (**FigS1E-F**). To better visualize the glucose uptake in the fat depots, we excluded regions of high 18F-FDG uptake (e.g., heart, and bladder) using the software ORS Dragonfly. Remarkably,

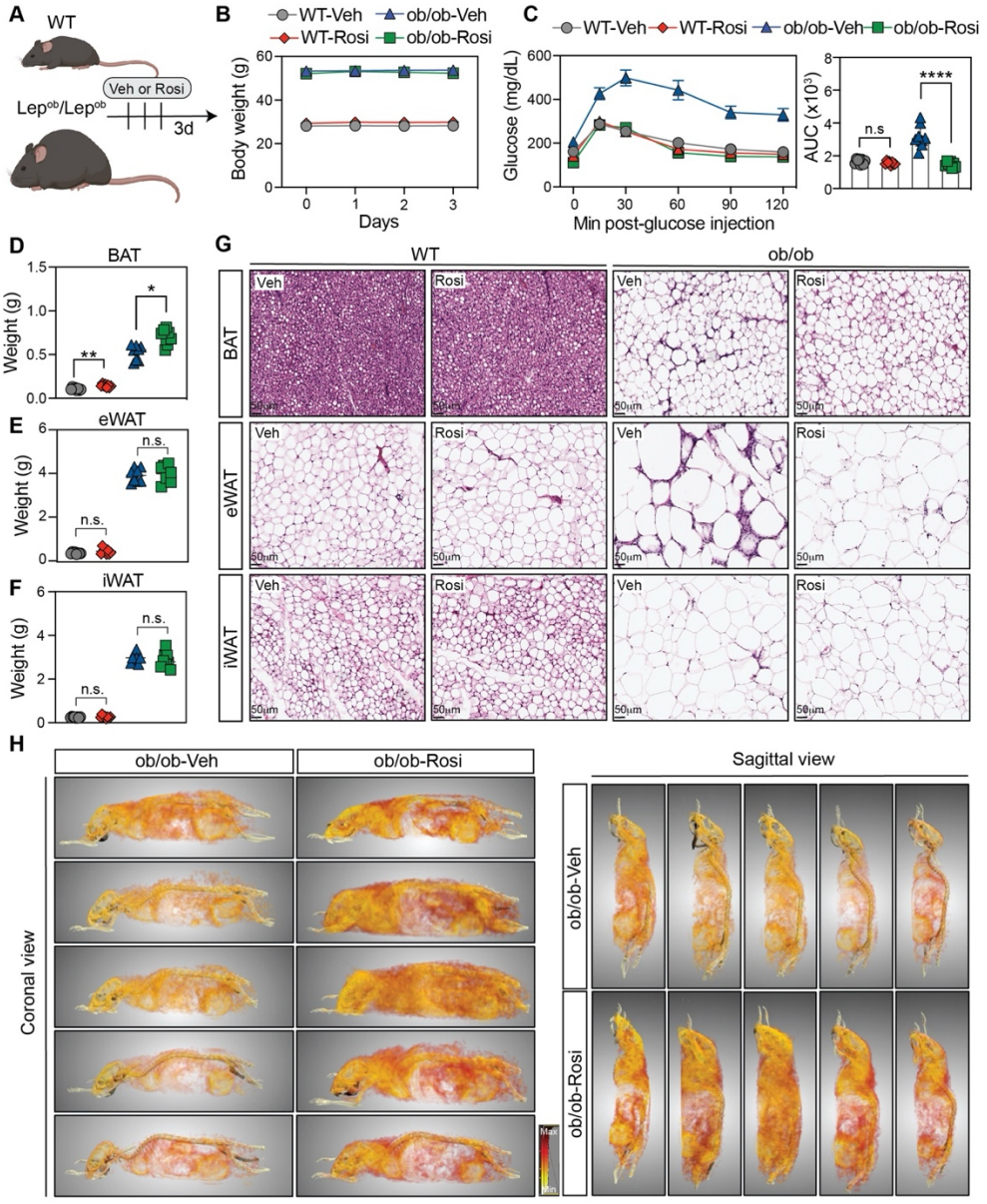

Figure 7 Adipose tissue remodeling after acute rosiglitazone treatment.

A) Schematic experimental design: lean (WT) and obese (ob/ob) mice were orally gavage with either vehicle or rosiglitazone 30mg/Kg for 3 days. (**B**) Total mice body weight. (**C**) Glucose tolerance test 1g/Kg. (**D-F**) Adipose tissue weight: brown adipose tissue (BAT), epididymal adipose tissue (eWAT), and inguinal adipose tissue (iWAT). (**G**) Histological analysis of BAT, eWAT, and iWAT (hematoxylin and eosin stain). (**H**) Visualization of adipose tissue [^{18}F]-FDG (100μCi) accumulation after one-hour conscious uptake. Data represent mean ± SEM (n = 8 mice per group). GP pvalue style: *p= 0.0332; **p < 0.0021; ***p < 0.0002 by one-way ANOVA, multiple comparisons followed by Tukey post hoc test, (C) two-way ANOVA followed by Bonferroni post hoc test.

ob/ob-Rosi mice had a much greater glucose uptake in the adipose tissues compared to ob/ob-Veh mice (**Fig7H**).

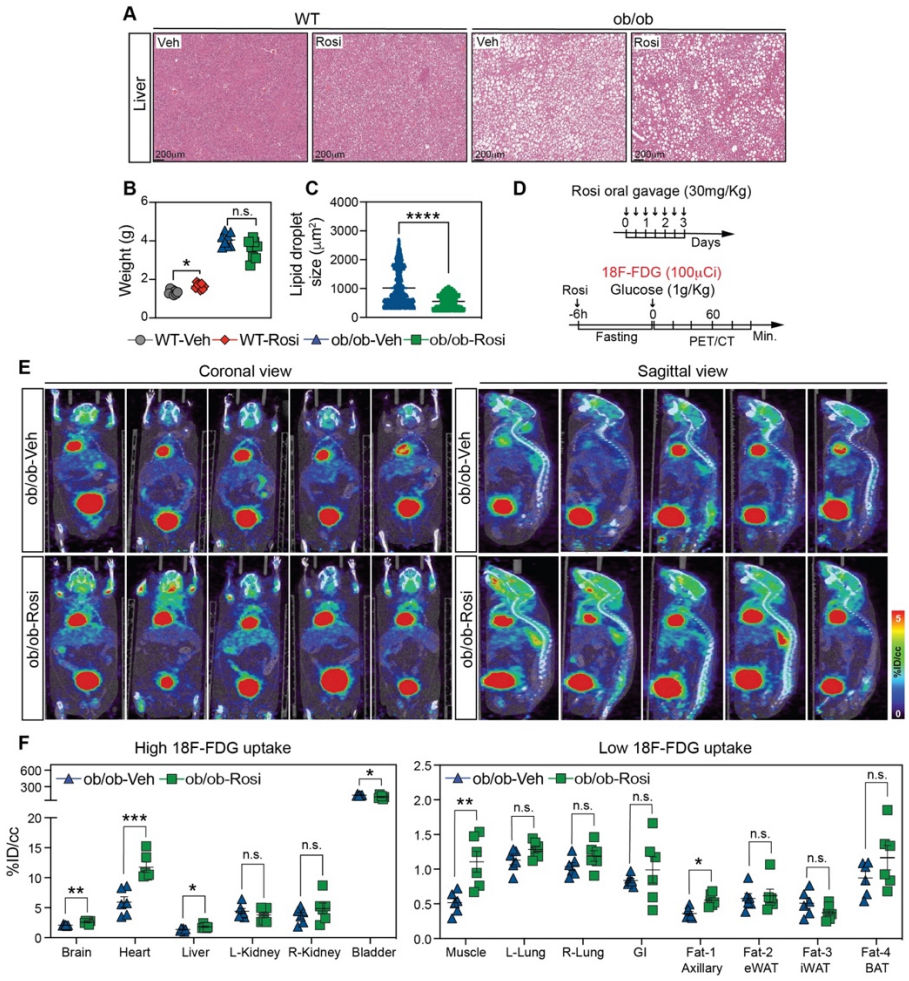

SFigure 1 Host physiology remodeling after rosiglitazone treatment.

(**A**) Histological analysis of the liver after acute rosiglitazone treatment (30mg/Kg). (**B**) Liver weight. (**C**) Lipid droplet area quantification of ob/ob mice treated with either vehicle or rosiglitazone. (**D**) Schematic overview of conscious glucose uptake in vivo using a bolus of glucose (1g/Kg) and [^{18}F]-FDG (100μCi). (**E**) PET/CTs at coronal and sagittal view of ob/ob mice treated either vehicle or rosiglitazone. (**F**) Quantification of percent injected dose per cubic centimeter in tissue (%ID/cc) ID, injected dose. Data represent mean ± SEM (n = 6-8 mice per group). GP pvalue style: *p= 0.0332; **p < 0.0021; ***p < 0.0002 by (B) one-way ANOVA, multiple comparisons followed by Tukey post hoc test, (C) two-tailed Student's t-test, and (F) multiple comparisons two-tailed Student's t-test.

Overall, acute Rosi treatment presented a major remodeling in the obese host physiology, specifically decreasing hepatic lipid accumulation, reducing cellular infiltration in eWAT,

increasing BAT mass, improving glucose tolerance, and increasing glucose uptake in adipose depots and other major tissues with high metabolism rate.

2.2.2 Single-Cell RNA Sequencing Uncovers Stromal Vascular Cell Remodeling after PPARγ agonist treatment

Although TZDs exhibit a clearly defined role in modulating adipocyte functions, the influence and remodeling effects on the adipose stromal vascular fraction remain unclear. Therefore, we set out to understand how Rosi treatment affects the stromal vascular fraction in the adipose tissue by using single-cell RNA sequencing (scRNASeq) in both eWAT and iWAT.

Since the major Rosi responses were observed in obese mice, we treated ob/ob mice with either vehicle or Rosi for 3 days. Additionally, we included a WT-Veh group to compare the baseline of lean mice (**Fig8A**)**.** Briefly, datasets from both eWAT and iWAT were separately processed through the 10X Genomics Cell Ranger version 3.0.2 single-cell software to perform sample demultiplexing, sequence alignment to mouse genome mm10, quality control assessment, and filtering unique molecular identifiers (UMIs) counting to generate gene count matrices. Single cells were identified from background noise with a default setting in Cell Ranger. The filtered matrix was further selected with the proportion of mitochondrial reads < 25%, the number of UMI ranging from 700-22,000, and the number of detected genes ranging from 200-6,000 (**FigS2A-B**).

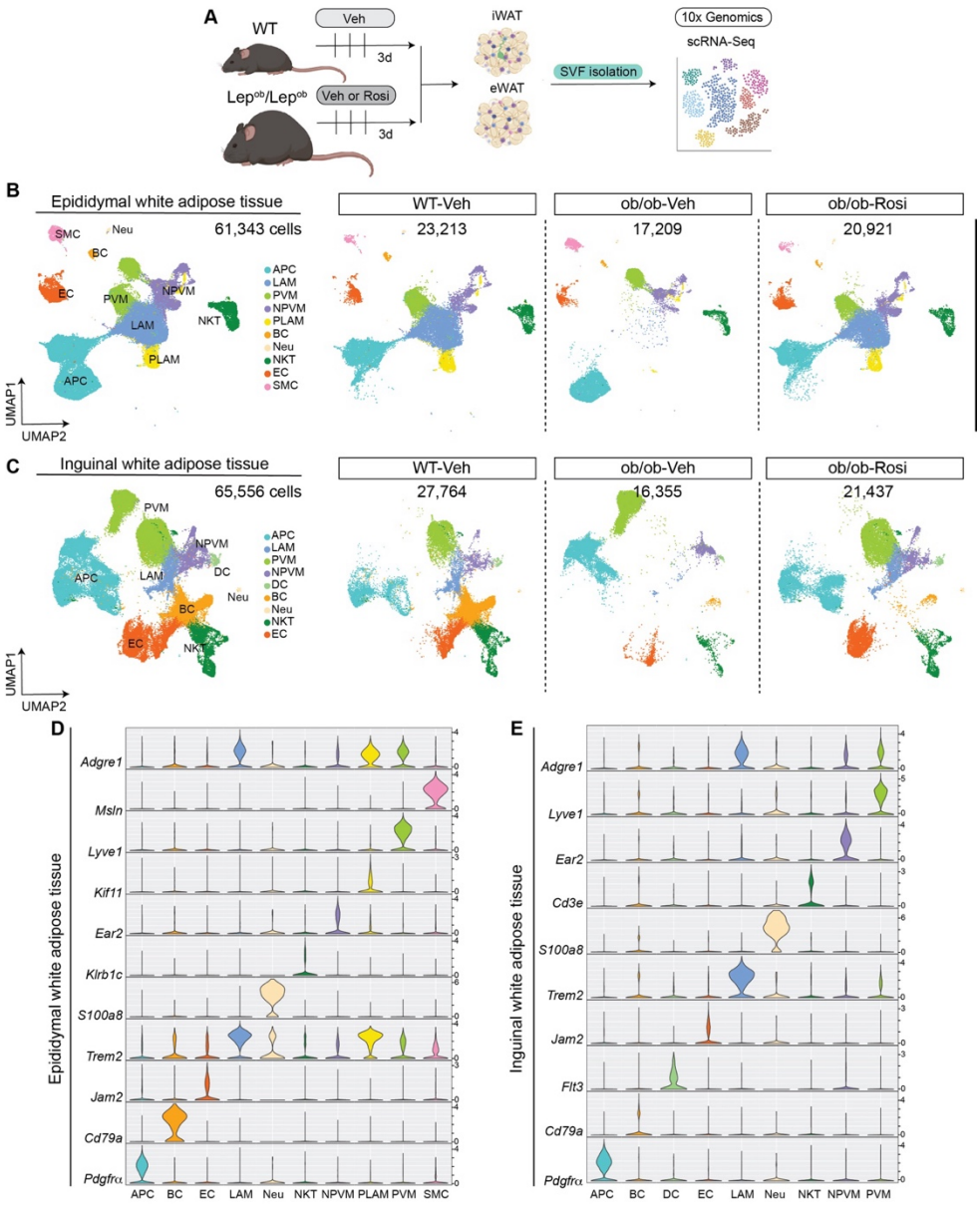

Figure 8 PPARγ-driven adipose tissue heterogeneity.

(**A**) Schematic overview of scRNA-Seq: lean (WT) and obese (ob/ob) mice were treated with either vehicle or rosiglitazone for 3 days (30 mg/Kg). Single-cell RNA Sequencing was conducted on the stromal vascular fraction extracted from epididymal white adipose tissue (eWAT) and inguinal white adipose tissue (iWAT) separately. (**B-C**) Uniform Manifold Approximation and Projection (UMAP) plot illustrates the cell clusters among 61,343 eWAT cells and 65,556 iWAT cells. The right three panels separately represent cells from WT-Veh, ob/ob-Veh, and ob/ob-Rosi. Each colored dot signifies a cell, with distinct colors indicating various cell types. The Louvain algorithm was utilized to determine cell clusters. (**D-E)** Cluster-specific expression of known cell markers: Adipocyte Precursor Cells (APC): *Pdgfrα;* B Lymphocytes (BC): *Cd79a*; Dendric Cells (DC): *Flt3*; Endothelial cells (EC): *Jam2*; Lipid-Associated Macrophages (LAM): *Trem2* and *Adgre1*; Neutrophils (Neu): *S100a8*, Natural Killer T cells (NKT): *Klrb1c* and *Cd3e*; Non-Perivascular-like Macrophages (NPVM): *Ear2* and *Adgre1*, Proliferating-LAM (P-LAM): *Kif11, Trem2* and *Adgre1*, Perivascular Macrophages (PVM): *Lyve1* and *Adgre1*, Smooth Muscle Cells (SMC): *Msln*. Data shown a single scRNA-Seq experiment (n=2 per group).

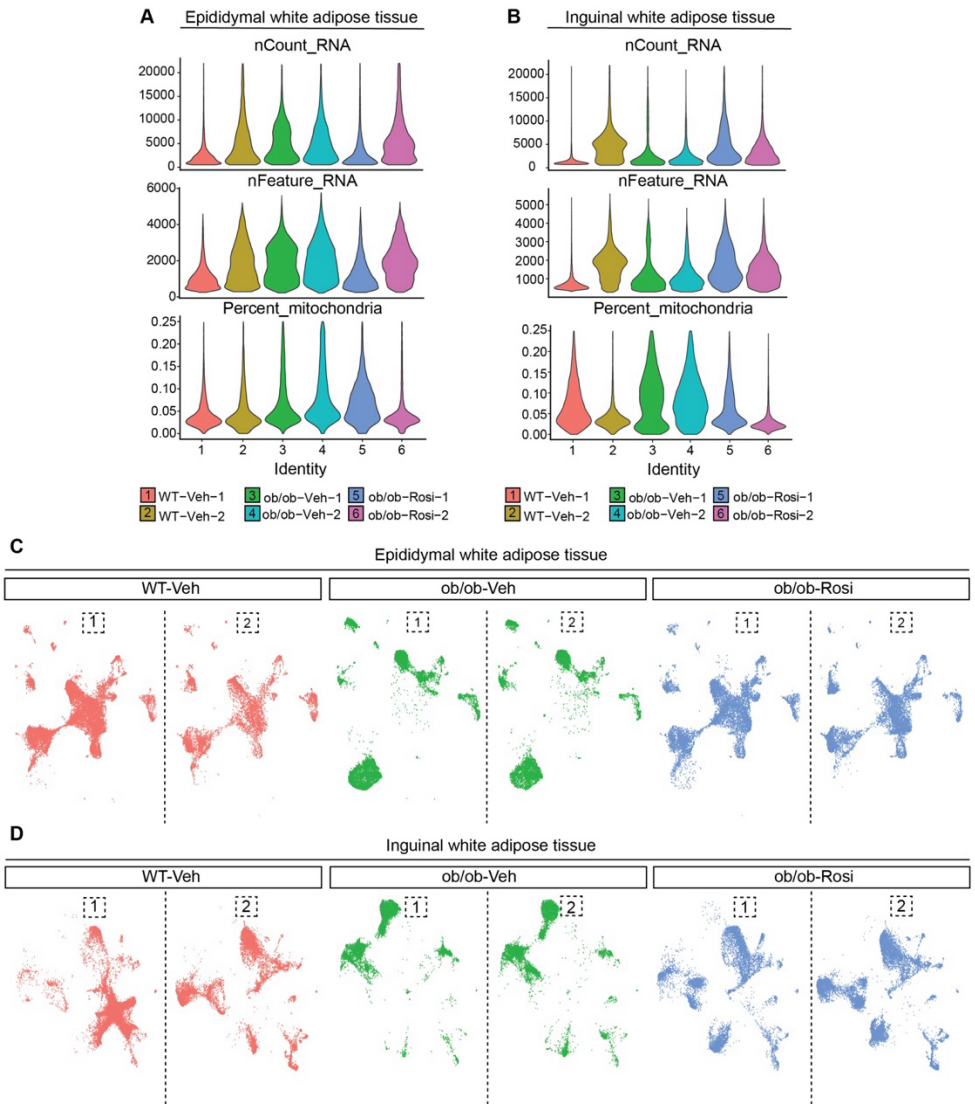

SFigure 2 Adipose stromal vascular fraction Single-Cell RNA Sequencing quality control.

(**A-B**) Violin plots display the distribution of the number of Unique Molecular Identifiers (UMI) (nCount_RNA), the number of detected genes (nFeature_RNA), and the proportion of mitochondrial reads (Percent_mitochondria) across each sample in eWAT (**A**) and iWAT (**B**). Cells were selected based on the number of UMIs (with a threshold range of 700-22,000), the number of detected genes (with a threshold range of 200-6,000), and the proportion of mitochondrial reads (with a threshold of less than 25%). (**C-D**) UMAP plot illustrates the cell clusters among 61,343 eWAT cells (**C**) and 65,556 iWAT cells (**D**) by each sample. The three panels separately represent cells from WT-Veh, ob/ob-Veh, and ob/ob-Rosi groups. Each colored dot signifies a cell. Data shown a single scRNA-Seq experiment (n=2 per group).

We were able to identify the major cell types described to be present in the adipose tissue: Smooth Muscle Cells (SMC), Neutrophils (Neu), B Lymphocytes (BC), Endothelial cells (EC), Adipocyte Progenitor Cells (APC), Natural Killer T cells (NKT), Dendritic Cells (DC), Perivascular

Macrophages (PVM), Lipid-Associated Macrophages (LAM), Non-Perivascular-like Macrophages (NPVM), and Proliferating-Lipid Associated Macrophages (PLAM) (**Fig8B-E**). Visualization of the cell clusters using t-SNE plots of the individual mice showed high reproducibility within groups (**FigS2C-D**). Interestingly, tissue-specific differences between eWAT and iWAT were evident, such as the presence of SMCs and PLAMs in the eWAT and DCs in the iWAT (**Fig8B-C**). Remarkably, ob/ob-Rosi samples from both eWAT and iWAT presented a huge shift in the cell clusters away from those in the ob/ob group to resemble the microenvironment in the lean WT-Veh mice (**Fig8B-C**).

2.2.3 Rosiglitazone Treatment Leads to Major Shifts in Macrophages Subpopulations

Despite the presence of crown-like structures in the histology of the ob/ob-Veh mice (**Fig7G**), we did not observe the presence of a large population of Lipid-Associated Macrophages (LAM) by scRNASeq in the ob/ob-Veh samples (iWAT and eWAT) (**Fig8B-C**). We, therefore, hypothesized that due to the high lipid content of those cells, and a gentle dissociation (**see Methods**), LAM may have floated away with the mature adipocyte fraction. To test this, we collected the top floating layer after iWAT/eWAT enzymatic digestion, plated cells overnight, and then performed confocal imaging. We found numerous F4/80 positive cells within the mature adipocyte fraction in both eWAT and iWAT of ob/ob-Veh mice (**FigS3A**). A few of these macrophages were in the process of phagocytosing apoptotic adipocytes, which also showed Plin1 staining, a lipid droplet marker found in adipocytes. By contrast, ob/ob-Rosi samples showed a decrease in the number of macrophages, as well as drastic morphological differences in macrophages, likely reflecting a different state of activation, with less classically activated cells (**FigS3A**). The effect of Rosi on macrophages switching from an inflammatory to an anti-inflammatory profile has been previously described (Tontonoz, Nagy et al. 1998, Odegaard, Ricardo-Gonzalez et al. 2007, Szanto, Balint et al. 2010), and PPARγ activation directs an

alternative-activation profile by the IL4-PPARγ-STAT6 pathway. To better understand the changes in macrophage composition in response to Rosi, we performed flow cytometry to quantify Macrophages (Macs), Inflammatory Macrophages (IM), Lipid-laden Macrophages (LAM), and Perivascular Macrophages (PVM) (**FigS3B**). We confirmed that Rosi treatment decreased the number of inflammatory and lipid-associated macrophages in both eWAT and iWAT, with a stronger response in the eWAT (**FigS3C-F**).

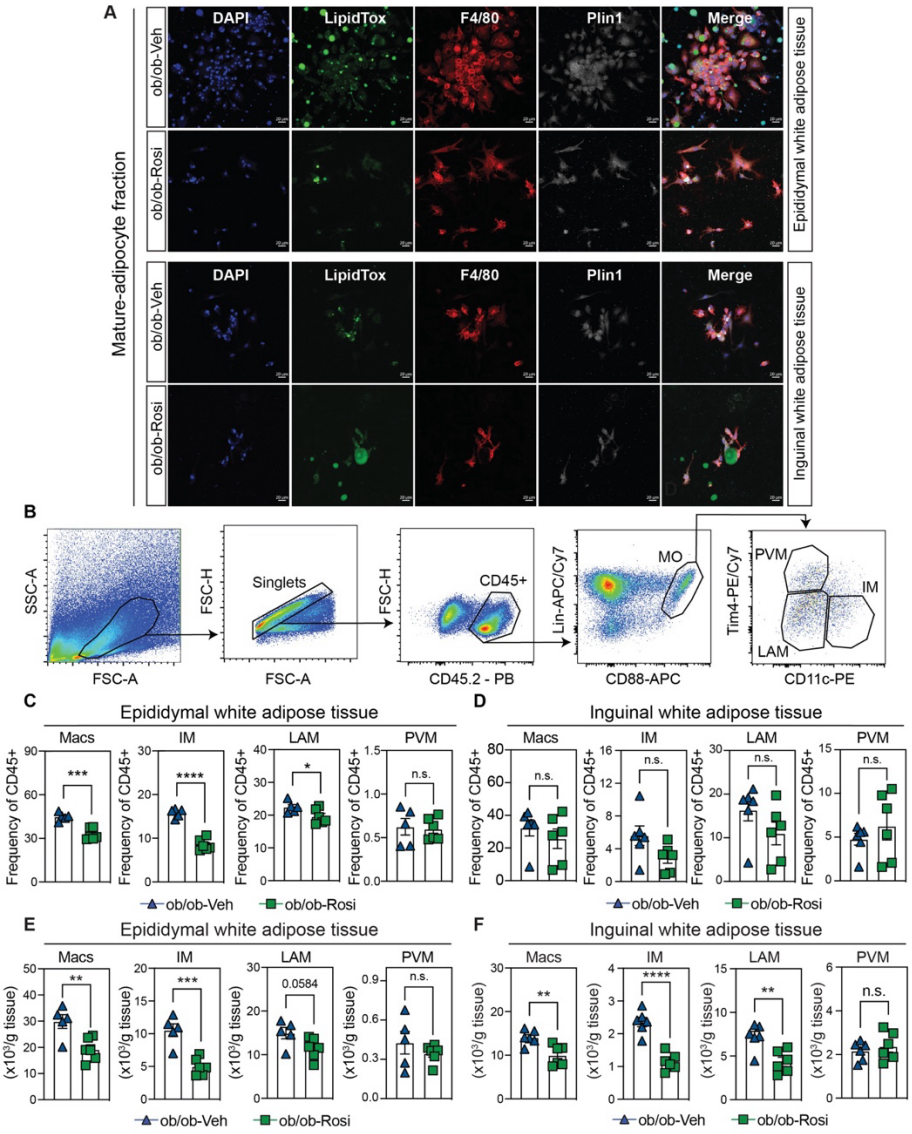

SFigure 3 Adipose-specific macrophage profile remodeling after PPARγ agonist treatment.

(**A**) Confocal images of macrophages (F4/80+) cultured overnight from mature-adipocyte fraction from either ob/ob-Veh or ob/ob-Rosi: DAPI (nuclei- blue), LipidTox (neutral lipids-green), F4/80 (macrophages-red), Plin1 (adipocyte-specific perilipin - white). (**B**) Flow

cytometry gate strategy for macrophages: Tim4+: perivascular macrophages (PVM), Cd11c+: inflammatory macrophages (IM), Tim4-, Cd11c-: lipid-laden macrophages (LAM). (**C-F**) Frequency and absolute number of Macrophages (Mac), IM, LAM, and PVM from epididymal and inguinal adipose tissue. Data represent mean ± SEM (n = 6 mice per group). GP pvalue style: *p= 0.0332; **p < 0.0021; ***p < 0.0002 by two-tailed Student's t-test.

2.2.4 *Response of Adipocyte Progenitors Cells after PPARγ Agonist Treatment*

Further evaluation of adipose histological sections of both eWAT (**Fig9**) and iWAT (**FigS4**) showed the presence of small multi-locular cells that could be indicative of newly forming adipocytes in ob/ob-Rosi mice (**Fig9A, FigS4A** - arrowheads). To evaluate whether acute Rosi treatment could impact the adipocyte progenitor populations that give rise to adipocytes, we focused on the cluster of Adipocyte Progenitor Cells (APC) that were then subclustered into progenitors and preadipocytes (**Fig9B** and **FigS4B**)**.** Interestingly, the Rosi treatment remodeled the clusters of progenitors and preadipocytes to states that are transcriptionally similar to those observed in lean mice (**Fig9B** and **FigS4B**). To confirm the progenitors and preadipocyte identities, we checked the expression of classical markers of progenitors (*Pi16* and *Dpp4*), and preadipocytes (*Icam1* and *Cd36*) [4]. eWAT presented a very clear and distinguishing expression of progenitor markers and a more diffused expression of preadipocyte markers potentially exemplifying a gradient of commitment to the adipogenic lineage (**Fig9C**). In contrast, the iWAT had a very clear separation between the progenitors and preadipocytes (**FigS4C**).

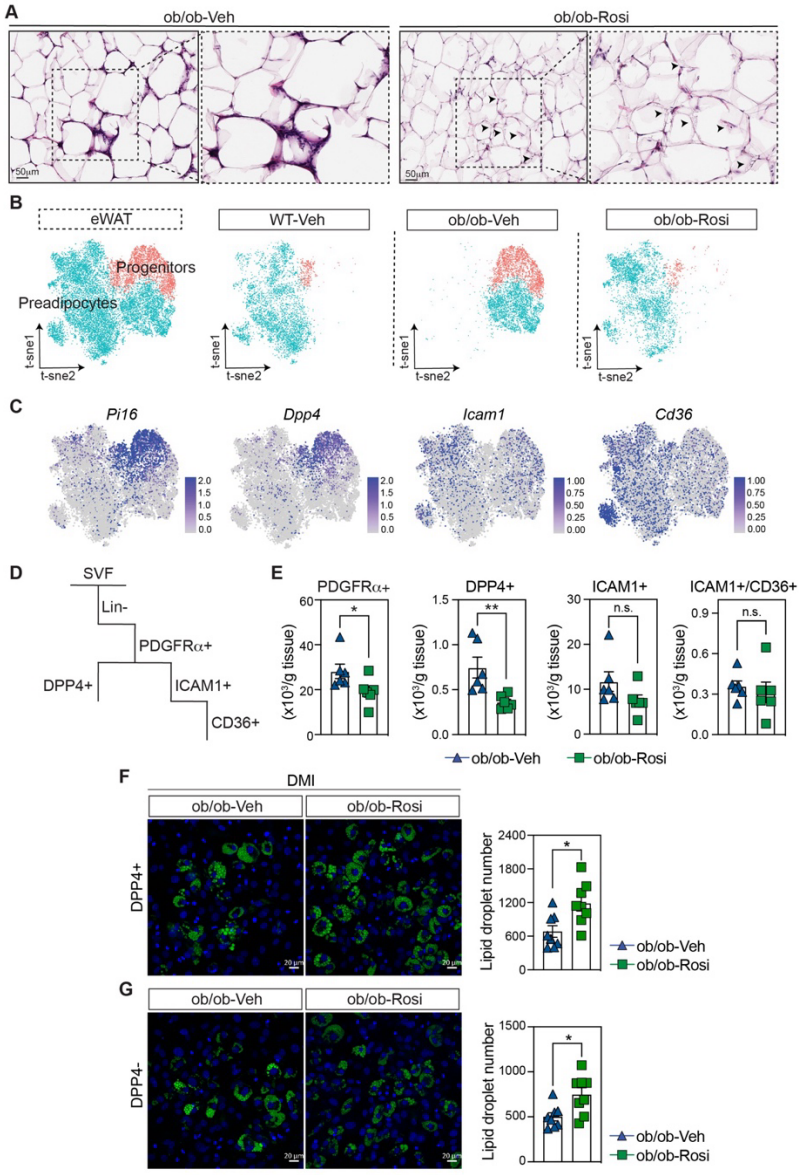

Figure 9 Remodeling of epididymal adipocyte precursor cells in response to PPARγ agonist.

(**A**) Histological analysis of epididymal adipose tissue (hematoxylin and eosin stain) from either ob/ob-Veh or ob/ob-Rosi mice. (**B**) t-distributed stochastic neighbor embedding (t-SNE) plot illustrates two subclusters of adipocyte precursor cells in the eWAT: progenitors and preadipocytes. The right three panels separately represent cells from WT-Veh, ob/ob-Veh, and ob/ob-Rosi. Each color-coded dot represents a cell, with progenitors being represented by red and preadipocytes by cyan. The Louvain algorithm was utilized to determine cell clusters. (**C**) Individual gene t-SNE ploys showing the expression and distribution of representative marker genes: *Pi16* and *Dpp4* for progenitors, *Icam1* and *Cd36* for preadipocytes. (**D**) Gate strategy to characterize progenitor cells: Lineage negative (CD45-, CD31-), PDGFRα+, DPP4+ (progenitors), and ICAM1+/CD36+ (preadipocytes). (**E**) Absolute number of progenitor and preadipocytes from ob/ob-Veh and ob/ob-Rosi mice. (**F-G**) Confocal of sorted lineage negative (CD45-, CD31-), PDGFRα+, DPP4+, and DPP4- cells differentiated for 4 days on DMI (dexamethasone, IBMX, and insulin) media, DAPI (nuclei- blue), LipidTox (neutral lipids- green). Data represent mean ± SEM (n = 6 mice per group). Confocal images: 4 wells per condition, 2 representative images per well were acquired. GP pvalue style: *p= 0.0332; **p < 0.0021; ***p < 0.0002 by two-tailed Student's t-test.

We made several comparisons to understand how our APC annotations compare with previously published single-cell analyses to validate our progenitors and preadipocyte populations

(**FigS5A-B**). First, we compared our data set with Burl and collaborators (Burl, Ramseyer et al. 2018). They have identified two populations in the eWAT and iWAT at steady state and in response to β3-adrenergic receptor agonist: adipocyte stem cells 1 and 2 (ASC1 and ASC2). In agreement with their data, our progenitor population matched with their ASC2 population, and our preadipocytes matched with their ASC1 population in both tissues (**FigS5A-B**). Second, we evaluated Sarvari *et al* (Sárvári, Van Hauwaert et al. 2021). They focused specifically on the context of diet-induced obesity and tackled the adipose progenitor's heterogeneity using single nuclei RNA sequencing. They characterized four fibro-adipogenic progenitor subpopulations in the eWAT: FAP1, FAP2, FAP3, and FAP4. Our data set presented a gradient between progenitors and preadipocyte gene expression in populations FAP2 and FAP3 potentially showing a spectrum of differentiation. FAP1 and FAP4 however, did match with our preadipocytes and progenitors, respectively. Finally, we compared and contrasted our dataset with Schwalie *et al* (Schwalie, Dong et al. 2018). They described three populations in the iWAT after depletion of lineage negative or Lin- (CD31-, CD45-, TER119-), and CD29+, CD34+, SCA1+: P1, P2, and P3 (adipogenesis regulator: Aregs). Our scRNASeq data showed that our progenitor cells and preadipocytes had similar expression as P1 and P2 respectively. Interestingly, their Aregs (P3) cells had a similar but lower expression matching with our preadipocytes, potentially exemplifying the existence of such cells in the genetic model of obesity Lep^{ob}/ Lep^{ob} as well.

To determine whether Rosi impacts the total number of ob/ob progenitor and preadipocytes in WAT, we performed flow cytometry (**Fig9D, FigS4D**). Since both eWAT and iWAT showed high expression of *Pdgfrα* (**FigS5C-D**), we defined our gating strategy as follows: lineage exclusion or Lin- (CD31-, CD45-), PDGFRα+, followed by the isolation of progenitors (DPP4+) and preadipocytes (ICAM1+ and ICAM1+/CD36+) (**FigS5E**). In both tissues, we observed a reduction in both frequency and absolute numbers of the less committed populations

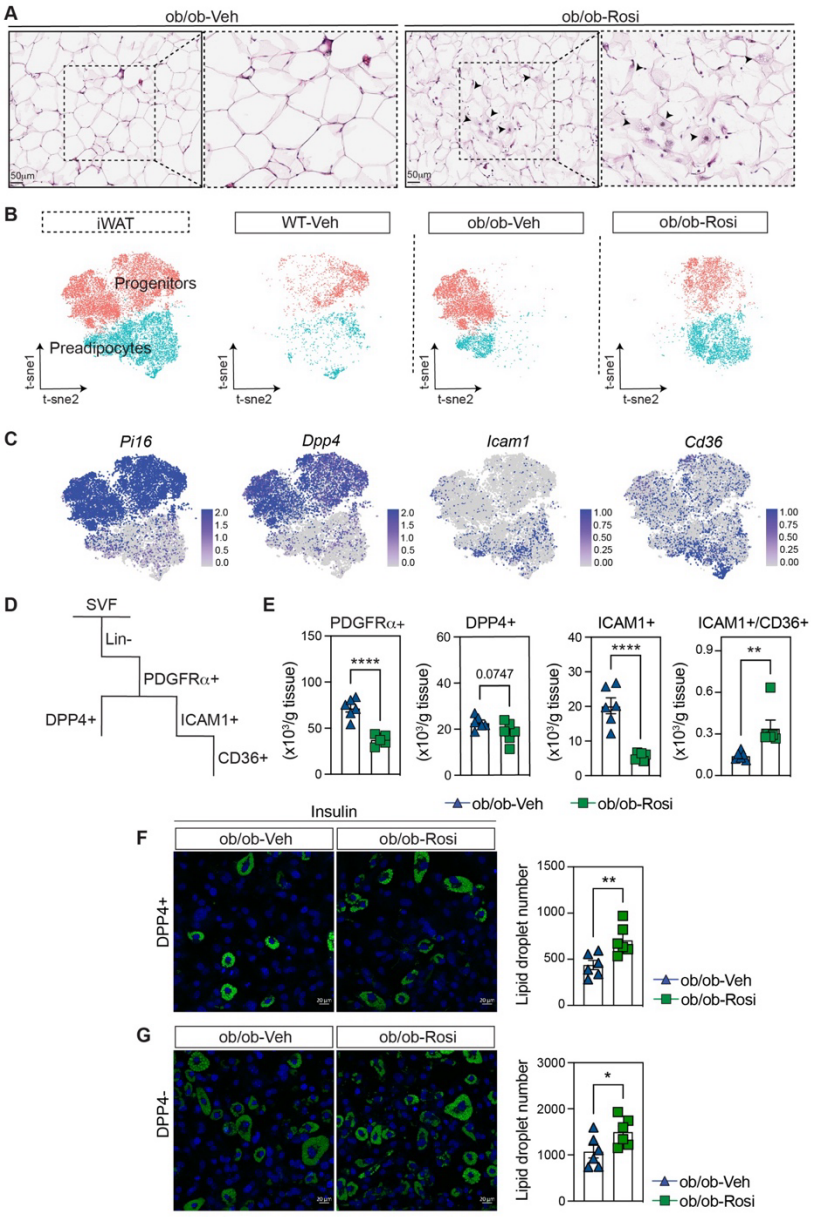

SFigure 4 Rosiglitazone-driven enhancement of adipocyte differentiation in inguinal adipose tissue.

(**A**) Histological analysis of inguinal adipose tissue (hematoxylin and eosin stain) from either ob/ob-Veh or ob/ob-Rosi mice. (**B**) t-distributed stochastic neighbor embedding (t-SNE) plot illustrates two sub-clusters of Adipocyte Precursor Cells (APC) in iWAT: Progenitors and preadipocytes. The right three panels separately represent cells from WT-Veh, ob/ob-Veh, and ob/ob-Rosi. Each color-coded dot represents a cell, with progenitors being represented by red and preadipocytes by cyan. The Louvain algorithm was utilized to determine cell clusters. (**C**) Individual gene t-SNE ploys showing the expression and distribution of representative marker genes: *Pi16* and *Dpp4* for progenitors, *Icam1* and *Cd36* for preadipocytes. (**D**) Gate strategy to characterize progenitor cells: Lineage negative (CD45-, CD31-), PDGFRα+, DPP4+ (progenitors), and ICAM1+/CD36+ (preadipocytes). (**E**) Absolute number of progenitor and preadipocytes from ob/ob-Veh and ob/ob-Rosi mice. (**F-G**) Confocal of sorted lineage negative (CD45-, CD31-), PDGFRα+, DPP4+, and DPP4- cells differentiated for 4 days on insulin-containing media, DAPI (nuclei-blue), LipidTox (neutral lipids-green). Data represent mean ± SEM (n = 3 mice per group). Confocal images: 4 wells per condition, 2 representative images per well were acquired. GP pvalue style: *p= 0.0332; **p < 0.0021; ***p < 0.0002 by two-tailed Student's t-test.

(PDGFRα+ and DPP4+) in the ob/ob-Rosi mice compared to ob/ob-Veh (**Fig9E, FigS4E, FigS5F-G**). Interestingly, we also observed a reduction in the preadipocytes ICAM1+ cells in the eWAT at frequency level (**FigS5F**) and in iWAT at both absolute number and frequency levels in ob/ob-Rosi mice (**FigS4E, FigS5G**). We then hypothesized that such reduction could reflect more differentiation of those progenitors/preadipocytes into fully mature fat cells. We subsequently gated those preadipocytes with CD36+ as a marker of a more differentiated preadipocyte. Even though the eWAT ICAM1+ cells did not show a significant change in the expression of CD36+ after Rosi treatment, we did observe an induction of expression in the iWAT cells (**Fig9E, FigS4E**). Such stronger response in the iWAT agrees with the previous literature showing a more robust response to rosiglitazone in this tissue (Soccio, Li et al. 2017).

To fully test the differentiation potential of those cells after the Rosi treatment we sorted the cells from mice acutely treated for three days with vehicle or Rosi into a culture plate. We hypothesized that those progenitor/preadipocyte cells would have an *ex-vivo* imprint towards a more committed adipogenic lineage. In order to have enough primary cells we used a simpler gating strategy: Lin-, PDGFRα+, DPP4+ (progenitors), and DPP4- (preadipocytes) to increase the number of cells sorted since those are very rare populations in obese mice (**Fig9E, FigS4E**). eWAT DPP4+ and DPP4- cells from ob/ob-Rosi mice both showed an increased adipocyte differentiation after 4 days in the complete differentiation media (dexamethasone, IBMX, and insulin - DMI) without any PPARγ agonist compared to ob/ob-Veh samples, reflecting an *ex-vivo* imprint in those cells towards the adipogenic lineage (**Fig9F-G**). iWAT DPP4+ and DPP4- cells from ob/ob-Rosi mice, however, showed a very high adipogenic capacity in the same media making it hard to precisely quantify lipid droplet number and size (**FigS6A-B**). Even though both populations of iWAT DPP4+ and DPP4- presented a trend towards more differentiation and smaller lipid droplets in the ob/ob-Rosi samples compared to ob/ob-Veh mice, we decided to replicate the same experiment in two additional conditions: (1) dexamethasone and insulin media

(DI), and (2) minimal media with insulin. In a similar way, iWAT DPP4+ and DPP4- cells from ob/ob-Rosi mice treated with DI media presented a trend towards more adipogenic differentiation compared to ob/ob-Veh cells (**FigS6C-D**). However, when we challenged iWAT DPP4+ and DPP4- cells from ob/ob-Rosi mice with a minimal media containing only insulin we observed a significant increase in adipocyte differentiation in both populations compared to DPP4+ and DPP4- cells from ob/ob-Veh mice (**FigS4F-G**).

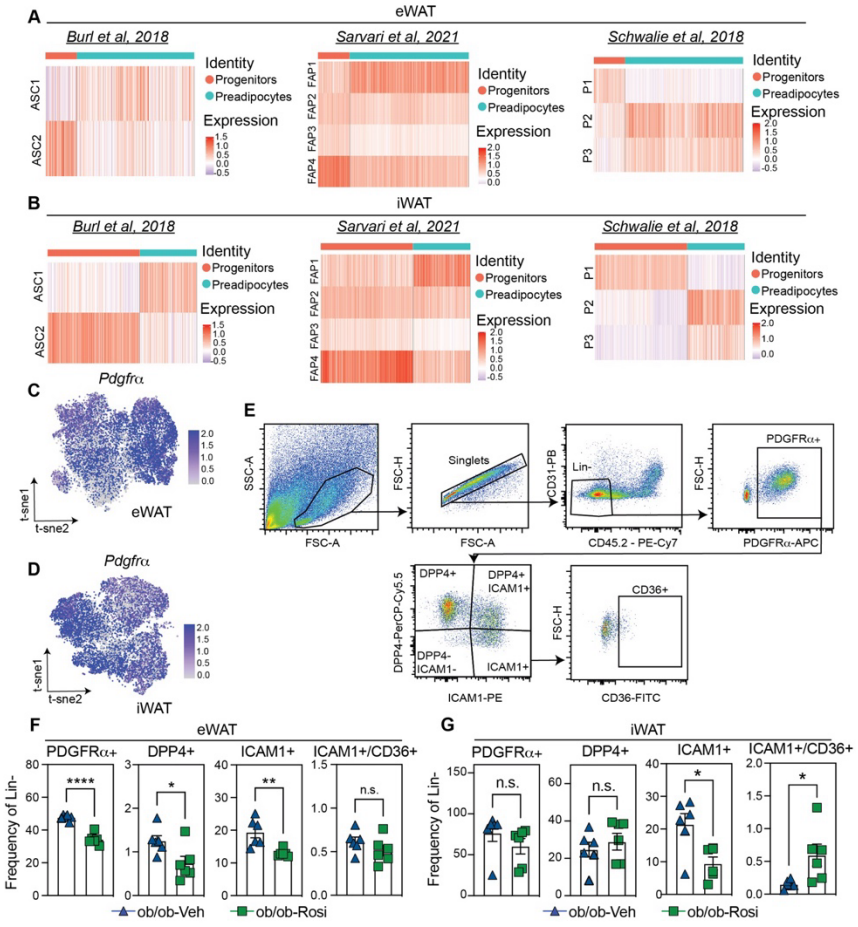

SFigure 5 Validation of progenitor and preadipocyte populations.

(A-B) Heatmap illustrates gene module scores within eWAT (**A**) and iWAT (**B**) cells by APC subtype identities. The gene module scores feature the top 50 significant markers from each reference cell type, as delineated in the research findings of Burl et al., Sarvari et al., and Schwalie et al. (**C-D**) t-SNE visualization visualizes the expression of Pdgfrα in eWAT and iWAT cells respectively. (**E**) Flow cytometry gate strategy for progenitors and preadipocytes: Lin- (CD45-, CD31-), PDGFRα+, DPP4+ (progenitors), and ICAM1+ and/or ICAM1+/CD36+ (preadipocytes). (**F-G**) Frequency of progenitors and preadipocytes from epididymal and inguinal adipose tissue. Data represent mean ± SEM (n = 6 mice per group). GP pvalue style: *p= 0.0332; **p < 0.0021; ***p < 0.0002 by two-tailed Student's t-test.

These data highlight the impressive capacity of Rosi to initiate a restructuring of the transcriptional network within progenitor/preadipocyte cells *in vivo*, as well as their ability to retain this enhancement in adipogenic commitment when cultured *in vitro*.

2.2.5 Rosiglitazone-dependent Remodeling of Specific Gene Networks in Adipocyte Progenitor Cells

To investigate how rosiglitazone promotes adipogenic capacity in progenitor/preadipocyte cells in eWAT and iWAT, we analyzed the obesity-associated gene sets being reversed after the treatment in the ob/ob mice (**Fig10**). First, we defined the obesity-associated gene sets as either downregulated or upregulated in obesity by comparing ob/ob-Veh versus WT-Veh mice. Next, we evaluated sets of genes as follows: (a) downregulated by Rosi (upregulated in ob/ob-Veh mice and now reversed in ob/ob-Rosi mice, blue outer circle), (b) upregulated by Rosi (downregulated in ob/ob-Veh mice and now reversed in ob/ob-Rosi mice, red outer circle), (c) sets of genes upregulated in both ob/ob-Veh and ob/ob Rosi groups, (d) sets of genes downregulated in both ob/ob-Veh and ob/ob Rosi groups, and (e) unique sets of genes that are regulated exclusively in each group but are not being reversed by the Rosi treatment (dark brown columns) (**Fig10A-D, FigS7- S8**).

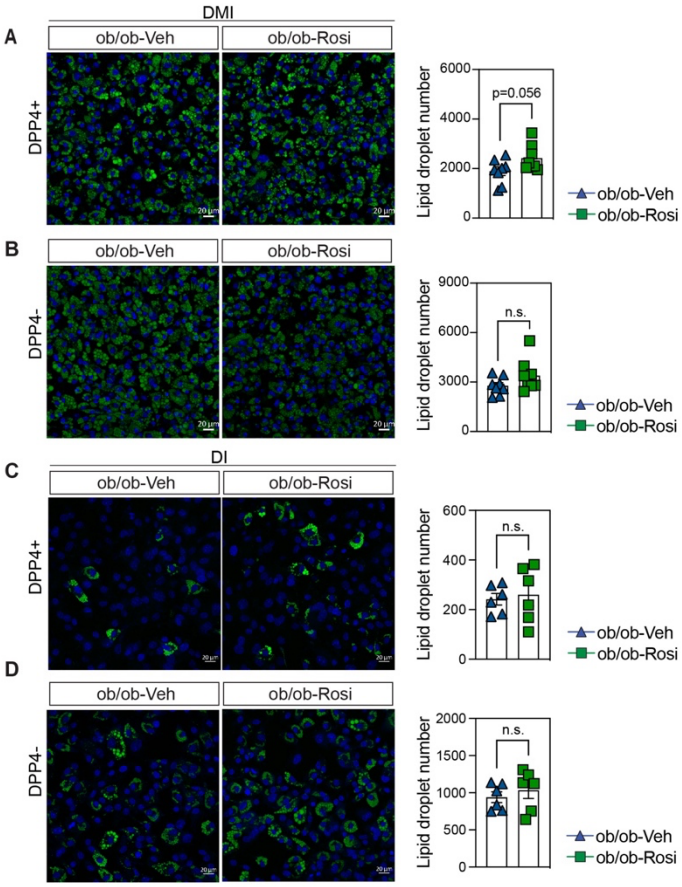

SFigure 6 Inguinal adipose tissue progenitors differentiation potential after rosiglitazone treatment.

(**A**-**D**) Confocal of sorted lineage negative (CD45-, CD31-), PDGFRα+, DPP4+, and DPP4- cells differentiated for 4 days on DMI (dexamethasone, IBMX, and insulin) media, DAPI (nuclei- blue), LipidTox (neutral lipids- green) (**A-B**). 4 days on DI (dexamethasone, and insulin) media, DAPI (nuclei- blue), LipidTox (neutral lipids- green) (**C-D**). Right panels: quantification of lipid droplet number. Data represent mean ± SEM (n = 3-6 mice per group). Confocal images: 4 wells per condition, 2 representative images per well were acquired. GP pvalue style: *p= 0.0332; **p < 0.0021; ***p < 0.0002 by two-tailed Student's t-test.

In general, Rosi treatment mainly decreased the upregulated obesity-associated genes in the eWAT progenitor/preadipocyte cells (**Fig10A-B**). In addition to that, eWAT progenitor and preadipocyte subclusters presented a very distinguishing profile. eWAT preadipocytes showed a bigger intersection size of reverted genes upregulated and downregulated by Rosi than the progenitor cells (**Fig10A-B**). These reversed pathways which were upregulated in obesity but downregulated by Rosi were enriched for inflammatory response processes such as the NFκB pathway (**Fig10E**).

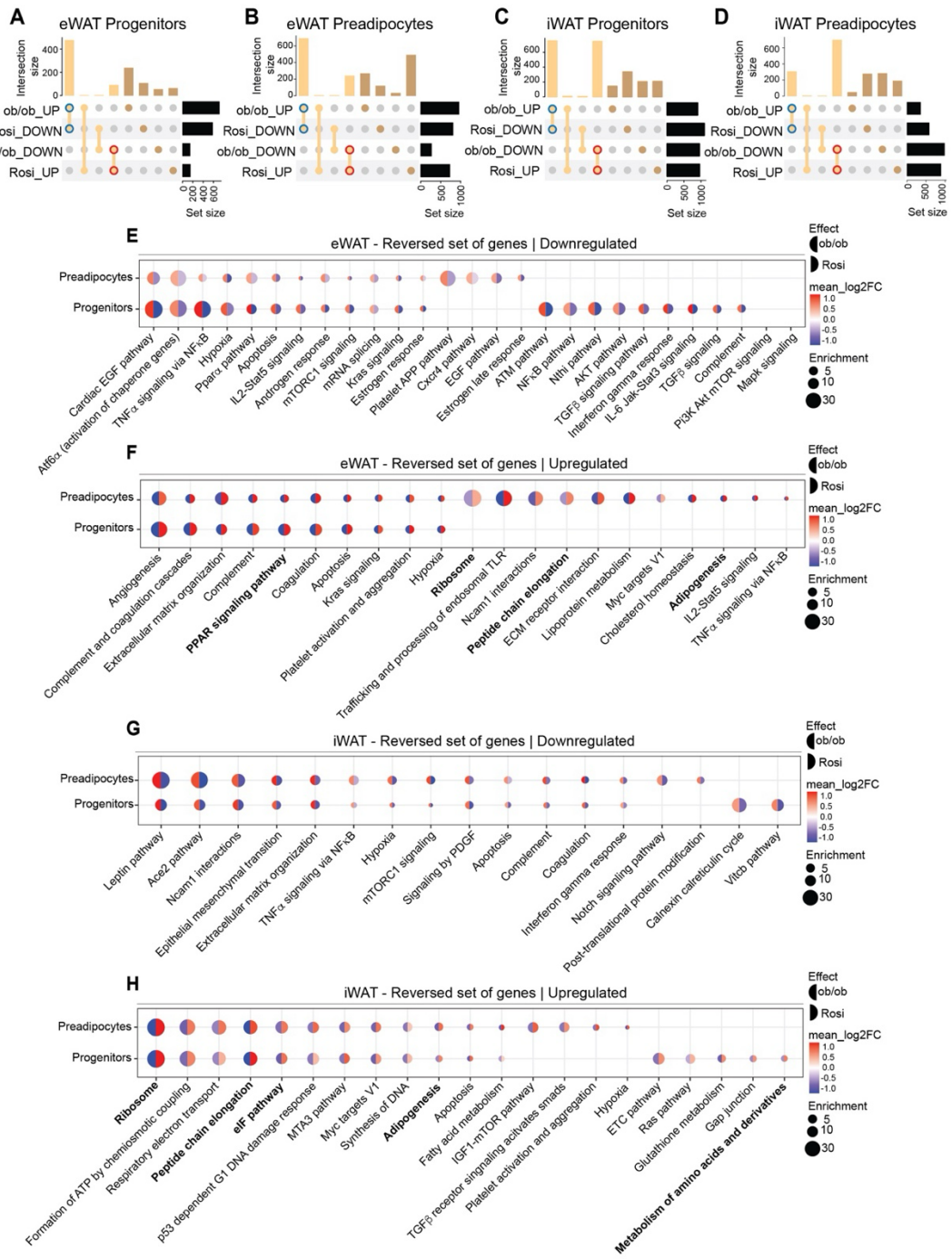

Figure 10 Comparison of differently expressed and enriched pathways in response to obesity and rosiglitazone treatment in the eWAT and iWAT.

(**A-D**) UpSet plot illustrates intersections of differentially expressed genes (DEGs) in 4 categories for the eWAT progenitors (**A**), eWAT preadipocytes (**B**), iWAT progenitors (**C**), and iWAT preadipocytes (**D**) all at a Bonferroni-adjusted p-value < 0.05. The 4 categories include upregulated DEGs in obese mice compared to lean mice (ob/ob_UP), downregulated DEGs in obese mice compared to lean mice (ob/ob_DOWN), up-regulated DEGs in response to Rosiglitazone treatment compared to ob/ob-Veh (Rosi_UP), and downregulated DEGs in response to Rosiglitazone treatment compared to ob/ob-Veh (Rosi_DOWN). Horizontal bars (set size) indicate total DEGs for each cluster in each plot. In the UpSet plots, dots point to the specific clusters for which the vertical bars for DEG counts are shown, and vertical lines between dots represent the intersections between two or more clusters. The blue circle

signifies the set of DEGs that are upregulated in obese mice and downregulated in response to rosiglitazone treatment. The red circle represents the DEGs that are downregulated in obese mice and upregulated following rosiglitazone treatment. (**E-H**) Dot plot illustrates the top enriched pathways in response to rosiglitazone treatment, which acts to reverse the effects of obesity. All pathways displayed meet the cut-off for statistical significance at Bonferroni corrected p values < 0.05. The size of each dot corresponds to the enrichment score for each pathway, reflecting the ratio of overlapping genes to total genes within the cell type-specific gene set, adjusted by a scale factor of 20,000, and then divided by the total number of genes within the pathway. Color of the left side of each dot represents the log2(fold-change), calculated based on the average fold change across all overlapping DEGs within a pathway in obese mice than in lean mice. Color of the right side of each dot represents the log2 (fold-change), calculated based on the average fold change across all overlapping DEGs within a pathway in response to rosiglitazone treatment. (**E**) Represented pathways enriched from DEGs that are downregulated in eWAT obese mice and upregulated following rosiglitazone treatment. (**F**) Represented pathways enriched from DEGs that are upregulated in eWAT obese mice and downregulated following rosiglitazone treatment. (**G**) Represented pathways enriched from DEGs that are downregulated in iWAT obese mice and upregulated following rosiglitazone treatment. (**H**) Represented pathways enriched from DEGs that are upregulated in iWAT obese mice and downregulated following rosiglitazone treatment.

Interestingly, eWAT progenitor cells had very unique downregulated pathways such as TGFβ signaling, conceivably reflecting a decrease in the progenitor fibro-inflammatory profile (**Fig10E**) (Sárvári, Van Hauwaert et al. 2021). In contrast, the reversed pathways that were downregulated in obesity but upregulated by Rosi were related to expected pathways such as PPAR signaling and adipogenesis pathways (**Fig10F**). Surprisingly, we also observed an increase in ribosome and peptide chain elongation pathways in the preadipocytes, potentially highlighting an enhancement in the translation machinery in those cells (**Fig10F**).

Unlike the eWAT, the iWAT progenitor/preadipocyte cells showed a different pattern in response to Rosi (**Fig10C-D**). In the iWAT progenitors, Rosi reversed similar numbers of up- and down-regulated obesity-associated genes. However, in the iWAT preadipocytes, Rosi mainly increased the down-regulated obesity-associated genes, which is opposite to the trend in eWAT preadipocytes where Rosi primarily inhibited the upregulated genes in obesity (**Fig 10A-D**). These data highlight a depot-dependent response to Rosi treatment in the progenitor and preadipocyte populations. At pathway level, similar to eWAT, iWAT progenitor/preadipocyte cells also showed a major decrease in inflammation in the reserved set of genes that were downregulated by Rosi, such as activation of complement and TNFα signaling via NFκB (**Fig10G**). Among the upregulated pathways by Rosi, we observed an increase in adipogenesis and fatty acid metabolism in both iWAT APC populations (**Fig10H**). In contrast to the eWAT cells, however, in the iWAT we observed more shared pathways between progenitors and preadipocytes both in the downregulated and upregulated sets (**Fig10E-H**). Interestingly, we again observed an

upregulation in the ribosome, peptide chain elongation, and now with the addition of the eukaryotic initiation factors (eIF) pathway in both iWAT progenitors and preadipocytes. Moreover, upstream regulators of translation such as metabolism of amino acids and mTOR signaling (Valvezan and Manning 2019) were also upregulated in the progenitor cells (**Fig10H**).

These results emphasized a potential uncharacterized role of PPARγ agonists in remodeling not only the transcription landscape in APCs but also the translation machinery to enhance translation efficiency.

2.2.6. Rosiglitazone-dependent Remodeling of the Transcriptional Landscape in Other Cell Populations in the Adipose Stromal Vascular Fraction

To fully access the effects of Rosi in the entire stromal vascular fraction of the eWAT and iWAT we analyzed all the cell populations identified in scRNASeq and examined all gene sets reversed in both upregulated and downregulated directions (**FigS7**, **FigS8**). For the eWAT cells (**FigS7**), we were able to assess all the nine populations: Macrophages (LAM, PLAM, NPVM, PVM), NKT cells, B lymphocyte Cells (BC), Neutrophils (NEU), Endothelial Cells (EC), and Smooth Muscle Cells (SMC). Overall, every single cell type had a unique profile of regulation, with cells described as potentially expressing PPARγ, such as macrophages, NKT, EC, and SMC having a very robust response to Rosi (Nagy, Tontonoz et al. 1998, Faveeuw, Fougeray et al. 2000, Gosset, Charbonnier et al. 2001, Padilla, Leung et al. 2002, Yang, Kim et al. 2013, Kotlinowski and Jozkowicz 2016) (**FigS7A-E, FigS7H-I**). The only exceptions were the BCs and NEUs that had a very small gene intersection between genes altered in obesity and those being modulated by Rosi (**FigS7F, FigS7G**). In a similar manner to the eWAT progenitors/preadipocytes, the rest of the stromal vascular fraction also had a more robust Rosi response towards the downregulation of genes previously upregulated in the ob/ob-Veh mice (**FigS7A-I**). Collectively, the downregulated pathways involved several inflammatory and fibrosis

pathways, with pathways such as IL-7 being reversed uniquely in the NKT cells (**FigS7J**). These results emphasized a shift towards a less inflammatory microenvironment in the eWAT after Rosi treatment. The upregulated pathways by Rosi again included the ribosome pathway as shown in the progenitors/preadipocytes, highlighting a remodeling in the translation machinery in the entire stromal vascular fraction. In addition, Rosi treatment upregulated pathways such as cholesterol metabolism and respiratory electron chain transport (ECT) in the macrophages (PLAM, NPVM, PVM) and NKT cells, and also uniquely upregulated glycolysis and peroxisomes pathways in the PLAM cells (**FigS7K**).

Similar to the iWAT progenitors/preadipocytes, iWAT stromal cells had a strong upregulation by Rosi of genes downregulated in obesity, which is opposite to the eWAT cells in general (**FigS7-8**). We were able to analyze seven populations: Macrophages (LAM, NPVM, PVM), NKT cells, B lymphocyte Cells (BC), Dendritic Cells (DC), and Endothelial Cells (EC). The only population we were not able to assess the Rosi response was the neutrophils due to a low number of genes being reversed by Rosi (**FigS8A-G**). The upregulated pathways by Rosi included anabolic pathways such as the ribosome, peptide chain elongation, and synthesis of DNA, as well as the ECT pathway, fatty acid metabolism, and cholesterol homeostasis across cell types. Cell-type specific pathways were also observed, such as increased lysosomes and glycolysis in LAM macrophages (**FigS8I**). There were fewer downregulated pathways by Rosi as expected since fewer upregulated genes in obesity were downregulated by Rosi. These included inflammation, extracellular matrix organization, and hypoxia pathways and were shared by multiple cell types such as macrophages (NPVM, PVM), NKT cells, and EC (**FigS8H**).

In summary, Rosi treatment remodeled the transcriptome of the entire stromal vascular fraction in a depot-specific specific manner.

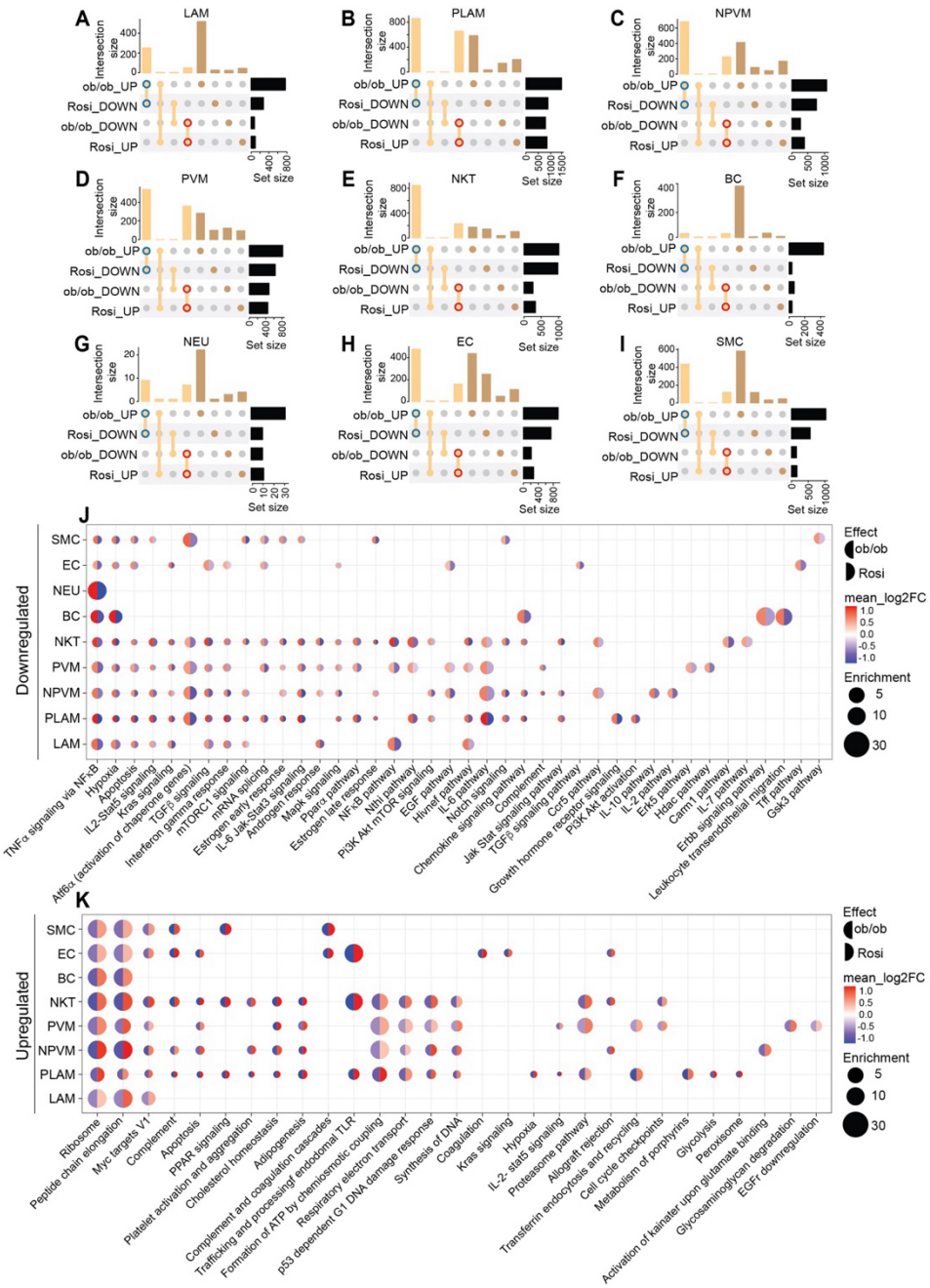

SFigure 7 Effects of rosiglitazone treatment in the stromal vascular fraction of epididymal adipose tissue.

(**A**-**I**) UpSet plot illustrates intersections of DEGs for the cell types in eWAT. (**J**-**K**) Dot plot illustrates the top enriched pathways in response to rosiglitazone treatment in each cell type, which acts to reverse the effects of obesity. (**J**) represent pathways enriched from DEGs that are downregulated in obese mice and upregulated following rosiglitazone treatment. (**K**) represent pathways enriched from DEGs that are upregulated in obese mice and downregulated following rosiglitazone treatment.

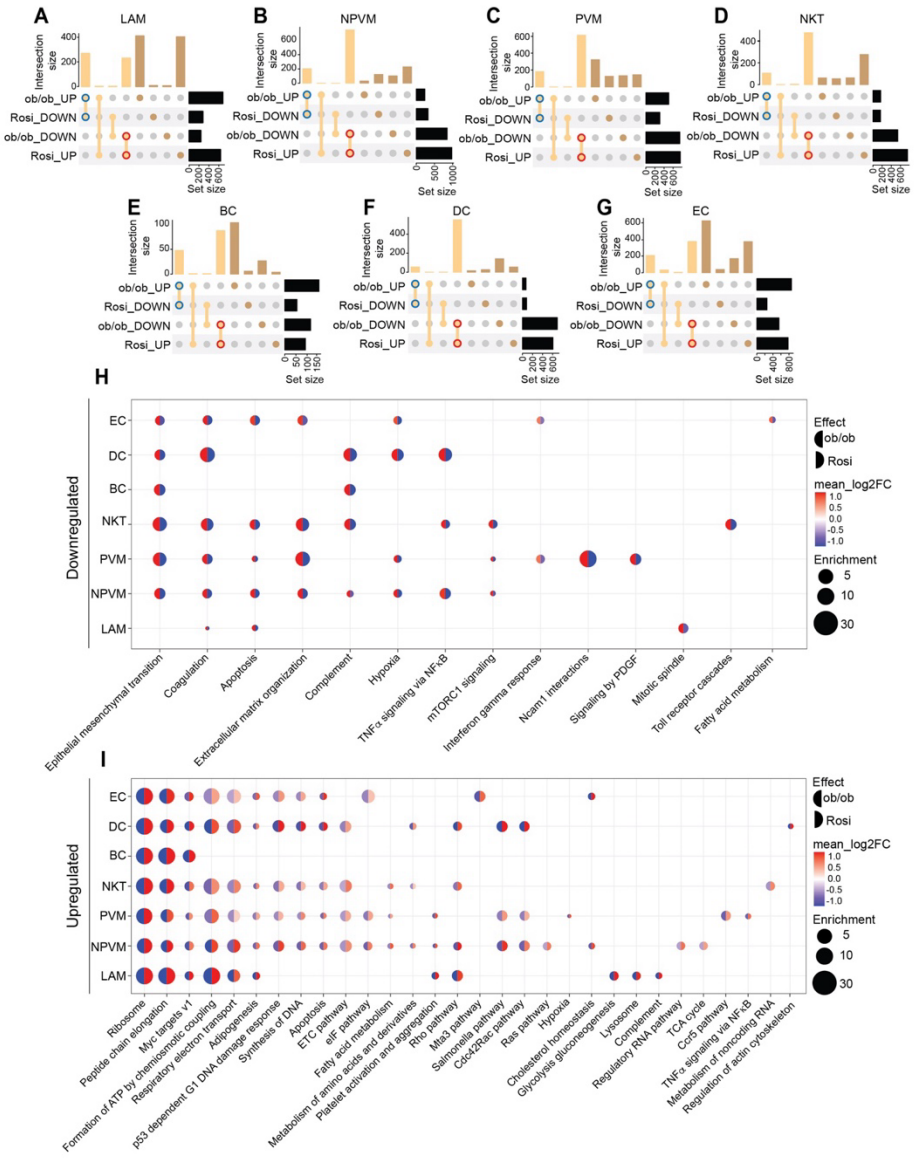

SFigure 8 Effects of rosiglitazone treatment in the stromal vascular fraction of inguinal adipose tissue.

(**A-G**) UpSet plot illustrates intersections of DEGs for the cell types in iWAT. (**H-I**) Dot plot illustrates the top enriched pathways in response to rosiglitazone treatment in each cell type, which act to reverse the effects of obesity. (**H**) represent pathways enriched from DEGs that are downregulated in obese mice and upregulated following rosiglitazone treatment. Conversely, (**I**) represents pathways enriched from DEGs that are upregulated in obese mice and downregulated following rosiglitazone treatment.

2.2.7. Induction of Ribosomal Transcriptional Signature with PPARγ Agonist Treatment in Adipocyte Progenitor Cells

Since we observed a potential uncharacterized role of PPARγ agonists in remodeling not only the transcription landscape in the adipose cells, but also the translation machinery, we further mechanistically characterized the progenitors/preadipocyte cells to understand how Rosi was changing the ribosomal transcriptional signature. Among the genes related to ribosome homeostasis that were modulated by Rosi (**Fig11A**), iWAT progenitors and preadipocyte cells from ob/ob-Rosi mice had a robust upregulation of several small ribosomal (Rps) and large ribosomal (Rpl) transcripts (lanes 4 and 8) compared to ob/ob-Veh mice (**Fig11A**). In contrast, the eWAT ob/ob-Rosi samples had a major upregulation of ribosome genes mainly in the preadipocyte population compared to eWAT ob/ob-Veh mice (lanes 2 and 6) (**Fig11A**), likely reflecting the increase in protein synthesis necessary for final adipocyte differentiation.

The induction of ribosomal gene expression suggested that some of these genes have binding sites for PPARγ. Therefore, we accessed and re-analyzed a publicly available PPARγ ChIP-Seq dataset with a similar study design to ours (Siersbæk, Loft et al. 2012) to evaluate PPARγ binding sites near those targets. This ChIP-Seq study isolated stromal vascular fraction from BAT, eWAT, and iWAT, and differentiated the cells *in vitro* for nine days using insulin and Rosi. Re-analysis of this dataset revealed a total of 41 PPARγ binding sites in the eWAT and 24 PPARγ binding sites in the iWAT that are located either at proximal sites to certain ribosome genes such as on *Rpl23a* and *Rps3a1* or at more distant sites of select ribosome genes such as *Rpl11*, *Rpl19*, *Rps14,* and *Rps27a* (**Fig11B**). These results emphasize a potential novel role of PPARγ in the direct regulation of ribosomal targets and potentially translation.

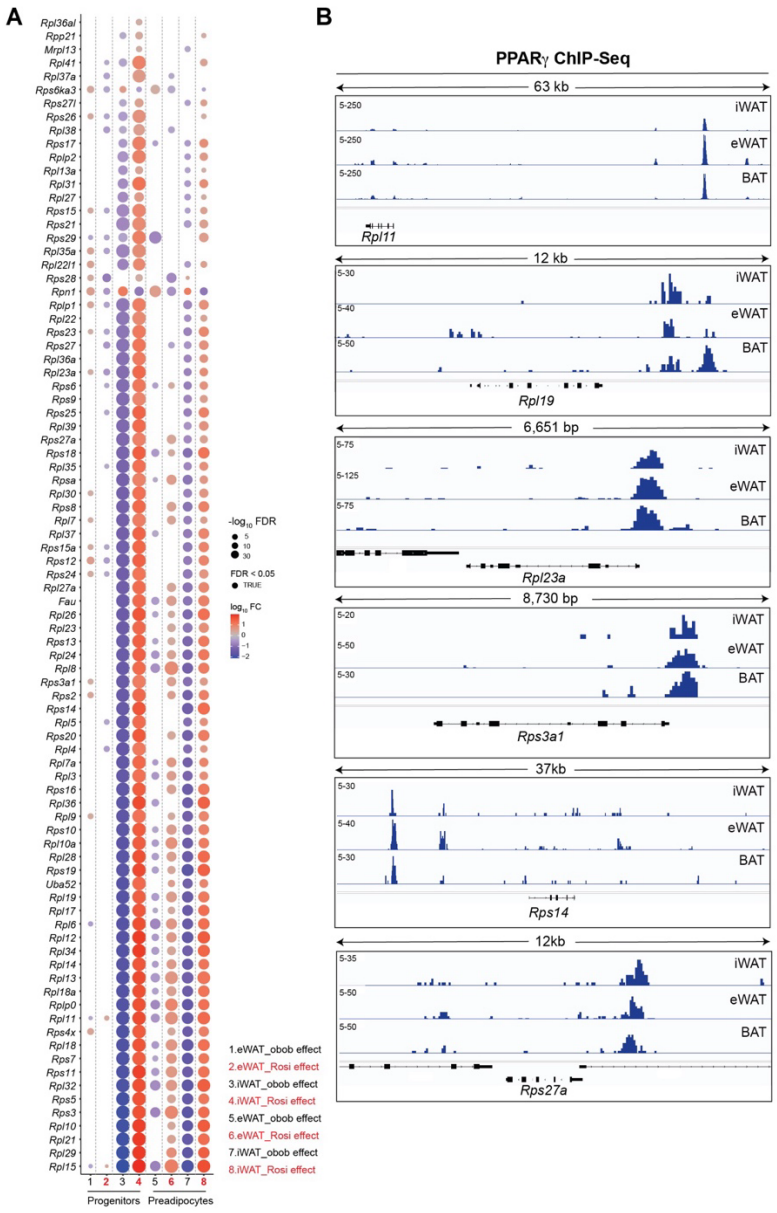

Figure 11 PPARγ-driven enhancement in the transcriptional network of ribosomal genes.

(**A**) Dot plot showing differentially expressed ribosomal genes influenced by the ob/ob effect or Rosi effect in eWAT and iWAT progenitors or preadipocytes all at a Bonferroni- adjusted p-value < 0.05. The size of the dots reflects the -log10(FDR) of the DEGs and the color of the dots reflects the fold change of the DEGs. (**B**) Visualization of peaks of PPARγ binding sites in ribosomal genes: *Rpl11, Rpl19, Rpl23a, Rps3a1, Rps14,* and *Rps27a* in eWAT, iWAT and BAT.

2.2.8. Adipocyte-Specific Translational Selectivity Induced by Rosiglitazone

Plasticity is one of the main hallmarks of the adipose tissue. Fat depots can be remodeled to attend to the needs of the host by increasing storage or catabolic process, differentiating or de-differentiating to accommodate different biological and environmental stressors among other processes (Sakers, De Siqueira et al. 2022). Adipogenesis, for instance, is one of these processes, and it involves the commitment of progenitor cells to the fat cell lineage and subsequent transcription and translation of adipocyte-specific mRNA networks (Siersbæk, Nielsen et al. 2012). The major organelle orchestrating this process are the ribosomes. They are central organelles in translation, very dynamic, heterogenic, and with a fast turnover in eukaryotes (Guo 2018). Recent studies have shown significant heterogeneity of ribosomes (Shi, Fujii et al. 2017), ribosome-mediated specificity (Li, Huo et al. 2022), 5' UTRs functional structures directing translation (Leppek, Das et al. 2018), and post-translational modifications (Spitale, Flynn et al. 2015, Lin, Choe et al. 2016). However, how this process is regulated in the context of obesity or type 2 diabetes is poorly understood. Based on our scRNASeq and ChIP-Seq analysis results we hypothesized that PPARγ drives not only the expression of fat-specific genes but also the expression of several ribosomal genes to build up the machinery necessary for cellular specialization.

To understand the role of PPARγ agonists on translation, we first measured *in vivo* protein synthesis in the adipose tissue using the Surface-Sensing of Translation (SUnSET) assay (**Fig12A**). Briefly, mice received an injection of puromycin, which is a structural analog of tyrosyl-tRNA. Consequently, newly produced proteins would bear a peptide tagged with puromycin. After one hour of conscious labeling, protein synthesis efficiency was evaluated by immunoblot using an antibody that detects puromycin. eWAT and iWAT puromycilation showed an increase in protein synthesis in the ob/ob-Rosi treated mice when compared to ob/ob-Veh treated mice (**Fig12B**).

Nex, to characterized if the remodeling in the ribosome-related pathways had an impact in translation and to understand which mRNA networks were differentially translated in response to Rosi, we carried out polysome profiling followed by sequencing. Briefly, primary SVF from ob/ob mice was differentiated with either DMI-Veh or DMI-Rosi for four days *in vitro* (to mimic the *in vivo* Rosi treatment). Polysomes from eWAT SVF of ob/ob-Veh and ob/ob-Rosi at day 4 of differentiation were found to be similar in both eWAT (**Fig12C**) and iWAT (**FigS9A**). Subsequently, we conducted polysome sequencing on eWAT SVF to profile highly translated mRNAs. This choice was driven by eWAT's (a) robust tissue environment remodeling after Rosi treatment (**Fig7G-8B**); (b) substantial difference in *ex-vivo* adipogenesis between Veh and Rosi; coupled with (c) its comparatively less understood response to Rosi relative to iWAT. Briefly, input total RNA (control samples) and mRNA from polysome fractions containing more than 3 ribosomes, were extracted and sequenced (**Fig12D**). To reflect transcriptional alterations in response to Rosi treatment, we first performed differential gene expression analysis on the

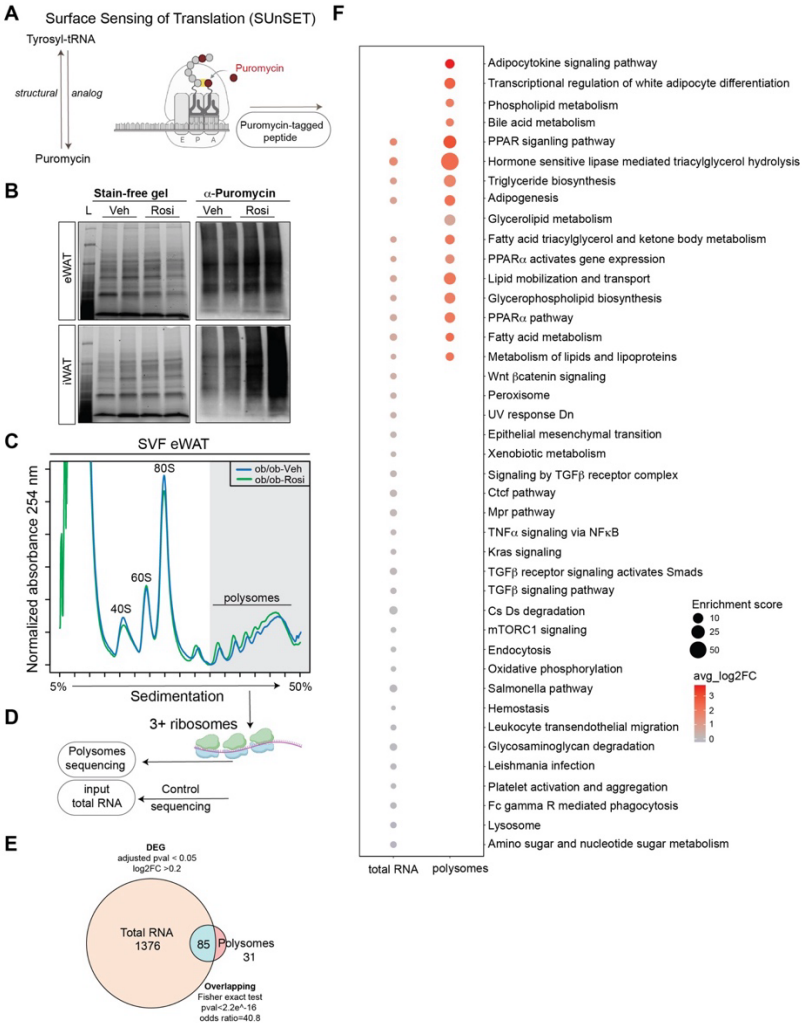

Figure 12 PPARγ-driven translation selectivity.

(**A**) Surface Sensing of Translation (SUnSET) scheme. Puromycin is used as a tyrosyl-tRNA analog therefore being incorporated in the newly synthesized proteins during translation (puromycin-tagged peptide). (**B**) Immunoblots of eWAT and iWAT. Left panel: total protein in stain-free gel. Right-panel: immunoblot anti-puromycin. (**C**) Polysome profile of primary stromal vascular fraction (SVF) of eWAT after four days of adipocyte differentiation. (**D**) Experimental design for the polysome sequencing: fractions containing more than 3 ribosomes were pooled together for RNA extraction and sequencing. Control samples: input total RNA before samples were submitted to polysome fractionation. (**E**) Venn Diagram illustrates the intersection of DEGs derived from total RNA sequencing and polysome sequencing. Both sets of DEGs satisfy the criteria of an adjusted p-value less than 0.05 and a log2 (fold-change) greater than 0.2. The significance of overlap was assessed using Fisher's exact test. (**F**) Dot Plot visualizing the significant pathways that are enriched within the total RNA sequencing DEG set and polysome sequencing DEG set considering all pathways at a Bonferroni-adjusted p-value < 0.05. The size of each dot corresponds to the enrichment score for each pathway, reflecting the ratio of overlapping genes to total genes within the cell type-specific gene set, adjusted by total number of genes detected by total RNA sequencing or polysome sequencing. Dot color represents the log2 (fold-change), calculated based on the average fold change across all overlapping genes within a pathway.

mRNA-seq dataset derived from the polysome fractions between the ob/ob-Rosi group and the ob/ob-Veh group. For comparison and to reflect overall transcriptional changes, differential gene expression analysis was also carried out on the total RNA-seq dataset. In both datasets, genes

satisfying the criteria of an adjusted p-value below 0.05 and a log2 (fold change) exceeding 0.2 were designated as differentially expressed. Surprisingly, we observed a huge translational buffering response in the polysomes, as reflected by the identification of >1400 DEGs from the total RNA-seq but only 116 DEGs from the polysome fraction. Translational buffering opposes the impact of alterations in mRNA levels on the proteome by compensating, equilibrating, and offsetting the translation (Kusnadi, Timpone et al. 2022) (**Fig12E**). Such response was expected since our treatment involved a transcriptional factor agonist causing a major enhancement in gene expression. From the 116 DEG identified in the polysome fraction, 85 are shared with those that are transcriptionally induced by Rosi. Finally, we characterized the enriched pathways among the 85 transcripts being translated versus the ones being buffered. Among the pathways enriched in the DEGs identified from total RNA-seq (input) are lysosomes, immune response (TNFα, TGFβ), and oxidative phosphorylation pathways (**Fig12F**). In contrast, DEGs being highly translated in the polysome fraction were enriched for more selective pathways pertaining to adipocyte functions including adipokine signaling pathway, triglyceride biosynthesis, and adipogenesis (**Fig12F**). These results highlight how eWAT switches its translatome from inflammatory pathways to a metabolic/adipogenic profile after Rosi treatment.

To validate the above findings from eWAT SVF, we also examined the response in the primary SVF cells in the iWAT (**FigS9A-B**). We selected the highly ranked targets based on the degree of change between groups (log2FC), which included several fat-specific genes such as *Adipoq, Arxes1, Fabp4, Plin1,* and *Aqp7*. We measured differences in these genes by quantitative real-time PCR in both the isolated polysome fraction and the total input RNA from both EWAT and iWAT (**FigS9C-D**). Surprisingly we found unique patterns of selectivity in the eWAT SVF, with *Adipoq, Arxes1*, and *Fabp4* presenting higher expression in the polysome fraction than in the total RNA, highlighting robust translational induction, whereas *Plin1* and *Aqp7* showing a more modest trend (**FigS9C**). In contrast, the iWAT SVF presented a similar pattern of higher polysome

occupancy for all those targets, emphasizing a fat-depot specialization in response to Rosi (**FigS9D**) and potentially explaining its stronger response to Rosi.

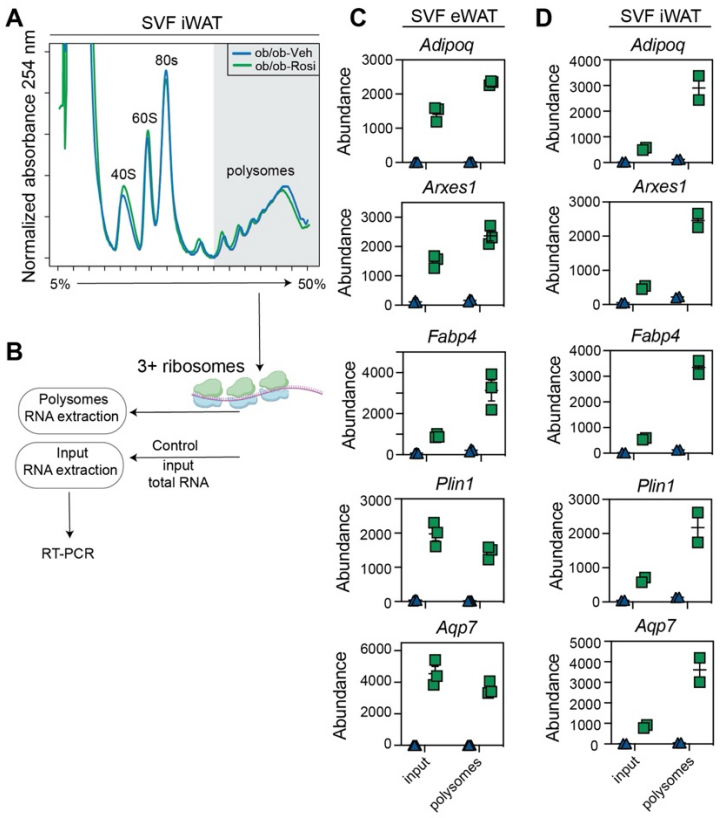

SFigure 9 Adipose-specific polysome profile.

(**A**) Polysome profile of primary stromal vascular fraction (SVF) of iWAT after four days of adipocyte differentiation. (**B**) Experimental design for the RT-PCR: fractions containing more than 3 ribosomes were pooled together for RNA extraction and cDNA synthesis. Control samples: input total RNA before samples were submitted to polysome fractionation. (**C-D**) Gene expression of *Adipoq, Arxes1, Fabp4, Plin1*, and *Aqp7* in the input (total RNA) vs polysomes in eWAT and iWAT (eWAT polysomes: triplicates, iWAT polysomes: duplicates).

Together, these studies highlight an unexplored role for PPARγ in driving the expression of defined ribosomal transcripts that are essential for cellular specialization and translational regulation of select mRNAs important for adipose tissue homeostasis.

2.2.9. Structural Modifications in the 5' Untranslated Region Induced by Rosi Treatment

Translation is a predominant process for protein synthesis that regulates the global level of gene expression products (Gebauer and Hentze 2004). To analyze the translation efficiency and confirm the hypothesized enhancement by Rosi we re-analyzed the polysome sequencing data now focusing on the transcripts level instead of gene level. Analyses conducted at the transcript level can thus identify different sequences within various isoforms. We first systematically identified the transcripts with differential translation efficiency (DTETs) with normalization of the total RNA abundance in polysome fractions (**Fig13A, see Methods** (Chothani, Adami et al. 2019)). A total of 135 transcripts were defined as being upregulated by Rosi and 206 as being downregulated (**Fig13B**). Intriguingly, upregulated transcripts were not necessarily direct targets of PPARγ (**Fig13B**), highlighting an enhancement in translation efficiency independent of the increase in gene expression caused by the PPARγ-agonist treatment. Notably, one of the isoforms of *Pnpla2* (ENSMUST00000169665) was identified as one of the translationally upregulated targets after Rosi treatment (**Fig13C**). *Pnpla2* encodes for adipose triglyceride lipase (ATGL), a pivotal enzyme in triglycerides hydrolyses. ATGL initiates adipose lipolysis by the breakdown of triglycerides into diacylglycerol (DAG) and free fatty acid (FFA) (Liu, Purushotham et al. 2009). Therefore, this data highlights a significant and novel Rosi-induced remodeling in the translation efficiency of crucial adipose mRNA networks.

Next, we decided to delve into potential mechanisms driving this Rosi-dependent translation efficiency. Translation rates are controlled by various processes, with the initiation stage playing a predominant role. There are several primary sequences or secondary structures in the context of 5' untranslated regions (5'UTR) that could serve as modulators of translation initiation (Leppek, Das et al. 2018). Thus, we further decided to analyze the sequence and structure in the 5'UTR of the transcripts being upregulated by Rosi to see if there was a common feature between them. First, we extracted the hexamers in up- and down-regulated transcripts and identified highly enriched hexamers using k-mer enrichment analysis (**Fig13A**). Interestingly,

we found that the 5'UTR of Rosi-upregulated transcripts contain guanine (G)-rich sequences (**Fig13D**), which are capable of forming G-quadruplexes (G4) and other secondary structures that serve as roadblocks in the translation process (Rhodes and Lipps 2015). Secondary structures such as G4 can impact the ability of the initiation machinery to scan the untranslated region in order to identify the start codon (Dumas, Herviou et al. 2021). For instance, DNA G4 structures are lost during stem cell differentiation to drive cellular specialization by enhancing translation (Zyner, Simeone et al. 2022). Furthermore, the modulation of certain RNA-binding proteins (RBPs) acts as a regulatory mechanism, impeding the formation of G quadruplex structures. Specifically, RBPs such as CNBP/ZNF9 can recognize G-rich elements within the mRNA coding region, thereby facilitating translation (Benhalevy, Gupta et al. 2017).

Next, to verify if the enrichment scores were robust when choosing different background sets, we calculated the correlations of the hexamers' enrichment scores and observed strong correlations (**FigS10A**). Additionally, we also performed the same analysis in coding regions

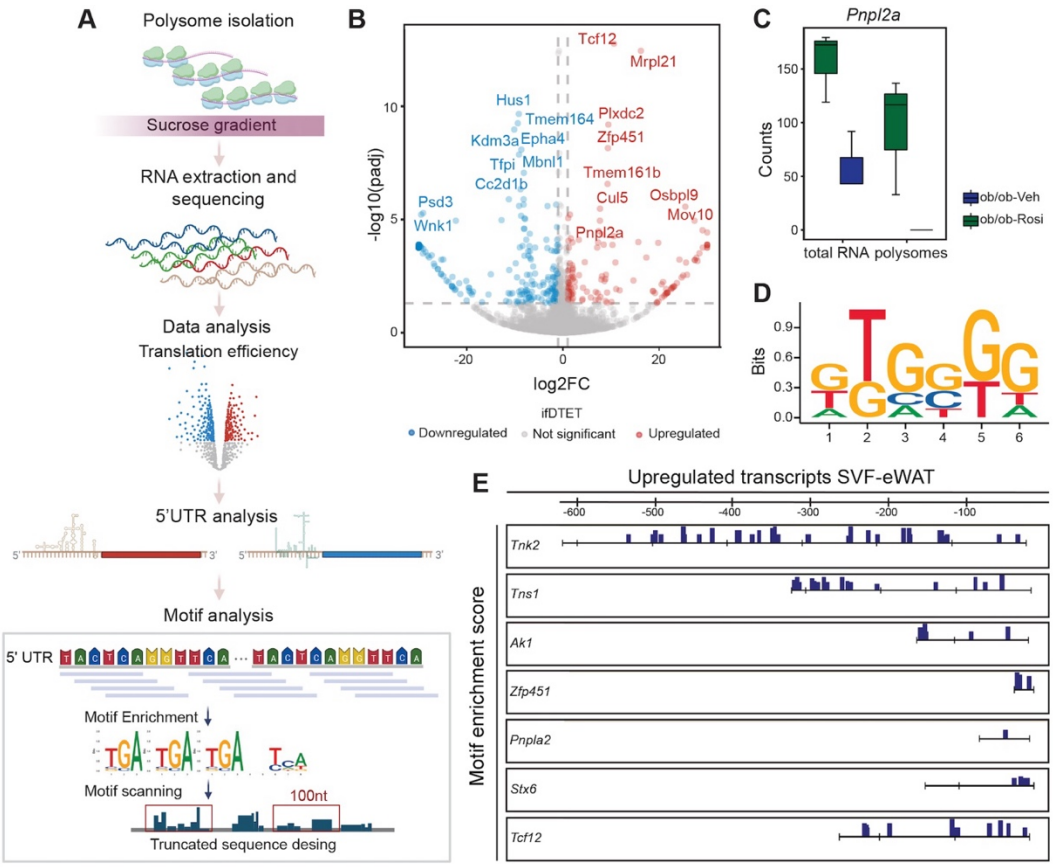

Figure 13 Translation regulation of rosiglitazone via the G-rich motifs in 5'UTR.

(**A**) Schematic overview of polysome profiling and sequence feature analysis in 5'UTR under acute rosiglitazone treatment. (**B**) Volcano plot illustrates the differentially translated transcripts between rosiglitazone and vehicle treatment. The X-axis shows the log2 transformed fold change, while the Y-axis shows the adjusted p-value. The red and blue dots label the up- and down-regulated transcripts separately. (**C**) Boxplot shows the normalized reads count on *Pnpla2* transcript between different treatments (rosiglitazone in red box and vehicle in blue box) in polysome fractions and total RNA. (**D**) Sequence motif enriched in the 5'UTR of up-regulated transcripts. (**E**) The feature map of the 5'UTR in some interesting up-regulated transcripts. Each deep blue bar indicates each significant site under the p-value lower than 0.05 calculated by the scan-matrix program.

(CDS) and 3' untranslated regions (3'UTR) and found notable differences between these different regions (**FigS10A**). The enriched hexamers in the CDS of Rosi-upregulated transcripts showed a strong AG-rich motif, whereas the motif in the 3'UTR was U-rich (**FigS10B-C**), highlighting the diverse translation regulation in different RNA regions. We then focused on the 5' untranslated regions (5'UTR), since it is well-established that secondary structures in mRNAs are essential to regulate translation initiation (Jia, Mao et al. 2020). We decided to characterize the transcripts containing this G-rich motif in the upregulated targets (**Fig13A, see Methods**). We did identify several transcripts presenting the G-rich motif in 5'UTR (**FigS10D**). Remarkably, we found several

zinc fingers containing transcripts such as *Zfp451, Zfp292, Zfp932, Zfp825, Zfp131, Zfp654, Zfp516* (**Fig13E- FigS10D**). *Zfp451* and *Zfp516* in particular are directly involved in driving stem cell differentiation and activation of UCP1 expression, respectively (Dempersmier, Sambeat et al. 2015, Antonio Urrutia, Ramachandran et al. 2021). Additionally, *Syntaxin 6* (*Stx6*), *Tensin 1* (*Tns1*), *Periostin* (*Post*), and *Pnpla2* (coding for ATGL) were directly involved in adipose-specific processes such as Glut4 trafficking (Perera, Clarke et al. 2003), cell-cell interactions (Bäckdahl, Franzén et al. 2021), and lipid metabolism (Liu, Purushotham et al. 2009, Graja, Garcia-Carrizo et al. 2018).

In conclusion, these studies emphasize a prospect new role of Rosi enhancing the translation of transcripts with G-rich 5'UTRs in a PPARγ-independent manner. These results shed light on a long-unanswered question of how Rosi remodels the adipose SVF independent of PPARγ. Mechanistically, these unique sequence features, which are capable to form G4 structures, exhibit diverse functions, from fine-tuning the translation of specific mRNAs to acting as molecular switches in response to various cellular cues, such as adipogenesis. Understanding the nuances of G-rich motifs-mediated regulation provides insights into the complexity of adipose cellular processes and may hold the key to unlocking new strategies for optimizing gene expression and protein synthesis in adipose tissue health and disease.

2.3 Discussion

Adipose tissue dysfunction represents a distinct risk factor for the development of type 2 diabetes. In particular, the enlargement of adipocytes (known as adipocyte hypertrophy) plays a pivotal role in disrupting metabolic adaptability. While adipose tissue has the capacity to expand, there is a finite threshold beyond which excess lipids can spill over into the bloodstream, contributing to the onset of metabolic syndrome (Unger 2003, Wang, Grayburn et al. 2008, Johnson and Olefsky 2013, Spalding, Bernard et al. 2017). The utilization of thiazolidinediones

as an antidiabetic treatment stimulates the production of new adipocytes, diminishes inflammation, and enhances metabolic adaptability. Notably, rosiglitazone stands out as a potent agent that bolsters insulin sensitivity in peripheral tissues, including both muscle and adipose tissue (Lebovitz 2019). Our data has indeed highlighted the acute and strong effects of Rosi normalizing glucose metabolism, but more importantly, we found enhanced glucose uptake in several tissues including the brain, heart, muscle, liver, and adipose tissue, providing an *in vivo* atlas of tissues involved in improving glucose homeostasis (**Fig7-FigS1**). While the rosiglitazone effect in the adipose tissue has been described, the precise mechanisms underlying the SVF remodeling in fat depots and the depot-specific response have not been completely elucidated.

Our data has provided for the first time a reference guide at single-cell levels of how cells respond to Rosi during obesity in the adipose tissue. As a potent anti-diabetic drug, Rosi has great clinical significance and interest. Therefore, understanding its PPARγ-dependent and independent actions will provide a unique source for the metabolic scientific community. We found extensive remodeling of almost all cell types in the SVF of both eWAT and iWAT. As previously described the macrophages highly respond to the obesity phenotype and also to the rosiglitazone treatment. We have shown a reduction of peri-vascular macrophage population at single cell level in obese mice (**Fig8B-C**), and a rapid response (decrease) of lipid-laden/inflammatory macrophages after rosiglitazone treatment in obese mice (**FigS3C-F**). The decrease of inflammatory cells is a remarkable function of Rosi, and it is essential to restore the immune tonus in the adipose tissue. In addition, to the macrophages, endothelial cells were also remodeled in the context of obesity, shown as a reduction in the ob/ob mice compared to lean-WT mice, and being restored by Rosi in both tissues (**Fig8B-C**). Ultimately, across the cell types, Rosi enhanced PPAR signaling and translation pathways but reduced inflammatory pathways. Numerous PPARγ targets are among the differentially expressed genes altered by Rosi treatment.

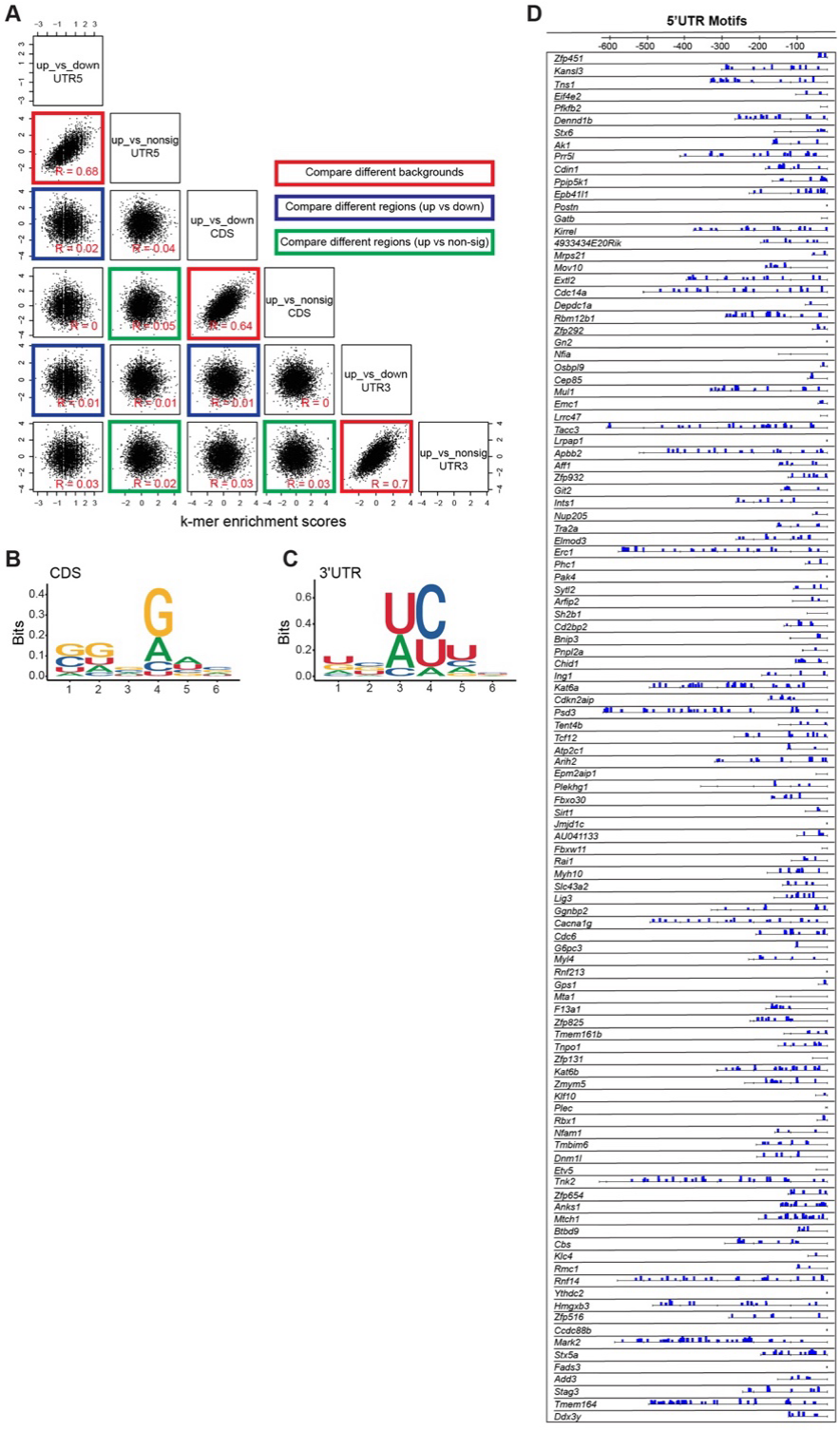

SFigure 10 Motif analysis of the 5'UTR of up-regulated transcripts under the regulation of rosiglitazone.

(**A**) The correlations of the hexamers enrichment scores between different regions (i.e., 5'UTR, CDS, and 3'UTR) or background choices regions (i.e., down-regulated transcripts and non-significantly expressed transcripts). The scatter plots in deep orange squares highlight the correlations between different background choices during motif enrichment analysis (the X-axis represents the enrichment z-scores calculated using down-regulated transcripts as background, while the Y-axis represents the enrichment z-scores calculated using non-significantly expressed transcripts as background). The scatter plots in deep green squares highlight the correlations between different regions, the hexamer enrichment z-scores of which are calculated using non-significantly expressed transcripts as background. The scatter plots in deep blue squares highlight the correlations between different regions, the hexamer enrichment z-scores of which are calculated using down-regulated transcripts as background. (**B**) Sequence motif enriched in the CDS of up-regulated transcripts. (**C**) Sequence motif enriched in the 3'UTR of up-regulated transcripts. (**D**) The feature map of the 5'UTR in all up-regulated transcripts. Each deep blue bar indicates each significant site under the p-value lower than 0.05 calculated by the scan-matrix program.

Most significantly, we have compared and contrasted those responses in the eWAT and iWAT (**Fig10** & **FigS7-8)**. iWAT presented a robust response to Rosi by upregulating numerous genes that were downregulated in obesity. The eWAT instead, mainly responds by downregulating several inflammatory processes and then upregulating metabolic-related responses. How this fine-tuned process happens *in vivo* is not well understood. However, our analysis suggests that expression of ribosomal genes increase through a rosiglitazone-dependent manner and that there is selectivity in which mRNA networks are being highly translated by them. The specialization of ribosomes is a current focal point across various fields of study (Guo 2018). It is crucial to comprehend how ribosomes specific to fat tissue select the mRNAs networks for translation in order to gain a comprehensive understanding of the physiology of this tissue.

It is well established that adipose-specific transcriptional regulation is an exceptionally dynamic process that involves extensive chromatin remodeling and the presence of transcription factor hotspots (Siersbæk, Baek et al. 2014). This is a core mechanism defining adipose molecular identity and maintaining tissue homeostasis. However, how post-transcriptional processes control the precise balance of protein production within adipocytes is not well understood. Our analysis suggests that while there is induction of translation, there is significant translational buffering. This buffering prevents abrupt fluctuations in protein levels due to changes in gene expression, ensuring that translation is finely tuned and responsive to specific cellular conditions. Translation buffering can be achieved through factors like ribosome pausing (Jobava, Mao et al. 2021), increasing mRNA stability (Wu, Medina et al. 2019), or regulating the availability

of transfer RNA (tRNA) molecules (Torrent, Chalancon et al. 2018). Rosi treatment causes a major transcriptional remodeling, inducing, and repressing the expression of several PPARγ targets. Our data has shown that most of these transcripts are under the translation buffering response though with a reduction in translation rate compared to the mRNA cytoplastic availability. Surprisingly, although a large number of genes are transcriptionally altered by Rosi, we found that in the eWAT there is a decrease in the translation of several immune-related pathways, oxidative phosphorylation, peroxisome, and Wnt β-catenin signaling. Instead, the polysomes are enriched with adipogenic-related targets, adipokines, and triglyceride biosynthesis mRNAs, allowing these genes to be selectively translated (**Fig12**). Ribosomes somehow bypass the overwhelming transcription remodeling of Rosi and selectively induce the translation of essential adipose-specific targets that promote fat homeostasis.

However, how is adipose-specific translation precisely adjusted? In general, the mechanism of translation regulation in cells is a finely tuned and dynamic process that plays a crucial role in the control of protein synthesis. Cells employ a variety of mechanisms to modulate translation, ensuring that the production of proteins is precisely regulated in response to various internal and external cues. The regulation of translation specific to the adipose tissue is an area that lacks extensive study, with only a few papers outlining its function. For example, in 3T3-L1 cells during adipogenesis, enhancement of the ribosome machinery, and a dynamic regulation of polysomes versus free mRNA fraction seems essential to drive full adipocyte differentiation (Fromm-Dornieden, von der Heyde et al. 2012, von der Heyde, Fromm-Dornieden et al. 2014). In addition, initiation factors, such as eIF6 controls translation of transcriptional factors C/EBPβ and C/EBPδ in a G/C-rich 5'UTR manner, contributing to lipid metabolism homeostasis in adipocytes and hepatocytes (Brina, Miluzio et al. 2015). However, adipose-translation regulation is still on its infancy and more studies are necessary to understand its plasticity.

2.4 Methods

Mice

Adult C57BL/6J (12-week-old) male mice (stock #000664) and *Lep^{ob}/Lep^{ob}* (stock #000632) were acquired through Jackson Laboratories. All mice were housed at a maximum of 5 animals per cage in temperature-controlled rooms under a 12-hour light/dark cycle and provided water and chow *ad libitum.* All mouse procedures were performed under animal study proposals approved by the University of California, Los Angeles Animal Research Committee (ARC 2019-066).

Rosiglitazone treatment

To examine the effects of PPARγ agonist, C56BL/6 and *Lep^{ob}/Lep^{ob}* mice were given 30 mg/kg rosiglitazone (Sigma R2408), or vehicle [2.6% methylcellulose (StemCell Technologies, M3120) diluted 1:5 in Dulbecco's modified medium (GIBCO)] by oral gavage in the morning and evening for three consecutive days as previously described (Davies, Waki et al. 2008).

Stromal vascular fraction isolation for scRNASeq

To ensure high quality and viability of the single cell suspensions, stromal vascular fractions were isolated as previously described (Majka, Miller et al. 2014) with small modifications from Dr. Xia Yang laboratory. Briefly, 300mg of the white adipose tissue (eWAT or iWAT) were collected (small biopsies from several locations of the fat depot to represent tissue environment), cut into small pieces, suspended in phosphate-buffered saline (PBS) (calcium, magnesium free) (GIBCO) containing 2mg/mL of type II collagenase (Worthington), and digested for 40 minutes at 37°C with agitation (100 rpm). The resulting dissociated tissue was resuspended in DMEM (GIBCO) with 10% FBS, gently mixed, passed through 100μm strainers, and centrifuged at 150g for 8 min at 4C. Next, supernatant and floating adipocytes were removed, and pellet was resuspended in DMEM (GIBCO) with 10% FBS and centrifuged at 150g for 8 min at 4C. Red blood cells were

lysed using ACK lysis buffer (GIBCO). Lysate pellets were first washed with DMEM (GIBCO) with 10% FBS, centrifuged at 150g for 8 min at 4C and then PBS with 0.04% BSA (Gemini). The resulting pellets were finally resuspended in 200uL of PBS, 0.04% BSA (Gemini), passed through 40µm tip-strainers, counted, and further used for 10X 3'GEX library preparation and sequencing.

10X 3'GEX library preparation and sequencing

The Chromium Single Cell Gene Expression Solution upgrades short read sequencers to deliver a scalable microfluidic platform for 3' digital gene expression by profiling 500-10,000 individual cells per sample. A pool of ~3,500,000 10x Barcodes are sampled separately to index each cell's transcriptome. It is done by partitioning thousands of cells into nanoliter-scale Gel Beads-in-emulsion (GEMs), where all generated cDNA shares a common 10x Barcode. Libraries are generated and sequenced from the cDNA and 10x Barcodes are used to associate individual reads back to the individual partitions. In addition to the poly(dT) primer that enables the production of barcoded, full-length cDNA from poly-adenylated mRNA, the Single Cell 3' v3.1 Gel Beads also include two additional primer sequences (Capture Sequence 1 and Capture Sequence 2), that enable capture and priming of Feature Barcoding technology compatible targets or analytes of interest. Only the poly(dT) primers are used in this protocol for generating Single Cell 3' Gene Expression libraries. GEMs are generated by combining barcoded Single Cell 3' v3.1 Gel Beads, a Master Mix containing cells, and Partitioning Oil onto Chromium Next GEM Chip G. To achieve single-cell resolution, cells are delivered at a limiting dilution, such that the majority (~90-99%) of generated GEMs contain no cell, while the remainder largely contains a single cell. Immediately following GEM generation, the Gel Bead is dissolved, primers are released, and any co-partitioned cell is lysed. Primer containing (1) an Illumina TruSeq Read 1 (read 1 sequencing primer), (2) 10x Barcode, (3) 12nt unique molecular identifier (UMI), and (3) 30nt poly(dT) sequence are mixed with the cell lysate and a Master Mix containing reverse transcription (RT)

reagents. Incubation of the GEMs produces barcoded, full-length cDNA from poly-adenylated mRNA. After incubation, GEMs are broken, and pooled fractions are recovered. Silane magnetic beads are used to purify the first-strand cDNA from the post GEM-RT reaction mixture, which includes leftover biochemical reagents and primers. Barcoded, full-length cDNA is amplified via PCR to generate sufficient mass for library construction. Enzymatic fragmentation and size selection are used to optimize the cDNA amplicon size. TruSeq Read 1 (read 1 primer sequence) is added to the molecules during GEM incubation. P5, P7, a sample index, and TruSeq Read 2 (read 2 primer sequence) are added via End Repair, A-tailing, Adaptor Ligation, and PCR. The final libraries contain the P5 and P7 primers used in Illumina bridge amplification. A Chromium Single Cell 3' Gene Expression library comprises standard Illumina paired-end constructs which begin and end with P5 and P7. The 10x Barcode and 12 bp UMI are encoded in Read 1, while Read 2 is used to sequence the cDNA fragment. Sample index sequences are incorporated as the sample index read. TruSeq Read 1 and TruSeq Read 2 are standard Illumina sequencing primer sites used in paired-end sequencing. These libraries were sequenced using Illumina's NovaSeq6000 platform in paired end 2x100bp configuration. Data quality check was done on Illumina SAV, and data de-multiplexing was performed with Illumina Bcl2fastq v2.19.1.403 software.

scRNA-Seq data processing and quality control

The 10X Genomics Cell Ranger version 3.0.2 single-cell software (Zheng, Terry et al. 2017) was used to perform sample demultiplexing sequencing alignment to mouse genome mm10, filtering, and unique molecular identifier (UMI) counting to generate gene count matrices. Single cells were identified from background noise by filtering on the proportion of mitochondrial reads (threshold: < 25%), the number of UMI (thresholds: 700-22,000), and the number of detected genes (thresholds: 200-6,000).

Cell clustering and cell type identification

The cell clustering and cell type identification were performed using the Seurat R package version 4.0.2. The Louvain algorithm was employed to determine cell clusters based on similarities in transcriptome patterns, and the resulting clusters were visualized using t-Distributed Stochastic Neighbor Embedding (t-SNE) and Uniform Manifold Approximation and Projection (UMAP). Highly variable genes selected using the FindVariableFeatures function with default parameters were subjected to principal component analysis (PCA). The number of principal components used for Louvain clustering and subsequent visualization was determined with the Jackstraw permutation approach (n=25 for clustering of all cells and n=15 for APC sub-clustering). Cell type identities of the clusters were resolved by comparing the cell cluster-specific marker genes expressed in each cluster in our own dataset, identified with a Wilcoxon rank sum test, with known cell-type-specific markers curated from literature, single-cell atlases, and previous studies in the white adipose tissue. For a gene to be considered in the cell cluster marker analysis, it had to be expressed in at least 10% of the single cells from the cluster of interest and exhibit at least a 0.25 log-fold change in the cell cluster of interest compared to other cells. Multiple testing was corrected using the Benjamini-Hochberg method to estimate the false discovery rate (FDR).

Identification of differentially expressed genes (DEGs) and pathways

To determine which genes were affected by genetic background or rosiglitazone treatment, we compared the cell transcriptome of each cell type between age groups using a Wilcoxon rank sum test. To be considered in the analysis, a gene had to be expressed in at least 10% of the single cells from at least one of the two groups for that cell type and there had to be at least a 1.1-fold change in gene expression between the groups. Multiple testing correction was done using the Benjamini–Hochberg method to estimate FDR. To assess pathway enrichment, we performed

Fisher's exact test to determine the overlap between the DEGs and pathways from KEGG, REACTOME, BIOCARTA, and HALLMARK. Multiple testing correction was performed using the Benjamini-Hochberg method to estimate FDR. The enrichment score was calculated as the number of overlapped genes divided by the number of genes in our cell type-specific gene set, multiplied by 20,000, and then divided by the total number of genes in the pathway.

Regular stromal vascular fraction isolation

Stromal vascular fractions were isolated as previously described (Church, Berry et al. 2014). Briefly, entire WAT depots were cut into small pieces, suspended in DMEM (GIBCO) + 50 mM HEPES (GIBCO) + 1mg/mL type II collagenase (Sigma), + 1% BSA - low fatty acid (Gemini), and digested for 30 minutes at 37°C with agitation (120 rpm). The resulting dissociated tissue was passed through 100μm strainers, and adipocytes were removed from the supernatant by centrifugation (750g, 10min, 4C). After a second filtration with 40μm strainers, red blood cells were lysed using ACK lysis buffer (GIBCO). The resulting pellets were processed further for flow cytometry, sorting or primary cell culture.

Flow cytometry and sorting

Cells were analyzed for cell-surface markers using fluorophore-conjugated antibodies (BioLegend, eBioscience). Cell surface staining was performed in HBSS (GIBCO). Flow cytometry was performed using the Attune NxT and data were analyzed with FlowJo software (BD). Cell surface and intracellular staining were performed using the following fluorophore-conjugated antibodies: (a) macrophages panel (Hildreth, Ma et al. 2021): CD45.2 (104), TCRβ (H57-597), CD3 (17A2), CD19 (6D5), NK1.1 (PK136), Ly6G (1A8), CD11c (N418), CD11b (M1/70), CD88 (20/70), CD9 (MZ3), Tim-4 (RMT4-54). (b) progenitors: Lineage negative: CD45.2 [104], and CD31 [390], PDGFRα (APA5), DPP4 (H194-112), ICAM-1 (YN1/1.7.4), CD36 (HM36).

For sorting, cell suspensions were stained with: CD45.2 [104], and CD31 [390], PDGFRα (APA5), DPP4 (H194-112), and DAPI (AAT Bioquest) and sorted on FACSAria III (BD).

Confocal

Sorted cells were plated in a 96-well plate and culture in DMEM (GIBCO), 5µg/mL insulin (GIBCO), 10% FBS (Omega FB#11), 1% PenStrep (GIBCO), and 50ng/mL Primocin (Invivogen) until confluency. Specific differentiation cocktails included: (a) complete adipogenic cocktail (0.5mM 3-isobutyl-1-methylxanthine (Sigma), 1µM dexamethasone (Sigma), 5µg/mL insulin (GIBCO), or (b) DI (dexamethasone (Sigma), and 5µg/mL insulin (GIBCO), or (c) minimal media (Insulin (GIBCO). Differentiation media was added for two days and then replaced with minimal media (DMEM, 10% FBS, 5µg/mL insulin) until day 4 of differentiation. Cells were fixed with 4% paraformaldehyde, permeabilized with 0.1% Triton, and stained with LipidTOX Green Neutral Lipid (Invitrogen) and DAPI (AAT Bioquest). For macrophage staining, cells from the adipose tissue were dissociated as previously described. Upper floating layer containing mature adipocytes was collected and plated in an 8-well chamber (Nunc Lab-Tek, Sigma) previously treated with poly-L-lysine. After overnight incubation at 37C, slides were washed four times with phosphate-buffered saline (PBS), fixed with 4% paraformaldehyde, permeabilized with 0.1% Triton, blocked with normal donkey serum 5% (Jackson Immuno Research) and stained overnight with PLIN1 (rabbit, 3526, Abcam), and F4/80 (rat, BM8, BioLegend). Next, slides were washed four times with PBS and incubated for one hour with LipidTOX Green Neutral Lipid (Invitrogen), DAPI (AAT Bioquest), donkey anti-rat IgG Alexa Fluor 568 (Abcam), and donkey anti-rabbit IgG Alexa Fluor 647 (Abcam). Images were acquired using Zeiss LSM900 microscope.

Histology and lipid droplet quantification

Tissues were fixed for 48h in 10% buffered formalin (ThermoFisher), after which they were washed with 70% ethanol (ThermoFisher), sectioned in paraffin (10 μm thickness for adipose tissues and 5 μm for liver), and stained with hematoxylin and eosin (H&E). The lipid droplet cell area from livers and progenitors/preadipocytes from confocal images were quantified using ImageJ.

Glucose tolerance test

For glucose tolerance tests, mice were fasted for 6 hours prior to the challenge with glucose (1 g/kg mouse) via intraperitoneal injection. Blood glucose levels were assessed by tail vein bleeding using a glucometer (Accu-Chek). AUC was determined using Prism software (GraphPad).

μPET/μCT

Lep^{ob}*/Lep*^{ob} mice (stock #000632) (12 weeks old, male) treated with either vehicle (n=6) or rosiglitazone (n=6) were fasted for six hours, prior to intravenous injections via tail vein with 85-90 μCi of [^{18}F]-FDG that had been mixed with glucose based on the weight of the mouse (1g/Kg). Following a 50-minute conscious uptake of [^{18}F]-FDG, mice were anesthetized with 2% vaporized isoflurane, and PET (energy window 350-650 keV, 10-min static scan) and CT (voltage 80 kVp, current 150 μA, 720 projections, 200μm resolution, scan time 1 min) images were acquired on a GNEXT PET/CT scanner (Sofie Biosciences, Dulles, VA). The PET images were reconstructed using a 3D-Ordered Subset Expectation Maximization (OSEM) algorithm (24 subsets and 3 iterations), with random, attenuation, and decay correction. The CT images were reconstructed using a modified Feldkamp algorithm. Amide software was used to analyze co-registered uPET/uCT images, and a full body panel was generated by placing ROIs for the brain, blood, liver, left and right kidney, bladder, muscle, left and right lung, gastrointestinal tract, and adipose

tissues. Visual representation of μPET signal from adipose tissues was generated using ORS Dragonfly software (Object Research Systems Inc, Montreal, Canada).

Surface Sensing of Translation (SUnSET)

The assay was performed as previously described with small modifications (Ravi, Jain et al. 2020). Briefly, mice were intraperitoneally injected with puromycin (40 nmol/g) (Santa Cruz) and returned to their cages with food/water *ad libitum* for one hour. Next, brown, epididymal, and inguinal adipose tissue were collected, and proteins were lysed using radioimmunoprecipitation assay buffer (RIPA) (50mM Tris-HCl pH 7.6, 150mM NaCl, 0.1% sodium dodecyl sulfate, 0.5% sodium deoxycholate, 1% NP40 and freshly added halt protease/phosphate inhibitor cocktail (ThermoFisher). Immunoblots were performed using 20μg of protein and total protein was assessed using UV light exposure to Mini-Protean TGX Stain-free gels (Biorad). Puromycilation was detected using anti-puromycin antibody (12D10, Sigma), and HRP AffiniPure Goat anti-mouse IgG, Fcγ subclass 2a specific (Jackson Immuno Research).

Polysome profile

Polysome profiles were obtained as described before (Gandin, Sikström et al. 2014, Gandin, Masvidal et al. 2016, Chan, Robert et al. 2019). Briefly, stromal vascular fraction of Lep^{ob}/Lep^{ob} was mice was isolated, and primary cells were grown to confluency in 15-cm dishes. Cells were then treated to differentiate with complete adipogenic cocktail (0.5mM 3-isobutyl-1-methylxanthine (Sigma), 1μM dexamethasone (Sigma), 5μg/mL insulin (GIBCO) plus either 1μM rosiglitazone (Novo Nordisk) or vehicle (DMSO) for 2 days. After that, media was replaced for minimal maintenance media (Insulin/Rosi or Insulin/DMSO) for 2 days. At day 4 of differentiation cells were boosted with fresh media for one hour and for the last 5 minutes cycloheximide (Sigma) was added to the media (final concentration 100μg/mL). Cells were lysed and collected in

hypotonic lysis buffer (5mM Tris HCl pH 7.5, 2.5 mM MgCl2, 1.5 mM KCl, 100 µg/mL cycloheximide, 2 mM DTT), and 0.5% Triton, 0.5% Sodium Deoxycholate were then added to the cell lysates after collection. The cytoplasmic extracts were resolved on 5-50% sucrose gradients by centrifugation in an SW40 rotor at 150,000 x g for 2 hours. The absorbance at 260 nm was measured using a Piston Gradient Fractionator Model 153 instrument (BioComp, Canada). The results were plotted in R as previously described (Hulea, Gravel et al. 2018).

Pparγ ChIP-Seq

Publicly available dataset GSE41481 was downloaded from Gene Expression Omnibus (Siersbæk, Loft et al. 2012). For each fat depot, sequenced reads from the ChIP-seq library were first aligned to mouse reference genome (mm9) with Bowtie2 (Langmead and Salzberg 2012). Uniquely aligning read per genomic position was kept with Picard for downstream peak calling. Enriched PPARγ-binding regions were identified using HOMER (Heinz, Benner et al. 2010) findPeaks program (with "factor" mode) where default parameters for tag count normalization (to 10 million reads), false-discovery rate (FDR) cutoff (< 0.1%), and filtering options (≥ 4-fold tag count enrichment compared to both input control and local tag density) were applied. Peaks were annotated to the nearest TSS using HOMER annotatePeaks.pl program. Lastly, enriched peaks were visualized with Integrative Genomics Viewer (IGV) (Robinson, Thorvaldsdóttir et al. 2011).

Total RNA sequencing and polysomes sequencing analysis

The RNA sample received was quantified using Qubit 2.0 Fluorometer (Life Technologies, Carlsbad, CA, USA) and RNA integrity was checked using TapeStation (Agilent Technologies, Palo Alto, CA, USA). The RNA sequencing library was prepared using the NEBNext Ultra RNA Library Prep Kit for Illumina using manufacturer's instructions (NEB, Ipswich, MA, USA). Briefly, mRNAs were initially enriched with Oligod(T) beads. Enriched mRNAs were fragmented for 15

minutes at 94 °C. First-strand and second-strand cDNA were subsequently synthesized. cDNA fragments were end-repaired and adenylated at 3'ends, and universal adapters were ligated to cDNA fragments, followed by index addition and library enrichment by PCR with limited cycles. The sequencing library was validated on the Agilent TapeStation (Agilent Technologies, Palo Alto, CA, USA), and quantified by using Qubit 2.0 Fluorometer (Invitrogen, Carlsbad, CA) as well as by quantitative PCR (KAPA Biosystems, Wilmington, MA, USA). The sequencing library was clustered on three lanes of a flowcell. After clustering, the flowcell was loaded on the Illumina HiSeq instrument (4000 or equivalent) according to the manufacturer's instructions. The sample was sequenced using a 2x150bp Paired End (PE) configuration. Image analysis and base calling were conducted by the HiSeq Control Software (HCS). Raw sequence data (.bcl files) generated from Illumina HiSeq was converted into fastq files and de-multiplexed using Illumina's bcl2fastq 2.17 software. One mismatch was allowed for index sequence identification. Quality control of raw sequencing data was conducted using FastQC (Andrews 2010), employing default parameters. Subsequently, sequencing reads were mapped to the mouse genome mm10 using Salmon (Patro, Duggal et al. 2017). Differential gene expression analysis was then undertaken with DESeq2 (Love, Huber et al. 2014). Genes meeting the criteria of an adjusted p-value less than 0.05 and a log2(fold change) greater than 0.2 were classified as differentially expressed. Pathway enrichment analysis was executed by examining the overlap between the identified DEGs and canonical pathways from databases such as KEGG, REACTOME, BIOCARTA, and HALLMARK using Fisher's exact test. Multiple testing corrections were applied using the Benjamini-Hochberg method to determine the false discovery rate (FDR). Additionally, an enrichment score was calculated, capturing the proportion of overlapping genes in relation to the entire gene set specific to a given cell type. This score was normalized by the total number of genes detected in either total RNA sequencing or polysome sequencing.

qPCR validation of selected genes

RNA from polysomes or total RNA pool was resuspended in Trizol reagent (ThermoFisher), and RNA was isolated using Direct-zol RNA Microprep kits as described by the manufacture (Zymo research). Isolated RNA was reverse transcribed using High-Capacity cDNA synthesis kit (ThermoFisher). Gene expression for selected genes was quantified using Quant Studio 6 Flex Real-Time PCR instrument, 384-well (Applied Biosystems by Invitrogen) with KAPA SYBR FAST qPCR 2x Master Mix Rox Low (Kapa Biosystems).

Differentially translated transcripts analysis

Differential expression analysis was performed using DESeq2 (Love, Huber et al. 2014). We designed an interaction term between RNA fractions (i.e., polysome vs total RNA) and treatment (i.e., rosiglitazone vs vehicle) during DESeq2 analysis, which could normalize the expression level of total RNA abundance in polysome fractions. The transcripts with differential translation efficiency (DTETs) were defined using the criteria of adjusted p-values less than 0.05 and absolute log2(Foldchange) greater than 1. The up-regulated transcripts after rosiglitazone treatments were classified as log2(Foldchange) greater than 1, while down-regulated ones are classified as log2(Foldchange) less than -1.

Identification and quantification of enriched motifs

To explore the sequence patterns in up-regulated transcripts, RNA sequences including 5'UTR, CDS, and 3'UTR were extracted based on the transcriptome annotations from GENCODE VM33. A statistic enrichment analysis was conducted to extract the enriched motifs from hexamer sequences in the up-regulated transcripts regions and we chose the sequences from down-regulated transcripts as the background group to measure the enrichment of hexamers. In brief, the sequences from the up-regulated transcripts regions were extracted by overlapping hexamers

using the window length as 6nt and step size as 1nt. The occurrences and frequencies of each hexamer were counted across sequences and the enrichment score was calculated using Z-test. The enriched hexamers between up- vs down-regulated transcripts were defined with the enrichment z-scores larger than 3. The motif analyses are performed using RSAT (Turatsinze, Thomas-Chollier et al. 2008). First, the position-specific scoring matrix (PSSM) of the enriched hexamers was obtained using the 'convert-matrix' program. Sequence motifs were generated using R package 'ggseqlogo'. Then, we scanned the enriched 5'UTR motif across each position of the 5'UTR in up-regulated transcripts using the 'matrix-scan' program, which is a pattern-matching method calculating the similarity between sequences with PSSM. The 5'UTR sites with p-values lower than 0.05 were selected as the possible regulatory sites to generate a feature map.

Design of truncated 5'UTRs

All significant motif sites were used to design the truncated 5'UTRs. We scanned each 5'UTR using the sliding windows in 100nt length with 1nt step size and then counted all the significant motif sites in each 100nt sliding window. The windows with more than 1 motif site were defined as potential functional windows. If there were at least two functional windows in adjacent positions,

2.5 Conclusions

Our studies propose that Rosi regulates fat-specific translation by (a) a direct mechanism on which PPARγ can drive the expression of ribosomal genes and build up the machinery necessary to translate specialized fat mRNAs; and (b) an indirect RNA G-rich mediated mechanism by which Rosi enhances the translation of mRNA containing this motif. This could be achieved by potentially removing G4 structures from defined mRNA as observed at DNA level (Zyner, Simeone et al. 2022) to drive cell differentiation. Additionally, we speculated that rosiglitazone could induce the expression of RBP that preferentially binds to G-riched sequences

(G4) and other structures driving more translation (Benhalevy, Gupta et al. 2017). In conclusion, we propose a novel and exciting new role of TZDs (rosiglitazone) regulating the translation machinery in the adipose SVF. Our studies suggest for the first time that rosiglitazone not only drives the fat-transcription networks but also regulate its translation in a very precise and sophisticated way to ensure fat-cell specialization. This opens up a completely new perspective about adipose tissue translation homeostasis and its adaptability to diverse stressors. We acknowledge that future studies will be necessary to fully characterize how the translation machinery is regulated or impaired in the context of obesity and how can we target it to restore adipose plasticity.

CHAPTER 3: ROLE OF PIXL IN WHITE AND BROWN ADIPOSE TISSUE

3.1 Introduction

Adipose tissue is a key regulator of systemic lipid metabolism. Adipocytes are specialized cells that store energy in the form of triglycerides and mobilize this energy as free fatty acids during times of caloric deficiency (Sakers, De Siqueira et al. 2022). Excess adipose tissue (i.e. obesity) increases the risk for metabolic disorders such as dyslipidemia, cardiovascular disease, insulin resistance, and type 2 diabetes (Alberti, Zimmet et al. 2005). In fact, increased visceral adipose tissue leads to increase in cardiometabolic risk, and chronic low-grade inflammation (Rosenquist, Pedley et al. 2013, Abraham, Pedley et al. 2015, Sahakyan, Somers et al. 2015). The local effects of this dysfunctional expansion of adipose tissue result in increased levels of proinflammatory cytokines, such as TNF-α and IL-6 (Park, Park et al. 2005, Sahakyan, Somers et al. 2015), oxidative stress, mitochondrial dysfunction, hypoxia, and increased expression of antiangiogenic genes (Ledoux, Queguiner et al. 2008, Gealekman, Guseva et al. 2011, An, Crewe et al. 2019). At systemic level, the inefficient storage of excess lipids in the adipose tissue leads to ectopic fat deposition in the liver, systemic inflammation, and consequently atherosclerosis (Reardon, Lingaraju et al. 2018, Ansaldo, Montecucco et al. 2019, Ben, Jiang et al. 2019, Zhang, Zhang et al. 2019). These studies highlight the essential role of functional adipose tissue in regulating systemic energy metabolism.

Pharmacological therapies, such as the use of thiazolidinediones (TZDs) can specifically target several of the dysfunctional consequences of obesity and rewire metabolism. For example, Rosiglitazone (Rosi) has potent anti-diabetic effects(Xu, Xing et al. 2022) by (a) increasing uptake of glucose on muscle (b) increasing triglyceride storage in the adipose tissue and production of adipokines such as adiponectin, (c) increasing fatty acid oxidation in the liver, (d) reducing lipid accumulation in muscle and liver and (e) reducing inflammation by targeting PPARγ in

macrophages, switching to an anti-inflammatory profile (Cariou, Charbonnel et al. 2012, Ahsan 2019). Most importantly, recent studies have demonstrated fewer cardiac side effects with the use of rosiglitazone in diabetic patients (Home, Jones et al. 2007, Home, Pocock et al. 2009, Florez, Reaven et al. 2015).

Here we identified, a novel adipose target of PPARγ, **Pparγ-Induced X-Linked (PIXL).** PIXL (also known as Kiaa1701, Bhlhb9 and p60Trp) is a cytoplastic protein, containing four armadillo repeats at the C-terminus and a completely disordered N-terminus. In particular, PIXL does not have a DNA biding domain despite its previous annotations (Uniprot Q6PB60). Interestingly, *Pixl* is upregulated by Rosi treatment in obese mice in both brown and white adipose depots and it has no defined adipose function. Previous work has demonstrated that *Pixl* expression increases during cellular differentiation in chondrocytes (Suwanwela, Farber et al. 2011) and its overexpression induces neurogenesis (Mishra and Heese 2011).Therefore we aimed to characterized the function of this protein in adipose biology. Since our previous work (Chapter 2) has shown the importance of Rosi increasing the expression of the translation machinery we hypothesized that TZDs promote adipocyte proteostasis by inducing the expression of translation-related proteins and specific regulators to fine tune the proteome tonus. As *Pixl* seems to enhance the differentiation process in other tissues we conjectured that *Pixl* could be involved in the regulation of protein synthesis and therefore regulating the translational status.

3.2 Results

3.2.1 Identification of PPARγ- Induced X-linked gene: Pixl

Rosiglitazone (Rosi) is a PPARγ agonist drug that has been shown to remodel adipose tissue architecture and it has a potent anti-diabetic function (Lebovitz 2019). To identify novel uncharacterized genes upregulated by a PPARγ agonist we acutely treated ob/ob mice with vehicle (Veh) or Rosi for 3 days and performed RNA sequencing of brown adipose tissue (BAT),

epididymal adipose tissue (eWAT), and inguinal adipose tissue (iWAT) (**Fig14A**). Venn diagram analysis revealed a remarkable depot-specific response and an overlapping signature (**Fig14B**). We first validated the main common pathways being upregulated by Rosi such as lipid metabolism and PPAR signaling (**Fig14C**). Next, we analyzed depot-specific pathways (**FigS11A-F**). Downregulated processes demonstrated decreased immune responses and metabolic processes (**FigS11B, D, F**). Interestingly, in the upregulated pathways, we did observe an upregulation of not only fat-specific processes but also several translation-related pathways (**FigS11A, C, E**). We then decided to refine the pathways involved in mRNA processing and translation and we observed that Rosi treatment indeed upregulates several processes to induce translation remodeling and protein synthesis in the adipose tissue (**Fig14D**). Since adipose-specific regulation of translation is a poorly studied field we aimed to identify novel targets induced by Rosi that may be involved in such regulation. To identify relevant targets, we ranked the upregulated transcripts by Rosi in the three fat depots-based fold changes. Among the classical PPARγ targets (e.g. E*lovl3, Rbp7, Clstn3*) and previously described genes involved in adipogenesis (e.g. *Arxes1* and *Arxes2*), we identified an uncharacterized gene *Bhlhb9 (a.k.a. Gprasp3*, *p60TRP*). Despite its name, *Bhlhb9* does not have a basic helix-loop-helix domain (Uniprot Q6PB60). Therefore, herein we are referring to it as PPARγ- Induced X-linked gene: *Pixl.* To validate that *Pixl* upregulation was dependent on the Rosi treatment, we checked a publicly available PPARγ ChIP-Seq dataset. Indeed, we identified PPARγ binding sites in the promoter region of *Pixl* (**Fig14F**).

In conclusion, we have demonstrated that Rosi treatment indeed enhances the translation machinery expression in the adipose tissue. Moreover, we have identified a novel candidate, *Pixl*, which may play a role in this process.

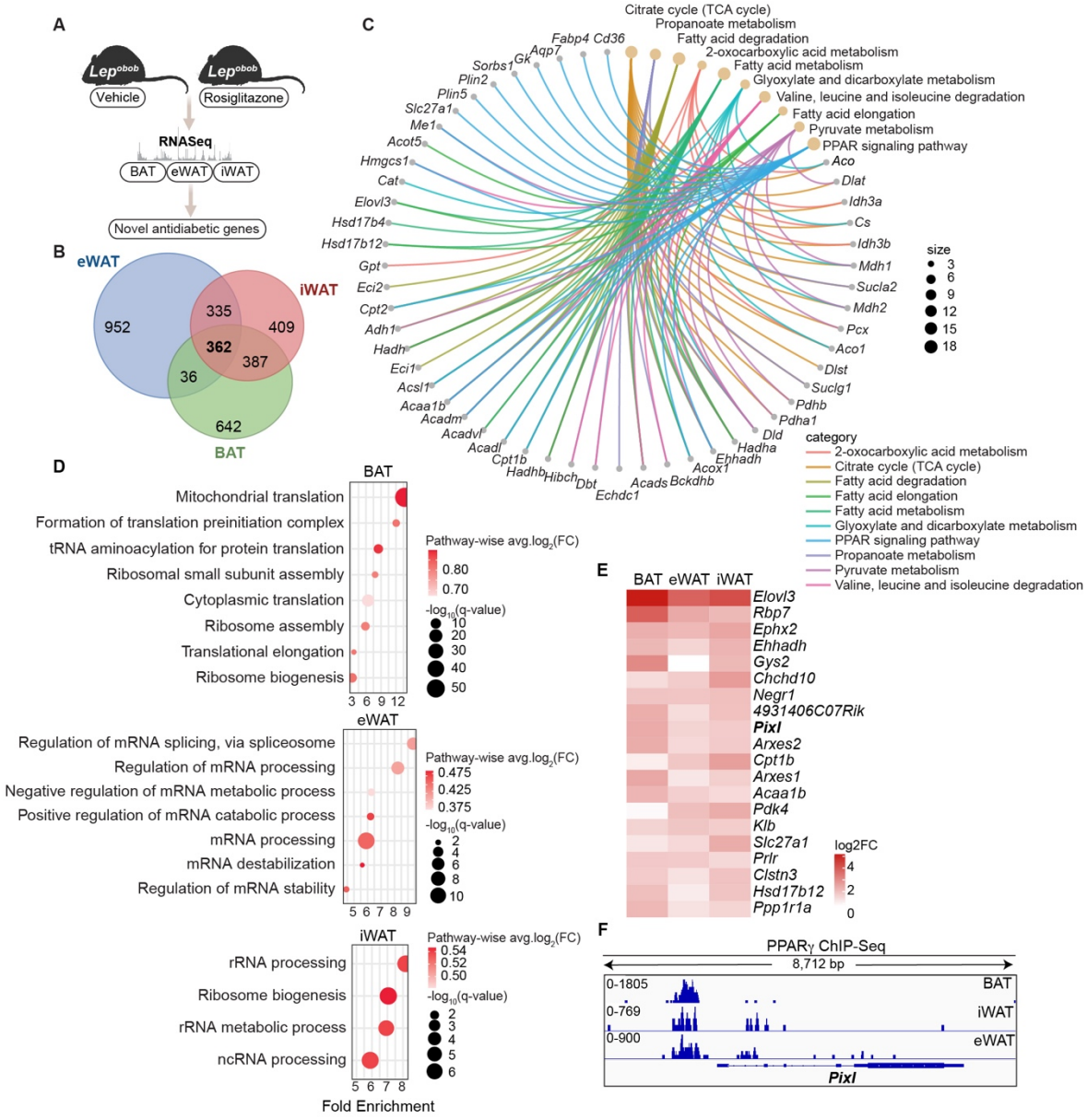

Figure 14 PPARγ-dependent induction of Pixl.

(A) Schematic experimental design: obese (ob/ob) mice were orally gavage with either vehicle or rosiglitazone (Rosi) 30mg/Kg for 3 days, and BAT, eWAT and iWAT were isolated for RNA sequencing. (**B**) Venn diagram of transcripts upregulated by Rosi in BAT, eWAT, and iWAT. (**C**) C-net of pathways enriched in the overlapping upregulated transcripts by Rosi. (**D**) Translation-related pathways upregulated by Rosi. (**E**) Heat-map of transcripts upregulated by Rosi by fold-change (>450 read counts, log2FC>1.3). (**F**) Visualization of peaks of PPARγ binding sites in BAT, iWAT and eWAT. (n = 3 mice per group).

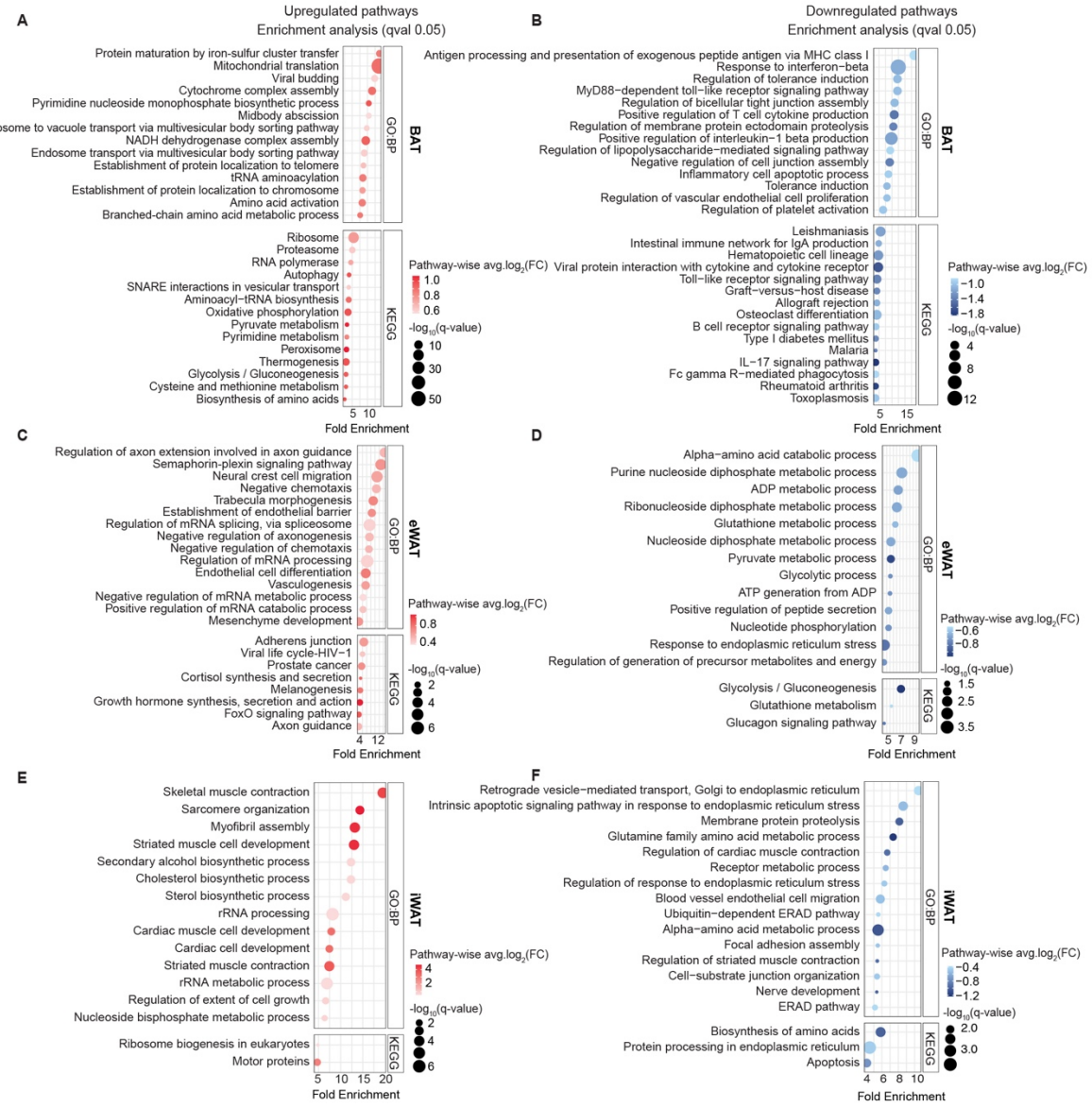

SFigure 11 Rosiglitazone-induced transcriptome remodeling.

(**A-B**) Upregulated and downregulated pathways by Rosi in BAT. GO: biological processes and KEGG. (**C-D)** Upregulated and downregulated pathways by Rosi in eWAT. GO: biological processes and KEGG. (**E-F**) Upregulated and downregulated pathways by Rosi in iWAT. GO: biological processes and KEGG. (n = 3 mice per group).

3.2.2. PIXL interacts with the translation machinery

Next, we aimed to define the function of *Pixl* in adipose biology. In order to do that, we first used AlphaFold and ChimeraX to define PIXL-predicted structures. PIXL secondary structures are predicted to be one alpha helix at the N-terminus, and four helices at the C-terminus, colored by hydrogen bonds in blue (**Fig15A**). Additionally, electrostatic, and hydrophobic properties

demonstrate that PIXL is composed of mainly positive (Lys, His, Arg) (**FigS12A**) and hydrophilic residues (**FigS12B**). Second, we used AlphaFold and Swiss-Model to predict specific structures and domains. The only high-confidence modeling we were able to predict was armadillo repeats like in the C-terminus (dark blue) (**Fig15B**). The entire N-terminus seems to be disordered and without any high-confidence predictions. Given that structure prediction was not insightful for us to define PIXL molecular function, we decided to characterize the *in vitro* function of PIXL. We first performed an adipocyte differentiation time course using 10T1/2 cells. *Pixl* mRNA levels increase during differentiation with the highest expression on day 2 of differentiation (**FigS12C**).

Since we could not validate an antibody to identify the protein levels of PIXL we tagged *Pixl* with either HA or flag tag at the C-terminus (**FigS12D**). PIXL-flag protein expression was very similar to the endogenous mRNA levels, with the highest expression at day 2 of differentiation (**FigS12E**). Next, we decide to evaluate PIXL cellular localization. Confocal images revealed that PIXL is a cytoplasmic-resident protein (**Fig15C**). To identify the molecular partners of PIXL, we performed an immunoprecipitation on day 2 of adipocyte differentiation (**Fig15D**).

Network analysis revealed that PIXL is part of the ribonucleoprotein/ translation complex (**Fig15D**). We identified upstream regulators of translation (e.g. LAMTOR3, RRAGA), and eukaryotic initiation factors – eIF (e.g. eIF5, eIF4E, eIF4H) (**Fig15D-E**). Since initiation factors such as eIF4E (Conn, Yang et al. 2021) and eIF6 (Brina, Miluzio et al. 2015) have been recently described as important proteins regulating the metabolic tone in the liver, we decided to characterize the role of PIXL and the eukaryotic initiation complex. To validate the complex interaction, we initially co-immunoprecipitated PIXL and eIF4E (**Fig15F**), and then we decided to analyze the polysome profile of 10T1/2 cells during adipocyte differentiation. Expression of PIXL-flag at day 2 (**Fig15G**) or day 4 (**FigS12F**) of differentiation did not cause changes in the polysome profile, nor in the polysomes/monosomes ratio (**FigS12G**).

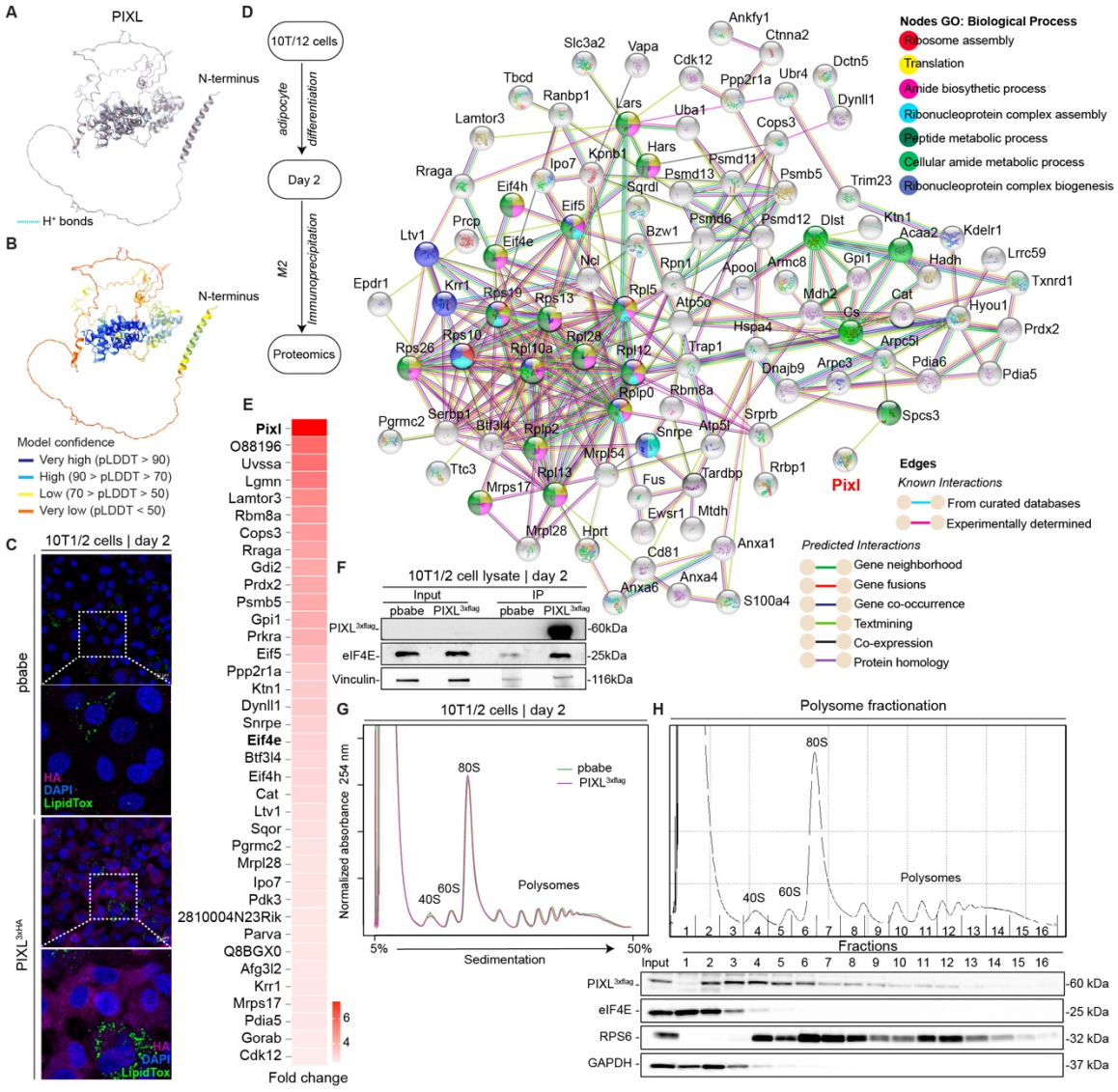

Figure 15 Molecular characterization of PIXL.

(A) AlphaFold prediction of PIXL secondary structures (visualization by ChimeraX). Hydrogen bonds depictable in blue. (**B**) Model confidence by AlphaFold (visualization by ChimeraX). (**C**) Confocal images of 10T/12 cells at day 2 of differentiation (PIXL-HA: purple; nuclei: DAPI, blue; Lipid droplets: LipidTox, green. (**D**) Left-panel: experimental design for proteomics of immunoprecipitated proteins with PIXL-flag. Right panel: interactome of proteins identified by proteomics (log2FC>1.2). (**E**) Heat-map of proteins identified by proteomics using a cut-off of log2FC>1.2, and adj p-value < 0.04. (**F**) Co-immunoprecipitation of PIXL and eIF4E at day 2 of differentiation. (**G**) Polysomes profile of 10T1/2 PIXL-flag and pBABE cells at day 2 of differentiation. (**H**) Western blot of polysome profile of PIXL-flag, eIF4E, RPS6, and GAPDH.

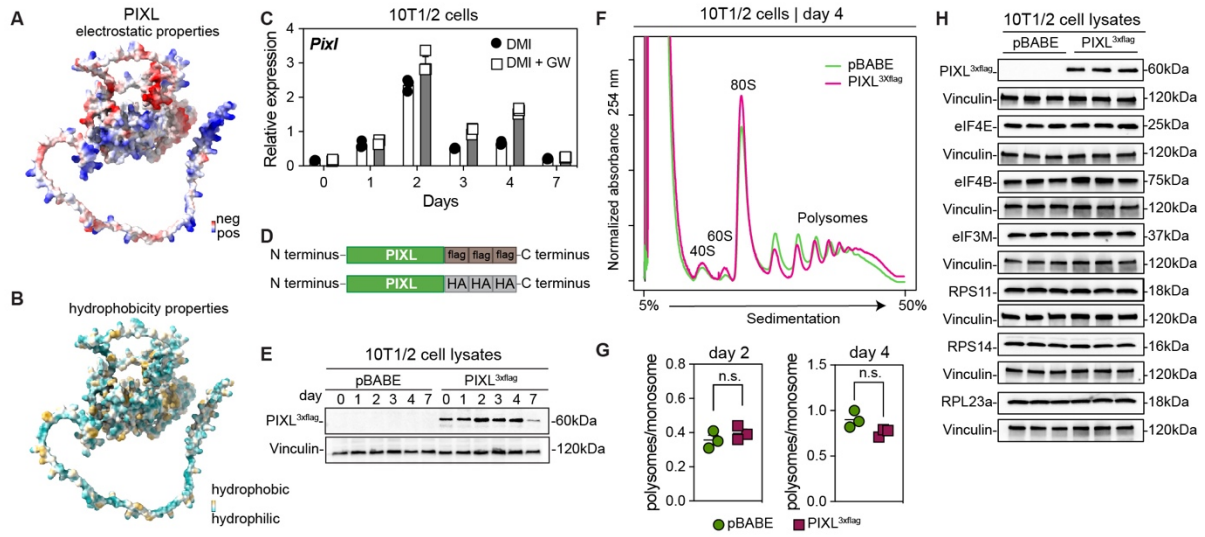

SFigure 12 Pixl expression during adipocyte differentiation.

(**A**) Visualization by ChimeraX of electrostatic properties of PIXL (blue: positive residues; red: negative residues). (**B**) Visualization by ChimeraX of hydrophobicity properties of PIXL (yellow: hydrophobic residues; cyan: hydrophilic residues). (**C**) mRNA levels of endogenous *Pixl* during adipocyte differentiation. (**D**) Schematic design for *Pixl*-3xflag and *Pixl*-3xHA at its C-terminus. (**E**) Protein levels of PIXL during adipocyte differentiation. (**F**) Polysomes profile of 10T1/2 PIXL-flag and pBABE cells at day 4 of differentiation. (**G**) Ratio of polysomes by monosome peaks from polysomes at day 2 and day 4 of differentiation. (**H**) Western blot analysis of initiation factors and ribosomal proteins at day 2 of adipocytes differentiation. GP pvalue style: n.s.= non-significant, *p= 0.0332; **p < 0.0021; ***p < 0.0002 by two-tailed Student's t-test.

Additionally, PIXL-flag expression only slightly increased the expression of initiation factors (eIF4E, eIF4B, eIF3M) with no changes in ribosomal proteins (RPS11, RPS14, RPL23a) (**FigS12H**). Nonetheless, when we immunoblotted for PIXL in the fractions of the polysome we did identify PIXL at the highest levels in the early fractions (F2-F6) of the polysome (**Fig15H**).

Overall, we have demonstrated that PIXL expression increases during early stages of adipocyte differentiation, and it interacts with the initiation complex.

3.2.3 Pixl deletion leads to remodeling in the polysome profile

Next, we decide to investigate how the absence of PIXL would impact the polysome profile. In order, to generate a knockout (KO), we used CRISPR-Cas9 ribonucleoprotein complex delivered by electroporation (**Fig16A**). After a first KO screening with a pooled population, we performed single clone isolation, expansion, and a second KO screening. Clones with a KO and

indel score higher than 90% were selected. Pixl or Pixl^{flag} were reintroduced in the KOs to serve as control (WT). Finally, after testing adipogenic potential, clone #10 was selected for downstream experiments. First, we checked gene expression to confirm a successful reintroduction of *Pixl* in the KO cells (**Fig16B**).

Second, we performed polysome profile at early (day 2) and late (day 4) adipogenic differentiation. At day 2 of differentiation, PIXL-KO cells presented a very similar profile to PIXL, and PIXL^{flag} cells (**Fig16C**). A minor decrease was observed in the pool of polysomes (more than 5 ribosomes), and an increased in the pool of 2+ and 3+ ribosomes. Interestingly, at day 4 of differentiation, we first observed how cells now have a very active translation, with very pronounced polysomes compared to day 2 (**Fig16D**). Next, we compared the control cells to PIXL-KO cells and did observe a shift in the polysomes. KO cells had more monosomes and polysomes with 2-3 ribosomes and a slight decrease in the highly translating polysomes (**Fig16D**).

These results highlight that the absence of PIXL does impact the overall polysome profile specially at day 4 of differentiation when cells are highly translating mRNA networks -a phenotype that may impact adipocyte functions *in vivo*.

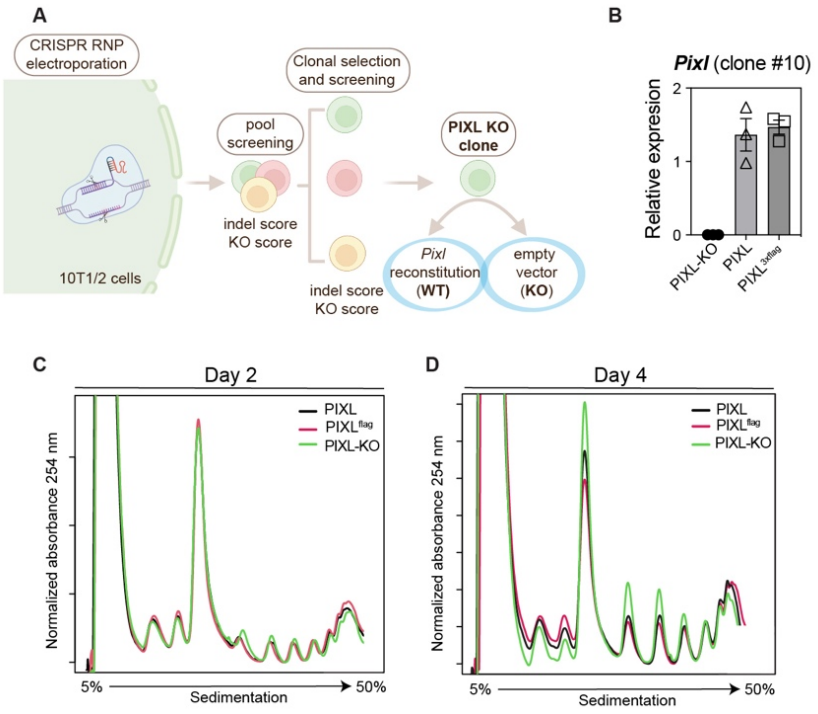

Figure 16 Characterization of adipogenesis in the absence of PIXL.

(A) Schematic experimental design: 10T1/2 cells were electroporated with the ribonucleoprotein complex (gRNA, Cas9), followed by a first screening at the pool level (indel score, KO score), and finally clonal selection was performed to select KO clones. Defined clones then had *Pixl* or *Pixl*^{flag} reintroduced to serve as a control (WT). (**B**) mRNA expression of *Pixl* in 10T1/2 clone #10. (**C-D**) Polysomes profile at day 2 and 4 of PIXL, PIXL^{flag} and PIXL-KO cells.

3.2.4 PIXL knockout perturbs cold adaptation

To investigate the role of *Pixl* in adipose biology *in vivo* we decided to create a mouse model using the Adiponectin-Cre (PIXL-AKO) (**Fig17A**). *Pixl* and *Cre* expression levels (**Fig17B**) indeed demonstrated a knockout of *Pixl*. Next, since BAT presented the major upregulation in the translation machinery pathways (**Fig14D**) and the highest expression of *Pixl* after Rosi treatment (**Fig14E**), we decided to challenge those mice with a cold exposure experiment (**Fig17A**). First, we checked the expression levels of *Pixl* during differentiation and activation of primary brown adipocytes. We observe that *Pixl* is highly expressed in those cells and that its expression increases in the course of brown adipocyte differentiation (**FigS13A**) similar to what we have seen in the 10T1/2 cells (**FigS12C**). However, norepinephrine stimulation does not seem to increase

Pixl expression as it does with UCP1 (**FigS13A-B**). Second, we challenged WT and PIXL-AKO mice with a 6h cold exposure (4C). PIXL-AKO mice are less cold tolerant than the WT mice and they were not able to restore temperature homeostasis (**Fig17C**). Cold exposure however does not change *Pixl* expression (**FigS13C**) so this phenotype may be due to *Pixl* function. Subsequently, we decided to explore how the proteome is modulated during cold exposure. WT mice exposed to cold presented an upregulation of thermogenesis, insulin signaling, and surprisingly ribosome pathways compared to WT at room temperature (RT) (**Fig17D**). Then we decided to analyze how the PIXL-AKO mice modulated their proteome compared to WT during cold exposure. We did observe a downregulation of ribosome pathways and PPAR signaling in PIXL-AKO mice compared to WT (**Fig17E**). Interestingly some of these down regulated proteins are very important for lipolysis (PLIN1, PLIN4, LPL) or long chain fatty acids uptake (CD36) and consequently, fundamental to fuel thermogenesis (**Fig17E- FigS13E**). We also compared PIXL-AKO versus WT at room temperature and there were not many changes in the BAT proteome (**FigS13D**). Therefore, challenging the translation machinery with an acute stress (cold exposure) revealed major impairments in the PIXL-AKO mice. Next, we decided to validate some of these findings, and indeed we observed a decrease in PLIN1 and RPS19 in PIXL-AKO mice compared to WT (**Fig17F-G**). Interestingly these changes are not reflected at mRNA levels (**Fig17H**) highlighting that this may be a translation impairment. We also analyzed histological sections of BAT, eWAT, and iWAT at RT and cold, and no apparent changes were observed (**Fig17I-FigS13F**). Finally, we performed indirect calorimetry in a gradient temperature. We observed that at 5C PIXL-AKO mice have a lower energy expenditure than WT mice (**Fig17J**).

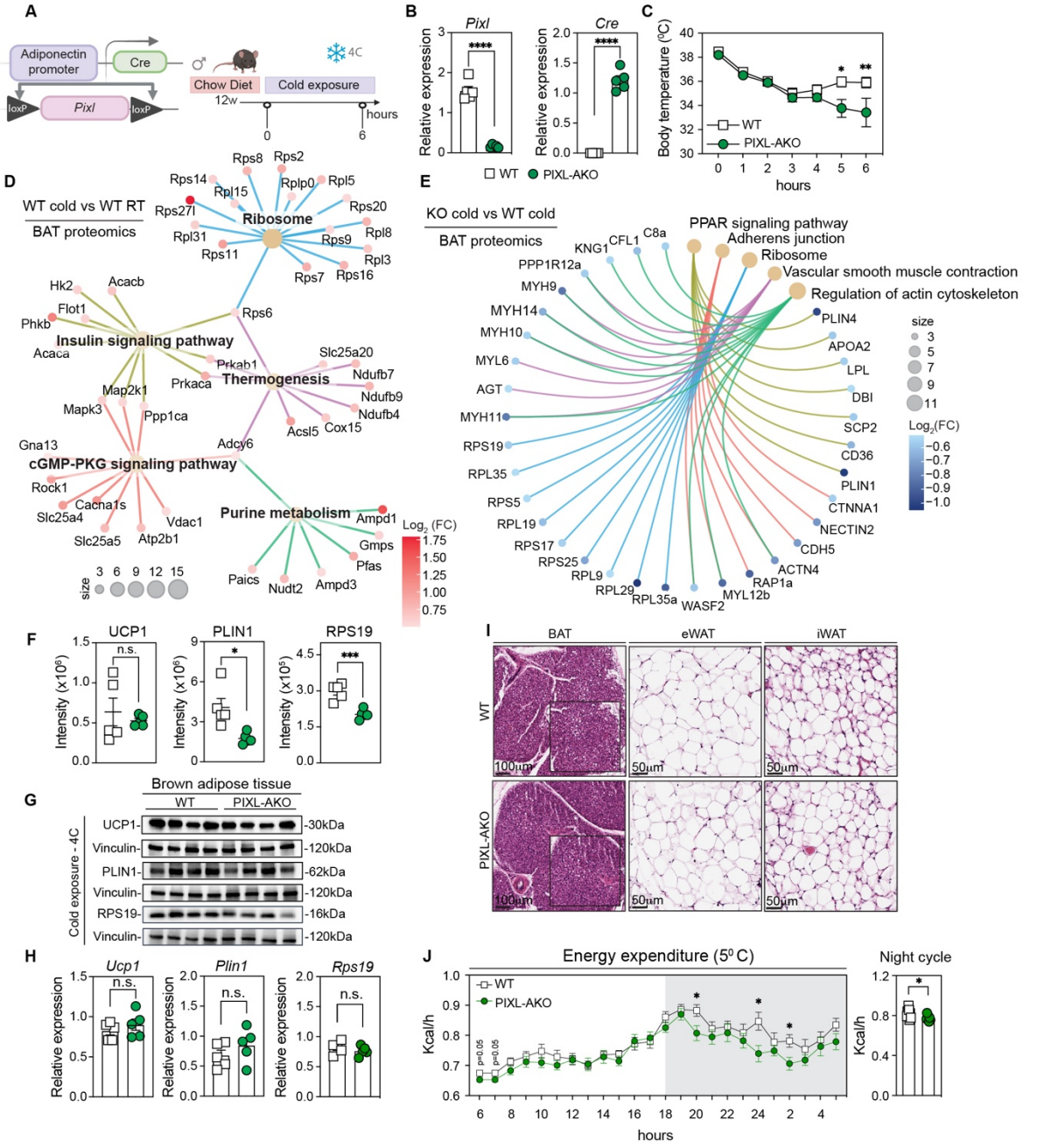

Figure 17 Absence of PIXL leads to cold sensitivity.

(A) PIXL-AKO mice model: floxed *Pixl* mice were crossed to Adiponectin-Cre mice to generate adipocyte-specific KOs (PIXL-AKO). (**B**) *Pixl* and *Cre* expression in brown adipose tissue (BAT) confirming knockout of *Pixl*. (**C**) Cold-exposure challenge in WT and PIXL-AKO mice for 6 h. (**D**) Network from proteomics analysis of upregulated proteins in BAT from WT mice in cold vs room temperature (adj. pvalue <0.05). (**E**) C-net proteomics analysis of downregulated proteins in BAT from PIXL-AKO vs WT during cold exposure (pvalue <0.05). (**F**) Proteomics intensity signal of UCP1, PLIN1, and RPS19. (**G**) Western blot analysis of UCP1, PLIN1, and RPS19 from BAT. (**H**) mRNA expression of *Ucp1*, *Plin1*, and *Rps19* from BAT. (**I**) Histological analysis of BAT, eWAT, and iWAT (hematoxylin and eosin stain) from either WT or PIXL-AKO mice at 4C (after 6h). (**J**) Energy expenditure from PIXL-AKO and WT mice at 5C. Data represent mean ± SEM (n = 5-9 mice per group). GP pvalue style: *p= 0.0332; **p < 0.0021; ***p < 0.0002 by one-way ANOVA, multiple comparisons followed by Tukey post hoc test.

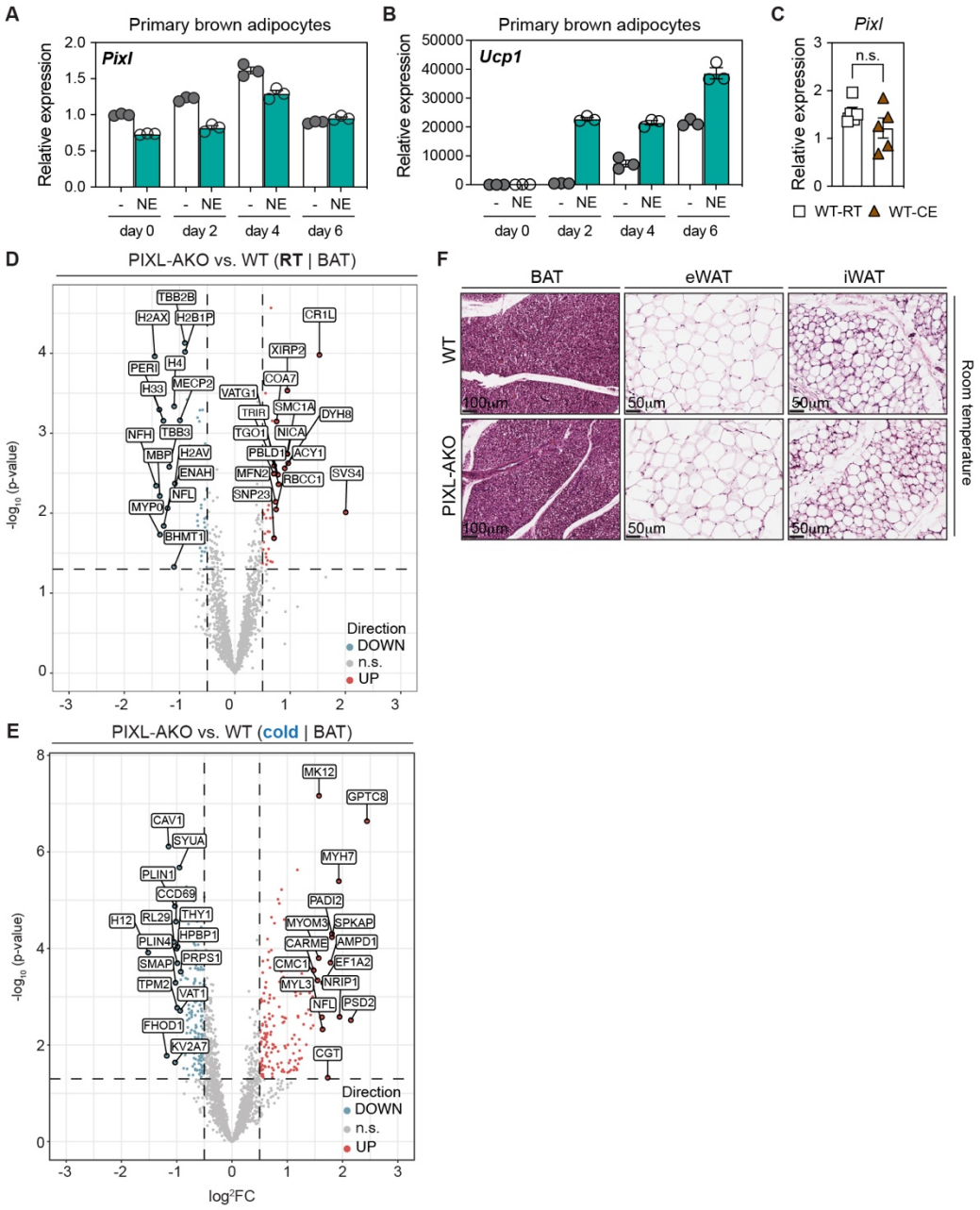

SFigure 13 Characterization of Pixl in brown adipose tissue.

(**A-B**) mRNA expression of *Pixl* and *Ucp1* in primary brown adipocytes during differentiation and stimulation with norepinephrine. (**C**) mRNA expression of *Pixl* during room temperature and cold exposure in BAT. (**D-E**) Volcano plot from PIXL-AKO vs WT at room temperature and cold exposure, respectively (pvalue<0.05) (**F**) Histological analysis of BAT, eWAT, and iWAT (hematoxylin and eosin stain) from either WT or PIXL-AKO mice at room temperature. Data represent mean ± SEM (n = 5-9 mice per group).

Therefore, we conclude that the absence of PIXL *in vivo* impairs cold adaption. A mechanism that in part seems to be mediated by a reduction in protein expression of essential

adipose proteins but not mRNA levels. As a consequence, PIXL-AKO mice presented a decreased energy expenditure compared to control mice.

3.2.5 PIXL-dependent maladaptation of adipose tissue during obesity

Next, we decided to evaluate how the absence of *Pixl* would impact a chronic process such as diet-induced obesity. First, we defined in each fraction of the adipose tissue Rosi upregulated *Pixl*. We dissociated eWAT and iWAT into stromal vascular fraction (SVF) and mature adipocytes (mAD). We observed that *Pixl* was upregulated exclusively in the mAD fraction (**Fig18A**). We also confirmed again our knockout model in the mAD of eWAT and iWAT (**FigS14A**). Subsequently, we evaluated if this upregulation of *Pixl* in the mAD was also present in lean mice. Indeed, we observed that Rosi robustly upregulated *Pixl* in mAD of lean mice in both eWAT and iWAT (**Fig18B**). Then we decided to challenge those mice with control (10% low-fat diet- LFD) and 60% high-fat diet (60% HFD) (**Fig18C**). Since *Pixl* is an X-linked gene we perform experiments in males and females. Male mice on a 10% LFD gained less body weight (**Fig18D**), had a slight decrease in fat mass (**Fig18E**), and a trend in being more glucose tolerant (**FigS14B**) and less insulin resistant (**FigS14C**) compared to their littermate controls. In contrast, male mice on a 60% HFD, gained more weight (**Fig18F**), increased fat mass (**Fig18G**), and became glucose intolerant (**Fig18H**) compared to control mice. We did not observe changes in the insulin tolerance test (**FigS14D**). We performed the same experiments with females on a 10% LFD (**FigS14E-H**) and a 60% high-fat diet (**FigS14I-L**) and did not observe any differences. Therefore, we decided to continue with the phenotype characterization using male mice. Lean male mice did not present any major histological changes in the liver, BAT, eWAT, or iWAT (**FigS14M**). On the other hand, PIXL-AKO obese mice macroscopic presented changes in the appearance and weight of the eWAT (**Fig18I-J**) compared to control mice. No significant alterations were observed in the liver, BAT, and iWAT (**Fig18J**).

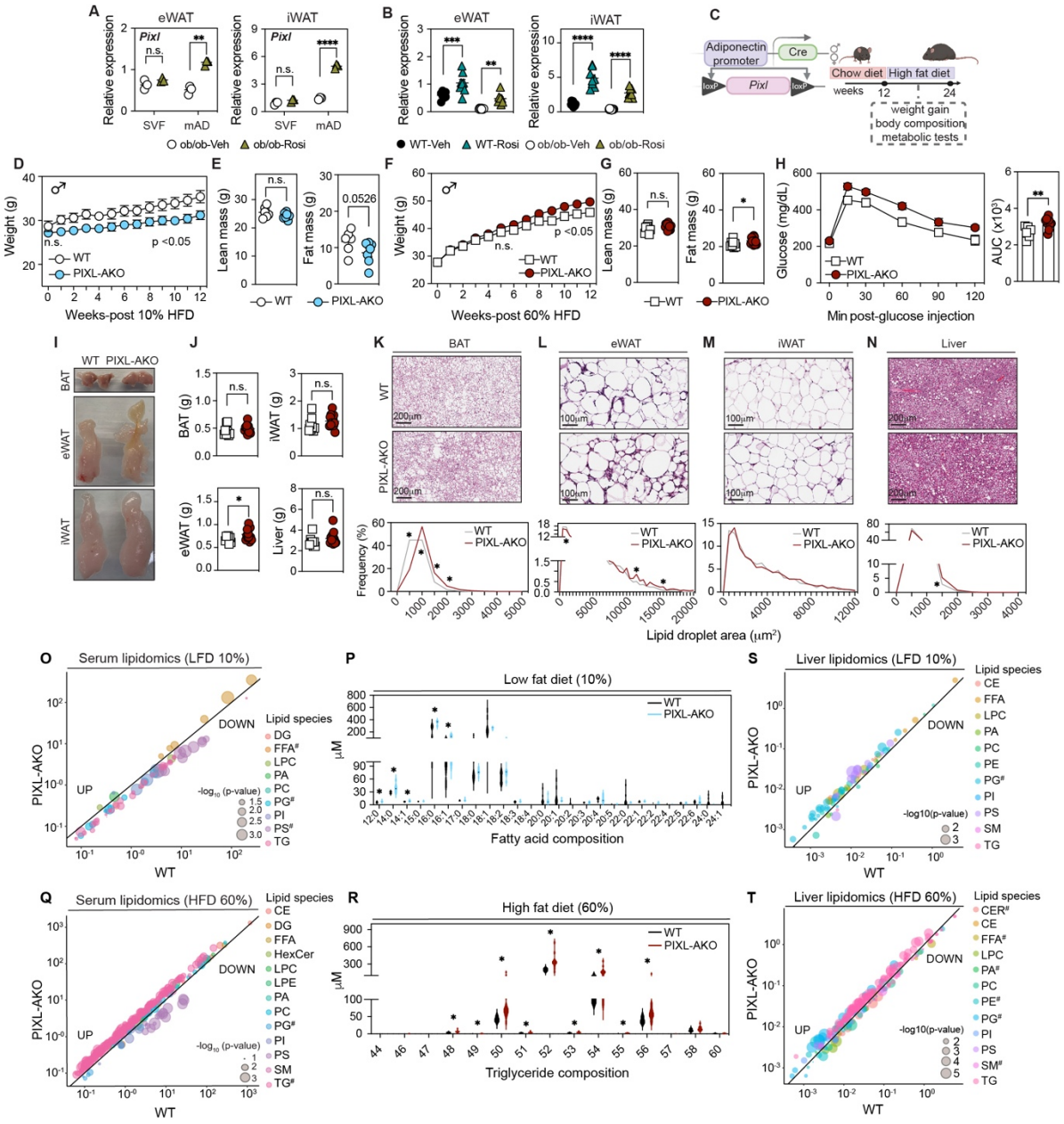

Figure 18 PIXL deletion exacerbates obesity.

(A) mRNA expression of *Pixl* in stromal vascular fraction (SVF) and mature adipocytes (mAD) of eWAT and iWAT. (**B**) mRNA expression of *Pixl* in mAD of lean (WT), and obese (ob/ob) mice treated with vehicle (Veh) or rosiglitazone (Rosi). (**C**) Schematic experimental design: WT and PIXL-AKO, males and females were placed on a low-fat diet (10%) or a high-fat diet (60%) for at least 12 weeks. Weight gain, body composition, and glucose/insulin tolerance were accessed. (**D-E**) Body weight and body composition of male WT and PIXL-AKO mice in a 10% low fat diet. (**F-G**) Body weight and body composition of male WT and PIXL-AKO mice in a 60% high fat diet. (**H**) Glucose tolerance test of male mice after 16 weeks on 60% HFD. (**I**) Macroscopic images of BAT, eWAT and iWAT of male mice after 20 weeks on 60% HFD. (**J**) Tissue weight of BAT, eWAT, iWAT and liver of WT and PIXL-AKO mice after 20 weeks on 60% HFD. (**K-L**) Histological analysis of BAT, eWAT, iWAT and Liver (hematoxylin and eosin stain) from either WT or PIXL-AKO mice after 20 weeks on high-fat diet. Bottom panel represent quantification of lipid droplet area and the frequency distribution. (**O**) Serum lipidomics of WT and PIXL-AKO mice after 20 weeks on 10% low-fat diet. (**P**) Fatty acid bond composition from WT and PIXL-AKO mice after 20 weeks on 10% low-fat diet. (**Q**) Serum lipidomics of WT and PIXL-AKO mice after 20 weeks on 60% high-fat diet. (**R**) Triglyceride bond composition from WT and PIXL-AKO mice after 20 weeks on 60% high-fat diet. (**S-T**) Liver lipidomics of

WT and PIXL-AKO mice after 20 weeks on 10 % and 60% high-fat diet, respectively. Data represent mean ± SEM (n = 8-11 mice per group). GP pvalue style: n.s.= non-significant, *p= 0.0332; **p < 0.0021; ***p < 0.0002 by two-tailed Student's t-test or by one-way ANOVA, multiple comparisons followed by Tukey post hoc test or two-way ANOVA followed by Bonferroni post hoc test (GTT).

Next, we decided to microscopically characterize these tissues by measuring the lipid droplet area. PIXL-AKO BAT and eWAT presented a decrease in the frequency of smaller lipid droplets and an increase in hypertrophic ones compared to control mice (**Fig18K-L**). iWAT did not present any alteration in both mice groups (**Fig18M**) and the liver had a slight increase in bigger lipid droplets in PIXL-AKO mice (**Fig18N**). Finally, we decided to study the impact of this obesity maladaptation on systemic metabolism. We first compared the serum lipidomic of PIXL-AKO mice on 10% LFD and 60% HFD to their respective controls. Under 10% LFD PIXL-AKO presented an upregulation in free fatty acids (FFA), and a decrease in phosphatidylserine (PS), and phosphatidylglycerol (PG) compared to their controls (**Fig18O**). Within the FFA composition, the main changes were in 12:0, 14:0, 14:1, 16:0, and 16:1 (**Fig18P**). Conversely, during 60% HFD PIXL-AKO mice substantially increased the levels of triglycerides (TG) in the serum compared to littermate controls (**Fig18Q**). TG composition revealed an increase in 48:0, 49:0, 50:0, 51:0, 52:0, 53:0, 54:0, 55:0, and 56:0 in the PIXL-AKO mice (**Fig18R**). Next, we analyzed the hepatic lipid composition of those animals. Similarly to the serum lipidomic, the liver lipidomic revealed a major remodeling during the 60% HFD challenge (**Fig18S-T**). PIXL-AKO mice presented a similar hepatic liver profile to control mice during 10% LFD, with only upregulation of phosphatidylglycerol (PG) (**Fig18S-FigS14N**). After 60% HFD, PIXL-AKO mice increased the levels of phosphatidic acid (PA) and phosphatidylglycerol (PG) and decreased FFA, ceramide (CER), and phosphatidylethanolamine (PE). Fatty acid composition revealed a major decrease at 16:0 and a minor decrease at 18:0 in PIXL-AKO mice compared to controls (**FigS14O-P**).

Overall, the deletion of PIXL in the adipose tissue exacerbated the onset of obesity and conferred PIXL-AKO mice a detrimental metabolic profile, with increases in glucose intolerance, macrophage infiltration, hypertrophic adipocytes, and hypertriglyceridemia compared to control mice.

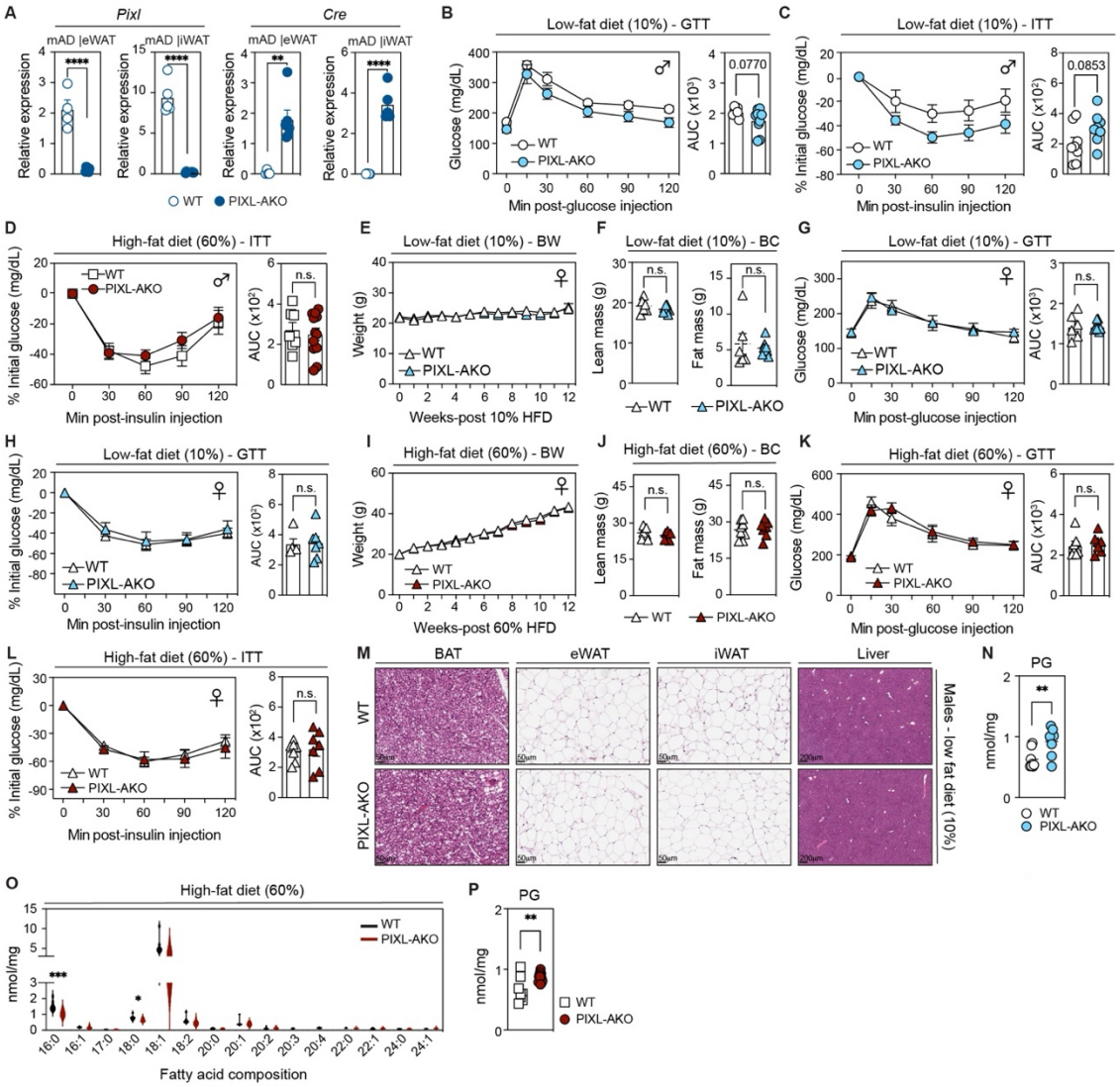

SFigure 14 Dietary and sex response of adipose tissue in the absence of PIXL.

(**A**) *Pixl* and *Cre* expression in mAD of eWAT and iWAT. (**B-C**) Glucose and insulin tolerance test of male mice after 16 weeks on 10% LFD. (**D**) Insulin tolerance test of male mice after 16 weeks on 60% HFD. (**E-F**) Body weight and body composition of female WT and PIXL-AKO mice in a 10% low fat diet. (**G-H**) Glucose and insulin tolerance test of female mice on 10% LFD. (**I-J**) Body weight and body composition of female WT and PIXL-AKO mice in a 60% high fat diet. (**K-L**) Glucose and insulin tolerance test of female mice on 60% HFD. (**M**) Histological analysis of BAT, eWAT, iWAT and Liver (hematoxylin and eosin stain) from either WT or PIXL-AKO mice after 20 weeks on low-fat diet (10%). (**N**) Phosphatidylglycerol (PG) quantification from liver lipidomics (10%LFD). (**O-P**) Hepatic fatty acid bond composition and Phosphatidylglycerol (PG) concentration from WT and PIXL-AKO male mice after 20 weeks on 60% high-fat diet. Data represent mean ± SEM (n = 8-11 mice per group). GP pvalue style: n.s.= non-significant, *p= 0.0332; **p < 0.0021; ***p < 0.0002 by two-tailed Student's t-test or by one-way ANOVA or two-way ANOVA followed by Bonferroni post hoc test (GTT, ITT).

3.2.6 Impact of PIXL deletion on eWAT adaptation during obesity

Finally, since the eWAT was the tissue that mostly changed in size, structure, and adipocyte morphology we decided to further define the underlying mechanisms driving this phenotype. Since we noticed an increase in cellular infiltration in the PIXL-AKO eWAT compared to WT (**Fig18L**), we decided to stain the adipose section with an F4/80 marker. Immunohistochemistry analysis revealed that PIXL-AKO mice presented an increase in macrophage/monocyte infiltration in the eWAT compared to control mice (**Fig19A**).

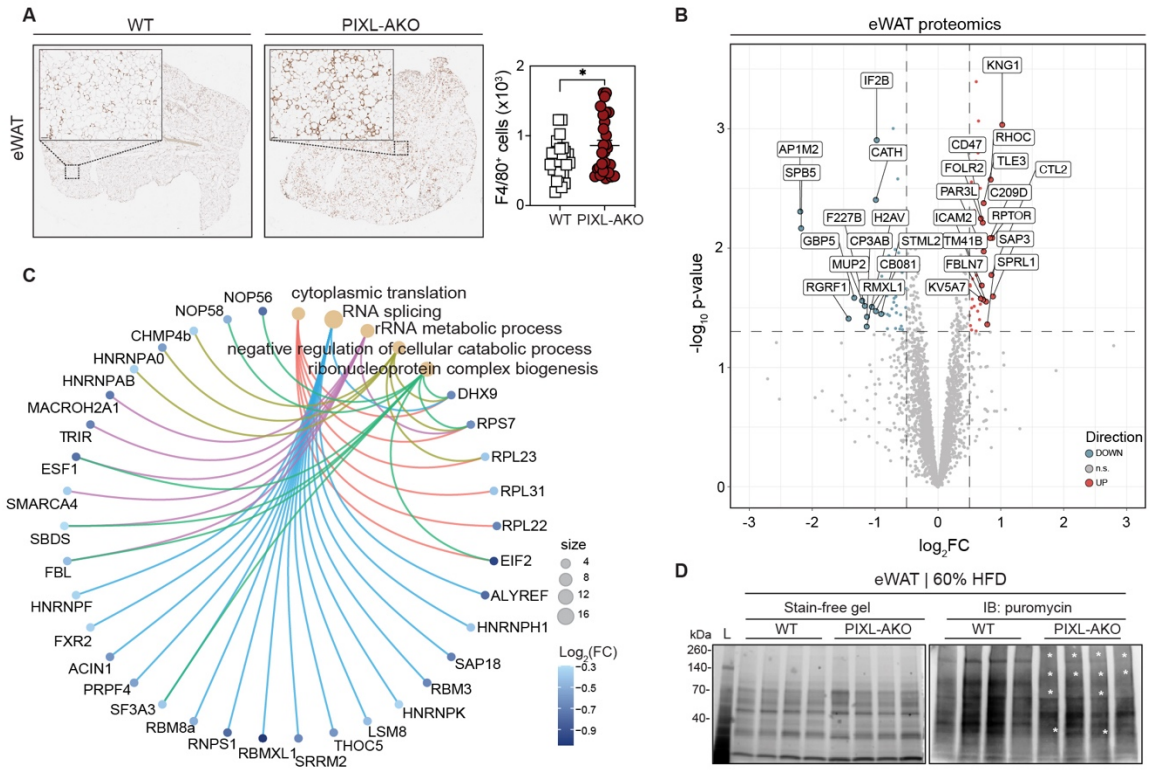

Figure 19 Absence of PIXL leads to eWAT maladaptation during obesity.

(**A**) F4/80 immunohistochemistry of eWAT from WT and PIXL-AKO male mice after 20 weeks on 60% HFD. (**B**) Volcano plot from eWAT proteomics of WT and PIXL- AKO mice (pvalue<0.05). (**C**) C-net proteomics analysis of downregulated proteins in eWAT from PIXL-AKO vs WT after 20 weeks in 60% HFD (pvalue <0.05). (**D**) Surface Sensing of Translation (SUnSET). Puromycin is used as a tyrosyl-tRNA analog therefore being incorporated in the newly synthesized proteins during translation (puromycin-tagged peptide). Immunoblots of eWAT. Left panel: total protein in stain-free gel. Right-panel: immunoblot anti-puromycin. Data represent mean ± SEM (n = 4-8 mice per group). GP pvalue style: n.s.= non-significant, *p= 0.0332; **p < 0.0021; ***p < 0.0002 by two-tailed Student's t-test.

This phenotype seems to be exclusive to the eWAT and no alterations were observed in the iWAT (**FigS15A**). Next, we performed RNA sequencing in the eWAT to identify the main pathway downregulated in the absence of *Pixl*. Overall, the main pathways downregulated in the eWAT of PIXL-AKO mice showed downregulation of pathways involved in mRNA processing, metabolism, and stabilization, suggesting an impact on the translation process (**FigS15B**). Subsequently, we performed proteomics using the same tissue to identify the main proteins downregulated. Volcano plot (**Fig19B**) and pathways analysis (**Fig19C**) revealed a downregulation in the ribonucleoprotein complex biogenesis and cytoplasmic translation. Finally, as a readout to evaluate overall eWAT protein synthesis, we performed the SUrface SEnsing of Translation (SUnSET) assay *in vivo.* Immunoblot analysis indeed revealed a decrease in the incorporation of puromycin into newly synthesized nascent peptides in PIXL-AKO mice compared to WT mice.

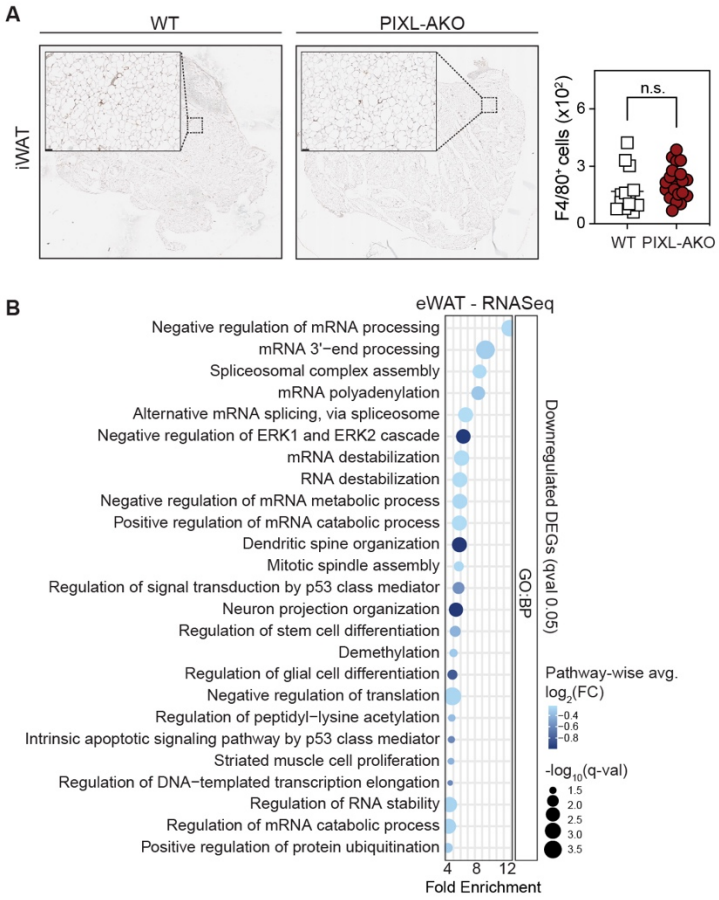

SFigure 15 Adipose transcriptomics remodeling after PIXL deletion.

(**A**) F4/80 immunohistochemistry of iWAT from WT and PIXL-AKO male mice after 20 weeks on 60% HFD. (**B**) Downregulated pathway from RNA-Seq of eWAT from eWAT from PIXL-AKO vs WT after 20 weeks in 60% HFD (pvalue <0.05). Data represent mean ± SEM (n = 4-8 mice per group). GP pvalue style: n.s.= non-significant, *p= 0.0332; **p < 0.0021; ***p < 0.0002 by two-tailed Student's t-test.

3.3. Discussion

Translation regulation is a fundamental process to cell development, differentiation, and function. Several reports have been presented elucidating a very controlled and health upregulation of translation during T cell activation (De Silva, Ferguson et al. 2021), and stem cell differentiation and proliferation (Sampath, Pritchard et al. 2008, Signer, Magee et al. 2014, Zhang, Shalaby et al. 2014, Forester, Oses-Prieto et al. 2022). However, an uncontrolled increase in protein synthesis can lead to development of cancer (Jewer, Lee et al. 2020, Morral, Stanisavljevic et al. 2020, Passarelli, Pinzaru et al. 2022).

Notably, not much is known about the regulation of the translation machinery during obesity. As discussed in the introduction, few studies have globally manipulated (downregulated) the expression of initiation factors and it seems to overall reduce lipid storage and enhance lipid oxidation (Tsukiyama-Kohara, Poulin et al. 2001, Brina, Miluzio et al. 2015, Conn, Yang et al. 2021). Nonetheless a fat-specific mechanism of translation regulation is still unknown.

We first, uncovered the role Rosi as a translation enhancer by driving the expression of PPARγ and consequently the induction of ribosomal proteins. In addition to that, on Chapter 3 we now demonstrated the function of a novel and uncharacterized protein in the adipose tissue, PIXL. We have demonstrated that PIXL overall interacts with the initiation complex and absence of PIXL drives cold sensitivity and obesity. A mechanism that seems to be related to which mRNAs are being translated to confer adipose tissue health adaptation to different environmental stressors.

In conclusion, we demonstrated that PPARγ agonist (Rosi) is essential to not only drive the transcription program of fat cells but also to modulate and remodel the translation machinery in order to accommodate cellular specialization.

3.4. Methods

Mice

Male and female mice, 12- weeks old, C57BL/6 background, will be used unless otherwise stated. We engineered mice with loxp sites flanking the *Pixl* exon. Notably, *Pixl* is an X-linked gene and contains only one exon that is flanked by 5' and 3' UTR. A conditionally targeted allele based on the Cre-Lox system has allowed us to generate both global and tissue specific knockout mice. In order to target mature adipocytes, used the Cre-lox system where *Pixl* flox mice were crossed with Adiponectin-Cre, generating a conditional knockout of *Pixl* in cells expressing adiponectin. Adult C57BL/6J (12-week-old) male mice (stock #000664) and Lep^{ob}/Lep^{ob} (stock #000632) were acquired through Jackson Laboratories. All mice were housed at a maximum of 5 animals per

cage in temperature-controlled rooms under a 12-hour light/dark cycle and provided water and chow *ad libitum.* All mouse procedures were performed under animal study proposals approved by the University of California, Los Angeles Animal Research Committee (ARC 2019-066).

Special diets

To induce obesity, mice were placed onto a high-fat diet (HFD) (Research diets D12492) with 60 kcal% fat. Control mice were placed onto a low-fat diet (Research diets D12450J) with 10 kcal% fat matching sucrose to D12492.

Rosiglitazone treatment

To examine the effects of PPARγ agonist, C56BL/6 and Lep^{ob}/Lep^{ob} mice were given 30 mg/kg rosiglitazone (Sigma R2408), or vehicle [2.6% methylcellulose (StemCell Technologies, M3120) diluted 1:5 in Dulbecco's modified medium (GIBCO)] by oral gavage in the morning and evening for three consecutive days as previously described (Davies, Waki et al. 2008).

RNA Sequencing and data processing

The RNA sample from BAT, eWAT, and iWAT received was quantified using Qubit 2.0 Fluorometer (Life Technologies, Carlsbad, CA, USA) and RNA integrity was checked using TapeStation (Agilent Technologies, Palo Alto, CA, USA). The RNA sequencing library was prepared using the NEBNext Ultra RNA Library Prep Kit for Illumina using manufacturer's instructions (NEB, Ipswich, MA, USA). Briefly, mRNAs were initially enriched with Oligod(T) beads. Enriched mRNAs were fragmented for 15 minutes at 94 °C. First-strand and second-strand cDNA were subsequently synthesized. cDNA fragments were end-repaired and adenylated at 3'ends, and universal adapters were ligated to cDNA fragments, followed by index addition and library enrichment by PCR with limited cycles. The sequencing library was validated on the Agilent TapeStation (Agilent Technologies, Palo Alto, CA, USA), and quantified by using Qubit 2.0

Fluorometer (Invitrogen, Carlsbad, CA) as well as by quantitative PCR (KAPA Biosystems, Wilmington, MA, USA). The sequencing library was clustered on three lanes of a flowcell. After clustering, the flowcell was loaded on the Illumina HiSeq instrument (4000 or equivalent) according to the manufacturer's instructions. The sample was sequenced using a 2x150bp Paired End (PE) configuration. Image analysis and base calling were conducted by the HiSeq Control Software (HCS). Raw sequence data (.bcl files) generated from Illumina HiSeq was converted into fastq files and de-multiplexed using Illumina's bcl2fastq 2.17 software. One mismatch was allowed for index sequence identification. Quality control of raw sequencing data was conducted using FastQC (Andrews 2010), employing default parameters to evaluate the quality of reads. Sequencing reads were mapped to the mouse reference genome (mm10) using Salmon (Patro, Duggal et al. 2017) with a quasi-mapping algorithm**.**

Differential expression genes analysis

The quantified transcripts were analyzed using DESeq2(Love, Huber et al. 2014) The raw count data input for DESeq2 was prepared using tximport to import Salmon output into R. Genes were classified as differentially expressed based on an adjusted p-value of less than 0.05 and a log2 fold change greater than 0.2.

Pathway enrichment analyses

We selected significant up/down-regulated genes and proteins as input for pathway enrichment analyses, respectively. Pathway enrichment analyses were performed using enrichGO and enrichKEGG functions in the clusterProfiler package (v4.6) (Wu, Hu et al. 2021). For transcriptomics data, significant pathways were defined with q-value < 0.05 and at least five genes enriched in the pathways. For proteomics data, significant pathways were defined with q-value < 0.05, Benjamini-Hochberg-corrected p-value < 0.05, and at least five proteins enriched in the

pathways. Pathway-wise avg.log2(FC) value was calculated as the mean of the avg.log_2FC of genes or proteins enriched in the pathway. Fold enrichment was calculated as the ratio of geneRatio by BgRatio associated with the enriched pathway. enrichDF2enrichResult and cnetplot functions were applied to visualize linkages of genes/proteins and enriched concepts (GO: BP categories and KEGG pathways).

Pparγ ChIP-Seq

Publicly available dataset GSE41481 was downloaded from Gene Expression Omnibus (Siersbæk, Loft et al. 2012). For each fat depot, sequenced reads from the ChIP-seq library were first aligned to mouse reference genome (mm9) with Bowtie2 (Langmead and Salzberg 2012). Uniquely aligning read per genomic position was kept with Picard for downstream peak calling. Enriched PPARγ-binding regions were identified using HOMER (Heinz, Benner et al. 2010) findPeaks program (with "factor" mode) where default parameters for tag count normalization (to 10 million reads), false-discovery rate (FDR) cutoff (< 0.1%), and filtering options (≥ 4-fold tag count enrichment compared to both input control and local tag density) were applied. Peaks were annotated to the nearest TSS using HOMER annotatePeaks.pl program. Lastly, enriched peaks were visualized with Integrative Genomics Viewer (IGV) (Robinson, Thorvaldsdóttir et al. 2011).

Lipidomics

For serum lipidomics 25μL of serum was used. For homogenized tissue, 50-100 mg of tissue were collected in a 2mL homogenizer tube pre-loaded with 2.8mm ceramic beads (Omni #19-628). .75mL PBS was added to the tube and homogenized in the Omni Bead Ruptor Elite (3 cycles of 10 seconds at 5 m/s with a 10 second dwell time). Homogenate containing 2-6mg of original tissue was transferred to a glass tube for extraction. A modified Bligh and Dyer extraction (Hsieh, Williams et al. 2021) was carried out on all samples. Prior to biphasic extraction, an

internal standard mixture consisting of 70 lipid standards across 17 subclasses was added to each sample (AB Sciex 5040156, Avanti 330827, Avanti 330830, Avanti 330828, Avanti 791642). Following two successive extractions, pooled organic layers were dried down in a Thermo SpeedVac SPD300DDA using ramp setting 4 at 35°C for 45 minutes with a total run time of 90 minutes. Lipid samples were resuspended in 1:1 methanol/dichloromethane with 10mM Ammonium Acetate and transferred to robovials (Thermo 10800107) for analysis. Samples were analyzed on the Sciex 5500 with DMS device (Lipidyzer Platform) with an expanded targeted acquisition list consisting of 1450 lipid species across 17 subclasses. Differential Mobility Device on Lipidyzer was tuned with EquiSPLASH LIPIDOMIX (Avanti 330731). Data analysis performed on an in-house data analysis platform comparable to the Lipidyzer Workflow Manager (Su, Bettcher et al. 2021). Instrument method including settings, tuning protocol, and MRM list available in (Su, Bettcher et al. 2021). Quantitative values were normalized to mg of tissue.

Stable cell lines

10T1/2 cells were used for expression of Pixl-HA/ Pixl-flag and Crispr-Cas9 knockout (KO). Briefly, Pixl cDNA was first PCR amplified and subcloned into Gateway pDONR vector (Addgene). The C-terminal 3xFLAG or 3XHA was then added through Gibson assembly (NEB). Gateway LR clonase was used to insert the construct on the mammalian retroviral vector pBABE-puro (Addgene). Retrovirus packing was performed using PhoE cells. Puromycin selection (4μg/mL) was performed to select cells. For Crispr-Cas9 Pixl knockout, experiments were performed according to (Hildreth, Riggan et al. 2020) without major changes. Briefly, 1x 10^6 10T1/2 cells were grown and used for each electroporation. Cell suspension was mixed with ribonucleoprotein complex (sgRNA (Synthego) and TrueCut Hifi Cas9 (ThermoFisher), and electroporated using Neon Nxt Electroporation System (Invitrogen). After 1 h incubation at 37°C, cells were platted and cultured until 70% confluency was reached. Genomic DNA was extracted

and purified according to manufactory protocol (Thermo), and edited regions were amplified by PCR. Sequencing results were analyzed using Synthego ICE CRISPR Analysis Tool. gRNAs with a KO score higher than 55% were used for further clonal selection. Shortly, single cell isolation was performed using FACSAria III (BD). Single clones were expanded, and KO and Indel scores higher than 90% were used as a cutoff for selection. KO clones were then reconstituted with either *Pixl* or *Pixl-flag* using the retrovirus system described earlier. Reconstituted clones with a high adipogenic potential were selected for the downstream experiments.

Acute cold challenge

Mice were first fasted for 1h at room temperature. Next mice were singly housed at 4°C in prechilled cages without food but with 50g of bedding, water and one nestlet. Core body temperature was monitored hourly for 6h (9am - 3pm) using RET-3 Rectal Probe (Physitemp). Mice were removed from the study and euthanized once their core body temperatures reached 28°C or lower.

Indirect calorimetry

Respiratory exchange ratio (EE) and energy expenditure were assessed using Promethion Core - Metabolic Analysis System CGF (Sable Systems International) for 96 hours. First, mice were acclimated at 22°C for 24h. Then, mice were kept under 30°C, 20°C, 10°C, and 5°C for 24 hours respectively. Mice had water and food *ad libitum*.

Protein extraction and western blots

Proteins were lysed using radioimmunoprecipitation assay buffer (RIPA) (50mM Tris-HCl pH 7.6, 150mM NaCl, 0.1% sodium dodecyl sulfate, 0.5% sodium deoxycholate, 1% NP40 and freshly added halt protease/phosphate inhibitor cocktail (ThermoFisher). Lysates were cleared by

centrifuging at 14,000g for 20 min at 4°C. Supernatants were retained, and protein concentration was determined using Pierce BCA Protein Assay Kit (ThermoFisher). Immunoblots were performed using 20µg of protein and total protein was assessed using UV light exposure to Mini-Protean TGX Stain-free gels (Biorad). Puromycilation was detected using anti-puromycin antibody (12D10, Sigma), and HRP AffiniPure Goat anti-mouse IgG, Fcγ subclass 2a specific (Jackson Immuno Research). The following antibodies were used for the regular western blots: UCP1 (D9D6X Cell Signaling), PLIN1 (D1D8 Cell Signaling), RPS19 (ProteinTech), VINCULIN (hVIN-1 Sigma), anti-flag M2 (D6W5B Cell Signaling), eIF4E (Cell Signaling), eIF4B (W17131B Biolegend), eIF3M (ThermoFisher), RPS11 (Abcam), RPS14(Abcam), RPL23a (ProteinTech), anti-mouse IgG, HRP-liked (Cell Signaling) and anti-rabbit IgG, HRP-liked (Cell Signaling).

Body composition

Lean and fat mass were accessed using nuclear magnetic resonance (NMR) Minispec Bruker Systems.

Immunohistochemistry

Adipose tissue was harvested from mice, fixed with 10% formalin for 48 h; 70% ethanol for 24 h, and, paraffin-embedded and sectioned at 10 µm. For immunohistochemical studies, slides were incubated overnight at 62°C to remove excess paraffin. Slides were rehydrated and antigens were retrieved using AR6 Buffer (Akoya Biosciences AR600250ML.) Slides were cooled at 4°C for 30 minutes and blocked in 3% hydrogen peroxide (Flinn Scientific H0008) for 10 minutes. Slides were then blocked with 5% Normal Goat Serum (Vector Laboratories S-1000-20 goat serum for 1 hour. Slides were incubated with AvidinD blocking solution and Biotin Blocking Solution for 15 minutes each (Vector Laboratories Sp-2001). To stain macrophages, slides were incubated overnight with purified anti-mouse F4/80 antibody at a 1:200 dilution (Biolegend 123102, clone

BM8). Slides were incubated with ImmPRESS HRP Goat Anti-Rat IgG for 1 hour at room temperature (Vector Laboratories MP-7404-50). Slides were then incubated with Vectastain Elite ABC reagent for 1 hour (Vector Laboratories PK-7100). Slides were developed for 1 minute using ImmPACT DAB Substrate (Vector Laboratories SK-4105). Slides were counterstained using Harris Modified Hematoxylin (Fisher Chemical PK-7100) for 3 minutes and dehydration steps were performed. Images were taken at 20 x magnification and analyzed with AperioImageScope. The number of F4/80 positive cells were counted using Qupath 0.2.3.

Primary brown adipocytes

Primary mouse brown adipocytes were prepared as previously described with some modifications (Veliova, Tol et al. 2023). BAT harvested from 3-4 new-born neonates (P+1) were minced for 30 sec, transferred into 15 ml conical tubes, and incubated with 7.5mL of digestion buffer (100 mM HEPES pH 7.4, 123 mM NaCl, 1.3 mM $CaCl_2$, 5 mM KCl, 5mM glucose, 2% essentially fatty acid-free BSA, 2mg/ml type 2 collagenase (Worthingon) for 40 min at 37°C under inverted rotation. Then, the digested BAT suspension was adjusted to 15 mL with ice-cold Dulbecco's modified Eagle's medium (DMEM: Corning 10-013-CM) and passed through 18.5G needle (8 times) for extra tissue disruption. Digested tissue was strained with 40 µm filters into 50mL conical tubes, followed by washing the filters with 30 mL ice-cold DMEM and spun down at 600 x g for 10 min. Collected preadipocytes were resuspended with 30mL ice-cold DMEM, spun down at 600 x g for 10 min, resuspended with warm pBA growth medium (DMEM supplemented with 15% Fetal Bovine Serum (GemCell^{TM}), Penicillin (50 U/mL), and streptomycin (50 µg/mL)) and plated in 10 cm dishes. After 48 hours, cells were rinsed with pBA growth medium and cultured with fresh pBA growth medium. Once cells reached ~80% confluence in a 10 cm dish, they were subcultured to experiment format. For the differentiation, preadipocytes were grown to confluence and treated with rosiglitazone (1 µM), indomethacin (125 µM), 3-isobutyl-1-methylxanthine (0.5

mM), dexamethasone (1μM), Humulin (100nM) and triiodothyronine (2 nM) for 48 h (day 0-2), rosiglitazone (1 μM), Humulin (100nM) and triiodothyronine (2 nM) for 48 h (day 2-4), and Humulin (100nM) and triiodothyronine (2 nM) for 48 h (day 4-6). For RNA isolation, the differentiation medium was replaced with fresh pBA growth medium and stimulated with 1μM norepinephrine (Baxter) for 4 h.

Immunoprecipitation

10T1/2 Pixl-flag cells were differentiated until day 2 (0.5mM 3-isobutyl-1-methylxanthine (Sigma), 1μM dexamethasone (Sigma), 5μg/mL insulin (GIBCO), 50nM GW1929 (Sigma)), washed twice with ice-cold PBS and incubated with lysis buffer (50mM Tris-HCl pH 7.6, 150mM NaCl, 0.5% sodium deoxycholate, 1% NP40 and freshly added halt protease/phosphate inhibitor cocktail (ThermoFisher)). Lysates were cleared by centrifuging at 14,000g for 20 min at 4°C. Supernatants were retained, and protein concentration was determined using Pierce BCA Protein Assay Kit (ThermoFisher). Lysates were incubated with pre-cleared anti-Flag M2 Magnetic Beads (Sigma) overnight at 4 °C with end-over-end rotation. Beads were collected using the DynaMag-2 magnetic stand (Invitrogen) and washed once with 50mM Tris-HCl pH 7.6, 150mM NaCl, 0.5% sodium deoxycholate, 1% NP40, protease/phosphate inhibitor cocktail, and twice with TBS, 0.1% Tween (TBS-T), and protease/phosphate inhibitor cocktail. Proteins were eluted from the beads with 3× Flag peptide (Sigma) in TBS-T buffer and samples were analyzed by western blot.

On-bead digestion of immunoprecipitated proteins

The beads obtained after immunoprecipitation were resuspended in 2M Urea, 50mM Tris-Cl, pH 8.0 followed by reduction and alkylation by the sequential addition of 5 mM tris (2-carboxyethyl) phosphine and 10 mM iodoacetamide. The samples were proteolytically digested overnight with Lys-C and trypsin at 37°C. The digestion was quenched by addition of formic acid to a final

concentration of 5%. The digested peptides were desalted using C18 pipette tips (Thermo Fisher, Prod. 87782). Dried peptides were resuspended in 5% formic acid and analyzed by LC-MS/MS.

Protein extraction and protease digestion for proteomics

Protein extraction and concentration were performed as described above. Equal amount of protein for each sample was reduced and alkylated by the sequential addition of 5 mM tris (2-carboxyethyl) phosphine and 10 mM iodoacetamide. This was followed by treatment with single-pot, solid-phase-enhanced sample preparation (SP3) protocol for protein clean-up (Hughes, Moggridge et al. 2019). Following SP3, eluates were proteolytically digested with Lys-C and trypsin at 37°C overnight in 18µl of 100mM triethylammonium bicarbonate (TEAB).

Isobaric labeling

Isobaric labeling of peptides was performed using 10-plex tandem mass tag (TMT) reagents. TMT reagents (0.8 mg) were dissolved in 41µL of dry acetonitrile (ACN). 9uL of 100% acetonitrile was added to the overnight tryptic digest of 30µg protein to which 3µL of TMT reagent was added. After 1 hour (RT, low speed vortexing), the reaction was quenched by adding 3.6µL of 5% hydroxylamine followed by incubation at RT for 15 minutes. The reaction mixture was acidified with formic acid added to a final concentration of 5%. The digested and labeled peptides were subjected to offline SP3-based peptide clean-up (Hughes, Moggridge et al. 2019). 2µL of each of the ten labelled peptide samples was pooled acidified with formic acid added to a final concentration of 5% and analyzed on LC-MS/MS for labeling efficiency.

Basic pH reversed-phase fractionation

The TMT labeled peptides were normalized based on median reporter intensity reported by Maxquant analysis, mixed and dried. The dried peptides were resuspended in 300uL of 0.1%

trifluoroacetic acid. High pH reversed phase fractionation was carried out using spin columns according to the manufacturer's protocol (Thermo Fisher). 8 fractions thus collected were dried, reconstituted in 30µL of 5% FA followed by LC-MS/MS analysis.

Mass spectrometry analysis of dried and digested tryptic peptides

Digested peptide samples from affinity purifications as well as peptide fractions resulting from the isobaric labeling experiment were separated by reversed phase chromatography using 75 µm inner diameter fritted fused silica capillary column packed in-house to a length of 25 cm with bulk 1.9mM ReproSil-Pur beads with 120 Å pores (Jami-Alahmadi, Pandey et al. 2021). The increasing gradient of acetonitrile was delivered by a Dionex Ultimate 3000 (Thermo Scientific) at a flow rate of 200nL/min. For affinity purification samples, the MS/MS spectra were collected using data dependent acquisition on Orbitrap Fusion Lumos Tribrid mass spectrometer (Thermo Fisher Scientific) with MS1 scans in orbitrap with resolution (r) of 120,000 followed by sequential MS2 scans at a resolution (r) of 15,000. For isobaric labeling experiment, data was collected on an Orbitrap Fusion Lumos Tribrid mass spectrometer (Thermo Fisher Scientific) using a synchronous precursor selection -MS3-based (SPS-MS3) method (McAlister, Nusinow et al. 2014). MS1 scans were collected in orbitrap with resolution (r) of 120,000 followed by sequential MS2 scans in the ion trap at a resolution (r) of 15,000. Synchronous precursor selection was enabled to include 10 MS2 fragment ions in MS3 spectrum which were collected in the orbitrap at 50,000 resolutions. For the analysis of affinity purification samples, the data generated by LC-MS/MS were analyzed on MaxQuant bioinformatic pipeline (Cox and Mann 2008). The Andromeda integrated in MaxQuant was employed as the peptide search engine and the data were searched against Mus musculus database (Uniprot Reference UP000000589). A maximum of two missed cleavages was allowed. The maximum false discovery rate for peptide and protein was specified as 0.01. For isobaric labeling experiment, raw data were analyzed by Maxquant with "variable

modifications" set for TMT10-plex 126, 127N, 127C, 128N, 128C, 129N, 129C, 130N, 130C, 131 to be at N-termini, as well as lysine for database searching and peptide identification. Group-specific parameters were set to "TMT10-plex labeled" and "reporter ion MS3". The parent and peptide ion search tolerances were set to 20 and 4.5 ppm respectively. The MaxQuant output files were subsequently processed for statistical analysis of differentially enriched proteins using MSstatsTMT (Huang, Choi et al. 2020).

Definition of differentially expressed proteins

For proteins in BAT, significant differentially expressed proteins were defined as $|\log_2 FC| > 0.5$ and adjusted p-value < 0.05. For proteins in eWAT, we applied $|\log_2 FC| > 0.1$ and p-value < 0.05 as cutoffs to define the significance of differential expression in order to obtain suggestive pathways due to the limited number of proteins that pass adjusted p-value < 0.05.

Stromal vascular fraction and mature adipocytes isolation

Stromal vascular fractions were isolated as previously described (Church, Berry et al. 2014). Briefly, entire WAT depots were cut into small pieces, suspended in DMEM (GIBCO) + 50 mM HEPES (GIBCO) + 1mg/mL type II collagenase (Sigma), + 1% BSA - low fatty acid (Gemini), and digested for 30 minutes at 37°C with agitation (120 rpm). The resulting dissociated tissue was centrifuged at 750g, 10 min, 4°C. Floating mature adipocytes layer were collected and processed for RNA or protein isolation as described in the methods. Stromal vascular fraction was resuspended and filtered using 100µm and 40µm cell strainers. After a second centrifugation at 750g, 3 min, 4°C cells collected and processed for RNA or protein isolation as described in the methods.

Confocal

Cells were grown to confluency and initiated in differentiation cocktail: complete adipogenic cocktail 0.5mM 3-isobutyl-1-methylxanthine (Sigma), 1μM dexamethasone (Sigma), 5μg/mL insulin (GIBCO), 50nM GW1929 Sigma for 2 days, and then maintenance media until defined end point (50nM GW1929, 5μg/mL insulin). For Pixl localization, cells were fixed with 4% paraformaldehyde, permeabilized with 0.1% Triton, blocked with normal donkey serum 5% (Jackson Immuno Research) and stained overnight with rabbit anti-HA (C29F4 Cell Signaling). Next, slides were washed four times with PBS and incubated for one hour with LipidTOX Green Neutral Lipid (Invitrogen), DAPI (AAT Bioquest), donkey anti-rat IgG Alexa Fluor 568 (Abcam). Images were acquired using Zeiss LSM900 microscope.

Histology and lipid droplet quantification

Tissues were fixed for 48h in 10% buffered formalin (ThermoFisher), after which they were washed with 70% ethanol (ThermoFisher), sectioned in paraffin (10 μm thickness for adipose tissues and 5 μm for liver), and stained with hematoxylin and eosin (H&E). The lipid droplet cell area from livers and progenitors/preadipocytes from confocal images were quantified using ImageJ.

Glucose and insulin tolerance test

For glucose and insulin tolerance tests, mice were fasted for 6 hours prior to the challenge with either glucose (1 g/kg mouse) or insulin (0.75U/Kg) via intraperitoneal injection. Blood glucose levels were assessed by tail vein bleeding using a glucometer (Accu-Chek). AUC was determined using Prism software (GraphPad).

Surface Sensing of Translation (SUnSET)

The assay was performed as previously described with small modifications (Ravi, Jain et al. 2020). Briefly, mice were intraperitoneally injected with puromycin (40 nmol/g) (Santa Cruz) and returned to their cages with food/water *ad libitum* for one hour. Next, brown, epididymal, and inguinal adipose tissue were collected, and proteins were lysed using radioimmunoprecipitation assay buffer (RIPA) (50mM Tris-HCl pH 7.6, 150mM NaCl, 0.1% sodium dodecyl sulfate, 0.5% sodium deoxycholate, 1% NP40 and freshly added halt protease/phosphate inhibitor cocktail (ThermoFisher). Immunoblots were performed using 20µg of protein and total protein was assessed using UV light exposure to Mini-Protean TGX Stain-free gels (Biorad). Puromycilation was detected using anti-puromycin antibody (12D10, Sigma), and HRP AffiniPure Goat anti-mouse IgG, Fcγ subclass 2a specific (Jackson Immuno Research).

Polysome profile

Polysome profiles were obtained as described before (Gandin, Sikström et al. 2014, Gandin, Masvidal et al. 2016, Chan, Robert et al. 2019). Cells were grown to confluency in 15-cm dishes. Cells were then treated to differentiate with complete adipogenic cocktail: 0.5mM 3-isobutyl-1-methylxanthine (Sigma), 1µM dexamethasone (Sigma), 5µg/mL insulin (GIBCO), 50nM GW1929 (Sigma) for 2 days, and then maintenance media until defined end point (50nM GW1929, 5µg/mL insulin). Before lysis, cells were boosted with fresh media for one hour and for the last 5 minutes cycloheximide (Sigma) was added to the media (final concentration 100µg/mL). Cells were lysed and collected in hypotonic lysis buffer (5mM Tris HCl pH 7.5, 2.5 mM MgCl2, 1.5 mM KCl, 100 µg/mL cycloheximide, 2 mM DTT), and 0.5% Triton, 0.5% Sodium Deoxycholate were then added to the cell lysates after collection. The cytoplasmic extracts were resolved on 5-50% sucrose gradients by centrifugation in an SW40 rotor at 150,000 x g for 2 hours. The absorbance at 260 nm was measured using a Piston Gradient Fractionator Model 153 instrument (BioComp, Canada). The results were plotted in R as previously described (Hulea, Gravel et al. 2018).

Protein and RNA extraction of polysome fractions

Fractions were collected in separate tubes and equal volume of TRIzol LS Reagent (Life Technologies) was added to each fraction. RNA was extracted according to manufacturer instructions. After removing the aqueous phase for RNA and discarding interphase, the lower phase was used for protein extraction. 4x volume cold acetone (-20^{0}C) was added to each fraction. Samples were left on ice for 30 min then centrifuged at max speed for 10 min at 4^{0}C. supernatants were discarded, and pellets were washed with 400 µL 100% Ethanol (centrifuged for 1 min and the supernatants were discarded). Samples were left to dry and then resuspended in 100 µL 1x Loading buffer in RIPA. Samples were boiled for 10 min at 100˚C and 10 µL (for GAPDH and RPS6) or 20 µL (for eIF4E and M2) was loaded on SDS-PAGE. Primary antibodies used were: GAPDH (14C10 Cell Signaling), RPS6 (C-8 Santa Cruz), eIF4E (A-10 Santa Cruz), anti-flag M2 (F1804 Sigma), and secondary antibodies anti-mouse IgG, HRP-liked (Cell Signaling) and anti-rabbit IgG, HRP-liked (Cell Signaling).

Gene expression

RNA was isolated using Trizol reagent (ThermoFisher). Isolated RNA was reverse transcribed using High-Capacity cDNA synthesis kit (ThermoFisher). Gene expression for selected genes was quantified using Quant Studio 6 Flex Real-Time PCR instrument, 384-well (Applied Biosystems by Invitrogen) with KAPA SYBR FAST qPCR 2x Master Mix Rox Low (Kapa Biosystems). The following primers were used: *36B4:* Forward: GGCCCTGCACTCTCGCTTTC, Reverse: TGCCAGGACGCGCTTGT; Ucp*1:* Forward: GCCCAATGAATACTGCCACT, Reverse: CTACGACACGGTCCAGGAGT; *Rps19:* Forward*:* CAGCAGGAGTTCGTCAGAGC, Reverse: CACCCATTCGGGGACTTTCA; *Cre:* Forward*:* GATTTCGACCAGGTTCGTTC, Reverse: GCTAACCAGCGTTTTCGTTC; *Pixl*: Forward: CTGGCCTCAAATGAAGAGGAAACT, Reverse:

TATGTATACCCATTGCAATCTGTGC; *Plin1*: Forward: AACGTGGTAGACACTGTGGTACA, Reverse: TCTCGGAATTCGCTCTCG.

3.5 Conclusions

Overall, we conclude that PPARγ-induced protein PIXL is an important player in adipose tissue homeostasis regulating the translation of defined mRNAs. Deletion of PIXL drives cold sensitivity in mice with a downregulation at protein levels of PLIN, CD36, LPL and PLIN4. On the other hand, during the onset of obesity the absence of PIXL drives adipocyte hypertrophy, adipose inflammation, fatty liver, and glucose intolerance. Therefore, PIXL seems to be an important protein maintaining adipose adaptation under different stress condition.

CONCLUSIONS

CHAPTER 4: FINAL CONCLUSIONS AND FUTURE DIRECTIONS

Adipose tissue plays a pivotal role in energy homeostasis, serving as a dynamic organ involved in the storage and release of lipids. However, the dysregulation of adipose tissue function, often associated with obesity, can lead to various metabolic disorders and health complications. Translation regulation emerges as a critical mechanism in adipose tissue biology and its link to obesity. Through intricate control of protein synthesis, translation regulation modulates key factors involved in adipogenesis, lipid metabolism, and inflammation, influencing the balance between adipose tissue expansion and metabolic health. Understanding the molecular mechanisms underlying translation regulation in adipose tissue offers promising avenues for therapeutic interventions aimed at mitigating the adverse effects of obesity and associated metabolic disorders. Thus, further exploration of translation regulation in adipose tissue holds significant promise for advancing our understanding and management of obesity-related health challenges.

Our work on Chapter 2 has demonstrated the intricate dynamics of adipose tissue plasticity, particularly focusing on the regulatory role of translation in response to obesity and pharmacological intervention with Rosi. Through comprehensive analysis, the research revealed a nuanced transcriptional and translational landscape within the adipose tissue stromal vascular fraction, shedding light on the mechanisms underlying its adaptability and dysregulation in obesity. The findings underscored the importance of ribosomal remodeling and translational efficiency in maintaining adipose tissue homeostasis, providing valuable insights into potential therapeutic targets for mitigating obesity-associated metabolic dysfunction. By elucidating these molecular pathways, this study not only expanded our understanding of adipose tissue biology but also laid a foundation for the development of novel interventions aimed at preserving adipose tissue health and combating the detrimental effects of obesity. Recent studies on obese humans

have indeed highlighted that enhancement of PPARγ signaling is a hallmark of health-obese individuals (Petersen, Smith et al. 2024).

Future directions based on Chapter 2 would include a deeper understanding into the concept of ribosome heterogeneity within adipose tissue, particularly in the context of obesity and therapeutic interventions like Rosi. Characterizing how different ribosomal subtypes contribute to translational control and tissue plasticity will be a focal point, as these dynamics play a crucial role in maintaining cellular homeostasis (Shi, Fujii et al. 2017, Genuth and Barna 2018). Detailed studies on ribosome remodeling, including how specific ribosomal proteins and post-translational modifications influence translational efficiency and selectivity, will be critical. Additionally, exploring the interaction between ribosome heterogeneity and PPARγ signaling could uncover new regulatory mechanisms that enhance adipose tissue function in health-obese individuals. Advanced techniques to track translation *in vivo* and the development of new genetic approaches to study ribosome heterogeneity will be essential to study translation control at physiological levels. Finally, this research direction could identify novel therapeutic targets to modulate ribosomal activity, potentially leading to interventions that can mitigate obesity-associated metabolic dysfunctions by preserving or restoring healthy adipose tissue function.

Our studies on Chapter 3, shifted to mature adipocytes and how Rosi influenced their translation machinery. Through transcriptional analysis of adipose tissue post-Rosi treatment, translation emerged as a significantly upregulated process, validating our first studies, and also suggesting a potential uncharacterized mechanism in enhancing translation efficiency within adipocytes. Our investigation centered on PIXL, an X-linked gene, responsive to PPARγ, primarily expressed in the cytoplasm and on mature adipocytes. *In vivo* studies demonstrated that PIXL loss-of-function in mature adipocytes led to dysfunctional tissue, characterized by adipocyte hypertrophy, impaired glucose metabolism, inflammation, hypertriglyceridemia, enhanced cold sensitivity, and decreased energy expenditure. Mechanistically, PIXL's interactome revealed

associations with eukaryotic initiation factors, suggesting its role in translational control. Co-immunoprecipitation studies demonstrated PIXL's association with the eIF4E complex, while polysome profiling revealed PIXL's presence in protein levels associated with initiation factors and ribosomal subunits. Altogether, our findings suggest that PPARγ induces PIXL expression to potentially regulate translational control and direct the translation of specific mRNA networks. In the absence of PIXL however we observe a downregulation of translation factors and ribosome proteins, highlighting an impairment in the translation efficiency.

Building on the insights from Chapter 3, future research directions will focus on further elucidating the role of PIXL in translational control within mature adipocytes. Key areas of interest include detailed mechanistic studies to pinpoint the exact interactions between PIXL and the eIF4E complex, as well as the broader translational machinery. For instance, elucidating if PIXL is associated with eIF4E during inactive (4EBP1-eIF4E), or active (eIF4E-eIF4G) states. Moreover, investigating how PIXL influences the translation of specific mRNA networks, especially those involved in metabolic regulation, will be crucial. Additionally, exploring therapeutic strategies to modulate PIXL expression or function could offer new avenues for treating metabolic disorders characterized by impaired adipocyte function (and potentially impaired translation efficiency). Advanced techniques such as single cell translatomics (Zeng, Huang et al. 2023) will be instrumental in mapping PIXL's impact on adipocyte biology at a granular level, elucidating its functions in different adipocyte populations. Finally, extending these findings to other models of adipose tissue dysfunction, including different types of obesity (metabolic healthy vs metabolic unhealthy), or lipodystrophy will help to generalize the therapeutic potential of targeting PIXL-mediated pathways.

In conclusion, our research highlights the critical importance of studying the regulation of translation in the context of obesity and health. By uncovering a novel layer of molecular regulation for thiazolidinediones (Rosi), specifically targeting translation efficiency and the adipose

translatome, we provide new insights into the intricate mechanisms that may be compromised during obesity and potentially restored with Rosi treatment. Understanding the different levels of regulation involved in translational control and their impact on adipose tissue function is essential for identifying the roots of metabolic dysfunction. For example, what are the main drivers regulating the tonus of translation besides growth factors and hormones in the adipose tissue? How is this process regulated in a chronic positive energy balance environment? Are there associated proteins regulating translation efficiency at the initiation step? How are ribosomes distributed in hypertrophic adipocytes and how spatial distribution affects translation? This knowledge opens up promising avenues for developing targeted therapeutic approaches that aim to enhance translation efficiency, thereby preserving adipose tissue health and mitigating the adverse effects of obesity. Through this work, we lay the groundwork for future studies to further explore and exploit these regulatory pathways, ultimately contributing to more effective treatments for obesity-related metabolic disorders.

REFERENCES

Abraham, T. M., A. Pedley, J. M. Massaro, U. Hoffmann and C. S. Fox (2015). "Association between visceral and subcutaneous adipose depots and incident cardiovascular disease risk factors." Circulation **132**(17): 1639-1647.

Acosta, J. R., I. Douagi, D. P. Andersson, J. Backdahl, M. Ryden, P. Arner and J. Laurencikiene (2016). "Increased fat cell size: a major phenotype of subcutaneous white adipose tissue in non-obese individuals with type 2 diabetes." Diabetologia **59**(3): 560-570.

Ahsan, W. (2019). "The Journey of Thiazolidinediones as Modulators of PPARs for the Management of Diabetes: A Current Perspective." Curr Pharm Des **25**(23): 2540-2554.

Albert, V., K. Svensson, M. Shimobayashi, M. Colombi, S. Munoz, V. Jimenez, C. Handschin, F. Bosch and M. N. Hall (2016). "mTORC2 sustains thermogenesis via Akt-induced glucose uptake and glycolysis in brown adipose tissue." EMBO Mol Med **8**(3): 232-246.

Alberti, K. G. M. M., P. Zimmet and J. Shaw (2005). "The metabolic syndrome—a new worldwide definition." The Lancet **366**(9491): 1059-1062.

Altshuler-Keylin, S., K. Shinoda, Y. Hasegawa, K. Ikeda, H. Hong, Q. Kang, Y. Yang, R. M. Perera, J. Debnath and S. Kajimura (2016). "Beige Adipocyte Maintenance Is Regulated by Autophagy-Induced Mitochondrial Clearance." Cell Metab **24**(3): 402-419.

Amano, S. U., J. L. Cohen, P. Vangala, M. Tencerova, S. M. Nicoloro, J. C. Yawe, Y. Shen, M. P. Czech and M. Aouadi (2014). "Local proliferation of macrophages contributes to obesity-associated adipose tissue inflammation." Cell Metab **19**(1): 162-171.

An, Y. A., C. Crewe, I. W. Asterholm, K. Sun, S. Chen, F. Zhang, M. Shao, J. B. Funcke, Z. Zhang, L. Straub, S. Klein, C. M. Kusminski and P. E. Scherer (2019). "Dysregulation of Amyloid Precursor Protein Impairs Adipose Tissue Mitochondrial Function and Promotes Obesity." Nat Metab **1**(12): 1243-1257.

Andersson, D. P., D. Eriksson Hogling, A. Thorell, E. Toft, V. Qvisth, E. Naslund, A. Thorne, M. Wiren, P. Lofgren, J. Hoffstedt, I. Dahlman, N. Mejhert, M. Ryden, E. Arner and P. Arner (2014). "Changes in subcutaneous fat cell volume and insulin sensitivity after weight loss." Diabetes Care **37**(7): 1831-1836.

Andrade, M. L., G. R. Gilio, L. A. Perandini, A. S. Peixoto, M. F. Moreno, É. Castro, T. E. Oliveira, T. S. Vieira, M. Ortiz-Silva, C. A. Thomazelli, A. B. Chaves-Filho, T. Belchior, P. Chimin, J. Magdalon, R. Ivison, D. Pant, L. Tsai, M. Y. Yoshinaga, S. Miyamoto and W. T. Festuccia (2021). "PPARγ-induced upregulation of subcutaneous fat adiponectin secretion, glyceroneogenesis and BCAA oxidation requires mTORC1 activity." Biochim Biophys Acta Mol Cell Biol Lipids **1866**(8): 158967.

Andrews, S. (2010). "FastQC: A Quality Control Tool for High Throughput Sequence Data."

Angueira, A. R., A. P. Sakers, C. D. Holman, L. Cheng, M. N. Arbocco, F. Shamsi, M. D. Lynes, R. Shrestha, C. Okada, K. Batmanov, K. Susztak, Y. H. Tseng, L. Liaw and P. Seale (2021). "Defining the lineage of thermogenic perivascular adipose tissue." Nat Metab **3**(4): 469-484.

Angueira, A. R., S. N. Shapira, J. Ishibashi, S. Sampat, J. Sostre-Colon, M. J. Emmett, P. M. Titchenell, M. A. Lazar, H. W. Lim and P. Seale (2020). "Early B Cell Factor Activity Controls Developmental and Adaptive Thermogenic Gene Programming in Adipocytes." Cell Rep **30**(9): 2869-2878 e2864.

Ansaldo, A. M., F. Montecucco, A. Sahebkar, F. Dallegri and F. Carbone (2019). "Epicardial adipose tissue and cardiovascular diseases." Int J Cardiol **278**: 254-260.

Antonio Urrutia, G., H. Ramachandran, P. Cauchy, K. Boo, S. Ramamoorthy, S. Boller, E. Dogan, T. Clapes, E. Trompouki, M. E. Torres-Padilla, J. J. Palvimo, A. Pichler and R. Grosschedl (2021). "ZFP451-mediated SUMOylation of SATB2 drives embryonic stem cell differentiation." Genes Dev **35**(15-16): 1142-1160.

Aouadi, M., P. Vangala, J. C. Yawe, M. Tencerova, S. M. Nicoloro, J. L. Cohen, Y. Shen and M. P. Czech (2014). "Lipid storage by adipose tissue macrophages regulates systemic glucose tolerance." Am J Physiol Endocrinol Metab **307**(4): E374-383.

Arner, P. (2005). "Human fat cell lipolysis: biochemistry, regulation and clinical role." Best Pract Res Clin Endocrinol Metab **19**(4): 471-482.

Arner, P., S. Bernard, L. Appelsved, K. Y. Fu, D. P. Andersson, M. Salehpour, A. Thorell, M. Ryden and K. L. Spalding (2019). "Adipose lipid turnover and long-term changes in body weight." Nat Med **25**(9): 1385-1389.

Bäckdahl, J., L. Franzén, L. Massier, Q. Li, J. Jalkanen, H. Gao, A. Andersson, N. Bhalla, A. Thorell, M. Rydén, P. L. Ståhl and N. Mejhert (2021). "Spatial mapping reveals human adipocyte subpopulations with distinct sensitivities to insulin." Cell Metab **33**(9): 1869-1882.e1866.

Baker, D. J., B. G. Childs, M. Durik, M. E. Wijers, C. J. Sieben, J. Zhong, R. A. Saltness, K. B. Jeganathan, G. C. Verzosa, A. Pezeshki, K. Khazaie, J. D. Miller and J. M. van Deursen (2016). "Naturally occurring p16(Ink4a)-positive cells shorten healthy lifespan." Nature **530**(7589): 184-189.

Barreau, C., E. Labit, C. Guissard, J. Rouquette, M. L. Boizeau, S. Gani Koumassi, A. Carriere, Y. Jeanson, S. Berger-Muller, C. Dromard, F. Plouraboue, L. Casteilla and A. Lorsignol (2016). "Regionalization of browning revealed by whole subcutaneous adipose tissue imaging." Obesity (Silver Spring) **24**(5): 1081-1089.

Bartelt, A., O. T. Bruns, R. Reimer, H. Hohenberg, H. Ittrich, K. Peldschus, M. G. Kaul, U. I. Tromsdorf, H. Weller, C. Waurisch, A. Eychmuller, P. L. Gordts, F. Rinninger, K. Bruegelmann, B. Freund, P. Nielsen, M. Merkel and J. Heeren (2011). "Brown adipose tissue activity controls triglyceride clearance." Nat Med **17**(2): 200-205.

Becher, T., S. Palanisamy, D. J. Kramer, M. Eljalby, S. J. Marx, A. G. Wibmer, S. D. Butler, C. S. Jiang, R. Vaughan, H. Schoder, A. Mark and P. Cohen (2021). "Brown adipose tissue is associated with cardiometabolic health." Nat Med **27**(1): 58-65.

Ben, J., B. Jiang, D. Wang, Q. Liu, Y. Zhang, Y. Qi, X. Tong, L. Chen, X. Liu, Y. Zhang, X. Zhu, X. Li, H. Zhang, H. Bai, Q. Yang, J. Ma, E. A. C. Wiemer, Y. Xu and Q. Chen (2019). "Major vault protein suppresses obesity and atherosclerosis through inhibiting IKK-NF-κB signaling mediated inflammation." Nat Commun **10**(1): 1801.

Benhalevy, D., S. K. Gupta, C. H. Danan, S. Ghosal, H. W. Sun, H. G. Kazemier, K. Paeschke, M. Hafner and S. A. Juranek (2017). "The Human CCHC-type Zinc Finger Nucleic Acid-Binding Protein Binds G-Rich Elements in Target mRNA Coding Sequences and Promotes Translation." Cell Rep **18**(12): 2979-2990.

Berry, D. C., Y. Jiang and J. M. Graff (2016). "Mouse strains to study cold-inducible beige progenitors and beige adipocyte formation and function." Nat Commun **7**: 10184.

Berry, R., E. Jeffery and M. S. Rodeheffer (2014). "Weighing in on adipocyte precursors." Cell Metab **19**(1): 8-20.

Berry, R. and M. S. Rodeheffer (2013). "Characterization of the adipocyte cellular lineage in vivo." Nat Cell Biol **15**(3): 302-308.

Bertholet, A. M. and Y. Kirichok (2017). "UCP1: A transporter for H(+) and fatty acid anions." Biochimie **134**: 28-34.

Bi, P., F. Yue, A. Karki, B. Castro, S. E. Wirbisky, C. Wang, A. Durkes, B. D. Elzey, O. M. Andrisani, C. A. Bidwell, J. L. Freeman, S. F. Konieczny and S. Kuang (2016). "Notch activation drives adipocyte dedifferentiation and tumorigenic transformation in mice." J Exp Med **213**(10): 2019-2037.

Bjorntorp, P. (1971). "Sjostrom L,+SJOSTROM L: Number and size of adipose tissue fat cells in relation to metabolism in human obesity." Metabolism **20**(7): 703-713.

Bjorntorp, P., G. Carlgren, B. Isaksson, M. Krotkiewski, B. Larsson and L. Sjostrom (1975). "Effect of an energy-reduced dietary regimen in relation to adipose tissue cellularity in obese women." Am J Clin Nutr **28**(5): 445-452.

Blanchard, P. G., W. T. Festuccia, V. P. Houde, P. St-Pierre, S. Brûlé, V. Turcotte, M. Côté, K. Bellmann, A. Marette and Y. Deshaies (2012). "Major involvement of mTOR in the PPARγ-induced stimulation of adipose tissue lipid uptake and fat accretion." J Lipid Res **53**(6): 1117-1125.

Brestoff, J. R., B. S. Kim, S. A. Saenz, R. R. Stine, L. A. Monticelli, G. F. Sonnenberg, J. J. Thome, D. L. Farber, K. Lutfy, P. Seale and D. Artis (2015). "Group 2 innate lymphoid cells promote beiging of white adipose tissue and limit obesity." Nature **519**(7542): 242-246.

Brina, D., A. Miluzio, S. Ricciardi, K. Clarke, P. K. Davidsen, G. Viero, T. Tebaldi, N. Offenhäuser, J. Rozman, B. Rathkolb, S. Neschen, M. Klingenspor, E. Wolf, V. Gailus-Durner, H. Fuchs, M. Hrabe de Angelis, A. Quattrone, F. Falciani and S. Biffo (2015). "eIF6 coordinates insulin sensitivity and lipid metabolism by coupling translation to transcription." Nature Communications **6**(1): 8261.

Buechler, M. B., R. N. Pradhan, A. T. Krishnamurty, C. Cox, A. K. Calviello, A. W. Wang, Y. A. Yang, L. Tam, R. Caothien, M. Roose-Girma, Z. Modrusan, J. R. Arron, R. Bourgon, S. Muller and S. J. Turley (2021). "Cross-tissue organization of the fibroblast lineage." Nature **593**(7860): 575-579.

Burl, R. B., V. D. Ramseyer, E. A. Rondini, R. Pique-Regi, Y. H. Lee and J. G. Granneman (2018). "Deconstructing Adipogenesis Induced by beta3-Adrenergic Receptor Activation with Single-Cell Expression Profiling." Cell Metab **28**(2): 300-309 e304.

Burl, R. B., V. D. Ramseyer, E. A. Rondini, R. Pique-Regi, Y. H. Lee and J. G. Granneman (2018). "Deconstructing Adipogenesis Induced by β3-Adrenergic Receptor Activation with Single-Cell Expression Profiling." Cell Metab **28**(2): 300-309.e304.

Burnett, P. E., R. K. Barrow, N. A. Cohen, S. H. Snyder and D. M. Sabatini (1998). "RAFT1 phosphorylation of the translational regulators p70 S6 kinase and 4E-BP1." Proc Natl Acad Sci U S A **95**(4): 1432-1437.

Cancello, R., A. Zulian, D. Gentilini, S. Maestrini, A. Della Barba, C. Invitti, D. Cora, M. Caselle, A. Liuzzi and A. M. Di Blasio (2013). "Molecular and morphologic characterization of superficial- and deep-subcutaneous adipose tissue subdivisions in human obesity." Obesity (Silver Spring) **21**(12): 2562-2570.

Cannon, B. and J. Nedergaard (2004). "Brown adipose tissue: function and physiological significance." Physiol Rev **84**(1): 277-359.

Cao, Q., J. Jing, X. Cui, H. Shi and B. Xue (2019). "Sympathetic nerve innervation is required for beigeing in white fat." Physiol Rep **7**(6): e14031.

Cao, W., K. W. Daniel, J. Robidoux, P. Puigserver, A. V. Medvedev, X. Bai, L. M. Floering, B. M. Spiegelman and S. Collins (2004). "p38 mitogen-activated protein kinase is the central regulator of cyclic AMP-dependent transcription of the brown fat uncoupling protein 1 gene." Mol Cell Biol **24**(7): 3057-3067.

Cao, Y., H. Wang, Q. Wang, X. Han and W. Zeng (2018). "Three-dimensional volume fluorescence-imaging of vascular plasticity in adipose tissues." Mol Metab **14**: 71-81.

Cao, Y., H. Wang and W. Zeng (2018). "Whole-tissue 3D imaging reveals intra-adipose sympathetic plasticity regulated by NGF-TrkA signal in cold-induced beiging." Protein Cell **9**(6): 527-539.

Cariou, B., B. Charbonnel and B. Staels (2012). "Thiazolidinediones and PPARγ agonists: time for a reassessment." Trends Endocrinol Metab **23**(5): 205-215.

Carpentier, A. C. (2021). "100(th) anniversary of the discovery of insulin perspective: insulin and adipose tissue fatty acid metabolism." Am J Physiol Endocrinol Metab **320**(4): E653-E670.

Caso, G., M. A. McNurlan, I. Mileva, A. Zemlyak, D. C. Mynarcik and M. C. Gelato (2013). "Peripheral fat loss and decline in adipogenesis in older humans." Metabolism **62**(3): 337-340.

Cattaneo, P., D. Mukherjee, S. Spinozzi, L. Zhang, V. Larcher, W. B. Stallcup, H. Kataoka, J. Chen, S. Dimmeler, S. M. Evans and N. Guimaraes-Camboa (2020). "Parallel Lineage-Tracing Studies Establish Fibroblasts as the Prevailing In Vivo Adipocyte Progenitor." Cell Rep **30**(2): 571-582 e572.

CDC. (2023). "Overweight & Obesity. Center for Disease Control and Prevention."

Chait, A. and L. J. den Hartigh (2020). "Adipose Tissue Distribution, Inflammation and Its Metabolic Consequences, Including Diabetes and Cardiovascular Disease." Front Cardiovasc Med **7**: 22.

Chan, K., F. Robert, C. Oertlin, D. Kapeller-Libermann, D. Avizonis, J. Gutierrez, A. Handly-Santana, M. Doubrovin, J. Park, C. Schoepfer, B. Da Silva, M. Yao, F. Gorton, J. Shi, C. J. Thomas, L. E. Brown, J. A. Porco, M. Pollak, O. Larsson, J. Pelletier and I. I. C. Chio (2019). "eIF4A supports an oncogenic translation program in pancreatic ductal adenocarcinoma." Nature Communications **10**(1): 5151.

Chao, L., B. Marcus-Samuels, M. M. Mason, J. Moitra, C. Vinson, E. Arioglu, O. Gavrilova and M. L. Reitman (2000). "Adipose tissue is required for the antidiabetic, but not for the hypolipidemic, effect of thiazolidinediones." J Clin Invest **106**(10): 1221-1228.

Chau, Y. Y., R. Bandiera, A. Serrels, O. M. Martinez-Estrada, W. Qing, M. Lee, J. Slight, A. Thornburn, R. Berry, S. McHaffie, R. H. Stimson, B. R. Walker, R. M. Chapuli, A. Schedl and N. Hastie (2014). "Visceral and subcutaneous fat have different origins and evidence supports a mesothelial source." Nat Cell Biol **16**(4): 367-375.

Chen, Y., K. Ikeda, T. Yoneshiro, A. Scaramozza, K. Tajima, Q. Wang, K. Kim, K. Shinoda, C. H. Sponton, Z. Brown, A. Brack and S. Kajimura (2019). "Thermal stress induces glycolytic beige fat formation via a myogenic state." Nature **565**(7738): 180-185.

Chi, J., Z. Wu, C. H. J. Choi, L. Nguyen, S. Tegegne, S. E. Ackerman, A. Crane, F. Marchildon, M. Tessier-Lavigne and P. Cohen (2018). "Three-Dimensional Adipose Tissue Imaging Reveals Regional Variation in Beige Fat Biogenesis and PRDM16-Dependent Sympathetic Neurite Density." Cell Metab **27**(1): 226-236 e223.

Chitraju, C., A. W. Fischer, R. V. Farese, Jr. and T. C. Walther (2020). "Lipid Droplets in Brown Adipose Tissue Are Dispensable for Cold-Induced Thermogenesis." Cell Rep **33**(5): 108348.

Cho, D. S., B. Lee and J. D. Doles (2019). "Refining the adipose progenitor cell landscape in healthy and obese visceral adipose tissue using single-cell gene expression profiling." Life Sci Alliance **2**(6): e201900561.

Cho, Y. K., Y. Son, A. Saha, D. Kim, C. Choi, M. Kim, J. H. Park, H. Im, J. Han, K. Kim, Y. S. Jung, J. Yun, E. J. Bae, J. K. Seong, M. O. Lee, S. Lee, J. G. Granneman and Y. H. Lee (2021). "STK3/STK4 signalling in adipocytes regulates mitophagy and energy expenditure." Nat Metab **3**(3): 428-441.

Chondronikola, M., E. Volpi, E. Borsheim, C. Porter, M. K. Saraf, P. Annamalai, C. Yfanti, T. Chao, D. Wong, K. Shinoda, S. M. Labbe, N. M. Hurren, F. Cesani, S. Kajimura and L. S. Sidossis (2016). "Brown Adipose Tissue Activation Is Linked to Distinct Systemic Effects on Lipid Metabolism in Humans." Cell Metab **23**(6): 1200-1206.

Chothani, S., E. Adami, J. F. Ouyang, S. Viswanathan, N. Hubner, S. A. Cook, S. Schafer and O. J. L. Rackham (2019). "deltaTE: Detection of Translationally Regulated Genes by Integrative Analysis of Ribo-seq and RNA-seq Data." Current Protocols in Molecular Biology **129**(1): e108.

Chouchani, E. T. and S. Kajimura (2019). "Metabolic adaptation and maladaptation in adipose tissue." Nat Metab **1**(2): 189-200.

Chouchani, E. T., L. Kazak, M. P. Jedrychowski, G. Z. Lu, B. K. Erickson, J. Szpyt, K. A. Pierce, D. Laznik-Bogoslavski, R. Vetrivelan, C. B. Clish, A. J. Robinson, S. P. Gygi and B. M. Spiegelman

(2016). "Mitochondrial ROS regulate thermogenic energy expenditure and sulfenylation of UCP1." Nature **532**(7597): 112-116.

Chu, A. Y., X. Deng, V. A. Fisher, A. Drong, Y. Zhang, M. F. Feitosa, C. T. Liu, O. Weeks, A. C. Choh, Q. Duan, T. D. Dyer, J. D. Eicher, X. Guo, N. L. Heard-Costa, T. Kacprowski, J. W. Kent, Jr., L. A. Lange, X. Liu, K. Lohman, L. Lu, A. Mahajan, J. R. O'Connell, A. Parihar, J. M. Peralta, A. V. Smith, Y. Zhang, G. Homuth, A. H. Kissebah, J. Kullberg, R. Laqua, L. J. Launer, M. Nauck, M. Olivier, P. A. Peyser, J. G. Terry, M. K. Wojczynski, J. Yao, L. F. Bielak, J. Blangero, I. B. Borecki, D. W. Bowden, J. J. Carr, S. A. Czerwinski, J. Ding, N. Friedrich, V. Gudnason, T. B. Harris, E. Ingelsson, A. D. Johnson, S. L. Kardia, C. D. Langefeld, L. Lind, Y. Liu, B. D. Mitchell, A. P. Morris, T. H. Mosley, Jr., J. I. Rotter, A. R. Shuldiner, B. Towne, H. Volzke, H. Wallaschofski, J. G. Wilson, M. Allison, C. M. Lindgren, W. Goessling, L. A. Cupples, M. L. Steinhauser and C. S. Fox (2017). "Multiethnic genome-wide meta-analysis of ectopic fat depots identifies loci associated with adipocyte development and differentiation." Nat Genet **49**(1): 125-130.

Chun, T. H., K. B. Hotary, F. Sabeh, A. R. Saltiel, E. D. Allen and S. J. Weiss (2006). "A pericellular collagenase directs the 3-dimensional development of white adipose tissue." Cell **125**(3): 577-591.

Church, C. D., R. Berry and M. S. Rodeheffer (2014). "Isolation and study of adipocyte precursors." Methods Enzymol **537**: 31-46.

Chusyd, D. E., D. Wang, D. M. Huffman and T. R. Nagy (2016). "Relationships between Rodent White Adipose Fat Pads and Human White Adipose Fat Depots." Front Nutr **3**(April): 10.

Cinti, S., R. Cancello, M. C. Zingaretti, E. Ceresi, R. De Matteis, A. Giordano, J. Himms-Hagen and D. Ricquier (2002). "CL316,243 and cold stress induce heterogeneous expression of UCP1 mRNA and protein in rodent brown adipocytes." J Histochem Cytochem **50**(1): 21-31.

Cohen, P. and S. Kajimura (2021). "The cellular and functional complexity of thermogenic fat." Nat Rev Mol Cell Biol **22**(6): 393-409.

Conn, C. S., H. Yang, H. J. Tom, K. Ikeda, J. A. Oses-Prieto, H. Vu, Y. Oguri, S. Nair, R. M. Gill, S. Kajimura, R. J. DeBerardinis, A. L. Burlingame and D. Ruggero (2021). "The major cap-binding protein eIF4E regulates lipid homeostasis and diet-induced obesity." Nat Metab **3**(2): 244-257.

Cote, J. A., G. Ostinelli, M. F. Gauthier, A. Lacasse and A. Tchernof (2019). "Focus on dedifferentiated adipocytes: characteristics, mechanisms, and possible applications." Cell Tissue Res **378**(3): 385-398.

Cox, J. and M. Mann (2008). "MaxQuant enables high peptide identification rates, individualized p.p.b.-range mass accuracies and proteome-wide protein quantification." Nature Biotechnology **26**(12): 1367-1372.

Crewe, C., Y. A. An and P. E. Scherer (2017). "The ominous triad of adipose tissue dysfunction: inflammation, fibrosis, and impaired angiogenesis." J Clin Invest **127**(1): 74-82.

Czech, M. P. (2020). "Mechanisms of insulin resistance related to white, beige, and brown adipocytes." Mol Metab **34**: 27-42.

Darcy, J. and Y. H. Tseng (2019). "ComBATing aging-does increased brown adipose tissue activity confer longevity?" Geroscience **41**(3): 285-296.

Davies, B. S., A. P. Beigneux, R. H. Barnes, 2nd, Y. Tu, P. Gin, M. M. Weinstein, C. Nobumori, R. Nyren, I. Goldberg, G. Olivecrona, A. Bensadoun, S. G. Young and L. G. Fong (2010). "GPIHBP1 is responsible for the entry of lipoprotein lipase into capillaries." Cell Metab **12**(1): 42-52.

Davies, B. S., H. Waki, A. P. Beigneux, E. Farber, M. M. Weinstein, D. C. Wilpitz, L. J. Tai, R. M. Evans, L. G. Fong, P. Tontonoz and S. G. Young (2008). "The expression of GPIHBP1, an endothelial cell binding site for lipoprotein lipase and chylomicrons, is induced by peroxisome proliferator-activated receptor-gamma." Mol Endocrinol **22**(11): 2496-2504.

De Silva, D., L. Ferguson, G. H. Chin, B. E. Smith, R. A. Apathy, T. L. Roth, F. Blaeschke, M. Kudla, A. Marson, N. T. Ingolia and J. H. D. Cate (2021). "Robust T cell activation requires an eIF3-driven burst in T cell receptor translation." eLife **10**: e74272.

Dempersmier, J., A. Sambeat, O. Gulyaeva, S. M. Paul, C. S. Hudak, H. F. Raposo, H. Y. Kwan, C. Kang, R. H. Wong and H. S. Sul (2015). "Cold-inducible Zfp516 activates UCP1 transcription to promote browning of white fat and development of brown fat." Mol Cell **57**(2): 235-246.

Di Angelantonio, E., S. N. Bhupathiraju, D. Wormser, P. Gao, S. Kaptoge, A. B. de Gonzalez, B. J. Cairns, R. Huxley, C. L. Jackson, G. Joshy, S. Lewington, J. E. Manson, N. Murphy, A. V. Patel, J. M. Samet, M. Woodward, W. Zheng, M. Zhou, N. Bansal, A. Barricarte, B. Carter, J. R. Cerhan, R. Collins, G. D. Smith, X. Fang, O. H. Franco, J. Green, J. Halsey, J. S. Hildebrand, K. J. Jung, R. J. Korda, D. F. McLerran, S. C. Moore, L. M. O'Keeffe, E. Paige, A. Ramond, G. K. Reeves, B. Rolland, C. Sacerdote, N. Sattar, E. Sofianopoulou, J. Stevens, M. Thun, H. Ueshima, L. Yang, Y. D. Yun, P. Willeit, E. Banks, V. Beral, Z. Chen, S. M. Gapstur, M. J. Gunter, P. Hartge, S. H. Jee, T.-H. Lam, R. Peto, J. D. Potter, W. C. Willett, S. G. Thompson, J. Danesh and F. B. Hu (2016). "Body-mass index and all-cause mortality: individual-participant-data meta-analysis of 239 prospective studies in four continents." The Lancet **388**(10046): 776-786.

Dichamp, J., C. Barreau, C. Guissard, A. Carriere, Y. Martinez, X. Descombes, L. Penicaud, J. Rouquette, L. Casteilla, F. Plouraboue and A. Lorsignol (2019). "3D analysis of the whole subcutaneous adipose tissue reveals a complex spatial network of interconnected lobules with heterogeneous browning ability." Sci Rep **9**(1): 6684.

Ding, H., S. Zheng, D. Garcia-Ruiz, D. Hou, Z. Wei, Z. Liao, L. Li, Y. Zhang, X. Han, K. Zen, C. Y. Zhang, J. Li and X. Jiang (2016). "Fasting induces a subcutaneous-to-visceral fat switch mediated by microRNA-149-3p and suppression of PRDM16." Nat Commun **7**(May): 11533.

Divoux, A., J. Tordjman, D. Lacasa, N. Veyrie, D. Hugol, A. Aissat, A. Basdevant, M. Guerre-Millo, C. Poitou, J. D. Zucker, P. Bedossa and K. Clement (2010). "Fibrosis in human adipose tissue:

composition, distribution, and link with lipid metabolism and fat mass loss." Diabetes **59**(11): 2817-2825.

Donohoe, C. L., J. Lysaght, J. O'Sullivan and J. V. Reynolds (2017). "Emerging Concepts Linking Obesity with the Hallmarks of Cancer." Trends Endocrinol Metab **28**(1): 46-62.

Dumas, L., P. Herviou, E. Dassi, A. Cammas and S. Millevoi (2021). "G-Quadruplexes in RNA Biology: Recent Advances and Future Directions." Trends in Biochemical Sciences **46**(4): 270-283.

Dumesic, D. A., A. L. Akopians, V. K. Madrigal, E. Ramirez, D. J. Margolis, M. K. Sarma, A. M. Thomas, T. R. Grogan, R. Haykal, T. A. Schooler, B. L. Okeya, D. H. Abbott and G. D. Chazenbalk (2016). "Hyperandrogenism Accompanies Increased Intra-Abdominal Fat Storage in Normal Weight Polycystic Ovary Syndrome Women." J Clin Endocrinol Metab **101**(11): 4178-4188.

During, M. J., X. Liu, W. Huang, D. Magee, A. Slater, T. McMurphy, C. Wang and L. Cao (2015). "Adipose VEGF Links the White-to-Brown Fat Switch With Environmental, Genetic, and Pharmacological Stimuli in Male Mice." Endocrinology **156**(6): 2059-2073.

El Agha, E., A. Moiseenko, V. Kheirollahi, S. De Langhe, S. Crnkovic, G. Kwapiszewska, M. Szibor, D. Kosanovic, F. Schwind, R. T. Schermuly, I. Henneke, B. MacKenzie, J. Quantius, S. Herold, A. Ntokou, K. Ahlbrecht, T. Braun, R. E. Morty, A. Gunther, W. Seeger and S. Bellusci (2017). "Two-Way Conversion between Lipogenic and Myogenic Fibroblastic Phenotypes Marks the Progression and Resolution of Lung Fibrosis." Cell Stem Cell **20**(2): 261-273 e263.

Esteve, D., N. Boulet, C. Belles, A. Zakaroff-Girard, P. Decaunes, A. Briot, Y. Veeranagouda, M. Didier, A. Remaury, J. C. Guillemot, S. Ledoux, C. Dani, A. Bouloumie and J. Galitzky (2019). "Lobular architecture of human adipose tissue defines the niche and fate of progenitor cells." Nat Commun **10**(1): 2549.

Faveeuw, C., S. Fougeray, V. Angeli, J. Fontaine, G. Chinetti, P. Gosset, P. Delerive, C. Maliszewski, M. Capron, B. Staels, M. Moser and F. Trottein (2000). "Peroxisome proliferator-

activated receptor gamma activators inhibit interleukin-12 production in murine dendritic cells." FEBS Lett **486**(3): 261-266.

Fedorenko, A., P. V. Lishko and Y. Kirichok (2012). "Mechanism of fatty-acid-dependent UCP1 uncoupling in brown fat mitochondria." Cell **151**(2): 400-413.

Ferrero, R., P. Rainer and B. Deplancke (2020). "Toward a Consensus View of Mammalian Adipocyte Stem and Progenitor Cell Heterogeneity." Trends Cell Biol **30**(12): 937-950.

Feuerer, M., L. Herrero, D. Cipolletta, A. Naaz, J. Wong, A. Nayer, J. Lee, A. B. Goldfine, C. Benoist, S. Shoelson and D. Mathis (2009). "Lean, but not obese, fat is enriched for a unique population of regulatory T cells that affect metabolic parameters." Nat Med **15**(8): 930-939.

Fischer, K., H. H. Ruiz, K. Jhun, B. Finan, D. J. Oberlin, V. van der Heide, A. V. Kalinovich, N. Petrovic, Y. Wolf, C. Clemmensen, A. C. Shin, S. Divanovic, F. Brombacher, E. Glasmacher, S. Keipert, M. Jastroch, J. Nagler, K. W. Schramm, D. Medrikova, G. Collden, S. C. Woods, S. Herzig, D. Homann, S. Jung, J. Nedergaard, B. Cannon, M. H. Tschop, T. D. Muller and C. Buettner (2017). "Alternatively activated macrophages do not synthesize catecholamines or contribute to adipose tissue adaptive thermogenesis." Nat Med **23**(5): 623-630.

Flaherty, S. E., 3rd, A. Grijalva, X. Xu, E. Ables, A. Nomani and A. W. Ferrante, Jr. (2019). "A lipase-independent pathway of lipid release and immune modulation by adipocytes." Science **363**(6430): 989-993.

Florez, H., P. D. Reaven, G. Bahn, T. Moritz, S. Warren, J. Marks, D. Reda, W. Duckworth, C. Abraira, R. Hayward and N. Emanuele (2015). "Rosiglitazone treatment and cardiovascular disease in the Veterans Affairs Diabetes Trial." Diabetes Obes Metab **17**(10): 949-955.

Fodor, P. B. (1993). "From the panniculus carnosum (PC) to the superficial fascia system (SFS)." Aesthetic Plast Surg **17**(3): 179-181.

Fontana, L., J. C. Eagon, M. E. Trujillo, P. E. Scherer and S. Klein (2007). "Visceral fat adipokine secretion is associated with systemic inflammation in obese humans." Diabetes **56**(4): 1010-1013.

Forester, C. M., J. A. Oses-Prieto, N. J. Phillips, S. Miglani, X. Pang, G. W. Byeon, R. DeMarco, A. Burlingame, M. Barna and D. Ruggero (2022). "Regulation of eIF4E guides a unique translational program to control erythroid maturation." Science Advances **8**(51): eadd3942.

Francisco, V., J. Pino, V. Campos-Cabaleiro, C. Ruiz-Fernandez, A. Mera, M. A. Gonzalez-Gay, R. Gomez and O. Gualillo (2018). "Obesity, Fat Mass and Immune System: Role for Leptin." Front Physiol **9**: 640.

Frayn, K. N. and F. Karpe (2014). "Regulation of human subcutaneous adipose tissue blood flow." Int J Obes (Lond) **38**(8): 1019-1026.

Fromm-Dornieden, C., S. von der Heyde, O. Lytovchenko, G. Salinas-Riester, B. Brenig, T. Beissbarth and B. G. Baumgartner (2012). "Novel polysome messages and changes in translational activity appear after induction of adipogenesis in 3T3-L1 cells." BMC Mol Biol **13**: 9.

Fruhbeck, G., L. Mendez-Gimenez, J. A. Fernandez-Formoso, S. Fernandez and A. Rodriguez (2014). "Regulation of adipocyte lipolysis." Nutr Res Rev **27**(1): 63-93.

Funcke, J. B. and P. E. Scherer (2019). "Beyond adiponectin and leptin: adipose tissue-derived mediators of inter-organ communication." J Lipid Res **60**(10): 1648-1684.

Gandin, V., L. Masvidal, L. Hulea, S. P. Gravel, M. Cargnello, S. McLaughlan, Y. Cai, P. Balanathan, M. Morita, A. Rajakumar, L. Furic, M. Pollak, J. A. Porco, Jr., J. St-Pierre, J. Pelletier, O. Larsson and I. Topisirovic (2016). "nanoCAGE reveals 5' UTR features that define specific modes of translation of functionally related MTOR-sensitive mRNAs." Genome Res **26**(5): 636-648.

Gandin, V., K. Sikström, T. Alain, M. Morita, S. McLaughlan, O. Larsson and I. Topisirovic (2014). "Polysome fractionation and analysis of mammalian translatomes on a genome-wide scale." J Vis Exp(87).

Gao, Z., A. C. Daquinag, F. Su, B. Snyder and M. G. Kolonin (2018). "PDGFRalpha/PDGFRbeta signaling balance modulates progenitor cell differentiation into white and beige adipocytes." Development **145**(1): dev155861.

Gastaldelli, A., M. Gaggini and R. A. DeFronzo (2017). "Role of Adipose Tissue Insulin Resistance in the Natural History of Type 2 Diabetes: Results From the San Antonio Metabolism Study." Diabetes **66**(4): 815-822.

Gealekman, O., N. Guseva, C. Hartigan, S. Apotheker, M. Gorgoglione, K. Gurav, K. V. Tran, J. Straubhaar, S. Nicoloro, M. P. Czech, M. Thompson, R. A. Perugini and S. Corvera (2011). "Depot-specific differences and insufficient subcutaneous adipose tissue angiogenesis in human obesity." Circulation **123**(2): 186-194.

Gebauer, F. and M. W. Hentze (2004). "Molecular mechanisms of translational control." Nat Rev Mol Cell Biol **5**(10): 827-835.

Genuth, N. R. and M. Barna (2018). "The Discovery of Ribosome Heterogeneity and Its Implications for Gene Regulation and Organismal Life." Mol Cell **71**(3): 364-374.

Ghaben, A. L. and P. E. Scherer (2019). "Adipogenesis and metabolic health." Nat Rev Mol Cell Biol **20**(4): 242-258.

Gingras, A. C., S. P. Gygi, B. Raught, R. D. Polakiewicz, R. T. Abraham, M. F. Hoekstra, R. Aebersold and N. Sonenberg (1999). "Regulation of 4E-BP1 phosphorylation: a novel two-step mechanism." Genes Dev **13**(11): 1422-1437.

Goldberg, E. L., I. Shchukina, Y. H. Youm, S. Ryu, T. Tsusaka, K. C. Young, C. D. Camell, T. Dlugos, M. N. Artyomov and V. D. Dixit (2021). "IL-33 causes thermogenic failure in aging by expanding dysfunctional adipose ILC2." Cell Metab **33**(11): 2277-2287 e2275.

Gonzalez-Hurtado, E., J. Lee, J. Choi and M. J. Wolfgang (2018). "Fatty acid oxidation is required for active and quiescent brown adipose tissue maintenance and thermogenic programing." Mol Metab **7**: 45-56.

Gosset, P., A. S. Charbonnier, P. Delerive, J. Fontaine, B. Staels, J. Pestel, A. B. Tonnel and F. Trottein (2001). "Peroxisome proliferator-activated receptor gamma activators affect the maturation of human monocyte-derived dendritic cells." Eur J Immunol **31**(10): 2857-2865.

Graja, A., F. Garcia-Carrizo, A. M. Jank, S. Gohlke, T. H. Ambrosi, W. Jonas, S. Ussar, M. Kern, A. Schürmann, K. Aleksandrova, M. Blüher and T. J. Schulz (2018). "Loss of periostin occurs in aging adipose tissue of mice and its genetic ablation impairs adipose tissue lipid metabolism." Aging Cell **17**(5): e12810.

Gulati, P., F. R. Day, F. Payne, H. Ongen, L. A. Lotta, F. R. Day, M. van de Bunt, K. J. Gaulton, J. D. Eicher, S. J. Sharp, J. a. Luan, E. De Lucia Rolfe, I. D. Stewart, E. Wheeler, S. M. Willems, C. Adams, H. Yaghootkar, N. G. Forouhi, K.-T. Khaw and A. D. Johnson (2017). Integrative genomic analysis implicates limited peripheral adipose storage capacity in the pathogenesis of human insulin resistance. New York, NY :, Nature Pub Co. **49:** 17-26.

Guo, H. (2018). "Specialized ribosomes and the control of translation." Biochem Soc Trans **46**(4): 855-869.

Gupta, R. K., Z. Arany, P. Seale, R. J. Mepani, L. Ye, H. M. Conroe, Y. A. Roby, H. Kulaga, R. R. Reed and B. M. Spiegelman (2010). "Transcriptional control of preadipocyte determination by Zfp423." Nature **464**(7288): 619-623.

Gustafson, B., A. Nerstedt and U. Smith (2019). "Reduced subcutaneous adipogenesis in human hypertrophic obesity is linked to senescent precursor cells." Nat Commun **10**(1): 2757.

Ha, C. W. Y., A. Martin, G. D. Sepich-Poore, B. Shi, Y. Wang, K. Gouin, G. Humphrey, K. Sanders, Y. Ratnayake, K. S. L. Chan, G. Hendrick, J. R. Caldera, C. Arias, J. E. Moskowitz, S. J. Ho Sui, S. Yang, D. Underhill, M. J. Brady, S. Knott, K. Kaihara, M. J. Steinbaugh, H. Li, D. P. B. McGovern, R. Knight, P. Fleshner and S. Devkota (2020). "Translocation of Viable Gut Microbiota to Mesenteric Adipose Drives Formation of Creeping Fat in Humans." Cell **183**(3): 666-683 e617.

Halberg, N., T. Khan, M. E. Trujillo, I. Wernstedt-Asterholm, A. D. Attie, S. Sherwani, Z. V. Wang, S. Landskroner-Eiger, S. Dineen, U. J. Magalang, R. A. Brekken and P. E. Scherer (2009). "Hypoxia-inducible factor 1alpha induces fibrosis and insulin resistance in white adipose tissue." Mol Cell Biol **29**(16): 4467-4483.

Hams, E., R. M. Locksley, A. N. McKenzie and P. G. Fallon (2013). "Cutting edge: IL-25 elicits innate lymphoid type 2 and type II NKT cells that regulate obesity in mice." J Immunol **191**(11): 5349-5353.

Han, X., Z. Zhang, L. He, H. Zhu, Y. Li, W. Pu, M. Han, H. Zhao, K. Liu, Y. Li, X. Huang, M. Zhang, H. Jin, Z. Lv, J. Tang, J. Wang, R. Sun, J. Fei, X. Tian, S. Duan, Q. D. Wang, L. Wang, B. He and B. Zhou (2021). "A suite of new Dre recombinase drivers markedly expands the ability to perform intersectional genetic targeting." Cell Stem Cell **28**(6): 1160-1176 e1167.

Harms, M. and P. Seale (2013). "Brown and beige fat: development, function and therapeutic potential." Nat Med **19**(10): 1252-1263.

Haslam, D. and N. Rigby (2010). "A long look at obesity." The Lancet **376**(9735): 85-86.

Heinz, S., C. Benner, N. Spann, E. Bertolino, Y. C. Lin, P. Laslo, J. X. Cheng, C. Murre, H. Singh and C. K. Glass (2010). "Simple combinations of lineage-determining transcription factors prime cis-regulatory elements required for macrophage and B cell identities." Mol Cell **38**(4): 576-589.

Henninger, A. M., B. Eliasson, L. E. Jenndahl and A. Hammarstedt (2014). "Adipocyte hypertrophy, inflammation and fibrosis characterize subcutaneous adipose tissue of healthy, non-obese subjects predisposed to type 2 diabetes." PLoS One **9**(8): e105262.

Henriques, F., A. H. Bedard, A. Guilherme, M. Kelly, J. Chi, P. Zhang, L. M. Lifshitz, K. Bellve, L. A. Rowland, B. Yenilmez, S. Kumar, Y. Wang, J. Luban, L. S. Weinstein, J. D. Lin, P. Cohen and M. P. Czech (2020). "Single-Cell RNA Profiling Reveals Adipocyte to Macrophage Signaling Sufficient to Enhance Thermogenesis." Cell Rep **32**(5): 107998.

Henriques, F., A. H. Bedard, A. Guilherme, M. Kelly, J. Chi, P. Zhang, L. M. Lifshitz, K. Bellvé, L. A. Rowland, B. Yenilmez, S. Kumar, Y. Wang, J. Luban, L. S. Weinstein, J. D. Lin, P. Cohen and M. P. Czech (2020). "Single-Cell RNA Profiling Reveals Adipocyte to Macrophage Signaling Sufficient to Enhance Thermogenesis." Cell Rep **32**(5): 107998.

Hepler, C. and R. K. Gupta (2017). "The expanding problem of adipose depot remodeling and postnatal adipocyte progenitor recruitment." Mol Cell Endocrinol **445**: 95-108.

Hepler, C., B. Shan, Q. Zhang, G. H. Henry, M. Shao, L. Vishvanath, A. L. Ghaben, A. B. Mobley, D. Strand, G. C. Hon and R. K. Gupta (2018). "Identification of functionally distinct fibro-inflammatory and adipogenic stromal subpopulations in visceral adipose tissue of adult mice." Elife **7**: 1-36.

Hepler, C., B. Shan, Q. Zhang, G. H. Henry, M. Shao, L. Vishvanath, A. L. Ghaben, A. B. Mobley, D. Strand, G. C. Hon and R. K. Gupta (2018). "Identification of functionally distinct fibro-inflammatory and adipogenic stromal subpopulations in visceral adipose tissue of adult mice." eLife **7**: e39636.

Herman, M. A., O. D. Peroni, J. Villoria, M. R. Schon, N. A. Abumrad, M. Bluher, S. Klein and B. B. Kahn (2012). "A novel ChREBP isoform in adipose tissue regulates systemic glucose metabolism." Nature **484**(7394): 333-338.

Hildreth, A. D., F. Ma, Y. Y. Wong, R. Sun, M. Pellegrini and T. E. O'Sullivan (2021). "Single-cell sequencing of human white adipose tissue identifies new cell states in health and obesity." Nat Immunol **22**(5): 639-653.

Hildreth, A. D., L. Riggan and T. E. O'Sullivan (2020). "CRISPR-Cas9 Ribonucleoprotein-Mediated Genomic Editing in Primary Innate Immune Cells." STAR Protoc **1**(3): 100113.

Hilgendorf, K. I., C. T. Johnson, A. Mezger, S. L. Rice, A. M. Norris, J. Demeter, W. J. Greenleaf, J. F. Reiter, D. Kopinke and P. K. Jackson (2019). "Omega-3 Fatty Acids Activate Ciliary FFAR4 to Control Adipogenesis." Cell **179**(6): 1289-1305 e1221.

Hill, D. A., H. W. Lim, Y. H. Kim, W. Y. Ho, Y. H. Foong, V. L. Nelson, H. C. B. Nguyen, K. Chegireddy, J. Kim, A. Habertheuer, P. Vallabhajosyula, T. Kambayashi, K. J. Won and M. A. Lazar (2018). "Distinct macrophage populations direct inflammatory versus physiological changes in adipose tissue." Proc Natl Acad Sci U S A **115**(22): E5096-E5105.

Hirosumi, J., G. Tuncman, L. Chang, C. Z. Gorgun, K. T. Uysal, K. Maeda, M. Karin and G. S. Hotamisligil (2002). "A central role for JNK in obesity and insulin resistance." Nature **420**(6913): 333-336.

Hirsch, J. and B. Batchelor (1976). "Adipose tissue cellularity in human obesity." Clin Endocrinol Metab **5**(2): 299-311.

Home, P. D., N. P. Jones, S. J. Pocock, H. Beck-Nielsen, R. Gomis, M. Hanefeld, M. Komajda and P. Curtis (2007). "Rosiglitazone RECORD study: glucose control outcomes at 18 months." Diabet Med **24**(6): 626-634.

Home, P. D., S. J. Pocock, H. Beck-Nielsen, P. S. Curtis, R. Gomis, M. Hanefeld, N. P. Jones, M. Komajda and J. J. McMurray (2009). "Rosiglitazone evaluated for cardiovascular outcomes in oral agent combination therapy for type 2 diabetes (RECORD): a multicentre, randomised, open-label trial." Lancet **373**(9681): 2125-2135.

Hong, K. Y., H. Bae, I. Park, D. Y. Park, K. H. Kim, Y. Kubota, E. S. Cho, H. Kim, R. H. Adams, O. J. Yoo and G. Y. Koh (2015). "Perilipin+ embryonic preadipocytes actively proliferate along growing vasculatures for adipose expansion." Development **142**(15): 2623-2632.

Hotamisligil, G. S., N. S. Shargill and B. M. Spiegelman (1993). "Adipose expression of tumor necrosis factor-alpha: direct role in obesity-linked insulin resistance." Science **259**(5091): 87-91.

Hsieh, W. Y., K. J. Williams, B. Su and S. J. Bensinger (2021). "Profiling of mouse macrophage lipidome using direct infusion shotgun mass spectrometry." STAR Protoc **2**(1): 100235.

Hu, B., C. Jin, X. Zeng, J. M. Resch, M. P. Jedrychowski, Z. Yang, B. N. Desai, A. S. Banks, B. B. Lowell, D. Mathis and B. M. Spiegelman (2020). "gammadelta T cells and adipocyte IL-17RC control fat innervation and thermogenesis." Nature **578**(7796): 610-614.

Huang, H., T. J. Song, X. Li, L. Hu, Q. He, M. Liu, M. D. Lane and Q. Q. Tang (2009). "BMP signaling pathway is required for commitment of C3H10T1/2 pluripotent stem cells to the adipocyte lineage." Proc Natl Acad Sci U S A **106**(31): 12670-12675.

Huang, T., M. Choi, M. Tzouros, S. Golling, N. J. Pandya, B. Banfai, T. Dunkley and O. Vitek (2020). "MSstatsTMT: Statistical Detection of Differentially Abundant Proteins in Experiments with Isobaric Labeling and Multiple Mixtures." Mol Cell Proteomics **19**(10): 1706-1723.

Hughes, C. S., S. Moggridge, T. Müller, P. H. Sorensen, G. B. Morin and J. Krijgsveld (2019). "Single-pot, solid-phase-enhanced sample preparation for proteomics experiments." Nature Protocols **14**(1): 68-85.

Hulea, L., S. P. Gravel, M. Morita, M. Cargnello, O. Uchenunu, Y. K. Im, C. Lehuédé, E. H. Ma, M. Leibovitch, S. McLaughlan, M. J. Blouin, M. Parisotto, V. Papavasiliou, C. Lavoie, O. Larsson, M. Ohh, T. Ferreira, C. Greenwood, G. Bridon, D. Avizonis, G. Ferbeyre, P. Siegel, R. G. Jones, W. Muller, J. Ursini-Siegel, J. St-Pierre, M. Pollak and I. Topisirovic (2018). "Translational and HIF-1α-Dependent Metabolic Reprogramming Underpin Metabolic Plasticity and Responses to Kinase Inhibitors and Biguanides." Cell Metab **28**(6): 817-832.e818.

Ikeda, K., Q. Kang, T. Yoneshiro, J. P. Camporez, H. Maki, M. Homma, K. Shinoda, Y. Chen, X. Lu, P. Maretich, K. Tajima, K. M. Ajuwon, T. Soga and S. Kajimura (2017). "UCP1-independent signaling involving SERCA2b-mediated calcium cycling regulates beige fat thermogenesis and systemic glucose homeostasis." Nat Med **23**(12): 1454-1465.

Ilan, Y., R. Maron, A. M. Tukpah, T. U. Maioli, G. Murugaiyan, K. Yang, H. Y. Wu and H. L. Weiner (2010). "Induction of regulatory T cells decreases adipose inflammation and alleviates insulin resistance in ob/ob mice." Proc Natl Acad Sci U S A **107**(21): 9765-9770.

Item, F. and D. Konrad (2012). "Visceral fat and metabolic inflammation: the portal theory revisited." Obes Rev **13 Suppl 2**: 30-39.

Iwayama, T., C. Steele, L. Yao, M. G. Dozmorov, D. Karamichos, J. D. Wren and L. E. Olson (2015). "PDGFRalpha signaling drives adipose tissue fibrosis by targeting progenitor cell plasticity." Genes Dev **29**(11): 1106-1119.

Jaitin, D. A., L. Adlung, C. A. Thaiss, A. Weiner, B. Li, H. Descamps, P. Lundgren, C. Bleriot, Z. Liu, A. Deczkowska, H. Keren-Shaul, E. David, N. Zmora, S. M. Eldar, N. Lubezky, O. Shibolet, D. A. Hill, M. A. Lazar, M. Colonna, F. Ginhoux, H. Shapiro, E. Elinav and I. Amit (2019). "Lipid-Associated Macrophages Control Metabolic Homeostasis in a Trem2-Dependent Manner." Cell **178**(3): 686-698 e614.

Jami-Alahmadi, Y., V. Pandey, A. K. Mayank and J. A. Wohlschlegel (2021). "A Robust Method for Packing High Resolution C18 RP-nano-HPLC Columns." J Vis Exp(171).

Jeffery, E., C. D. Church, B. Holtrup, L. Colman and M. S. Rodeheffer (2015). "Rapid depot-specific activation of adipocyte precursor cells at the onset of obesity." Nat Cell Biol **17**(4): 376-385.

Jeffery, E., A. Wing, B. Holtrup, Z. Sebo, J. L. Kaplan, R. Saavedra-Pena, C. D. Church, L. Colman, R. Berry and M. S. Rodeheffer (2016). "The Adipose Tissue Microenvironment Regulates Depot-Specific Adipogenesis in Obesity." Cell Metab **24**(1): 142-150.

Jespersen, N. Z., T. J. Larsen, L. Peijs, S. Daugaard, P. Homoe, A. Loft, J. de Jong, N. Mathur, B. Cannon, J. Nedergaard, B. K. Pedersen, K. Moller and C. Scheele (2013). "A classical brown adipose tissue mRNA signature partly overlaps with brite in the supraclavicular region of adult humans." Cell Metab **17**(5): 798-805.

Jewer, M., L. Lee, M. Leibovitch, G. Zhang, J. Liu, S. D. Findlay, K. M. Vincent, K. Tandoc, D. Dieters-Castator, D. F. Quail, I. Dutta, M. Coatham, Z. Xu, A. Puri, B.-J. Guan, M. Hatzoglou, A. Brumwell, J. Uniacke, C. Patsis, A. Koromilas, J. Schueler, G. M. Siegers, I. Topisirovic and L.-

M. Postovit (2020). "Translational control of breast cancer plasticity." Nature Communications **11**(1): 2498.

Jia, L., Y. Mao, Q. Ji, D. Dersh, J. W. Yewdell and S.-B. Qian (2020). "Decoding mRNA translatability and stability from the 5′ UTR." Nature Structural & Molecular Biology **27**(9): 814-821.

Jiang, H., X. Ding, Y. Cao, H. Wang and W. Zeng (2017). "Dense Intra-adipose Sympathetic Arborizations Are Essential for Cold-Induced Beiging of Mouse White Adipose Tissue." Cell Metab **26**(4): 686-692 e683.

Jiang, Y., D. C. Berry, W. Tang and J. M. Graff (2014). "Independent stem cell lineages regulate adipose organogenesis and adipose homeostasis." Cell Rep **9**(3): 1007-1022.

Jobava, R., Y. Mao, B. J. Guan, D. Hu, D. Krokowski, C. W. Chen, X. E. Shu, E. Chukwurah, J. Wu, Z. Gao, L. L. Zagore, W. C. Merrick, A. Trifunovic, A. C. Hsieh, S. Valadkhan, Y. Zhang, X. Qi, E. Jankowsky, I. Topisirovic, D. D. Licatalosi, S. B. Qian and M. Hatzoglou (2021). "Adaptive translational pausing is a hallmark of the cellular response to severe environmental stress." Mol Cell **81**(20): 4191-4208.e4198.

Joe, A. W. B., L. Yi, A. Natarajan, F. Le Grand, L. So, J. Wang, M. A. Rudnicki and F. M. V. Rossi (2010). "Muscle injury activates resident fibro/adipogenic progenitors that facilitate myogenesis." Nature Cell Biology **12**: 153-153.

Johnson, A. M. and J. M. Olefsky (2013). "The origins and drivers of insulin resistance." Cell **152**(4): 673-684.

Jung, S. M., C. M. Hung, S. R. Hildebrand, J. Sanchez-Gurmaches, B. Martinez-Pastor, J. M. Gengatharan, M. Wallace, D. Mukhopadhyay, C. Martinez Calejman, A. K. Luciano, W. Y. Hsiao, Y. Tang, H. Li, D. L. Daniels, R. Mostoslavsky, C. M. Metallo and D. A. Guertin (2019). "Non-canonical mTORC2 Signaling Regulates Brown Adipocyte Lipid Catabolism through SIRT6-FoxO1." Mol Cell **75**(4): 807-822 e808.

Kanda, H., S. Tateya, Y. Tamori, K. Kotani, K. Hiasa, R. Kitazawa, S. Kitazawa, H. Miyachi, S. Maeda, K. Egashira and M. Kasuga (2006). "MCP-1 contributes to macrophage infiltration into adipose tissue, insulin resistance, and hepatic steatosis in obesity." J Clin Invest **116**(6): 1494-1505.

Kang, J. G., C. Y. Park, S. H. Ihm, H. J. Yoo, H. Park, E. J. Rhee, J. C. Won, W. Y. Lee, K. W. Oh, S. W. Park and S. W. Kim (2010). "Mechanisms of adipose tissue redistribution with rosiglitazone treatment in various adipose depots." Metabolism **59**(1): 46-53.

Karastergiou, K. and S. K. Fried (2017). Cellular Mechanisms Driving Sex Differences in Adipose Tissue Biology and Body Shape in Humans and Mouse Models, Springer International Publishing**:** 29-51.

Kazak, L., E. T. Chouchani, M. P. Jedrychowski, B. K. Erickson, K. Shinoda, P. Cohen, R. Vetrivelan, G. Z. Lu, D. Laznik-Bogoslavski, S. C. Hasenfuss, S. Kajimura, S. P. Gygi and B. M. Spiegelman (2015). "A creatine-driven substrate cycle enhances energy expenditure and thermogenesis in beige fat." Cell **163**(3): 643-655.

Kazak, L., E. T. Chouchani, G. Z. Lu, M. P. Jedrychowski, C. J. Bare, A. I. Mina, M. Kumari, S. Zhang, I. Vuckovic, D. Laznik-Bogoslavski, P. Dzeja, A. S. Banks, E. D. Rosen and B. M. Spiegelman (2017). "Genetic Depletion of Adipocyte Creatine Metabolism Inhibits Diet-Induced Thermogenesis and Drives Obesity." Cell Metab **26**(4): 693.

Kelley, D. E., F. L. Thaete, F. Troost, T. Huwe and B. H. Goodpaster (2000). "Subdivisions of subcutaneous abdominal adipose tissue and insulin resistance." Am J Physiol Endocrinol Metab **278**(5): E941-948.

Khan, T., E. S. Muise, P. Iyengar, Z. V. Wang, M. Chandalia, N. Abate, B. B. Zhang, P. Bonaldo, S. Chua and P. E. Scherer (2009). "Metabolic dysregulation and adipose tissue fibrosis: role of collagen VI." Mol Cell Biol **29**(6): 1575-1591.

Khanh, V. C., A. F. Zulkifli, C. Tokunaga, T. Yamashita, Y. Hiramatsu and O. Ohneda (2018). "Aging impairs beige adipocyte differentiation of mesenchymal stem cells via the reduced expression of Sirtuin 1." Biochem Biophys Res Commun **500**(3): 682-690.

Kim, J. I., J. Park, Y. Ji, K. Jo, S. M. Han, J. H. Sohn, K. C. Shin, J. S. Han, Y. G. Jeon, H. Nahmgoong, K. H. Han, J. Kim, S. Kim, S. S. Choe and J. B. Kim (2019). "During Adipocyte Remodeling, Lipid Droplet Configurations Regulate Insulin Sensitivity through F-Actin and G-Actin Reorganization." Mol Cell Biol **39**(20).

Kim, J. Y., E. van de Wall, M. Laplante, A. Azzara, M. E. Trujillo, S. M. Hofmann, T. Schraw, J. L. Durand, H. Li, G. Li, L. A. Jelicks, M. F. Mehler, D. Y. Hui, Y. Deshaies, G. I. Shulman, G. J. Schwartz and P. E. Scherer (2007). "Obesity-associated improvements in metabolic profile through expansion of adipose tissue." J Clin Invest **117**(9): 2621-2637.

Kim, S. H., J. H. Chung, S. W. Song, W. S. Jung, Y. A. Lee and H. N. Kim (2016). "Relationship between deep subcutaneous abdominal adipose tissue and metabolic syndrome: a case control study." Diabetol Metab Syndr **8**(1): 10.

Kim, S. M., M. Lun, M. Wang, S. E. Senyo, C. Guillermier, P. Patwari and M. L. Steinhauser (2014). "Loss of white adipose hyperplastic potential is associated with enhanced susceptibility to insulin resistance." Cell Metab **20**(6): 1049-1058.

Klaver, M., C. J. M. de Blok, C. M. Wiepjes, N. M. Nota, M. Dekker, R. de Mutsert, T. Schreiner, A. D. Fisher, G. T'Sjoen and M. den Heijer (2018). "Changes in regional body fat, lean body mass and body shape in trans persons using cross-sex hormonal therapy: results from a multicenter prospective study." Eur J Endocrinol **178**(2): 163-171.

Kloting, N. and M. Bluher (2014). "Adipocyte dysfunction, inflammation and metabolic syndrome." Rev Endocr Metab Disord **15**(4): 277-287.

Knittle, J. L., K. Timmers, F. Ginsberg-Fellner, R. E. Brown and D. P. Katz (1979). "The growth of adipose tissue in children and adolescents. Cross-sectional and longitudinal studies of adipose cell number and size." J Clin Invest **63**(2): 239-246.

Koethe, J. R., C. Lagathu, J. E. Lake, P. Domingo, A. Calmy, J. Falutz, T. T. Brown and J. Capeau (2020). "HIV and antiretroviral therapy-related fat alterations." Nat Rev Dis Primers **6**(1): 48.

Kotlinowski, J. and A. Jozkowicz (2016). "PPAR Gamma and Angiogenesis: Endothelial Cells Perspective." J Diabetes Res **2016**: 8492353.

Kusminski, C. M., W. L. Holland, K. Sun, J. Park, S. B. Spurgin, Y. Lin, G. R. Askew, J. A. Simcox, D. A. McClain, C. Li and P. E. Scherer (2012). "MitoNEET-driven alterations in adipocyte mitochondrial activity reveal a crucial adaptive process that preserves insulin sensitivity in obesity." Nat Med **18**(10): 1539-1549.

Kusnadi, E. P., C. Timpone, I. Topisirovic, O. Larsson and L. Furic (2022). "Regulation of gene expression via translational buffering." Biochimica et Biophysica Acta (BBA) - Molecular Cell Research **1869**(1): 119140.

Labbe, S. M., M. Mouchiroud, A. Caron, B. Secco, E. Freinkman, G. Lamoureux, Y. Gelinas, R. Lecomte, Y. Bosse, P. Chimin, W. T. Festuccia, D. Richard and M. Laplante (2016). "mTORC1 is Required for Brown Adipose Tissue Recruitment and Metabolic Adaptation to Cold." Sci Rep **6**: 37223.

Langmead, B. and S. L. Salzberg (2012). "Fast gapped-read alignment with Bowtie 2." Nature Methods **9**(4): 357-359.

Lanktree, M. B. and R. A. Hegele (2017). "Metabolic Syndrome." Genomic and Precision Medicine: Primary Care: Third Edition **43**(1): 283-299.

Laurencikiene, J., T. Skurk, A. Kulyte, P. Heden, G. Astrom, E. Sjolin, M. Ryden, H. Hauner and P. Arner (2011). "Regulation of lipolysis in small and large fat cells of the same subject." J Clin Endocrinol Metab **96**(12): E2045-2049.

Le Bacquer, O., E. Petroulakis, S. Paglialunga, F. Poulin, D. Richard, K. Cianflone and N. Sonenberg (2007). "Elevated sensitivity to diet-induced obesity and insulin resistance in mice lacking 4E-BP1 and 4E-BP2." J Clin Invest **117**(2): 387-396.

Lebovitz, H. E. (2019). "Thiazolidinediones: the Forgotten Diabetes Medications." Curr Diab Rep **19**(12): 151.

Ledoux, S., I. Queguiner, S. Msika, S. Calderari, P. Rufat, J.-M. Gasc, P. Corvol and E. Larger (2008). "Angiogenesis Associated With Visceral and Subcutaneous Adipose Tissue in Severe Human Obesity." Diabetes **57**(12): 3247-3257.

Lee, M. J., P. Pramyothin, K. Karastergiou and S. K. Fried (2014). "Deconstructing the roles of glucocorticoids in adipose tissue biology and the development of central obesity." Biochim Biophys Acta **1842**(3): 473-481.

Lee, M. W., J. I. Odegaard, L. Mukundan, Y. Qiu, A. B. Molofsky, J. C. Nussbaum, K. Yun, R. M. Locksley and A. Chawla (2015). "Activated type 2 innate lymphoid cells regulate beige fat biogenesis." Cell **160**(1-2): 74-87.

Lee, Y. H. and J. G. Granneman (2012). "Seeking the source of adipocytes in adult white adipose tissues." Adipocyte **1**(4): 230-236.

Lee, Y. H., A. P. Petkova and J. G. Granneman (2013). "Identification of an adipogenic niche for adipose tissue remodeling and restoration." Cell Metab **18**(3): 355-367.

Lee, Y. H., A. P. Petkova, E. P. Mottillo and J. G. Granneman (2012). "In vivo identification of bipotential adipocyte progenitors recruited by beta3-adrenoceptor activation and high-fat feeding." Cell Metab **15**(4): 480-491.

Lee, Y. S., J. W. Kim, O. Osborne, D. Y. Oh, R. Sasik, S. Schenk, A. Chen, H. Chung, A. Murphy, S. M. Watkins, O. Quehenberger, R. S. Johnson and J. M. Olefsky (2014). "Increased adipocyte O2 consumption triggers HIF-1alpha, causing inflammation and insulin resistance in obesity." Cell **157**(6): 1339-1352.

Lefterova, M. I., A. K. Haakonsson, M. A. Lazar and S. Mandrup (2014). "PPARgamma and the global map of adipogenesis and beyond." Trends Endocrinol Metab **25**(6): 293-302.

Leppek, K., R. Das and M. Barna (2018). "Functional 5' UTR mRNA structures in eukaryotic translation regulation and how to find them." Nat Rev Mol Cell Biol **19**(3): 158-174.

Li, H., Y. Huo, X. He, L. Yao, H. Zhang, Y. Cui, H. Xiao, W. Xie, D. Zhang, Y. Wang, S. Zhang, H. Tu, Y. Cheng, Y. Guo, X. Cao, Y. Zhu, T. Jiang, X. Guo, Y. Qin and J. Sha (2022). "A male germ-cell-specific ribosome controls male fertility." Nature **612**(7941): 725-731.

Li, M., M. Wang, Y. Liu, S. Huang, X. Yi, C. Yin, S. Wang, M. Zhang, Q. Yu, P. Li and Y. Xiao (2019). "TNF-alpha Upregulates IKKepsilon Expression via the Lin28B/let-7a Pathway to Induce Catecholamine Resistance in Adipocytes." Obesity (Silver Spring) **27**(5): 767-776.

Li, X., Y. Zhao, C. Chen, L. Yang, H. H. Lee, Z. Wang, N. Zhang, M. G. Kolonin, Z. An, X. Ge, P. E. Scherer and K. Sun (2020). "Critical Role of Matrix Metalloproteinase 14 in Adipose Tissue Remodeling during Obesity." Mol Cell Biol **40**(8).

Lidell, M. E., M. J. Betz, O. Dahlqvist Leinhard, M. Heglind, L. Elander, M. Slawik, T. Mussack, D. Nilsson, T. Romu, P. Nuutila, K. A. Virtanen, F. Beuschlein, A. Persson, M. Borga and S. Enerback (2013). "Evidence for two types of brown adipose tissue in humans." Nat Med **19**(5): 631-634.

Lin, S., J. Choe, P. Du, R. Triboulet and R. I. Gregory (2016). "The m(6)A Methyltransferase METTL3 Promotes Translation in Human Cancer Cells." Mol Cell **62**(3): 335-345.

Liu, D., M. Bordicchia, C. Zhang, H. Fang, W. Wei, J. L. Li, A. Guilherme, K. Guntur, M. P. Czech and S. Collins (2016). "Activation of mTORC1 is essential for beta-adrenergic stimulation of adipose browning." J Clin Invest **126**(5): 1704-1716.

Liu, L. F., A. Purushotham, A. A. Wendel, K. Koba, J. DeIuliis, K. Lee and M. A. Belury (2009). "Regulation of adipose triglyceride lipase by rosiglitazone." Diabetes Obes Metab **11**(2): 131-142.

Liu, X., S. Wang, Y. You, M. Meng, Z. Zheng, M. Dong, J. Lin, Q. Zhao, C. Zhang, X. Yuan, T. Hu, L. Liu, Y. Huang, L. Zhang, D. Wang, J. Zhan, H. Jong Lee, J. R. Speakman and W. Jin

(2015). "Brown Adipose Tissue Transplantation Reverses Obesity in Ob/Ob Mice." Endocrinology **156**(7): 2461-2469.

Lockwood, T. E. (1991). "Superficial fascial system (SFS) of the trunk and extremities: a new concept." Plast Reconstr Surg **87**(6): 1009-1018.

Long, J. Z., K. J. Svensson, L. Tsai, X. Zeng, H. C. Roh, X. Kong, R. R. Rao, J. Lou, I. Lokurkar, W. Baur, J. J. Castellot, Jr., E. D. Rosen and B. M. Spiegelman (2014). "A smooth muscle-like origin for beige adipocytes." Cell Metab **19**(5): 810-820.

Love, M. I., W. Huber and S. Anders (2014). "Moderated estimation of fold change and dispersion for RNA-seq data with DESeq2." Genome Biology **15**(12): 550.

Lovejoy, J. C., C. M. Champagne, L. de Jonge, H. Xie and S. R. Smith (2008). "Increased visceral fat and decreased energy expenditure during the menopausal transition." Int J Obes (Lond) **32**(6): 949-958.

Lu, J., J. Zhao, H. Meng and X. Zhang (2019). "Adipose Tissue-Resident Immune Cells in Obesity and Type 2 Diabetes." Front Immunol **10**: 1173.

Lu, X., S. Altshuler-Keylin, Q. Wang, Y. Chen, C. Henrique Sponton, K. Ikeda, P. Maretich, T. Yoneshiro and S. Kajimura (2018). "Mitophagy controls beige adipocyte maintenance through a Parkin-dependent and UCP1-independent mechanism." Sci Signal **11**(527).

Lumeng, C. N., J. L. Bodzin and A. R. Saltiel (2007). "Obesity induces a phenotypic switch in adipose tissue macrophage polarization." J Clin Invest **117**(1): 175-184.

Lumeng, C. N., J. B. DelProposto, D. J. Westcott and A. R. Saltiel (2008). "Phenotypic switching of adipose tissue macrophages with obesity is generated by spatiotemporal differences in macrophage subtypes." Diabetes **57**(12): 3239-3246.

Lumeng, C. N., S. M. Deyoung, J. L. Bodzin and A. R. Saltiel (2007). "Increased Inflammatory Properties of Adipose Tissue Macrophages Recruited During Diet-Induced Obesity." Diabetes **56**(1): 16-23.

Mahlakoiv, T., A. L. Flamar, L. K. Johnston, S. Moriyama, G. G. Putzel, P. J. Bryce and D. Artis (2019). "Stromal cells maintain immune cell homeostasis in adipose tissue via production of interleukin-33." Sci Immunol **4**(35): eaax0416.

Majithia, A. R., J. Flannick, P. Shahinian, M. Guo, M. A. Bray, P. Fontanillas, S. B. Gabriel, T. D. C. Go, N. J. F. A. S. Project, S. T. D. Consortium, T. D. G. Consortium, E. D. Rosen and D. Altshuler (2014). "Rare variants in PPARG with decreased activity in adipocyte differentiation are associated with increased risk of type 2 diabetes." Proc Natl Acad Sci U S A **111**(36): 13127-13132.

Majka, S. M., H. L. Miller, K. M. Helm, A. S. Acosta, C. R. Childs, R. Kong and D. J. Klemm (2014). "Analysis and isolation of adipocytes by flow cytometry." Methods Enzymol **537**: 281-296.

Maniyadath, B., Q. Zhang, R. K. Gupta and S. Mandrup (2023). "Adipose tissue at single-cell resolution." Cell Metab **35**(3): 386-413.

Marangoni, R. G., B. D. Korman, J. Wei, T. A. Wood, L. V. Graham, M. L. Whitfield, P. E. Scherer, W. G. Tourtellotte and J. Varga (2015). "Myofibroblasts in murine cutaneous fibrosis originate from adiponectin-positive intradermal progenitors." Arthritis Rheumatol **67**(4): 1062-1073.

Marcelin, G., A. Ferreira, Y. Liu, M. Atlan, J. Aron-Wisnewsky, V. Pelloux, Y. Botbol, M. Ambrosini, M. Fradet, C. Rouault, C. Henegar, J. S. Hulot, C. Poitou, A. Torcivia, R. Nail-Barthelemy, J. C. Bichet, E. L. Gautier and K. Clement (2017). "A PDGFRalpha-Mediated Switch toward CD9(high) Adipocyte Progenitors Controls Obesity-Induced Adipose Tissue Fibrosis." Cell Metab **25**(3): 673-685.

Marcelin, G., A. L. M. Silveira, L. B. Martins, A. V. Ferreira and K. Clement (2019). "Deciphering the cellular interplays underlying obesity-induced adipose tissue fibrosis." J Clin Invest **129**(10): 4032-4040.

Markman, B. and F. E. Barton, Jr. (1987). "Anatomy of the subcutaneous tissue of the trunk and lower extremity." Plast Reconstr Surg **80**(2): 248-254.

McAlister, G. C., D. P. Nusinow, M. P. Jedrychowski, M. Wühr, E. L. Huttlin, B. K. Erickson, R. Rad, W. Haas and S. P. Gygi (2014). "MultiNotch MS3 enables accurate, sensitive, and multiplexed detection of differential expression across cancer cell line proteomes." Anal Chem **86**(14): 7150-7158.

McLaughlin, T., C. Craig, L. F. Liu, D. Perelman, C. Allister, D. Spielman and S. W. Cushman (2016). "Adipose Cell Size and Regional Fat Deposition as Predictors of Metabolic Response to Overfeeding in Insulin-Resistant and Insulin-Sensitive Humans." Diabetes **65**(5): 1245-1254.

Mehta, N. K., L. R. Abrams and M. Myrskyla (2020). "US life expectancy stalls due to cardiovascular disease, not drug deaths." Proc Natl Acad Sci U S A **117**(13): 6998-7000.

Merlotti, C., V. Ceriani, A. Morabito and A. E. Pontiroli (2017). "Subcutaneous fat loss is greater than visceral fat loss with diet and exercise, weight-loss promoting drugs and bariatric surgery: a critical review and meta-analysis." Int J Obes (Lond) **41**(5): 672-682.

Merrick, D., A. Sakers, Z. Irgebay, C. Okada, C. Calvert, M. P. Morley, I. Percec and P. Seale (2019). "Identification of a mesenchymal progenitor cell hierarchy in adipose tissue." Science **364**(6438).

Meyer, L. K., T. P. Ciaraldi, R. R. Henry, A. C. Wittgrove and S. A. Phillips (2013). "Adipose tissue depot and cell size dependency of adiponectin synthesis and secretion in human obesity." Adipocyte **2**(4): 217-226.

Meza-Perez, S. and T. D. Randall (2017). "Immunological Functions of the Omentum." Trends Immunol **38**(7): 526-536.

Mills, E. L., K. A. Pierce, M. P. Jedrychowski, R. Garrity, S. Winther, S. Vidoni, T. Yoneshiro, J. B. Spinelli, G. Z. Lu, L. Kazak, A. S. Banks, M. C. Haigis, S. Kajimura, M. P. Murphy, S. P. Gygi, C. B. Clish and E. T. Chouchani (2018). "Accumulation of succinate controls activation of adipose tissue thermogenesis." Nature **560**(7716): 102-106.

Min, S. Y., A. Desai, Z. Yang, A. Sharma, T. DeSouza, R. M. J. Genga, A. Kucukural, L. M. Lifshitz, S. Nielsen, C. Scheele, R. Maehr, M. Garber and S. Corvera (2019). "Diverse repertoire of human adipocyte subtypes develops from transcriptionally distinct mesenchymal progenitor cells." Proc Natl Acad Sci U S A **116**(36): 17970-17979.

Min, S. Y., J. Kady, M. Nam, R. Rojas-Rodriguez, A. Berkenwald, J. H. Kim, H. L. Noh, J. K. Kim, M. P. Cooper, T. Fitzgibbons, M. A. Brehm and S. Corvera (2016). "Human 'brite/beige' adipocytes develop from capillary networks, and their implantation improves metabolic homeostasis in mice." Nat Med **22**(3): 312-318.

Mishra, M. and K. Heese (2011). "P60TRP interferes with the GPCR/secretase pathway to mediate neuronal survival and synaptogenesis." J Cell Mol Med **15**(11): 2462-2477.

Miyazaki, Y., A. Mahankali, M. Matsuda, S. Mahankali, J. Hardies, K. Cusi, L. J. Mandarino and R. A. DeFronzo (2002). "Effect of pioglitazone on abdominal fat distribution and insulin sensitivity in type 2 diabetic patients." J Clin Endocrinol Metab **87**(6): 2784-2791.

Molofsky, A. B., J. C. Nussbaum, H. E. Liang, S. J. Van Dyken, L. E. Cheng, A. Mohapatra, A. Chawla and R. M. Locksley (2013). "Innate lymphoid type 2 cells sustain visceral adipose tissue eosinophils and alternatively activated macrophages." J Exp Med **210**(3): 535-549.

Morigny, P., M. Houssier, E. Mouisel and D. Langin (2016). "Adipocyte lipolysis and insulin resistance." Biochimie **125**: 259-266.

Morley, T. S., J. Y. Xia and P. E. Scherer (2015). "Selective enhancement of insulin sensitivity in the mature adipocyte is sufficient for systemic metabolic improvements." Nat Commun **6**: 7906.

Morral, C., J. Stanisavljevic, X. Hernando-Momblona, E. Mereu, A. Álvarez-Varela, C. Cortina, D. Stork, F. Slebe, G. Turon, G. Whissell, M. Sevillano, A. Merlos-Suárez, À. Casanova-Martí, C. Moutinho, S. W. Lowe, L. E. Dow, A. Villanueva, E. Sancho, H. Heyn and E. Batlle (2020). "Zonation of Ribosomal DNA Transcription Defines a Stem Cell Hierarchy in Colorectal Cancer." Cell Stem Cell **26**(6): 845-861.e812.

Morrison, S. F. (2016). "Central neural control of thermoregulation and brown adipose tissue." Auton Neurosci **196**: 14-24.

Mowers, J., M. Uhm, S. M. Reilly, J. Simon, D. Leto, S. H. Chiang, L. Chang and A. R. Saltiel (2013). "Inflammation produces catecholamine resistance in obesity via activation of PDE3B by the protein kinases IKKepsilon and TBK1." Elife **2**: e01119.

Murano, I., G. Barbatelli, A. Giordano and S. Cinti (2009). "Noradrenergic parenchymal nerve fiber branching after cold acclimatisation correlates with brown adipocyte density in mouse adipose organ." J Anat **214**(1): 171-178.

Nagy, L., P. Tontonoz, J. G. Alvarez, H. Chen and R. M. Evans (1998). "Oxidized LDL regulates macrophage gene expression through ligand activation of PPARgamma." Cell **93**(2): 229-240.

Neese, R. A., L. M. Misell, S. Turner, A. Chu, J. Kim, D. Cesar, R. Hoh, F. Antelo, A. Strawford, J. M. McCune, M. Christiansen and M. K. Hellerstein (2002). "Measurement in vivo of proliferation rates of slow turnover cells by 2H2O labeling of the deoxyribose moiety of DNA." Proc Natl Acad Sci U S A **99**(24): 15345-15350.

Ngo, D. T., M. G. Farb, R. Kikuchi, S. Karki, S. Tiwari, S. J. Bigornia, D. O. Bates, M. P. LaValley, N. M. Hamburg, J. A. Vita, D. T. Hess, K. Walsh and N. Gokce (2014). "Antiangiogenic actions of vascular endothelial growth factor-A165b, an inhibitory isoform of vascular endothelial growth factor-A, in human obesity." Circulation **130**(13): 1072-1080.

Nguyen, H. P., F. Lin, D. Yi, Y. Xie, J. Dinh, P. Xue and H. S. Sul (2021). "Aging-dependent regulatory cells emerge in subcutaneous fat to inhibit adipogenesis." Dev Cell **56**(10): 1437-1451 e1433.

Nguyen, M. T., S. Favelyukis, A. K. Nguyen, D. Reichart, P. A. Scott, A. Jenn, R. Liu-Bryan, C. K. Glass, J. G. Neels and J. M. Olefsky (2007). "A subpopulation of macrophages infiltrates hypertrophic adipose tissue and is activated by free fatty acids via Toll-like receptors 2 and 4 and JNK-dependent pathways." J Biol Chem **282**(48): 35279-35292.

Nielsen, S., Z. Guo, C. M. Johnson, D. D. Hensrud and M. D. Jensen (2004). "Splanchnic lipolysis in human obesity." J Clin Invest **113**(11): 1582-1588.

Nishimura, S., I. Manabe, M. Nagasaki, K. Eto, H. Yamashita, M. Ohsugi, M. Otsu, K. Hara, K. Ueki, S. Sugiura, K. Yoshimura, T. Kadowaki and R. Nagai (2009). "CD8+ effector T cells contribute to macrophage recruitment and adipose tissue inflammation in obesity." Nat Med **15**(8): 914-920.

Odegaard, J. I., R. R. Ricardo-Gonzalez, M. H. Goforth, C. R. Morel, V. Subramanian, L. Mukundan, A. Red Eagle, D. Vats, F. Brombacher, A. W. Ferrante and A. Chawla (2007). "Macrophage-specific PPARgamma controls alternative activation and improves insulin resistance." Nature **447**(7148): 1116-1120.

Oguri, Y., K. Shinoda, H. Kim, D. L. Alba, W. R. Bolus, Q. Wang, Z. Brown, R. N. Pradhan, K. Tajima, T. Yoneshiro, K. Ikeda, Y. Chen, R. T. Cheang, K. Tsujino, C. R. Kim, V. J. Greiner, R. Datta, C. D. Yang, K. Atabai, M. T. McManus, S. K. Koliwad, B. M. Spiegelman and S. Kajimura (2020). "CD81 Controls Beige Fat Progenitor Cell Growth and Energy Balance via FAK Signaling." Cell **182**(3): 563-577 e520.

Oguri, Y., K. Shinoda, H. Kim, D. L. Alba, W. R. Bolus, Q. Wang, Z. Brown, R. N. Pradhan, K. Tajima, T. Yoneshiro, K. Ikeda, Y. Chen, R. T. Cheang, K. Tsujino, C. R. Kim, V. J. Greiner, R. Datta, C. D. Yang, K. Atabai, M. T. McManus, S. K. Koliwad, B. M. Spiegelman and S. Kajimura (2020). "CD81 Controls Beige Fat Progenitor Cell Growth and Energy Balance via FAK Signaling." Cell **182**(3): 563-577.e520.

Ohashi, K., J. L. Parker, N. Ouchi, A. Higuchi, J. A. Vita, N. Gokce, A. A. Pedersen, C. Kalthoff, S. Tullin, A. Sams, R. Summer and K. Walsh (2010). "Adiponectin promotes macrophage polarization toward an anti-inflammatory phenotype." J Biol Chem **285**(9): 6153-6160.

Ouellet, V., S. M. Labbe, D. P. Blondin, S. Phoenix, B. Guerin, F. Haman, E. E. Turcotte, D. Richard and A. C. Carpentier (2012). "Brown adipose tissue oxidative metabolism contributes to energy expenditure during acute cold exposure in humans." J Clin Invest **122**(2): 545-552.

Ouellet, V., A. Routhier-Labadie, W. Bellemare, L. Lakhal-Chaieb, E. Turcotte, A. C. Carpentier and D. Richard (2011). "Outdoor temperature, age, sex, body mass index, and diabetic status determine the prevalence, mass, and glucose-uptake activity of 18F-FDG-detected BAT in humans." J Clin Endocrinol Metab **96**(1): 192-199.

Padilla, J., E. Leung and R. P. Phipps (2002). "Human B lymphocytes and B lymphomas express PPAR-gamma and are killed by PPAR-gamma agonists." Clin Immunol **103**(1): 22-33.

Padwal, R., W. D. Leslie, L. M. Lix and S. R. Majumdar (2016). "Relationship Among Body Fat Percentage, Body Mass Index, and All-Cause Mortality: A Cohort Study." Ann Intern Med **164**(8): 532-541.

Pal, A., T. M. Barber, M. Van de Bunt, S. A. Rudge, Q. Zhang, K. L. Lachlan, N. S. Cooper, H. Linden, J. C. Levy, M. J. Wakelam, L. Walker, F. Karpe and A. L. Gloyn (2012). "PTEN mutations as a cause of constitutive insulin sensitivity and obesity." N Engl J Med **367**(11): 1002-1011.

Pan, W. W. and M. G. Myers, Jr. (2018). "Leptin and the maintenance of elevated body weight." Nat Rev Neurosci **19**(2): 95-105.

Park, H. S., J. Y. Park and R. Yu (2005). "Relationship of obesity and visceral adiposity with serum concentrations of CRP, TNF-alpha and IL-6." Diabetes Res Clin Pract **69**(1): 29-35.

Park, J., S. Shin, L. Liu, I. Jahan, S. G. Ong, P. Xu, D. C. Berry and Y. Jiang (2021). "Progenitor-like characteristics in a subgroup of UCP1+ cells within white adipose tissue." Dev Cell **56**(7): 985-999 e984.

Passarelli, M. C., A. M. Pinzaru, H. Asgharian, M. V. Liberti, S. Heissel, H. Molina, H. Goodarzi and S. F. Tavazoie (2022). "Leucyl-tRNA synthetase is a tumour suppressor in breast cancer and regulates codon-dependent translation dynamics." Nature Cell Biology **24**(3): 307-315.

Patro, R., G. Duggal, M. I. Love, R. A. Irizarry and C. Kingsford (2017). "Salmon provides fast and bias-aware quantification of transcript expression." Nature Methods **14**(4): 417-419.

Patsouris, D., P. P. Li, D. Thapar, J. Chapman, J. M. Olefsky and J. G. Neels (2008). "Ablation of CD11c-positive cells normalizes insulin sensitivity in obese insulin resistant animals." Cell Metab **8**(4): 301-309.

Pause, A., G. J. Belsham, A. C. Gingras, O. Donzé, T. A. Lin, J. C. Lawrence, Jr. and N. Sonenberg (1994). "Insulin-dependent stimulation of protein synthesis by phosphorylation of a regulator of 5'-cap function." Nature **371**(6500): 762-767.

Pearson, S., A. Loft, P. Rajbhandari, J. Simcox, S. Lee, P. Tontonoz, S. Mandrup and C. J. Villanueva (2019). "Loss of TLE3 promotes the mitochondrial program in beige adipocytes and improves glucose metabolism." Genes Dev **33**(13-14): 747-762.

Pellegrinelli, V., J. Heuvingh, O. du Roure, C. Rouault, A. Devulder, C. Klein, M. Lacasa, E. Clement, D. Lacasa and K. Clement (2014). "Human adipocyte function is impacted by mechanical cues." J Pathol **233**(2): 183-195.

Perera, H. K., M. Clarke, N. J. Morris, W. Hong, L. H. Chamberlain and G. W. Gould (2003). "Syntaxin 6 regulates Glut4 trafficking in 3T3-L1 adipocytes." Mol Biol Cell **14**(7): 2946-2958.

Petersen, M. C. and G. I. Shulman (2018). "Mechanisms of Insulin Action and Insulin Resistance." Physiol Rev **98**(4): 2133-2223.

Petersen, M. C., G. I. Smith, H. H. Palacios, S. S. Farabi, M. Yoshino, J. Yoshino, K. Cho, V. G. Davila-Roman, M. Shankaran, R. A. Barve, J. Yu, J. H. Stern, B. W. Patterson, M. K. Hellerstein, G. I. Shulman, G. J. Patti and S. Klein (2024). "Cardiometabolic characteristics of people with metabolically healthy and unhealthy obesity." Cell Metab **36**(4): 745-761.e745.

Peurichard, D., F. Delebecque, A. Lorsignol, C. Barreau, J. Rouquette, X. Descombes, L. Casteilla and P. Degond (2017). "Simple mechanical cues could explain adipose tissue morphology." J Theor Biol **429**: 61-81.

Plikus, M. V., C. F. Guerrero-Juarez, M. Ito, Y. R. Li, P. H. Dedhia, Y. Zheng, M. Shao, D. L. Gay, R. Ramos, T. C. Hsi, J. W. Oh, X. Wang, A. Ramirez, S. E. Konopelski, A. Elzein, A. Wang, R. J. Supapannachart, H. L. Lee, C. H. Lim, A. Nace, A. Guo, E. Treffeisen, T. Andl, R. N. Ramirez, R. Murad, S. Offermanns, D. Metzger, P. Chambon, A. D. Widgerow, T. L. Tuan, A. Mortazavi, R. K. Gupta, B. A. Hamilton, S. E. Millar, P. Seale, W. S. Pear, M. A. Lazar and G. Cotsarelis (2017). "Regeneration of fat cells from myofibroblasts during wound healing." Science **355**(6326): 748-752.

Puigserver, P., Z. Wu, C. W. Park, R. Graves, M. Wright and B. M. Spiegelman (1998). "A cold-inducible coactivator of nuclear receptors linked to adaptive thermogenesis." Cell **92**(6): 829-839.

Qiu, Y., K. D. Nguyen, J. I. Odegaard, X. Cui, X. Tian, R. M. Locksley, R. D. Palmiter and A. Chawla (2014). "Eosinophils and type 2 cytokine signaling in macrophages orchestrate development of functional beige fat." Cell **157**(6): 1292-1308.

Raajendiran, A., G. Ooi, J. Bayliss, P. E. O'Brien, R. B. Schittenhelm, A. K. Clark, R. A. Taylor, M. S. Rodeheffer, P. R. Burton and M. J. Watt (2019). "Identification of Metabolically Distinct Adipocyte Progenitor Cells in Human Adipose Tissues." Cell Rep **27**(5): 1528-1540 e1527.

Rajbhandari, P., D. Arneson, S. K. Hart, I. S. Ahn, G. Diamante, L. C. Santos, N. Zaghari, A. C. Feng, B. J. Thomas, L. Vergnes, S. D. Lee, A. K. Rajbhandari, K. Reue, S. T. Smale, X. Yang and P. Tontonoz (2019). "Single cell analysis reveals immune cell-adipocyte crosstalk regulating the transcription of thermogenic adipocytes." Elife **8**.

Ramirez, A. K., S. N. Dankel, B. Rastegarpanah, W. Cai, R. Xue, M. Crovella, Y.-H. Tseng, C. R. Kahn and S. Kasif (2020). "Single-cell transcriptional networks in differentiating preadipocytes suggest drivers associated with tissue heterogeneity." Nature Communications **11**(1): 2117.

Rausch, M. E., S. Weisberg, P. Vardhana and D. V. Tortoriello (2008). "Obesity in C57BL/6J mice is characterized by adipose tissue hypoxia and cytotoxic T-cell infiltration." Int J Obes (Lond) **32**(3): 451-463.

Ravi, V., A. Jain, S. Mishra and N. R. Sundaresan (2020). "Measuring Protein Synthesis in Cultured Cells and Mouse Tissues Using the Non-radioactive SUnSET Assay." Curr Protoc Mol Biol **133**(1): e127.

Reardon, C. A., A. Lingaraju, K. Q. Schoenfelt, G. Zhou, C. Cui, H. Jacobs-El, I. Babenko, A. Hoofnagle, D. Czyz, H. Shuman, T. Vaisar and L. Becker (2018). "Obesity and Insulin Resistance Promote Atherosclerosis through an IFNγ-Regulated Macrophage Protein Network." Cell Rep **23**(10): 3021-3030.

Reubinoff, B. E., J. Wurtman, N. Rojansky, D. Adler, P. Stein, J. G. Schenker and A. Brzezinski (1995). "Effects of hormone replacement therapy on weight, body composition, fat distribution, and food intake in early postmenopausal women: a prospective study." Fertil Steril **64**(5): 963-968.

Rhodes, D. and H. J. Lipps (2015). "G-quadruplexes and their regulatory roles in biology." Nucleic Acids Research **43**(18): 8627-8637.

Rigamonti, A., K. Brennand, F. Lau and C. A. Cowan (2011). "Rapid cellular turnover in adipose tissue." PLoS One **6**(3): e17637.

Robinson, J. T., H. Thorvaldsdóttir, W. Winckler, M. Guttman, E. S. Lander, G. Getz and J. P. Mesirov (2011). "Integrative genomics viewer." Nat Biotechnol **29**(1): 24-26.

Rodeheffer, M. S., K. Birsoy and J. M. Friedman (2008). "Identification of white adipocyte progenitor cells in vivo." Cell **135**(2): 240-249.

Roh, H. C., M. Kumari, S. Taleb, D. Tenen, C. Jacobs, A. Lyubetskaya, L. T. Tsai and E. D. Rosen (2020). "Adipocytes fail to maintain cellular identity during obesity due to reduced PPARγ activity and elevated TGFβ-SMAD signaling." Mol Metab **42**: 101086.

Roh, H. C., L. T. Y. Tsai, M. Shao, D. Tenen, Y. Shen, M. Kumari, A. Lyubetskaya, C. Jacobs, B. Dawes, R. K. Gupta and E. D. Rosen (2018). "Warming Induces Significant Reprogramming of Beige, but Not Brown, Adipocyte Cellular Identity." Cell Metab **27**(5): 1121-1137 e1125.

Rosell, M., M. Kaforou, A. Frontini, A. Okolo, Y. W. Chan, E. Nikolopoulou, S. Millership, M. E. Fenech, D. MacIntyre, J. O. Turner, J. D. Moore, E. Blackburn, W. J. Gullick, S. Cinti, G. Montana, M. G. Parker and M. Christian (2014). "Brown and white adipose tissues: intrinsic differences in gene expression and response to cold exposure in mice." Am J Physiol Endocrinol Metab **306**(8): E945-964.

Rosen, E. D. and B. M. Spiegelman (2014). "What we talk about when we talk about fat." Cell **156**(1-2): 20-44.

Rosenquist, K. J., A. Pedley, J. M. Massaro, K. E. Therkelsen, J. M. Murabito, U. Hoffmann and C. S. Fox (2013). "Visceral and subcutaneous fat quality and cardiometabolic risk." JACC Cardiovasc Imaging **6**(7): 762-771.

Rosenwald, M., A. Perdikari, T. Rulicke and C. Wolfrum (2013). "Bi-directional interconversion of brite and white adipocytes." Nat Cell Biol **15**(6): 659-667.

Roux, P. P. and I. Topisirovic (2012). "Regulation of mRNA translation by signaling pathways." Cold Spring Harb Perspect Biol **4**(11).

Rytka, J. M., S. Wueest, E. J. Schoenle and D. Konrad (2011). "The portal theory supported by venous drainage-selective fat transplantation." Diabetes **60**(1): 56-63.

Sahakyan, K. R., V. K. Somers, J. P. Rodriguez-Escudero, D. O. Hodge, R. E. Carter, O. Sochor, T. Coutinho, M. D. Jensen, V. L. Roger, P. Singh and F. Lopez-Jimenez (2015). "Normal-Weight Central Obesity: Implications for Total and Cardiovascular Mortality." Ann Intern Med **163**(11): 827-835.

Sakaguchi, M., S. Fujisaka, W. Cai, J. N. Winnay, M. Konishi, B. T. O'Neill, M. Li, R. Garcia-Martin, H. Takahashi, J. Hu, R. N. Kulkarni and C. R. Kahn (2017). "Adipocyte Dynamics and Reversible Metabolic Syndrome in Mice with an Inducible Adipocyte-Specific Deletion of the Insulin Receptor." Cell Metab **25**(2): 448-462.

Sakers, A., M. K. De Siqueira, P. Seale and C. J. Villanueva (2022). "Adipose-tissue plasticity in health and disease." Cell **185**(3): 419-446.

Salans, L. B., S. W. Cushman and R. E. Weismann (1973). "Studies of human adipose tissue. Adipose cell size and number in nonobese and obese patients." J Clin Invest **52**(4): 929-941.

Sampath, P., D. K. Pritchard, L. Pabon, H. Reinecke, S. M. Schwartz, D. R. Morris and C. E. Murry (2008). "A hierarchical network controls protein translation during murine embryonic stem cell self-renewal and differentiation." Cell Stem Cell **2**(5): 448-460.

Sanchez-Gurmaches, J., W. Y. Hsiao and D. A. Guertin (2015). "Highly selective in vivo labeling of subcutaneous white adipocyte precursors with Prx1-Cre." Stem Cell Reports **4**(4): 541-550.

Sanchez-Gurmaches, J., C. M. Hung and D. A. Guertin (2016). "Emerging Complexities in Adipocyte Origins and Identity." Trends Cell Biol **26**(5): 313-326.

Sarvari, A. K., E. L. Van Hauwaert, L. K. Markussen, E. Gammelmark, A. B. Marcher, M. F. Ebbesen, R. Nielsen, J. R. Brewer, J. G. S. Madsen and S. Mandrup (2021). "Plasticity of Epididymal Adipose Tissue in Response to Diet-Induced Obesity at Single-Nucleus Resolution." Cell Metab **33**(2): 437-453 e435.

Sárvári, A. K., E. L. Van Hauwaert, L. K. Markussen, E. Gammelmark, A. B. Marcher, M. F. Ebbesen, R. Nielsen, J. R. Brewer, J. G. S. Madsen and S. Mandrup (2021). "Plasticity of Epididymal Adipose Tissue in Response to Diet-Induced Obesity at Single-Nucleus Resolution." Cell Metab **33**(2): 437-453.e435.

Schreiber, R., C. Diwoky, G. Schoiswohl, U. Feiler, N. Wongsiriroj, M. Abdellatif, D. Kolb, J. Hoeks, E. E. Kershaw, S. Sedej, P. Schrauwen, G. Haemmerle and R. Zechner (2017). "Cold-Induced Thermogenesis Depends on ATGL-Mediated Lipolysis in Cardiac Muscle, but Not Brown Adipose Tissue." Cell Metab **26**(5): 753-763 e757.

Schwalie, P. C., H. Dong, M. Zachara, J. Russeil, D. Alpern, N. Akchiche, C. Caprara, W. Sun, K. U. Schlaudraff, G. Soldati, C. Wolfrum and B. Deplancke (2018). "A stromal cell population that inhibits adipogenesis in mammalian fat depots." Nature **559**(7712): 103-108.

Sebo, Z. L. and M. S. Rodeheffer (2019). "Assembling the adipose organ: adipocyte lineage segregation and adipogenesis in vivo." Development **146**(7): dev172098.

Shahbazian, D., P. P. Roux, V. Mieulet, M. S. Cohen, B. Raught, J. Taunton, J. W. Hershey, J. Blenis, M. Pende and N. Sonenberg (2006). "The mTOR/PI3K and MAPK pathways converge on eIF4B to control its phosphorylation and activity." Embo j **25**(12): 2781-2791.

Shamsi, F., M. Piper, L. L. Ho, T. L. Huang, A. Gupta, A. Streets, M. D. Lynes and Y. H. Tseng (2021). "Vascular smooth muscle-derived Trpv1(+) progenitors are a source of cold-induced thermogenic adipocytes." Nat Metab **3**(4): 485-495.

Shan, B., M. Shao, Q. Zhang, Y. A. An, L. Vishvanath and R. K. Gupta (2021). "Cold-responsive adipocyte progenitors couple adrenergic signaling to immune cell activation to promote beige adipocyte accrual." Genes Dev **35**(19-20): 1333-1338.

Shan, B., M. Shao, Q. Zhang, C. Hepler, V. A. Paschoal, S. D. Barnes, L. Vishvanath, Y. A. An, L. Jia, V. S. Malladi, D. W. Strand, O. T. Gupta, J. K. Elmquist, D. Oh and R. K. Gupta (2020). "Perivascular mesenchymal cells control adipose-tissue macrophage accrual in obesity." Nat Metab **2**(11): 1332-1349.

Shao, M., C. Hepler, Q. Zhang, B. Shan, L. Vishvanath, G. H. Henry, S. Zhao, Y. A. An, Y. Wu, D. W. Strand and R. K. Gupta (2021). "Pathologic HIF1alpha signaling drives adipose progenitor dysfunction in obesity." Cell Stem Cell **28**(4): 685-701 e687.

Shao, M., J. Ishibashi, C. M. Kusminski, Q. A. Wang, C. Hepler, L. Vishvanath, K. A. MacPherson, S. B. Spurgin, K. Sun, W. L. Holland, P. Seale and R. K. Gupta (2016). "Zfp423 Maintains White Adipocyte Identity through Suppression of the Beige Cell Thermogenic Gene Program." Cell Metab **23**(6): 1167-1184.

Shao, M., L. Vishvanath, N. C. Busbuso, C. Hepler, B. Shan, A. X. Sharma, S. Chen, X. Yu, Y. A. An, Y. Zhu, W. L. Holland and R. K. Gupta (2018). "De novo adipocyte differentiation from Pdgfrbeta(+) preadipocytes protects against pathologic visceral adipose expansion in obesity." Nat Commun **9**(1): 890.

Shao, M., Q. A. Wang, A. Song, L. Vishvanath, N. C. Busbuso, P. E. Scherer and R. K. Gupta (2019). "Cellular Origins of Beige Fat Cells Revisited." Diabetes **68**(10): 1874-1885.

Shao, M., Q. Zhang, A. Truong, B. Shan, L. Vishvanath, L. Li, P. Seale and R. K. Gupta (2021). "ZFP423 controls EBF2 coactivator recruitment and PPARgamma occupancy to determine the thermogenic plasticity of adipocytes." Genes Dev **35**(21-22): 1461-1474.

Shapira, S. N. and P. Seale (2019). "Transcriptional Control of Brown and Beige Fat Development and Function." Obesity (Silver Spring) **27**(1): 13-21.

Shearin, A. L., B. R. Monks, P. Seale and M. J. Birnbaum (2016). "Lack of AKT in adipocytes causes severe lipodystrophy." Mol Metab **5**(7): 472-479.

Shen, W., M. Punyanitya, A. M. Silva, J. Chen, D. Gallagher, L. B. Sardinha, D. B. Allison and S. B. Heymsfield (2009). "Sexual dimorphism of adipose tissue distribution across the lifespan: a cross-sectional whole-body magnetic resonance imaging study." Nutr Metab (Lond) **6**(1): 17.

Shi, Z., K. Fujii, K. M. Kovary, N. R. Genuth, H. L. Röst, M. N. Teruel and M. Barna (2017). "Heterogeneous Ribosomes Preferentially Translate Distinct Subpools of mRNAs Genome-wide." Mol Cell **67**(1): 71-83.e77.

Shimizu, I., T. Aprahamian, R. Kikuchi, A. Shimizu, K. N. Papanicolaou, S. MacLauchlan, S. Maruyama and K. Walsh (2014). "Vascular rarefaction mediates whitening of brown fat in obesity." J Clin Invest **124**(5): 2099-2112.

Shin, H., Y. Ma, T. Chanturiya, Q. Cao, Y. Wang, A. K. G. Kadegowda, R. Jackson, D. Rumore, B. Xue, H. Shi, O. Gavrilova and L. Yu (2017). "Lipolysis in Brown Adipocytes Is Not Essential for Cold-Induced Thermogenesis in Mice." Cell Metab **26**(5): 764-777 e765.

Shirakawa, K., X. Yan, K. Shinmura, J. Endo, M. Kataoka, Y. Katsumata, T. Yamamoto, A. Anzai, S. Isobe, N. Yoshida, H. Itoh, I. Manabe, M. Sekai, Y. Hamazaki, K. Fukuda, N. Minato and M. Sano (2016). "Obesity accelerates T cell senescence in murine visceral adipose tissue." J Clin Invest **126**(12): 4626-4639.

Shook, B. A., R. R. Wasko, O. Mano, M. Rutenberg-Schoenberg, M. C. Rudolph, B. Zirak, G. C. Rivera-Gonzalez, F. Lopez-Giraldez, S. Zarini, A. Rezza, D. A. Clark, M. Rendl, M. D. Rosenblum, M. B. Gerstein and V. Horsley (2020). "Dermal Adipocyte Lipolysis and Myofibroblast Conversion Are Required for Efficient Skin Repair." Cell Stem Cell **26**(6): 880-895 e886.

Siersbæk, M. S., A. Loft, M. M. Aagaard, R. Nielsen, S. F. Schmidt, N. Petrovic, J. Nedergaard and S. Mandrup (2012). "Genome-wide profiling of peroxisome proliferator-activated receptor γ in primary epididymal, inguinal, and brown adipocytes reveals depot-selective binding correlated with gene expression." Mol Cell Biol **32**(17): 3452-3463.

Siersbæk, R., S. Baek, A. Rabiee, R. Nielsen, S. Traynor, N. Clark, A. Sandelin, O. N. Jensen, M. H. Sung, G. L. Hager and S. Mandrup (2014). "Molecular architecture of transcription factor hotspots in early adipogenesis." Cell Rep **7**(5): 1434-1442.

Siersbaek, R., R. Nielsen and S. Mandrup (2012). "Transcriptional networks and chromatin remodeling controlling adipogenesis." Trends Endocrinol Metab **23**(2): 56-64.

Siersbæk, R., R. Nielsen and S. Mandrup (2012). "Transcriptional networks and chromatin remodeling controlling adipogenesis." Trends Endocrinol Metab **23**(2): 56-64.

Signer, R. A., J. A. Magee, A. Salic and S. J. Morrison (2014). "Haematopoietic stem cells require a highly regulated protein synthesis rate." Nature **509**(7498): 49-54.

Smith, G. I., B. Mittendorfer and S. Klein (2019). "Metabolically healthy obesity: facts and fantasies." J Clin Invest **129**(10): 3978-3989.

Soccio, R. E., Z. Li, E. R. Chen, Y. H. Foong, K. K. Benson, J. R. Dispirito, S. E. Mullican, M. J. Emmett, E. R. Briggs, L. C. Peed, R. K. Dzeng, C. J. Medina, J. F. Jolivert, M. Kissig, S. R.

Rajapurkar, M. Damle, H. W. Lim, K. J. Won, P. Seale, D. J. Steger and M. A. Lazar (2017). "Targeting PPARγ in the epigenome rescues genetic metabolic defects in mice." J Clin Invest **127**(4): 1451-1462.

Song, A., W. Dai, M. J. Jang, L. Medrano, Z. Li, H. Zhao, M. Shao, J. Tan, A. Li, T. Ning, M. M. Miller, B. Armstrong, J. M. Huss, Y. Zhu, Y. Liu, V. Gradinaru, X. Wu, L. Jiang, P. E. Scherer and Q. A. Wang (2020). "Low- and high-thermogenic brown adipocyte subpopulations coexist in murine adipose tissue." J Clin Invest **130**(1): 247-257.

Song, Z., A. M. Xiaoli and F. Yang (2018). "Regulation and Metabolic Significance of De Novo Lipogenesis in Adipose Tissues." Nutrients **10**(10): 1383.

Spalding, K. L., E. Arner, P. O. Westermark, S. Bernard, B. A. Buchholz, O. Bergmann, L. Blomqvist, J. Hoffstedt, E. Naslund, T. Britton, H. Concha, M. Hassan, M. Ryden, J. Frisen and P. Arner (2008). "Dynamics of fat cell turnover in humans." Nature **453**(7196): 783-787.

Spalding, K. L., S. Bernard, E. Näslund, M. Salehpour, G. Possnert, L. Appelsved, K. Y. Fu, K. Alkass, H. Druid, A. Thorell, M. Rydén and P. Arner (2017). "Impact of fat mass and distribution on lipid turnover in human adipose tissue." Nat Commun **8**: 15253.

Spallanzani, R. G., D. Zemmour, T. Xiao, T. Jayewickreme, C. Li, P. J. Bryce, C. Benoist and D. Mathis (2019). "Distinct immunocyte-promoting and adipocyte-generating stromal components coordinate adipose tissue immune and metabolic tenors." Sci Immunol **4**(35): eaaw3658.

Spallanzani, R. G., D. Zemmour, T. Xiao, T. Jayewickreme, C. Li, P. J. Bryce, C. Benoist and D. Mathis (2019). "Distinct immunocyte-promoting and adipocyte-generating stromal components coordinate adipose tissue immune and metabolic tenors." Sci Immunol **4**(35).

Spitale, R. C., R. A. Flynn, Q. C. Zhang, P. Crisalli, B. Lee, J. W. Jung, H. Y. Kuchelmeister, P. J. Batista, E. A. Torre, E. T. Kool and H. Y. Chang (2015). "Structural imprints in vivo decode RNA regulatory mechanisms." Nature **519**(7544): 486-490.

Stefkovich, M., S. Traynor, L. Cheng, D. Merrick and P. Seale (2021). "Dpp4+ interstitial progenitor cells contribute to basal and high fat diet-induced adipogenesis." Mol Metab **54**: 101357.

Steger, D. J., G. R. Grant, M. Schupp, T. Tomaru, M. I. Lefterova, J. Schug, E. Manduchi, C. J. Stoeckert, Jr. and M. A. Lazar (2010). "Propagation of adipogenic signals through an epigenomic transition state." Genes Dev **24**(10): 1035-1044.

Stine, R. R., S. N. Shapira, H. W. Lim, J. Ishibashi, M. Harms, K. J. Won and P. Seale (2016). "EBF2 promotes the recruitment of beige adipocytes in white adipose tissue." Mol Metab **5**(1): 57-65.

Su, B., L. F. Bettcher, W. Y. Hsieh, D. Hornburg, M. J. Pearson, N. Blomberg, M. Giera, M. P. Snyder, D. Raftery, S. J. Bensinger and K. J. Williams (2021). "A DMS Shotgun Lipidomics Workflow Application to Facilitate High-Throughput, Comprehensive Lipidomics." J Am Soc Mass Spectrom **32**(11): 2655-2663.

Sun, C., W. L. Berry and L. E. Olson (2017). "PDGFRalpha controls the balance of stromal and adipogenic cells during adipose tissue organogenesis." Development **144**(1): 83-94.

Sun, C., H. Sakashita, J. Kim, Z. Tang, G. M. Upchurch, L. Yao, W. L. Berry, T. M. Griffin and L. E. Olson (2020). "Mosaic Mutant Analysis Identifies PDGFRalpha/PDGFRbeta as Negative Regulators of Adipogenesis." Cell Stem Cell **26**(5): 707-721 e705.

Sun, K., N. Halberg, M. Khan, U. J. Magalang and P. E. Scherer (2013). "Selective inhibition of hypoxia-inducible factor 1alpha ameliorates adipose tissue dysfunction." Mol Cell Biol **33**(5): 904-917.

Sun, K., C. M. Kusminski, K. Luby-Phelps, S. B. Spurgin, Y. A. An, Q. A. Wang, W. L. Holland and P. E. Scherer (2014). "Brown adipose tissue derived VEGF-A modulates cold tolerance and energy expenditure." Mol Metab **3**(4): 474-483.

Sun, K., J. Tordjman, K. Clement and P. E. Scherer (2013). "Fibrosis and adipose tissue dysfunction." Cell Metab **18**(4): 470-477.

Sun, W., H. Dong, M. Balaz, M. Slyper, E. Drokhlyansky, G. Colleluori, A. Giordano, Z. Kovanicova, P. Stefanicka, L. Balazova, L. Ding, A. S. Husted, G. Rudofsky, J. Ukropec, S. Cinti, T. W. Schwartz, A. Regev and C. Wolfrum (2020). "snRNA-seq reveals a subpopulation of adipocytes that regulates thermogenesis." Nature **587**(7832): 98-102.

Suwanwela, J., C. R. Farber, B. L. Haung, B. Song, C. Pan, K. M. Lyons and A. J. Lusis (2011). "Systems genetics analysis of mouse chondrocyte differentiation." J Bone Miner Res **26**(4): 747-760.

Sveidahl Johansen, O., T. Ma, J. B. Hansen, L. K. Markussen, R. Schreiber, L. Reverte-Salisa, H. Dong, D. P. Christensen, W. Sun, T. Gnad, I. Karavaeva, T. S. Nielsen, S. Kooijman, C. Cero, O. Dmytriyeva, Y. Shen, M. Razzoli, S. L. O'Brien, E. N. Kuipers, C. H. Nielsen, W. Orchard, N. Willemsen, N. Z. Jespersen, M. Lundh, E. G. Sustarsic, C. M. Hallgren, M. Frost, S. McGonigle, M. S. Isidor, C. Broholm, O. Pedersen, J. B. Hansen, N. Grarup, T. Hansen, A. Kjaer, J. G. Granneman, M. M. Babu, D. Calebiro, S. Nielsen, M. Ryden, R. Soccio, P. C. N. Rensen, J. T. Treebak, T. W. Schwartz, B. Emanuelli, A. Bartolomucci, A. Pfeifer, R. Zechner, C. Scheele, S. Mandrup and Z. Gerhart-Hines (2021). "Lipolysis drives expression of the constitutively active receptor GPR3 to induce adipose thermogenesis." Cell **184**(13): 3502-3518 e3533.

Szanto, A., B. L. Balint, Z. S. Nagy, E. Barta, B. Dezso, A. Pap, L. Szeles, S. Poliska, M. Oros, R. M. Evans, Y. Barak, J. Schwabe and L. Nagy (2010). "STAT6 transcription factor is a facilitator of the nuclear receptor PPARγ-regulated gene expression in macrophages and dendritic cells." Immunity **33**(5): 699-712.

Sztalryd, C. and D. L. Brasaemle (2017). "The perilipin family of lipid droplet proteins: Gatekeepers of intracellular lipolysis." Biochim Biophys Acta Mol Cell Biol Lipids **1862**(10 Pt B): 1221-1232.

Tabula Muris, C. (2020). "A single-cell transcriptomic atlas characterizes ageing tissues in the mouse." Nature **583**(7817): 590-595.

Tang, H. N., C. Y. Tang, X. F. Man, S. W. Tan, Y. Guo, J. Tang, C. L. Zhou and H. D. Zhou (2017). "Plasticity of adipose tissue in response to fasting and refeeding in male mice." Nutr Metab (Lond) **14**: 3.

Tang, W., D. Zeve, J. Seo, A. Y. Jo and J. M. Graff (2011). "Thiazolidinediones regulate adipose lineage dynamics." Cell Metab **14**(1): 116-122.

Tang, W., D. Zeve, J. M. Suh, D. Bosnakovski, M. Kyba, R. E. Hammer, M. D. Tallquist and J. M. Graff (2008). "White fat progenitor cells reside in the adipose vasculature." Science **322**(5901): 583-586.

Tang, Y., M. Wallace, J. Sanchez-Gurmaches, W. Y. Hsiao, H. Li, P. L. Lee, S. Vernia, C. M. Metallo and D. A. Guertin (2016). "Adipose tissue mTORC2 regulates ChREBP-driven de novo lipogenesis and hepatic glucose metabolism." Nat Commun **7**(1): 11365.

Tilg, H., N. Zmora, T. E. Adolph and E. Elinav (2020). "The intestinal microbiota fuelling metabolic inflammation." Nat Rev Immunol **20**(1): 40-54.

Tontonoz, P., Hu, E., & Spiegelman, B. M. (1994). "Stimulation of adipogenesis in fibroblasts by PPARγ2, a lipid-activated transcription factor." Cell **79**(7).

Tontonoz, P., L. Nagy, J. G. Alvarez, V. A. Thomazy and R. M. Evans (1998). "PPARgamma promotes monocyte/macrophage differentiation and uptake of oxidized LDL." Cell **93**(2): 241-252.

Tontonoz, P. and B. M. Spiegelman (2008). "Fat and beyond: the diverse biology of PPARgamma." Annu Rev Biochem **77**: 289-312.

Torrent, M., G. Chalancon, N. S. de Groot, A. Wuster and M. Madan Babu (2018). "Cells alter their tRNA abundance to selectively regulate protein synthesis during stress conditions." Sci Signal **11**(546).

Tran, C. M., S. Mukherjee, L. Ye, D. W. Frederick, M. Kissig, J. G. Davis, D. W. Lamming, P. Seale and J. A. Baur (2016). "Rapamycin Blocks Induction of the Thermogenic Program in White Adipose Tissue." Diabetes **65**(4): 927-941.

Trayhurn, P. (2013). "Hypoxia and adipose tissue function and dysfunction in obesity." Physiol Rev **93**(1): 1-21.

Tsukiyama-Kohara, K., F. Poulin, M. Kohara, C. T. DeMaria, A. Cheng, Z. Wu, A. C. Gingras, A. Katsume, M. Elchebly, B. M. Spiegelman, M. E. Harper, M. L. Tremblay and N. Sonenberg (2001). "Adipose tissue reduction in mice lacking the translational inhibitor 4E-BP1." Nat Med **7**(10): 1128-1132.

Turatsinze, J. V., M. Thomas-Chollier, M. Defrance and J. van Helden (2008). "Using RSAT to scan genome sequences for transcription factor binding sites and cis-regulatory modules." Nat Protoc **3**(10): 1578-1588.

Uezumi, A., S. Fukada, N. Yamamoto, S. Takeda and K. Tsuchida (2010). "Mesenchymal progenitors distinct from satellite cells contribute to ectopic fat cell formation in skeletal muscle." Nat Cell Biol **12**(2): 143-152.

Uezumi, A., T. Ito, D. Morikawa, N. Shimizu, T. Yoneda, M. Segawa, M. Yamaguchi, R. Ogawa, M. M. Matev, Y. Miyagoe-Suzuki, S. Takeda, K. Tsujikawa, K. Tsuchida, H. Yamamoto and S. Fukada (2011). "Fibrosis and adipogenesis originate from a common mesenchymal progenitor in skeletal muscle." J Cell Sci **124**(Pt 21): 3654-3664.

Ukropec, J., R. P. Anunciado, Y. Ravussin, M. W. Hulver and L. P. Kozak (2006). "UCP1-independent thermogenesis in white adipose tissue of cold-acclimated Ucp1-/- mice." J Biol Chem **281**(42): 31894-31908.

Unger, R. H. (2003). "Lipid overload and overflow: metabolic trauma and the metabolic syndrome." Trends Endocrinol Metab **14**(9): 398-403.

Valvezan, A. J. and B. D. Manning (2019). "Molecular logic of mTORC1 signalling as a metabolic rheostat." Nat Metab **1**(3): 321-333.

Vazirani, R. P., A. Verma, L. A. Sadacca, M. S. Buckman, B. Picatoste, M. Beg, C. Torsitano, J. H. Bruno, R. T. Patel, K. Simonyte, J. P. Camporez, G. Moreira, D. J. Falcone, D. Accili, O. Elemento, G. I. Shulman, B. B. Kahn and T. E. McGraw (2016). "Disruption of Adipose Rab10-Dependent Insulin Signaling Causes Hepatic Insulin Resistance." Diabetes **65**(6): 1577-1589.

Veliova, M., M. J. Tol, P. Tontonoz, O. S. Shirihai and M. Liesa (2023). "Measuring Mitochondrial Uncoupling in Mouse Primary Brown Adipocytes Differentiated Ex Vivo." Methods Mol Biol **2662**: 53-65.

Vijay, J., M. F. Gauthier, R. L. Biswell, D. A. Louiselle, J. J. Johnston, W. A. Cheung, B. Belden, A. Pramatarova, L. Biertho, M. Gibson, M. M. Simon, H. Djambazian, A. Staffa, G. Bourque, A. Laitinen, J. Nystedt, M. C. Vohl, J. D. Fraser, T. Pastinen, A. Tchernof and E. Grundberg (2020). "Single-cell analysis of human adipose tissue identifies depot and disease specific cell types." Nat Metab **2**(1): 97-109.

Villanueva, C. J., L. Vergnes, J. Wang, B. G. Drew, C. Hong, Y. Tu, Y. Hu, X. Peng, F. Xu, E. Saez, K. Wroblewski, A. L. Hevener, K. Reue, L. G. Fong, S. G. Young and P. Tontonoz (2013). "Adipose subtype-selective recruitment of TLE3 or Prdm16 by PPARgamma specifies lipid storage versus thermogenic gene programs." Cell Metab **17**(3): 423-435.

Vishvanath, L. and R. K. Gupta (2019). "Contribution of adipogenesis to healthy adipose tissue expansion in obesity." J Clin Invest **129**(10): 4022-4031.

Vishvanath, L., K. A. MacPherson, C. Hepler, Q. A. Wang, M. Shao, S. B. Spurgin, M. Y. Wang, C. M. Kusminski, T. S. Morley and R. K. Gupta (2016). "Pdgfrbeta+ Mural Preadipocytes Contribute to Adipocyte Hyperplasia Induced by High-Fat-Diet Feeding and Prolonged Cold Exposure in Adult Mice." Cell Metab **23**(2): 350-359.

von der Heyde, S., C. Fromm-Dornieden, G. Salinas-Riester, T. Beissbarth and B. G. Baumgartner (2014). "Dynamics of mRNA and polysomal abundance in early 3T3-L1 adipogenesis." BMC Genomics **15**(1): 381.

von Manteuffel, S. R., A. C. Gingras, X. F. Ming, N. Sonenberg and G. Thomas (1996). "4E-BP1 phosphorylation is mediated by the FRAP-p70s6k pathway and is independent of mitogen-activated protein kinase." Proc Natl Acad Sci U S A **93**(9): 4076-4080.

Vydelingum, N., R. L. Drake, J. Etienne and A. H. Kissebah (1983). "Insulin regulation of fat cell ribosomes, protein synthesis, and lipoprotein lipase." Am J Physiol **245**(2): E121-131.

Wang, M. Y., P. Grayburn, S. Chen, M. Ravazzola, L. Orci and R. H. Unger (2008). "Adipogenic capacity and the susceptibility to type 2 diabetes and metabolic syndrome." Proc Natl Acad Sci U S A **105**(16): 6139-6144.

Wang, Q. A., A. Song, W. Chen, P. C. Schwalie, F. Zhang, L. Vishvanath, L. Jiang, R. Ye, M. Shao, C. Tao, R. K. Gupta, B. Deplancke and P. E. Scherer (2018). "Reversible De-differentiation of Mature White Adipocytes into Preadipocyte-like Precursors during Lactation." Cell Metab **28**(2): 282-288 e283.

Wang, Q. A., C. Tao, R. K. Gupta and P. E. Scherer (2013). "Tracking adipogenesis during white adipose tissue development, expansion and regeneration." Nat Med **19**(10): 1338-1344.

Wang, Q. A., F. Zhang, L. Jiang, R. Ye, Y. An, M. Shao, C. Tao, R. K. Gupta and P. E. Scherer (2018). "Peroxisome Proliferator-Activated Receptor γ and Its Role in Adipocyte Homeostasis and Thiazolidinedione-Mediated Insulin Sensitization." Mol Cell Biol **38**(10).

Wang, W., J. Ishibashi, S. Trefely, M. Shao, A. J. Cowan, A. Sakers, H. W. Lim, S. O'Connor, M. T. Doan, P. Cohen, J. A. Baur, M. T. King, R. L. Veech, K. J. Won, J. D. Rabinowitz, N. W. Snyder, R. K. Gupta and P. Seale (2019). "A PRDM16-Driven Metabolic Signal from Adipocytes Regulates Precursor Cell Fate." Cell Metab **30**(1): 174-189 e175.

Weisberg, S. P., D. Hunter, R. Huber, J. Lemieux, S. Slaymaker, K. Vaddi, I. Charo, R. L. Leibel and A. W. Ferrante, Jr. (2006). "CCR2 modulates inflammatory and metabolic effects of high-fat feeding." J Clin Invest **116**(1): 115-124.

Weisberg, S. P., D. McCann, M. Desai, M. Rosenbaum, R. L. Leibel and A. W. Ferrante, Jr. (2003). "Obesity is associated with macrophage accumulation in adipose tissue." J Clin Invest **112**(12): 1796-1808.

West-Eberhard, M. J. (2019). "Nutrition, the visceral immune system, and the evolutionary origins of pathogenic obesity." Proc Natl Acad Sci U S A **116**(3): 723-731.

Westcott, G. P., M. P. Emont, J. Li, C. Jacobs, L. Tsai and E. D. Rosen (2021). "Mesothelial cells are not a source of adipocytes in mice." Cell Rep **36**(2): 109388.

Weyer, C., J. E. Foley, C. Borgadus, P. A. Tataranni and R. E. Pratley (2000). "Enlarged subcutaneous adbominal adipocyte size, but not obesity itself, predicts Type II diabetes independent of insulin resistance." Diabetologia **43**: 1498-1506.

WHO, W. H. O. (2023). "Health topics: Obesity."

Wildman, R. P., P. Muntner, K. Reynolds, A. P. McGinn, S. Rajpathak, J. Wylie-Rosett and M. R. Sowers (2008). "The obese without cardiometabolic risk factor clustering and the normal weight with cardiometabolic risk factor clustering: prevalence and correlates of 2 phenotypes among the US population (NHANES 1999-2004)." Arch Intern Med **168**(15): 1617-1624.

Wu, H., S. Ghosh, X. D. Perrard, L. Feng, G. E. Garcia, J. L. Perrard, J. F. Sweeney, L. E. Peterson, L. Chan, C. W. Smith and C. M. Ballantyne (2007). "T-cell accumulation and regulated on activation, normal T cell expressed and secreted upregulation in adipose tissue in obesity." Circulation **115**(8): 1029-1038.

Wu, J., P. Bostrom, L. M. Sparks, L. Ye, J. H. Choi, A. H. Giang, M. Khandekar, K. A. Virtanen, P. Nuutila, G. Schaart, K. Huang, H. Tu, W. D. van Marken Lichtenbelt, J. Hoeks, S. Enerback,

P. Schrauwen and B. M. Spiegelman (2012). "Beige adipocytes are a distinct type of thermogenic fat cell in mouse and human." Cell **150**(2): 366-376.

Wu, Q., S. G. Medina, G. Kushawah, M. L. DeVore, L. A. Castellano, J. M. Hand, M. Wright and A. A. Bazzini (2019). "Translation affects mRNA stability in a codon-dependent manner in human cells." Elife **8**.

Wu, T., E. Hu, S. Xu, M. Chen, P. Guo, Z. Dai, T. Feng, L. Zhou, W. Tang, L. Zhan, X. Fu, S. Liu, X. Bo and G. Yu (2021). "clusterProfiler 4.0: A universal enrichment tool for interpreting omics data." The Innovation **2**(3): 100141.

Xiao, L., X. Yang, Y. Lin, S. Li, J. Jiang, S. Qian, Q. Tang, R. He and X. Li (2016). "Large adipocytes function as antigen-presenting cells to activate CD4(+) T cells via upregulating MHCII in obesity." Int J Obes (Lond) **40**(1): 112-120.

Xu, B., A. Xing and S. Li (2022). "The forgotten type 2 diabetes mellitus medicine: rosiglitazone." Diabetol Int **13**(1): 49-65.

Xu, M., A. K. Palmer, H. Ding, M. M. Weivoda, T. Pirtskhalava, T. A. White, A. Sepe, K. O. Johnson, M. B. Stout, N. Giorgadze, M. D. Jensen, N. K. LeBrasseur, T. Tchkonia and J. L. Kirkland (2015). "Targeting senescent cells enhances adipogenesis and metabolic function in old age." Elife **4**(DECEMBER2015): e12997.

Xue, Y., N. Petrovic, R. Cao, O. Larsson, S. Lim, S. Chen, H. M. Feldmann, Z. Liang, Z. Zhu, J. Nedergaard, B. Cannon and Y. Cao (2009). "Hypoxia-independent angiogenesis in adipose tissues during cold acclimation." Cell Metab **9**(1): 99-109.

Yang, H.-M., B.-K. Kim, J.-Y. Kim, Y.-W. Kwon, S. Jin, J.-E. Lee, H.-J. Cho, H.-Y. Lee, H.-J. Kang, B.-H. Oh, Y.-B. Park and H.-S. Kim (2013). "PPARγ modulates vascular smooth muscle cell phenotype via a protein kinase G-dependent pathway and reduces neointimal hyperplasia after vascular injury." Experimental & Molecular Medicine **45**(11): e65-e65.

Yang, Q., A. Vijayakumar and B. B. Kahn (2018). "Metabolites as regulators of insulin sensitivity and metabolism." Nat Rev Mol Cell Biol **19**(10): 654-672.

Ye, Y., H. Liu, F. Zhang and F. Hu (2019). "mTOR signaling in Brown and Beige adipocytes: implications for thermogenesis and obesity." Nutr Metab (Lond) **16**(1): 74.

Yilmaz, M., K. C. Claiborn and G. S. Hotamisligil (2016). "De Novo Lipogenesis Products and Endogenous Lipokines." Diabetes **65**(7): 1800-1807.

Yki-Jarvinen, H. (2004). "Thiazolidinediones." N Engl J Med **351**(11): 1106-1118.

Yoneshiro, T., Q. Wang, K. Tajima, M. Matsushita, H. Maki, K. Igarashi, Z. Dai, P. J. White, R. W. McGarrah, O. R. Ilkayeva, Y. Deleye, Y. Oguri, M. Kuroda, K. Ikeda, H. Li, A. Ueno, M. Ohishi, T. Ishikawa, K. Kim, Y. Chen, C. H. Sponton, R. N. Pradhan, H. Majd, V. J. Greiner, M. Yoneshiro, Z. Brown, M. Chondronikola, H. Takahashi, T. Goto, T. Kawada, L. Sidossis, F. C. Szoka, M. T. McManus, M. Saito, T. Soga and S. Kajimura (2019). "BCAA catabolism in brown fat controls energy homeostasis through SLC25A44." Nature **572**(7771): 614-619.

Yoon, M. S. (2016). "The Emerging Role of Branched-Chain Amino Acids in Insulin Resistance and Metabolism." Nutrients **8**(7): 405.

Yore, M. M., I. Syed, P. M. Moraes-Vieira, T. Zhang, M. A. Herman, E. A. Homan, R. T. Patel, J. Lee, S. Chen, O. D. Peroni, A. S. Dhaneshwar, A. Hammarstedt, U. Smith, T. E. McGraw, A. Saghatelian and B. B. Kahn (2014). "Discovery of a class of endogenous mammalian lipids with anti-diabetic and anti-inflammatory effects." Cell **159**(2): 318-332.

Yoshino, J., B. W. Patterson and S. Klein (2019). "Adipose Tissue CTGF Expression is Associated with Adiposity and Insulin Resistance in Humans." Obesity (Silver Spring) **27**(6): 957-962.

Young, D. A., Y. S. Choi, A. J. Engler and K. L. Christman (2013). "Stimulation of adipogenesis of adult adipose-derived stem cells using substrates that mimic the stiffness of adipose tissue." Biomaterials **34**(34): 8581-8588.

Zaragosi, L. E., B. Wdziekonski, P. Villageois, M. Keophiphath, M. Maumus, T. Tchkonia, V. Bourlier, T. Mohsen-Kanson, A. Ladoux, C. Elabd, M. Scheideler, Z. Trajanoski, Y. Takashima, E. Z. Amri, D. Lacasa, C. Sengenes, G. Ailhaud, K. Clement, A. Bouloumie, J. L. Kirkland and C. Dani (2010). "Activin a plays a critical role in proliferation and differentiation of human adipose progenitors." Diabetes **59**(10): 2513-2521.

Zatterale, F., M. Longo, J. Naderi, G. A. Raciti, A. Desiderio, C. Miele and F. Beguinot (2019). "Chronic Adipose Tissue Inflammation Linking Obesity to Insulin Resistance and Type 2 Diabetes." Front Physiol **10**(1607): 1607.

Zeng, H., J. Huang, J. Ren, C. K. Wang, Z. Tang, H. Zhou, Y. Zhou, H. Shi, A. Aditham, X. Sui, H. Chen, J. A. Lo and X. Wang (2023). "Spatially resolved single-cell translatomics at molecular resolution." Science **380**(6652): eadd3067.

Zeng, W., R. M. Pirzgalska, M. M. Pereira, N. Kubasova, A. Barateiro, E. Seixas, Y. H. Lu, A. Kozlova, H. Voss, G. G. Martins, J. M. Friedman and A. I. Domingos (2015). "Sympathetic neuro-adipose connections mediate leptin-driven lipolysis." Cell **163**(1): 84-94.

Zeng, X., M. Ye, J. M. Resch, M. P. Jedrychowski, B. Hu, B. B. Lowell, D. D. Ginty and B. M. Spiegelman (2019). "Innervation of thermogenic adipose tissue via a calsyntenin 3beta-S100b axis." Nature **569**(7755): 229-235.

Zhang, F., G. Hao, M. Shao, K. Nham, Y. An, Q. Wang, Y. Zhu, C. M. Kusminski, G. Hassan, R. K. Gupta, Q. Zhai, X. Sun, P. E. Scherer and O. K. Oz (2018). "An Adipose Tissue Atlas: An Image-Guided Identification of Human-like BAT and Beige Depots in Rodents." Cell Metab **27**(1): 252-262 e253.

Zhang, Q., N. A. Shalaby and M. Buszczak (2014). "Changes in rRNA transcription influence proliferation and cell fate within a stem cell lineage." Science **343**(6168): 298-301.

Zhang, X., Y. Zhang, P. Wang, S. Y. Zhang, Y. Dong, G. Zeng, Y. Yan, L. Sun, Q. Wu, H. Liu, B. Liu, W. Kong, X. Wang and C. Jiang (2019). "Adipocyte Hypoxia-Inducible Factor 2α Suppresses Atherosclerosis by Promoting Adipose Ceramide Catabolism." Cell Metab **30**(5): 937-951.e935.

Zhang, Z., M. Shao, C. Hepler, Z. Zi, S. Zhao, Y. A. An, Y. Zhu, A. L. Ghaben, M. Y. Wang, N. Li, T. Onodera, N. Joffin, C. Crewe, Q. Zhu, L. Vishvanath, A. Kumar, C. Xing, Q. A. Wang, L. Gautron, Y. Deng, R. Gordillo, I. Kruglikov, C. M. Kusminski, R. K. Gupta and P. E. Scherer (2019). "Dermal adipose tissue has high plasticity and undergoes reversible dedifferentiation in mice." J Clin Invest **129**(12): 5327-5342.

Zhao, S., Y. Zhu, R. D. Schultz, N. Li, Z. He, Z. Zhang, A. Caron, Q. Zhu, K. Sun, W. Xiong, H. Deng, J. Sun, Y. Deng, M. Kim, C. E. Lee, R. Gordillo, T. Liu, A. K. Odle, G. V. Childs, N. Zhang, C. M. Kusminski, J. K. Elmquist, K. W. Williams, Z. An and P. E. Scherer (2019). "Partial Leptin Reduction as an Insulin Sensitization and Weight Loss Strategy." Cell Metab **30**(4): 706-719 e706.

Zheng, G. X. Y., J. M. Terry, P. Belgrader, P. Ryvkin, Z. W. Bent, R. Wilson, S. B. Ziraldo, T. D. Wheeler, G. P. McDermott, J. Zhu, M. T. Gregory, J. Shuga, L. Montesclaros, J. G. Underwood, D. A. Masquelier, S. Y. Nishimura, M. Schnall-Levin, P. W. Wyatt, C. M. Hindson, R. Bharadwaj, A. Wong, K. D. Ness, L. W. Beppu, H. J. Deeg, C. McFarland, K. R. Loeb, W. J. Valente, N. G. Ericson, E. A. Stevens, J. P. Radich, T. S. Mikkelsen, B. J. Hindson and J. H. Bielas (2017). "Massively parallel digital transcriptional profiling of single cells." Nature Communications **8**(1): 14049.

Zhou, P., A. Santoro, O. D. Peroni, A. T. Nelson, A. Saghatelian, D. Siegel and B. B. Kahn (2019). "PAHSAs enhance hepatic and systemic insulin sensitivity through direct and indirect mechanisms." J Clin Invest **129**(10): 4138-4150.

Zwick, R. K., C. F. Guerrero-Juarez, V. Horsley and M. V. Plikus (2018). "Anatomical, Physiological, and Functional Diversity of Adipose Tissue." Cell Metab **27**(1): 68-83.

Zyner, K. G., A. Simeone, S. M. Flynn, C. Doyle, G. Marsico, S. Adhikari, G. Portella, D. Tannahill and S. Balasubramanian (2022). "G-quadruplex DNA structures in human stem cells and differentiation." Nature Communications **13**(1): 142.